Identification of Dynamic Ankle Stiffness during Time-Varying Conditions

Diego L. Guarín

Doctor of Philosophy

Biomedical Engineering Department

McGill University

Montreal, Québec

March 8, 2017

A thesis submitted to McGill University in partial fulfillment of the requirements of the degree of Doctor of Philosophy

ABSTRACT

The neuromechanical properties of a joint can be described in terms of its dynamic stiffness that describes the dynamic relation between joint position and torque. Dynamic stiffness is generated by intrinsic (mechanical) and reflex (neural) mechanisms that act and change together; therefore, their individual contributions cannot be measured directly. During stationary conditions, the neuromechanical properties of a joint can be estimated using nonlinear mathematical models, specialized systems identification algorithms, and disturbance experiments. Stationary results have shown that dynamic joint stiffness is heavily modulated by joint position and voluntary torque. Consequently, during movement, when these undergo large, rapid changes, dynamic joint stiffness will be time-varying.

This thesis develops new analytical tools to estimate time-varying, dynamic joint stiffness during function. These methods were validated and their performance characterized using realistic simulations. Pilot experiments demonstrated that the methods accurately decompose the overall dynamic joint stiffness into its intrinsic and reflex components, and track how they change throughout functionally relevant activities. Therefore, these new methods make it possible for the first time to characterize the neuromechanical properties of joints during functional activities. This information is essential to understand how the central nervous system controls posture and movement and for the objective characterization of neuromuscular diseases.

ABRÉGÉ

Les propriétés neuromécaniques d'une articulation peuvent être décrites en termes de sa rigidité dynamique qui décrit la relation dynamique entre la position de l'articulation et le couple. La rigidité dynamique est générée par des mécanismes intrinsèques (mécaniques) et réflexes (neuronaux) qui agissent et changent ensemble; Par conséquent, leurs contributions individuelles ne peuvent pas être mesurées directement. En conditions stationnaires, les propriétés neuromécaniques d'une articulation peuvent être estimées à l'aide de modèles mathématiques non linéaires, d'algorithmes d'identification de systèmes spécialisés et d'expériences de perturbation. Les résultats stationnaires ont montré que la rigidité dynamique des articulations est fortement modulée par la position des joints et le couple volontaire. Par conséquent, lors du mouvement, lorsque ceux-ci subissent de grands changements rapides, la rigidité articulaire dynamique va varier dans le temps.

Cette thèse développe de nouveaux outils analytiques pour estimer la rigidité articulaire dynamique et variable dans le temps pendant la fonction. Ces méthodes ont été validées et leurs performances ont été caractérisées par des simulations réalistes. Des expériences pilotes ont démontré que les méthodes décomposent avec précision la rigidité articulaire globale dynamique dans ses composantes intrinsèque et réflexe et suivent comment elles évoluent tout au long des activités fonctionnellement pertinentes. Par conséquent, ces nouvelles méthodes permettent pour la première fois de caractériser les propriétés neuromécaniques des articulations au cours des activités fonctionnelles. Cette information est essentielle pour comprendre comment

le système nerveux central contrôle la posture et le mouvement et pour la caractérisation objective des maladies neuromusculaires.

DEDICATION

To my family

ACKNOWLEDGMENTS

I wish to express my sincere gratitude to my advisor, Dr. Robert E. Kearney, for his support, patience, and encouragement throughout my graduate studies. His technical and editorial advice was essential to the completion of this thesis.

I would like to thank my PhD committee members, Dr. Henrieta Galiana and Dr. Georgios Mitsis, for their guidance through this process. The discussion and feedback provided during our meetings was invaluable.

I would also like to thank the members and former members of REKlab for the helpful discussions and suggestions. Special thanks to my friend Kian Jalaleddini for his support in the early stages of my research. My thanks also go to Dr. Ross Wagner for his invaluable technical support, to Pina Sorrini, Daniel Caron and the BME department staff for all their help and support.

Finally, I would like to thank my wife Natalia for giving me the greatest joy in life, and her unconditional love and support during all these years. My parents, Martha and Fernando, receive my deepest gratitude for their love and support. Everything that I am now is because of them.

Financial support for this work was provided by The Fonds de recherche du Québec - Nature et technologies (FRQNT) and the Canadian Institutes of Health Research.

CONTRIBUTION OF AUTHORS

Diego L. Guarín designed the algorithms, simulations and experiments, performed the simulation studies and experiments, analyzed the data, interpreted the results, drafted the manuscripts and prepared the final versions. Robert E. Kearney provided overall supervision and advice in the design of the algorithms, simulations and experimental studies, assisted in the interpretation of results, and provided editorial input in writing the manuscripts.

ORIGINAL CONTRIBUTIONS

This thesis develops and validates new algorithms for the identification of linear, and non-linear, time-varying systems. The are applied to estimate the neuromechanical properties of joints during function. These methods and algorithms represent a significant contribution to the modeling and identification of biomedical systems allowing us to track the large, rapid changes commonly seen in the dynamics of these systems using a few, short input-output segments. The original contributions to the research and scientific knowledge are the following:

Parametric identification of linear, time-varying systems:

1. I developed and validated a novel algorithms for the identification of time-varying, Box-Jenkins models, which are useful to model biomedical systems because of their ability to accurately described the system dynamics even in the presence of complex, non-white, physiological noise. The major contribution of the new algorithm is that it can accurately track large, rapid, periodic parameter changes using a few, short input-output trials. Previous methods for identification of time-varying, Box-Jenkins models could only be used when the system parameters varied slowly with time. This algorithm represents an important contribution to the modeling and identification of biomedical systems since: i) time-varying, Box-Jenkins model structure is useful to model many biological system, ii) it can track the rapid changes frequently seen in biological systems, and iii) has only moderate data requirements simplifying experimental needs.

Non-parametric identification of linear, time-varying systems:

2. I developed and validated novel algorithms for identification of time-varying, non-parametric models using periodic, input-output data segments of short duration. Non-parametric models are useful to describe systems whose model structure is unknown and therefore commonly used to model biomedical systems. The new algorithm accurately estimates the time-varying parameters using just a few input-output realizations. This represents a great improvement over previous methods for identification of non-parametric, linear models that require hundreds of input-output realizations presenting the same time behavior. The reduction in data requirement results in much shorter experiments which makes it much easier to acquire enough trials with the same time-varying behavior.

Identification of time-varying, Hammerstein systems:

3. I developed a novel algorithms for the identification of time-varying, Hammerstein systems, consisting of the series connection of a time-varying static-nonlinearity and time-varying, Box-Jenkins model. Hammerstein systems are useful in describing biomedical systems as they combine the simplicity of linear systems with the generalization capacity of nonlinear models. The new algorithm improves on existing methods because: i) it does not require the inversion of the static-nonlinearity, ii) is guaranteed to converge to the true values under general conditions, and iii) it can provide accurate estimates of the time-varying model parameters from one single input-output realization.

Identification of time-varying, parallel-cascade systems:

4. I introduced a new method for the identification of the time-varying, parallel-cascade model of joint dynamic stiffness able to decompose the torque at the joint into its intrinsic and reflex components. The new algorithm improves on existing methods because: i) it accurately estimates the time-varying intrinsic and reflex stiffness models using just a few input-output realizations, ii) it does not make *a priori* assumptions about the linear dynamics and the shape of the static-nonlinearity, and iii) it does not assume that the model parameters remain over short time-windows, rather it estimates the model parameters at each point in time, and iv) it produces unbiased parameter estimates in the presence of complex, non-white, physiological noise. Using this algorithm I showed that both intrinsic and reflex dynamic stiffness present large, fast changes throughout the a simulated gait cycle, demonstrating that the joint neuromechanical properties during function cannot be appropriately described using time-invariant models, and that the results obtained from constant posture experiments cannot be interpolated to described the joint properties during movement.

TABLE OF CONTENTS

LIST OF TABLES

LIST OF FIGURES

CHAPTER 1
Introduction

Human joints serve as the interface between the body and the physical world. The mechanical properties of the joints must be constantly adapted or modulated to allow for natural interaction with the environment. For example, when handling a manual drill, the shoulder, elbow, wrist and digits must become stiff to secure the tool in place and facilitate its handling; this can be achieved by activation of surrounding musculature and/or by selecting a posture that provides higher joint stiffness and limb stability. Conversely, when interacting with delicate or soft objects, the joints must be compliant to prevent damage; this is commonly achieved by reducing the activation of related muscles. These activities are performed without much thought and for trained subjects these adaptations become natural parts of their behavior. These changes in the mechanical properties of the joints occur constantly during function to guarantee a natural interaction with the environment.

The complex tasks that the central, peripheral and neuromuscular systems perform to achieve these adaptations are not completely understood. Consequently, there is not yet a clear understanding of how the neuromechanical properties of joints are modulated during function and what mechanisms drive these modulations. Some of these mechanisms are voluntary, e.g. boosting the activation of certain muscles, adopting a new posture [11]. Others are involuntary, e.g. rapid increases in joint torque via spinal reflexes [12]. And still others results from intrinsic joint properties,

e.g. the modulation of skeletal muscle force with length and velocity [6]. A better understanding of how healthy humans interact with the environment and how the neuromechanical properties of joints are modulated to facilitate this interaction will have important implication in different research areas such as:

Motor control: Understanding of how the neuromechanical properties of joints are modulated during movement is essential to elucidate the mechanisms and strategies used by the central nervous system (CNS) to control posture and movement. Some theories of motor control suggest that the CNS controls movement and posture by modulating the neuromechanical properties of joints, so that the modulation of the joint dynamic stiffness should precede the movement [13, 14]. Others suggest that the CNS has an internal model of the limbs dynamics and can predict the forces required to generate movement under different conditions, so that the modulation of the dynamic joint stiffness is a consequence of the movement [15, 16]. Measurements of the modulation of neuromechanical joint properties during function are needed to provide the evidence required to test different hypothesis regarding the mechanisms used by the CNS to control movement and posture. For example, determining if the changes in intrinsic and reflex stiffness associated with a movement precede of succeed the movement will provide new evidence to support the equilibrium point or internal model hypotheses.

Neuromuscular disease: Many neuromuscular disorders cause changes in the joint properties, which are currently assessed in terms of the clinicians' subjective impression of the resistance offered by the joint during passive manipulations.

Measures of the intrinsic and reflexively mediated properties of joints will provide objective information of these neuromuscular diseases, and provide tools for the quantitative assessment of joint neuromechanical properties throughout the course of a disease or treatment [17].

Rehabilitation engineering: The informed design of prosthesis and orthosis requires a quantitative understanding of the neuromechanical joint properties. A complete characterization of joint mechanics during function will permit the development of biomimetic devices that will be easier to control by human operators as they behave and interact with the environment as real joints [18]

Robotics: Studies of joint mechanics will inform the development of biomimetic robots that can interact with humans and the environment in more natural ways. These new robots use adjustable compliant actuators that minimize large forces due to shocks, safely interact with the user, and store/release energy in passive elastic elements [19].

The neuromechanical properties of a joint can be described in terms of dynamic joint stiffness, it defines the relation between joint position and the torque acting about it [1]. Its inverse, joint compliance, defines the relation between joint torque and the resulting position changes [20]. Dynamic joint stiffness may be decomposed into two components:

- An intrinsic component arising from the limb's inertia, and the visco-elastic properties of the joint surface, connective tissue, and muscle.

- A reflex component arising from changes in muscle activation resulting from stretch reflex mechanisms.

These two components act and change together, and in practice it is not possible to measure the effects of the intrinsic or reflex mechanisms separately.

There are several methods to estimate the intrinsic and reflex components of dynamic joint stiffness. Some techniques involve the suppression of spinal reflexes using either cuffing, neural blockage or surgery. These methods involve performing two experimental trials, before and after neural blockade, and comparing the results to differentiate between the intrinsic and reflex components of dynamic joint stiffness. However, even if both experimental trials can be done under the same conditions, e.g, same muscle length, velocity, force; it is difficult to validate how the intrinsic joint properties are affected by this process. Therefore, comparing values before and after suppression of spinal reflexes might over- or under- estimate the role of the neural mechanisms.

An alternative, non-invasive, analytical approach, is to use mathematical models and system identification techniques analytically separate the intrinsic and reflex components of dynamic joint stiffness from one single trial. This analytical approach will be employed in this thesis for the estimation of dynamic joint stiffness during functional situations. During stationary experiments, dynamic joint stiffness can be modeled by a parallel-cascade structure composed of intrinsic and reflex components. In this structure, dynamic intrinsic stiffness is described by a linear system relating

joint position and intrinsic torque. Reflex dynamic stiffness is described by a Hammerstein system, which consist of a series connection of a static-nonlinearity and a linear system that relates joint velocity and reflex torque [12].

There are some major challenges in the quantification of dynamic joint stiffness from experimental data. First, the torque produced by the intrinsic and reflex mechanisms cannot be measured separately; only the noisy version of the total torque, which is the sum of intrinsic, reflex and voluntary contributions can be measured. Second, intrinsic and reflex mechanisms are heavily modulated by joint position, torque, functional task and a variety of other factors. Moreover, the properties of the intrinsic and reflex systems are modulated together during function and the complex, nonlinear interactions between these mechanisms make it difficult to dissociate their individual contributions. Finally, the output noise has complex amplitude and temporal structures; consequently, the system identification techniques used to characterize dynamic joint stiffness must be able to: decompose the total torque into its different components; track the large, rapid changes in the system dynamics expected during function; and must be robust to the presence of non-white, additive noise.

The general objective of this thesis was to develop and validate novel analytical and experimental methods to measure the neuromechanical properties of human joints and how they are modulated during function. This thesis focuses on the study of the ankle joint, because of its significant role during human locomotion and balance. Nevertheless, the methods described here can be applied to study other joints.

The developments presented in this thesis are based on the following specific objectives (SO):

SO 1: Develop and validate parametric system identification methods for the unbiased estimation of time-varying, linear systems.

SO 2: Develop and validate system identification methods for the unbiased estimation of time-varying, nonlinear, Hammerstein systems.

SO 3: Develop and validate system identification methods for the unbiased estimation of the time-varying, parallel-cascade, dynamic ankle stiffness model.

1.1 Thesis Outline

This thesis comprises four scholarly articles, one accepted by an international journal, one submitted to an international journal, one published in the proceedings of an international conference and one that will be submitted shortly to an international journal.

Chapter 2 describes the concept of dynamic joint stiffness, its different components and mechanism. It also presents a critical review of the literature on experimental and analytical methods used to estimate dynamic joint stiffness. Next, it discusses the analytical methods that involve system identification techniques for the estimation of dynamic joint stiffness, with an emphasis on the parallel-cascade model structure and related algorithms. It then summarizes the current state of knowledge of dynamic joint stiffness obtained with these methods. Finally, the rationale for the thesis is presented.

Chapter 3 presents a short summary describing the different methods for the identification of linear, Hammerstein, and time-varying systems that are the basis of the novel algorithms developed in this thesis.

The parallel-cascade model of dynamic joint stiffness describes the overall joint stiffness as a parallel combination of a linear system, representing the intrinsic mechanisms, and a Hammerstein system, formed as a series connection of a static-nonlinearity and a linear system, representing the reflex mechanisms. Therefore, the unbiased identification of linear systems is an important aspect in the characterization of joint biomechanics. There are several well-known methods for the identification of linear, time-invariant systems that provide unbiased parameter estimates even in the presence of non-white, additive noise. However, the identification of linear, time-varying systems is a research field in development, and available methods for the estimation of linear, time-varying systems from input-output data cannot accurately track the parameters time-course or require very large data records for its estimation, which severely limits their applicability.

Chapter 4 develops a novel algorithm for the identification of linear, time-varying, transfer function models in the presence of non-white, additive noise. This model structure is commonly known as Box-Jenkins model and is characterized by an independent parametrization of the system and noise dynamics. Simulations are used to demonstrate the time-varying, Box-Jenkins structure can describe the intrinsic joint compliance, and that the new algorithm can accurately tracks the changes in intrinsic joint compliance expected during walking. This chapter was published in IEEE Transactions on Neural System and Rehabilitation Engineering, authored

by D. L. Guarin and R. E. Kearney, entitled "Identification of a Time-Varying, Box-Jenkins Model of Intrinsic Joint Compliance" in October, 2016.

One limitation of the transfer function models is that the model order needs to be defined *a priori*, and the usefulness of the results depends on the validity of the selected model order. An alternative approach is to describe the system's dynamics by means of a non-parametric model, which do not require the definition of a model order. However, non-parametric models usually have more free parameters than transfer function models, so that when the model order is known, a transfer function model provides a more parsimonious representation of the system's dynamics.

Chapter 5 develops a novel algorithm for the identification of, linear, time-varying, non-parametric models. The new methodology that can track the parameters' time-course using only a few segments of periodic, input-output data records of short duration. This chapter was submitted to IEEE Transactions on Neural System and Rehabilitation Engineering, authored by D. L. Guarin and R. E. Kearney, entitled "Identification of Time Varying, Intrinsic, Dynamic Ankle Stiffness during Passive, Imposed Walking Movements" in August, 2016.

One of the main complexities in the estimation of dynamic joint stiffness is due to the nonlinear, Hammerstein structure used to represent the stretch reflex mechanism. The estimation of time-invariant, Hammerstein systems is a mature subject and many different techniques for the identification of the model parameters are available. However, to our knowledge there are no publicly available algorithms for the estimation of time-varying, Hammerstein systems. Chapter 6 develops a method for the identification of time-varying, Hammerstein system, composed by

a series combination of a time-varying, static-nonlinearity and Box-Jenkins model. This chapter was published in the proceedings of the 17th IFAC System Identification Symposium, authored by D. L. Guarin and R. E. Kearney, entitled "An Instrumental Variable Approach for the Identification of Time-Varying, Hammerstein Systems" in October, 2015.

Chapter 7 develops a new methodology for the identification of overall joint dynamic stiffness during time-varying conditions. Joint dynamic stiffness is modeled by a parallel-cascade structure composed of intrinsic and reflex pathways. The algorithms developed in previous chapters are used to estimate the intrinsic and reflex components of the dynamic joint stiffness sequentially, iterations are used to refine the parameters estimates. This method is applied to measure the intrinsic and reflex dynamic stiffness from one subject in an imposed walking movement experiment with constant muscle activation. The identified TV models predicted the measured torque very well, accounting for more than 95% of the measured torque variance. This chapter was submitted to Frontiers in Computational Neuroscience, authored by D. L. Guarin and R. E. Kearney, entitled "Estimation of Time-Varying, Intrinsic and Reflex Dynamic Ankle Stiffness during Movement" in January, 2017.

Chapter 8 summarizes the original contributions of this thesis and provides a general discussion and suggestions for future developments, applications and improvements.

Finally, Appendix A presents a short summary of the background material in anatomy and physiology required to clearly understand the subject.

CHAPTER 2
Literature Review

This chapter describes dynamic joint stiffness, its different components and underlying mechanisms. It then presents a critical review of the literature on experimental and analytical methods used to estimate dynamic joint stiffness. Next, it reviews system identification techniques for the estimation of dynamic joint stiffness, with an emphasis on the parallel-cascade model structure and related algorithms. It then summarizes the current state of knowledge of dynamic joint stiffness obtained with these methods. The chapter ends with the rationale for the thesis.

2.1 Dynamic Joint Stiffness

2.1.1 Definition

Dynamic joint stiffness is defined as the dynamic relation between the angular position of a joint and the torques acting about it [1]. It defines the interactions between a joint, the associated limbs, and the external environment. Measuring dynamic joint stiffness has important implications in a variety of research areas, including basic motor control research, neuromuscular diseases, rehabilitation engineering, and robotics.

Dynamic joint stiffness is usually described using a lumped model relating joint position and torque rather than considering the detailed mechanisms that compose it. However, having a clear idea of the mechanisms that underlie joint dynamics

is fundamental to the interpretation of results. This section briefly reviews these mechanisms.

Figure 2–1 shows an information flow diagram for the dynamics of a single joint. Here torque is considered as the input and position as the output, so that this model represents dynamic joint compliance; the inverse formulation, in which position is regarded as the input and torque is the output is known as dynamic joint stiffness. Overall joint dynamics are generated by three mechanisms: passive, intrinsic, and reflex dynamics. Each mechanisms is composed of different subsystems that will be described next.

Passive dynamics

It consist of two parts: limb dynamics and articular dynamics.

Limb dynamics: can be attributed to inertia if assumed that the limb is rigid and the joint rotates about a single, fixed axis. In this case, limb dynamics is a consequence of Newton's second law and can be defined as the relation between the second derivative of the joint angular position and the torque acting about it. More complex formulations, that consider the movements in different planes, are required for movements other than pure single axis rotations [21, 22].

Articular dynamics: encompasses the viscoelastic properties of the joint surface, ligaments, and connective tissue. Torques produced by these mechanisms are likely small in the middle of the range of motion and become significant as the joint approaches the limits of its range of motion [23, 24].

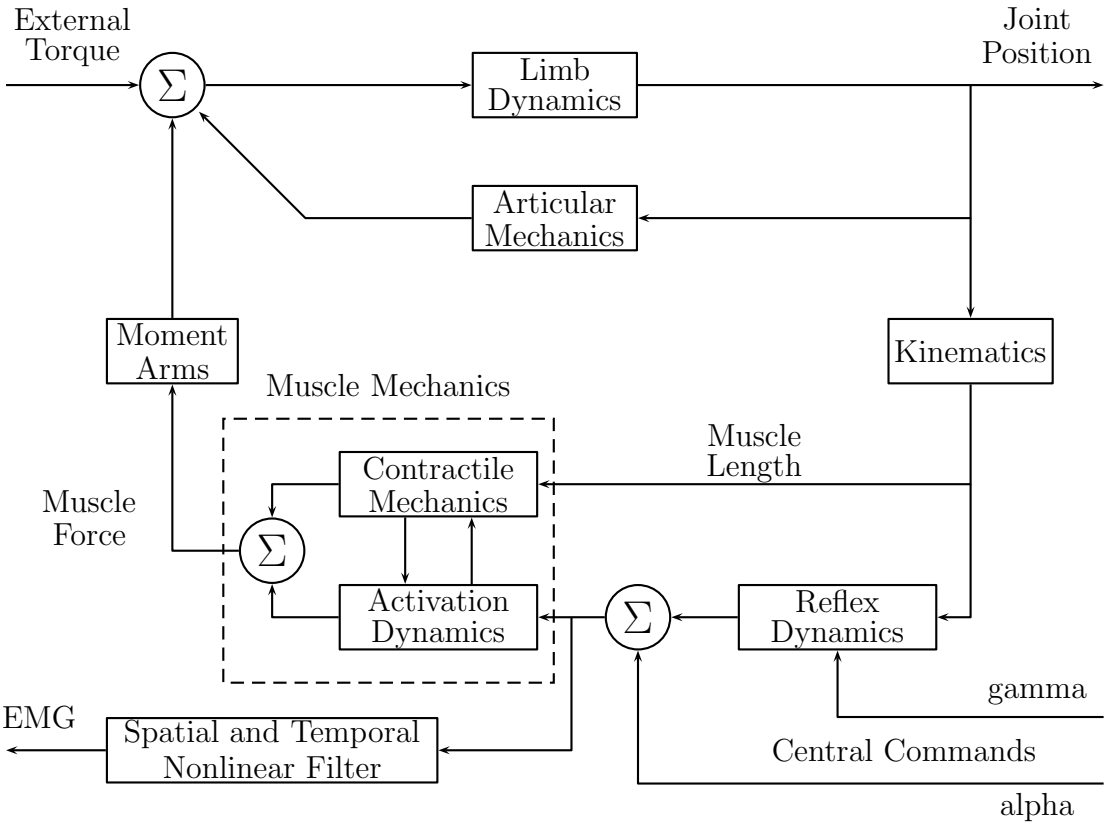

Figure 2–1: Information flow diagram of the peripheral neuromuscular system. Adapted from [1].

Intrinsic dynamics

It is represented by muscle mechanics in Figure 2–1. It arises from intrinsic properties of active muscle and consist of two components: contractile mechanics and activation dynamics.

Contractile Mechanics: determines the forces produced by the muscle in response to changes in length when the level of activation remains constant. These forces are a nonlinear function of the level of activation, the displacement amplitude, direction, velocity and several other factors [25].

Activation Dynamics: determines the forces produced by the muscle as a result of voluntary or reflex changes in the level of activation. Activation dynamics are complex because activation level changes results in changes in the number of active motor units (recruitment) and/or the firing rate of active motor units (rate coding). Activation dynamics have been measured indirectly in terms of the relation between the average electrical activity of the whole muscle (EMG signal) and the torque produced at the joint, this relation changes as a function of muscle length and the type of contraction [26].

Interactions: under physiological conditions muscle length and activation level often change together, and so interactions between the contractile mechanics and the activation dynamics will occur. However, the nature of these interactions is not fully understood. It has been suggested that contractile mechanics and activation dynamics can be treated as independent processes for small perturbations about an operating point, defined by the joint position and muscle activation level [1, 27]. However, this assumption is not valid in more general conditions involving large changes in joint position and/or activation level. Contractile mechanics change drastically with the level of activation, and it is likely that activation dynamics will change as a function of muscle length.

Reflex dynamics

Propioreceptive receptors are the source of reflex muscle activation most likely to influence joint dynamics. Muscle spindle receptors respond to changes in joint position (and its derivatives), and their dynamic response is under central control

via the gamma system. They have direct reflex connection to the muscles controlling the joint. Other reflex pathways might have an important role in determining the effect of reflexes in joint dynamics, in particular golgi tendon organs are very sensitive to muscle force. They have autogenetic, inhibitory connections to the motor neuron pool and may play and important role in determining the effects of reflexes in joint dynamics

Relation between muscle force and torque

The relation between muscle force and joint torque is determined by the muscles' lines of action and their moment arms. Several biomechanical models that predict joint torque from individual muscle forces have been described and validated [28, 29, 30]. However, the inverse problem, determining the force in the muscles about a joint from torque measurements is more difficult because generally there are more muscles than equations describing the joint motion, resulting in an overdetermined system of equations with infinite number of solutions [7]. Methods that rely on EMG recordings, muscle geometry, and/or the optimization of certain criterion to predict individual muscle forces have been used [31, 32, 33, 34]. However, is difficult to validate such prediction experimentally because measuring the individual muscle force in humans is challenging.

Relation between joint position and muscle length

Physiological studies of muscle and propioreceptor dynamics are often performed in terms of muscle length rather than joint position. Therefore, the transformation from muscle length to joint position must be known to understand the functional implication of these results. However, changes in overall muscle length arise from

the deformation of both muscle and tendons, which are connected in series, and their individual deformation is determined by their relative stiffness. Tendon has a nonlinear stress-stain relation and the mechanical properties of the muscle are complex [1]. Consequently, it is difficult to estimate the change in muscle length associated with a change in joint position.

Thus, joint dynamics arise from the interaction of different subsystems operating in a nested feedback structure and modulated by different factors. It is difficult to determine the characteristics of each subsystem independently because it is not possible to directly measure and manipulate their individual inputs and outputs. Joint position and torque are the only signals that can be readily measured and manipulated. Therefore, measuring dynamic joint stiffness can be seen as a classical system identification problem, where the system dynamics are estimated though the analysis of the relation between the input (position or torque) and the output (torque or position) records. However, accurate description of joint neuromechanical properties requires the decomposition of the overall joint dynamic stiffness in its components: passive, intrinsic and reflex dynamics. The methods commonly used for this task are discussed next.

2.2 Decomposition of Intrinsic and Reflex Mechanisms

One of the most challenging aspects of measuring dynamic joint stiffness is that the intrinsic and reflex components act and change together, so that is not possible to measure their mechanical consequences individually under normal conditions. Moreover, intrinsic and reflex components have different underlying mechanisms, intrinsic stiffness arises from the limb's inertia and the visco-elastic properties of the joint

surface, connective tissue and muscle; reflex stiffness is generated by stretch reflex mechanisms. Consequently, study each component individually, and understanding their roles during function, is fundamental to determine how the central nervous systems controls movement and posture. Furthermore, measuring the individual contributions of the intrinsic and reflex mechanisms to the overall joint dynamics might provide new means to characterize and diagnose neuromuscular diseases. For example, spastic patients have an altered reflex response to stimuli but their intrinsic response are not significantly different from normal subjects [17]; in contrast, in small children with cerebral palsy only the intrinsic component of joint dynamic stiffness was altered with respect to healthy, aged matched subjects [35].

Multiple experimental and analytical methods have been proposed to decompose the intrinsic and reflex mechanisms of dynamic joint stiffness. Among those, the most commonly used are: de-afferentation, reflex EMG and analytical methods. These are discussed in detail next.

2.2.1 De-afferentation methods

One approach to evaluate the contributions of intrinsic and reflex mechanisms to dynamic joint stiffness is to compare the mechanical responses to disturbances before and after eliminating reflexes. Differences between the responses are attributed to reflex contributions. De-afferentation techniques include removing the neural feedback using surgery [36, 37], or nerve block [38, 39, 40]. The reflex response has also been blocked by inducing ischemia using a pneumatic cuff fitted around the limb [41, 42, 43], or by applying high-frequency ($>$ 50Hz) vibrations to the tendon [44, 45].

A major concern with all de-afferentation techniques is that the operating point must be matched carefully before and after removing the reflex response to ensure that intrinsic mechanisms do not change. However, it is very difficult to match muscle activation levels between the two trials, as the stretch reflex plays an important part in voluntary activation of muscle [46]. Furthermore, it is not possible to ensure that only the stretch reflex mechanisms will be affected by the de-afferentation procedure. Likely, the motor control of the muscle is also affected [47].

Some groups have applied electrical stimulation to muscles in human subjects to activate the muscle and suppress reflex-mediated responses at the same time [48, 49, 50]. This technique encounters some problems. First, it cannot completely suppress the reflex response. Secondly, it can be painful and elicit spasm and co-contraction. Thirdly, the order of recruitment during electrical stimulation is different than that during normal voluntary contractions, so that different motor units will be active at the same level of force during voluntary and electrical activation [51]. Consequently, intrinsic mechanisms might differ and the contribution of reflex mechanisms to overall joint stiffness may be over- or under- estimated.

2.2.2 EMG methods

Stretch reflex activity has been studied often using EMG as the output measure [52, 53, 54, 55]. Kearney and Hunter identified the dynamic relation between velocity and reflex EMG in the triceps surae and tibialis anterior [56, 57]. They showed that the reflex gain was dependent on torque level and ankle position. Others have tried to characterize the mechanical properties of the joint using EMG signals. For example, Gottlieb and Agarwal defined the reflex compliance as the

ratio of the reflex EMG to velocity, and found that it increased linearly with level of voluntary contraction [58]. Stein and Kearney found similar results for the reflex EMG; however, the reflex gain increased less than linear with the level of voluntary contraction [59].

Although EMG studies have provided important information about reflex behavior, they do not necessarily reflect joint dynamics: the relation between EMG and joint torque is not fully understood, and therefore EMG signals cannot be used quantify the mechanical contribution of the stretch reflex mechanisms. Models relating EMG and torque have been proposed for isometric or isotonic conditions [60, 61, 26]. However, they cannot describe the EMG-force relation under general conditions. Furthermore, EMG is influenced by reflex response and other factors, such as voluntary activity [54], so that it is difficult to estimate the mechanical contribution of reflex activity using EMG only.

2.2.3 Analytical methods

A number of analytical methods involving random disturbances and system identification techniques have been developed to estimate the intrinsic and reflex mechanisms of dynamic joint stiffness. Kearney *et.al.* took advantage of the stretch reflex delay to separate the intrinsic and reflex stiffness from measurements of joint position and torque. In this method, a non-parametric, impulse response function (IRF) with a maximum memory of 40ms is estimated between joint position and torque using a correlation-based identification approach. Since there is no reflex response prior to 40ms from the onset of the perturbation, the model described only the intrinsic mechanisms. The position is then convolved with the identified IRF

to estimate the intrinsic torque. Reflex torque is then estimated by subtracting the intrinsic from the measured torque. Reflex stiffness is then found by estimating an IRF between half-wave rectified velocity and reflex torque, and this model is used to update the reflex torque. This process is repeated iteratively until further iterations fail to reduce the prediction error [12]. Despite its utility, this iterative approach may not converge to the true values and cannot be used with data acquired in closed-loop [62, 63].

Recently, I introduced a modification of this algorithm that used an *a priori* parametric model of intrinsic and reflex stiffness. The algorithm iteratively estimates the intrinsic and reflex components of dynamic joint stiffness using an instrumental variable approach [64, 65]. This method does not suffer from the convergence issues of the non-parametric approach and can be directly applied to data measured in closed-loop.

Zhao *et.al.*, considered an *a priori* parametric model of intrinsic and reflex stiffness and developed a non-iterative subspace approach for parameter estimation [63]. The main issue with this approach was that the second-order model used to describe the intrinsic stiffness could not capture the complex system dynamics. Jalaleddini *et.al.* extended the subspace approach to model the intrinsic stiffness with a non-parametric, IRF, successfully capturing the system dynamics [62]. The non-iterative approaches assume that the response of the intrinsic and reflex mechanism are independent; however, these mechanism might show complex, nonlinear interactions during function.

Zhang and Rymer modeled the joint stiffness as non-linear delay differential equation. They solved the differential equation using numerical integration. After performing the integration they carried out least-squares linear regression to estimate the parameter values. They compared the predictive capacity of their model to that of a simple second-order model that did not account for reflex responses and noted only a slight improvement. This result indicates that either their model was not correct or that reflex responses were too weak to be detected in their particular experimental conditions. [66].

Van der Helm *et.al.*, described a linear, closed-loop model to describe the intrinsic and reflex components of the human arm during postural control. The model parameters were estimated using a frequency domain technique that provided unbiased estimates for data acquired in closed-loop [47]. However, this technique is only valid for linear systems and therefore cannot be used when as the reflex response is nonlinear, as in the case of the ankle [59].

This thesis, develops and validates analytical methods to estimate the intrinsic and reflex components of joint dynamic stiffness. The approach has several advantages, including that is non-invasive, can decompose the intrinsic and reflex torques from its noisy measurement of joint position and torque, and does not use of EMG signals to quantify the mechanical consequences of the reflex mechanism.

2.3 Estimation of Dynamic Joint Stiffness

Before describing the analytical techniques used to estimate dynamic joint stiffness, it is important to clarify the different concepts and terminologies that are used in the literature.

Dynamic joint stiffness: refers to the dynamic relation between joint position and torque [12]; it includes: passive dynamics, intrinsic dynamics and reflex dynamics. The term joint impedance is often used as a synonym [67, 68, 69].

Joint compliance: Refers to the dynamic relation between joint torque and position, it is the inverse of dynamic stiffness [70], and sometimes is called joint admittance [71, 72].

Joint static stiffness: refers to the steady-state or DC component of intrinsic joint stiffness. It describes only the elastic properties of the joint, muscle and connective tissue, without characterizing the dynamic behavior of the joint [73].

Joint quasi-stiffness: is the instantaneous relation between joint position and torque when the joint position is changing significantly [73, 74]. Quasi-stiffness and static stiffness are equivalent during static conditions when there is no significant changes in joint position [75]. However, under TV conditions, when the joint is moving, they differ greatly as the joint quasi-stiffness is influenced by the joint biomechanical properties, movement speed, acceleration, and jerk [73].

A complete characterization of the neuromechanical properties of a joint requires the description of the static and dynamic properties of this neuromuscular systems. Consequently, this thesis focus of the developments of methods to describe dynamic joint stiffness and compliance. This rest of this section provides a critical review on the methods that have been used to estimate dynamic joint stiffness in a variety of tasks and comments on their strengths and weaknesses.

2.3.1 Dynamic stiffness

Quasi-stationary methods

Linear techniques have been used to characterize dynamic joint stiffness, under the assumption that stiffness dynamics are linear and time-invariant under stationary conditions.

Brown et al. [76] applied sinusoidal position inputs and used Nyquist analyses to study thumb stiffness. They calculated the viscosity and elasticity at each frequency and plotted viscosity versus elasticity as a Nyquist diagram of angular stiffness. This diagram was a function of frequency where the vector sum of the elastic and viscous components was the intrinsic dynamic stiffness. Similar techniques were applied at the elbow [77], and ankle [78]. One problem with this technique is that Fourier analyses is used to extract the components of the output at the same frequency as the input and all other components are discarded. However, joint dynamic stiffness is nonlinear, so that the output will have significant power in frequencies different from those of the input, and by ignoring the additional frequencies is possible to obtain only a linear approximation of a non-linear model [59].

Another analytical approach uses the amplitude and phase of the response to sinusoidal input to estimate the frequency response [70, 79]. The gain is the ratio of output to input amplitude and the phase is the difference between the output and input phases. One disadvantage of this approach is that the experiment must be repeated at many different frequencies. Thus, experiments will be lengthy. Furthermore, sinusoidal stimuli are predictable and so subjects may generate an undesirable,

periodic, voluntary response at the same frequency of the stimulus. Additionally, this technique is best suited for linear systems.

The use of stochastic stimuli can overcome the disadvantages of sinusoidal stimuli since stochastic signals can have power over a wide range of frequencies, which evoke an output response with the full range of frequencies required to characterize joint dynamics in a single experimental trial. In addition, stochastic perturbations cannot be predicted by the subject, so the voluntary contributions to the output will be reduced.

Broad-band, random, position perturbations have been used as input to characterize the intrinsic component of joint dynamic stiffness [23, 52, 80, 81]. However, high-frequency position vibrations inhibit stretch reflexes because of their high mean velocities [1], so that this type of position perturbations cannot be used to estimate the reflex component of dynamic joint stiffness. On the other hand, broad-band, random, torque perturbations have been used to characterize the intrinsic [1, 22, 69, 82, 83], and reflex [47, 84, 85, 86] components of ankle, forearm, and elbow compliance. However, these methods wrongly assume that the reflex component of joint compliance is linear.

Some studies have used *a priori*, parametric, nonlinear models to describe reflex stiffness. By using nonlinear optimization to estimate the model parameters [87, 88, 89]. However, the usefulness of the parameter estimates depends on the validity of the selected model, if the model is incorrect then its parameters will have no physical meaning [90].

Kearney *et.al.,* developed nonlinear, non-parametric techniques to estimate the intrinsic and reflex components of joint dynamic stiffness. These methods use pseudo-random, binary sequence (PRBS) as input perturbations; as these signals do not inhibit the stretch reflex response because of their low mean velocity. They also developed a non-parametric, parallel-cascade model structure that models the intrinsic and reflex mechanical responses to small, random position perturbations by a parallel combination of linear and nonlinear systems. Figure 2–2 presents this parallel-cascade model structure, intrinsic stiffness is represented by a non-parametric, linear, dynamical system, while reflex stiffness is represented by a block-oriented, nonlinear pathway comprised of a series combination of a differentiator, a static nonlinearity and a non-parametric, linear, dynamical system. They used an iterative, correlation-based, identification algorithm for the estimation of the two parallel pathways using joint position and total torque signals [12].

This model and associated identification algorithms, has been used to characterize the intrinsic and reflex components of dynamic stiffness in the ankle, trunk and wrist joints in both normal and pathological subjects during quasi-stationary experiments [12, 17, 62, 63, 64, 91, 92, 93, 94, 95, 96, 97, 98, 99, 100]. Results show that in spinal cord injured and stroke patients there is significant increase in reflex gain compared to that of aged matched controls [17, 91]. Moreover, the parallel-cascade model has been used to characterize the modulation of the intrinsic and reflex components of ankle dynamic stiffness as a function of joint position and torque in healthy subjects [11]. Intrinsic and reflex gain increase when the ankle is moved from a neutral position towards dorsiflexion and decreased when moved towards plantarflexion.

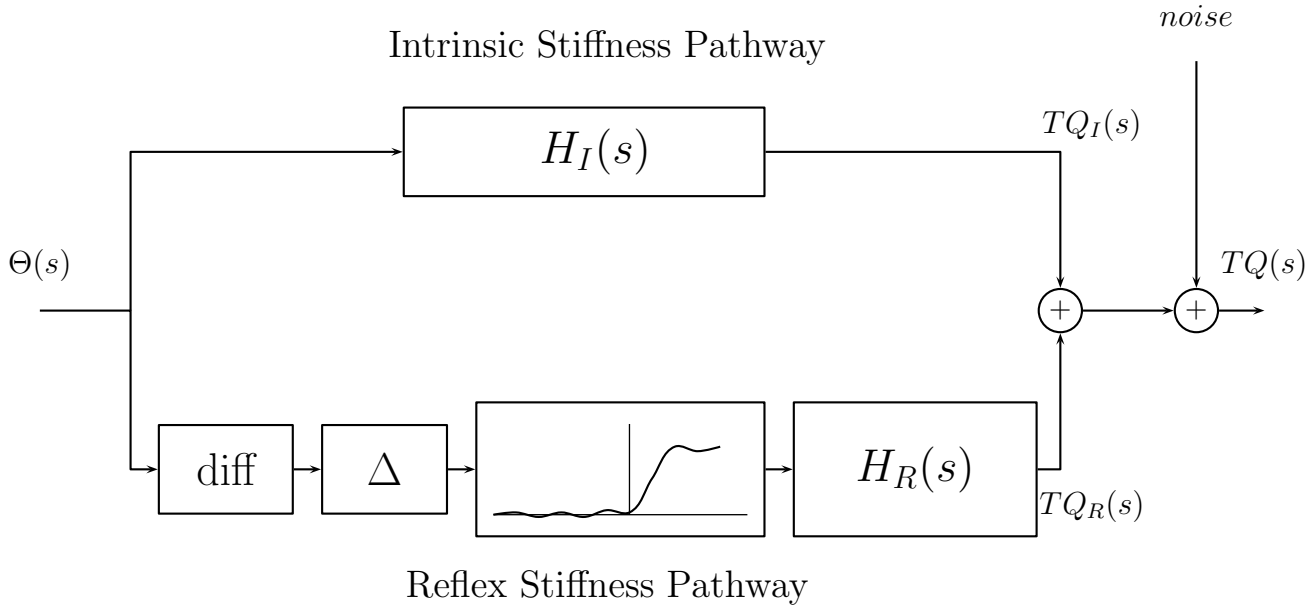

Figure 2–2: Overall representation of joint dynamics with two parallel pathways representing the intrinsic and reflex contributions. $\Theta(s)$, $TQ_I(s)$, $TQ_R(s)$ and $TQ(s)$ are the Laplace transform of the joint position, intrinsic, reflex and total torque respectively.

Intrinsic gain increased steadily with voluntary torque, whereas reflex gain showed an initial increment and the decreased as the voluntary torque increased.

One drawback of the non-parametric approach is that it is difficult to relate the model parameters to physiological meaningful variables. Intrinsic gain, or joint elasticity, can be obtained directly from the estimated non-parametric, intrinsic model by simple integration. However, extracting other physiologically relevant parameters, such as joint viscosity, or reflex gain and natural frequency requires non-linear optimization methods [92, 62]. These methods are not guarantee to converge to the

true values, and if a good initial estimate is not provided they it will often fail to converge [101].

Our laboratory has also proposed several parametric models to describe the intrinsic and reflex components of dynamic joint stiffness. These include autoregressive [102, 103], state-space [62, 63, 104], and transfer function models [64, 65]. The autoregressive model of Kukreja *et.al*, represents the linear dynamics in the intrinsic and reflex components with second order, discrete-time, autoregressive, moving-average models with exogenous inputs, and approximates the reflex nonlinearity with a second-order polynomial [102]. The authors claim that the estimated parameters can be easily related to physiologically relevant variable; however, simulations showed that the model estimates were biased when noise was added to the output so that the true model parameters cannot be retrieved.

A recent survey found that both state-space and transfer function based approaches provide superior results than the non-parametric approach. Likely due to the significantly reduction in the number of free-parameters, and the ability of both methods to handle complex, non-white, biological noise. Both approaches provided similar results; however, the transfer function model for dynamic joint stiffness has significantly fewer free-parameters than the state-space model, and its estimated parameters can be directly linked with physiologically relevant parameters [105].

Time-varying methods

Several studies have characterized intrinsic dynamic stiffness during time-varying conditions ignoring stretch reflex contributions [106, 107, 108, 109, 110]. We have introduced methods to estimate intrinsic and stretch reflex mechanisms using the

parallel-cascade model structure during time-varying conditions; however, these methods require very large data sets for parameter estimation, which severely limits their application [103, 111, 112, 113]. These studies have demonstrated that the values obtained during quasi-stationary experiments are significantly larger than those observed during time-varying conditions at matched operating points; consequently, time-varying methods are required to characterize joint dynamics during function.

Linear, time-varying techniques have been developed to characterize intrinsic stiffness during time-varying conditions. These methods usually employ an ensemble identification approach for parameter estimation, which requires many input-output trials showing the same time-varying behavior [108]. Using this methodology, studies have estimated the time-varying, intrinsic dynamics during imposed [107, 108, 114], and voluntary movements [106, 110, 109, 115].

When the changes in the time-varying, model parameters are fast and large, ensemble identification algorithms require hundreds (and sometime thousands) of input-output realization showing the same time-varying behavior for estimation of the parameters' time-course. Obtaining these hundreds of input-output trials presenting the same underlying time-varying behavior is challenging as it requires long, fatigue inducing experiments.

Another approach is to use adaptive methods for estimation of ankle dynamics stiffness to produce on-line estimates of intrinsic and reflex torque [116, 117]. However, these methods are limited to a particular type of input and the identification algorithm only provides a coarse estimate of the parameters' time-course.

Linear-parameter-varying methods

A limitation of time-varying methods is that models are identified for a particular trajectory of the operating point and cannot be used to predict the joint torque for a new trajectory. Therefore, it is necessary to create a new time-varying model for each trajectory of the operating point.

An alternative to time-varying models, is to assume that the model parameters are modulated by a measurable or estimable signal called scheduling variable. Such linear-parameter-varying (LPV) Models relate the changes in the model parameters with an underlying modulating signal, the scheduling variable. LPV methods have been recently used to estimate intrinsic stiffness in trials when only joint torque [118] or joint position changed [119] so that the scheduling variable was easily defined.

The advantage of the LPV approach over time-varying methods is that is possible to obtain accurate estimates of the system dynamics for all possible trajectories of the operating point from a single trial, provided that the scheduling variable has a rich enough amplitude distribution. This facilitates physiological interpretation by explicitly describing the relationship between stiffness parameters and the scheduling variable. Moreover, it provides models that can predict torques for novel operating point trajectories. The main drawback of this approach is that the scheduling variable and its relation to the model parameters must be defined *a priori*. This task has been achieved for simple experiments where only the joint position or torque changes. However, under general conditions this task is non-trivial and sometimes impossible. For example, Ludvig and Perreault reported that a proper choice of scheduling variable was not found in estimating the knee stiffness in a position varying task [120].

To summarize, estimation of joint dynamic stiffness is an important and challenging problem. Joint dynamics are nonlinear and the model parameters are heavily modulated during function. During static conditions, where the operating point does not change significantly, non-parametric and parametric, nonlinear models have been successfully used to describe intrinsic and reflex stiffness. However, during function, where there are large changes in the trajectory of the operating point, results have been limited to describe the time-varying intrinsic dynamics, ignoring the complex, nonlinear, reflex mechanisms.

2.4 Modulation of Dynamic Joint Stiffness

Ankle dynamic stiffness is heavily modulated by different factors, including joint trajectory, voluntary torque, and functional task. Next I will discuss the different factors known to influence dynamic joint stiffness.

2.4.1 Modulation with operating point

Quasi-stationary results

Quasi-stationary results have shown that both intrinsic and reflex dynamic stiffness are strongly modulated by joint position and torque. Weiss *et.al.* studied how intrinsic ankle stiffness changed with joint position and found that the joint viscosity and elasticity increased when the ankle was moved from a neutral position toward dorsiflexion or plantarflexion [52]. They also found that the reflex EMG increased significantly when the ankle was moved toward plantarflexion and decreased when moved towards dorsiflexion [121]. Mirbagheri *et.al.* studied the modulation of intrinsic and reflex components of dynamic ankle stiffness with joint position on healthy [11], and spinal cord injured subjects [17]. The gain of intrinsic and reflex

pathway increased when the ankle was moved from dorsiflexion towards plantarflexion. Jaleleddini *et.al.* studied the modulation of the reflex, static-nonlinearity as a function of ankle position. They found that the threshold of reflex, static-nonlinearity decreases when moving from dorsiflexion towards plantarflexion whereas the slope, or reflex gain, increased [62]. Furthermore, MacKay *et al.* found that the elbow elasticity increased with elbow flexion [122].

Multiple studies have shown that intrinsic joint stiffness is at a minimum at rest and increases steadily with joint torque [11, 66, 23, 80, 123]. Mirbagheri *et.al.* studied the modulation of reflex ankle stiffness with voluntary torque during stationary experiments [11]. Reflex gain increased when the subjects exerted a small level of torque and then decreased when further torque was produced. Schouten *et.al.* found similar results for the arm [86].

Time-varying results

The modulation of dynamic joint stiffness have also been studied during imposed movements that included large changes in the joint trajectory using linear, time-varying identification techniques. Kirsch *et.al* demonstrated that the ankle elasticity changed significantly when there is a transient change in joint position [107], they found that stationary results were consistent with the joint elasticity and viscosity found before and after the movement but the values observed during the movement were not attainable in stationary experiment with matched positions. Others found that joint dynamics stiffness decreased, compared with stationary results, during movement initiation at the wrist [89], elbow [72] and knee [124].

Modulation of dynamic joint stiffness during voluntary movements have also been studied using linear, time-varying identification techniques. Bennett *et al.* estimated the elbow intrinsic stiffness during cyclic movements and found that the elasticity and viscosity were much lower than those during posture experiments [106]. Recent studies of ankle intrinsic stiffness during the gait cycle, showed that the ankle elasticity and viscosity increased during the stance phase of walking and decreased before the beginning of the swing phase [34, 109, 110, 125].

2.4.2 Task dependency

Stretch reflex gain has been shown to change during function and to depend on the instructions given to the subject. EMG reflex response are smaller when the subject is asked to maintain a constant force than when instructed to maintain a constant position [126]. This might be linked to the fact that during constant force experiments, the reflex response from muscle spindle activation results in undesired force changes which do not contribute to the task [47].

Capaday and Stein showed that EMG reflex gain was heavily modulated throughout the gait cycle; the reflex response was largest for walking and smaller during running [127, 128]. They suggested that this adaptation of the reflex response is dependent on joint position and torque, and is influenced by central mechanisms.

2.4.3 Additional dependencies

In addition, stochastic perturbations to the ankle decrease the EMG reflex response to a sudden stretch in proportion to the main absolute velocity [59]. Static stretches decrease joint intrinsic stiffness [129]. Finally, joint dynamic stiffness depends on muscle history and is affected by fatigue [130].

To summarize, dynamic joint stiffness is a complex and highly nonlinear system. An approach to deal with these nonlinear dependencies is to assume that the system is time-varying. In this way, is possible to estimate time-varying models that describe the system behavior for a particular trajectory of the modulation signals. Another approach is to explicitly relate the joint dynamics with each of the modulation signals (*e.g.* joint position, joint velocity, muscle activation level) and find a global, nonlinear model of joint dynamics stiffness able to predict the intrinsic and reflex torque in all possible conditions. However, this is impossible to do during function as the joint dynamics is modulated by a variety factors many of which are not measurable, not completely understood or simply not known.

2.5 Thesis Rationale

Considerable work has been done in the characterization of joint biomechanics during stationary conditions. These experiments have demonstrated that the joint dynamic stiffness is modulated by multiple factors, including changes in joint position and torque. However, quasi-stationary estimates cannot be interpolated to describe the dynamic joint stiffness during time-varying conditions; the joint elasticity and viscocity measured during posture is significantly larger than those observed during movement.

The limited number of studies that have examined dynamic joint stiffness during time-varying conditions used an ensemble-based algorithm for parameter estimation. This approach requires hundreds of input-output trials having the same time-varying behavior, which is very difficult to achieve experimentally and requires long, fatigue

inducing experiments. Moreover, these studies focused only in the intrinsic component of joint dynamic stiffness, ignoring completely the complex, nonlinear reflex mechanisms. Other alternatives, such as LPV methods, that can characterize the system from one single trial, require significant *a priori* information that is often not available.

The objective of this thesis is to develop and validates novel time-varying, identification algorithms able to characterize joint dynamics stiffness during function. The novel methodology will make use of a time-varying, parallel-cascade structure to describe the intrinsic and reflex components of dynamic stiffness. The novel, time-varying identification algorithms will estimate the linear and nonlinear components of the parallel-cascade model of joint dynamic stiffness using significantly less data than ensemble approaches.

CHAPTER 3
Review of Relevant System Identification Methods

This chapter reviews the system identification approaches that are the basis of the novel algorithms developed in this thesis.

There are two main approaches to the modeling of biomedical systems: *A priori* and data-driven or black-box models. A priori models are based on first principles, knowledge of the system structure, and the function of each subsystem. This information is combined to describe the behavior of the system. Normally, each parameter in the model corresponds to a physiologically relevant component and so analysis of *a priori* models can provide physiologically relevant information [131].

A priori models typically includes a large set of parameters that must be adjusted to provide a desired behavior or estimated directly from data. This is a daunting task for systems that include nonlinear relations between variables, as it commonly occurs in biomedical systems. In addition, the data records are contaminated by noise which increases the uncertainty in the parameter estimates [131].

In contrast, data-driven models make few assumptions about the system. The system is described a black-box that mimics the behavior of the physiological system. This class of system is useful to describe the relation between input and outputs but it can be difficult to assign a physiological interpretation to the model parameters [132, 133].

A common use for system identification is to determine a model to predict the plant's response to design a controller that will produce a desired output [134]. In this context it is beneficial to have the simplest possible model that can describe the system dynamics, and accurately predict the plant's response. In this application, the estimated model parameters provide no direct information about the system properties.

Another application of system identification is to gain insight into the characteristics of a system. In this case, the input/output data is used to extract information about the characteristics of the systems. For such application, models do not necessarily need to be simple. Rather, they should reflect the current knowledge of the system structure so that estimating its parameters will provide information about the system properties [132, 133].

The system identification problem may be understood with the aid Fig. 3–1, which is based on that given in M. Verhaegen and P. Dewilde [2]. The *system* consists in everything inside the dotted box; it is composed of a deterministic and a stochastic component. The stochastic part of the system is driven by a white-noise sequence $e_2(t)$, which cannot be measured. The deterministic component or *plant* is driven by a controlled input $u(t)$ combined with the filtered version of a non-measurable white-noise process $e_1(t)$. In addition, it is assumed that the controlled input is not directly accessible, rather, only a noise corrupted version of it, $\widehat{u}(t)$, can be measured.

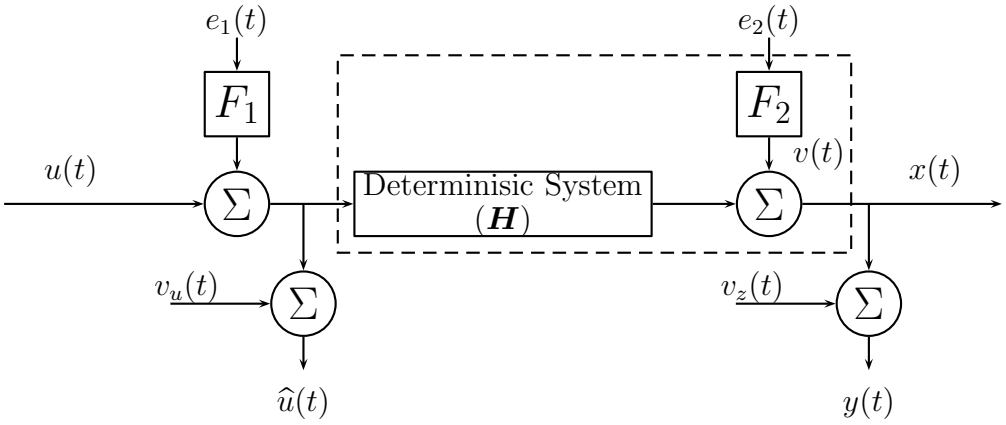

Figure 3–1: Block diagram representing the system identification problem. Adapted from [2].

The noise-free output, $x(t)$, is the sum of outputs from the deterministic and stochastic components. However, only $y(t)$, a noise corrupted version of output signal, can be measured.

Given this general structure, several different problems can be described:

- Identification of the deterministic system or plant. The objective is to determine the relation between the input and output $u(t)$ and $x(t)$, assuming that the stochastic components $e_2(t)$ is zero. In general, both input and output may be corrupted by noise. However, it is usually assumed that the input noise, $v_u(t)$, is negligible. This is the problem that will be addressed for the rest of this thesis.
- Identification of the noise process, F_2. In this case, the objective is to find the relation between $e_2(t)$ and $x(t)$, given that only the measured output, $y(t)$ is available. Usually the controlled input, $u(t)$ is assumed to be constant or

periodic. This identification problem is of interest for situations where the controlled input cannot be measured or it not known.

- Identification of the complete system. The objective is to use the input and output signals to determine the stochastic and deterministic component of the systems, in addition, the characteristics of $e_2(t)$ should also be estimated. This problem formulation is of interest when input and output signals are influenced by noise, as in the case of closed-loop identification.

3.1 Linear systems

A linear system obeys two properties: superposition and scaling. Thus, if H is a linear system, $u_1(t)$ and $u_2(t)$ are two input signals, $y_1(t)$ and $y_2(t)$ are two output signals, k is a constant, and

$$y_1(t) = H\left(u_1(t)\right),$$
$$y_2(t) = H\left(u_2(t)\right),$$

then

$$H\left(ku_1(t) + ku_2(t)\right) = k\left[y_1(t) + y_2(t)\right].$$

3.1.1 Models of linear systems

Parametric models: A continuous-time parametric model of a linear system consist of a differential equation relating the input(s) and output(s) of the systems

and describing its dynamics. In discrete-time, this representation may be approximated by a difference equation. This procedure involves the approximation of the differential operator (s) by means of a numerical approximation. This is commonly achieved using the bilinear transformation [135].

In discrete-time, the relation between input and output can be expressed in terms of a linear difference equation as [136]:

$$\begin{aligned} y(t_k) + a_1 y(t_k - 1) + \cdots + a_{n_a} x(t_k - n_a) = \\ b_0 u(t_k) + \cdots + b_{n_b} u(t_k - n_b) + \\ e(t_k) + c_1 e(t_k - 1) \cdots + c_{n_c} e(t_k - n_c), \end{aligned}$$

or more compactly as

$$A(q^{-1})y(t_k) = B(q^{-1})u(t_k) + C(q^{-1})e(t_k), \tag{3.1}$$

where $A(q^{-1}) = 1 + a_1 q^{-1} + \cdots + a_{n_a} q^{-n_a}$, and q^{-1} is the backward shift operator. This is an auto-regressive, moving average exogenous (ARMAX) model, the current output depends on an exogenous input, $u(t_k)$, that is usually known, and an innovation process, $e(t_k)$, that is usually unknown, and past values of the output. For the model in Fig. 3–1, the fraction $B(q^{-1})/A(q^{-1})$ corresponds to the deterministic model H, whereas the fraction $C(q^{-1})/A(q^{-1})$ corresponds to the stochastic model F_2. This model has several special cases:

Auto-regressive (AR) model

$$A(q^{-1})y(t_k) = e(t_k),$$

the current output depends on the current disturbance ($e(t_k)$) and past output values.

Moving-Average (MA) model

$$A(q^{-1})y(t_k) = C(q^{-1})e(t_k),$$

the current output depends on current and past values of the disturbance ($e(t_k)$) and past output values.

Auto-regresive, exogenous input (ARX)

$$A(q^{-1})y(t_k) = B(q^{-1})u(t_k) + e(t_k),$$

the current output depends on the current value of the disturbance ($e(t_k)$), the current and past values of the exogenous input ($u(t_k)$) and past output values.

Finite Impulse Response (FIR)

$$y(t_k) = B(q^{-1})u(t_k) + e(t_k),$$

the current output only depends on the current value of the disturbance ($e(t_k)$), and the current and past values of the exogenous input ($u(t_k)$). This model structure is a *non-parametric model* and due to its simplicity is commonly used to model biomedical systems. Fast, and accurate algorithms have been developed for parameter estimation [133].

It can be noticed that in all these model structures (except for the FIR model) assume that the fraction representing the deterministic and stochastic models

share the same denominator ($A(q^{-1})$); this is a strong assumption that is often not valid [137]. A generalization of these model structures is to assume that the deterministic and stochastic models have different numerators and denominators; this gives the **Box-Jenkins model** [136, 138]:

$$y(t_k) = \frac{B(q^{-1})}{A(q^{-1})}u(t_k) + \frac{C(q^{-1})}{D(q^{-1})}e(t_k). \tag{3.2}$$

For the model in Fig. 3–1, the fraction $B(q^{-1})/A(q^{-1})$ corresponds to the deterministic model H, whereas the fraction $C(q^{-1})/D(q^{-1})$ corresponds to the stochastic model F_2. The Box-Jenkins model structure contains all the other structures as special cases and therefore the methods used to estimate its parameters can be adapted to identify the other model structures. An important characteristic of the Box-Jenkins structure is the independent characterization of the deterministic and stochastic components of the model, that is, the linear system that processes the exogenous input does not share the same dynamics as the linear system that processes the random disturbances. It will be made clear through this thesis, that this independent parametrization of the deterministic and stochastic components make this model particularly useful for describing biomedical systems, including dynamic joint stiffness.

A key property of the Box-Jenkins model, that results from the independent parametrization of the deterministic and stochastic components, is that the estimates of the process ($B(q^{-1})/A(q^{-1})$) and noise ($C(q^{-1})/D(q^{-1})$) plants are asymptotically independent [139, 65]. In consequence, when the noise model is not of interest or its structure is unknown, the noise can be treated as white,

i.e. $C(q^{-1}) = D(q^{-1}) = 1$, and the estimates of the process plant will still be unbiased. This result does not hold for any other parametric model structure.

State Space models: An alternative structure is a state space model. In the discrete case, the system is represented by the set of equations

$$x(t_k + 1) = \boldsymbol{A}x(t_k) + \boldsymbol{B}u(t_k),$$
$$y(t_k) = \boldsymbol{C}x(t_k) + \boldsymbol{D}u(t_k),$$

where $u(t_k)$, $y(t_k)$ and $x(t_k)$ are the system's input, output and states. And $\boldsymbol{A}$, $\boldsymbol{B}$, $\boldsymbol{C}$ and $\boldsymbol{D}$ are matrices that describe the system dynamics. There are methods for estimating these matrices directly from input-output data [140]. However, these methods estimate the system matrices within a similarity transformation, making it difficult to relate the estimated model to the parameters of the original differential equation.

Methods for estimating dynamic joint stiffness using non-parametric [12], state-space [63, 62], and Box-Jenkins models [64] have been previously developed. A recent survey found that the state-space and Box-Jenkins based approaches provide better estimates than the non-parametric approach. This because they had many fewer free-parameters [105]. Both parametric approaches provided similar estimates; however, the Box-Jenkins model for dynamic joint stiffness has fewer free-parameters than the state-space model. This is important for the modeling of time-varying systems, where each model parameter must be estimated at each point in time. For this reason, this thesis will focus in the parametric identification of Box-Jenkins and FIR model structures.

3.1.2 Identification of linear systems

The study of linear systems has a rich history; many methods and algorithms have been developed to identify them, and linear identification methods have served as the kernels for the developments of tools for the analysis of more complex systems. Therefore, it is important to review the basics of linear systems identification.

The simplest linear statistical model is a linear combination of input variables:

$$x(t) = \omega_0 + \omega_1\phi_1(t) + \cdots + \omega_D\phi_D(t), \tag{3.3}$$

where $\phi_j(t)$ are, possibly nonlinear, functions of input ($u(t)$) and output ($x(t)$) variables.

For example, this model structure is general and can be used to represent continuous-time, differential equations:

$$\frac{dx^2(t)}{dt^2} + a_1\frac{dx(t)}{dt} + a_2x(t) = b_2\frac{du(t)}{dt} + b_1u(t) + b_0,$$

by using the notation of (3.3) and setting

$$\phi_0(t) = 1, \quad \phi_1(t) = u(t), \quad \phi_2(t) = \frac{du(t)}{dt}, \quad \phi_3(t) = \frac{dy(t)}{dt}, \quad \phi_4(t) = \frac{dy^2(t)}{dt^2},$$

and

$$\omega_0 = \frac{b_0}{a_2}, \quad \omega_1 = \frac{b_1}{a_2}, \quad \omega_2 = \frac{b_2}{a_2}, \quad \omega_3 = -\frac{a_1}{a_2}, \quad \omega_4 = -\frac{1}{a_2}.$$

The discrete-time, difference equation

$$x(t_k) + a_1x(t_k - 1) + \cdots + a_{n_a}x(t_k - n_a) = b_0u(t_k) + \cdots + b_{n_b}u(t_k - n_b),$$

can be re-parametrized similarly.

Using vector notation, (3.3) can be expressed as

$$x(t_k) = \boldsymbol{\omega}^T \boldsymbol{\phi}, \tag{3.4}$$

where

$$\boldsymbol{\omega} = [w_0, \cdots, w_D]^T,$$
$$\boldsymbol{\phi}(t) = [\phi_0(t_k), \cdots, \phi_D(t_k)],$$

where $\phi_0(t_k) = 1, \ \forall t$.

The system represented by the models (3.3) and (3.4) are not linear systems as they do not satisfy the superposition and/or scaling properties. Rather, these models are linear in the parameters [101] and are important in system identification as there are efficient algorithms to estimate its parameters from input and output data. However, the model (3.4) represents an ideal situation where neither the input nor output are contaminated by noise. For this thesis, the input noise will not be considered, however, the output noise cannot be ignored and its properties will play a major role in the selection of parameter estimation algorithms. Therefore, the models to be studied in this thesis have the form:

$$y(t_k) = x(t_k) + v(t_k) = \boldsymbol{\omega}^T \boldsymbol{\phi}(t) + v(t), \tag{3.5}$$

as shown in Fig. 3–1, $v(t)$ is a zero-mean, non-i.i.d, unmeasurable signal that is independent of the controlled input $u(t)$.

In the context of Box-Jenkins model structure, the following relations hold:

$$x(t_k) = \frac{B(q^{-1})}{A(q^{-1})}u(t_k),$$
$$v(t_k) = \frac{C(q^{-1})}{D(q^{-1})}e(t_k).$$

The Box-Jenkins model structure is a general linear model which contains all other parametric models as special cases. Consequently, the model of (3.5) is also a general representation of linear systems.

Next I will discuss different approaches for the identification of linear systems models of the form (3.5):

Ordinary least-squares approach: The objective of the least-squares approach is to find the parameter set $\boldsymbol{\omega}$ that minimizes the sum of square errors between the measured, sampled data and the output of the model, that is

$$E(\boldsymbol{\omega}) = \frac{1}{2}\sum_{t_k=1}^{N}\left[y(t_k) - \boldsymbol{\omega}^T\boldsymbol{\phi}(t_k)\right]^2, \tag{3.6}$$

where N is the number of samples and the $1/2$ is added for mathematical convenience. Differentiating (3.6) with respect to $\boldsymbol{\omega}$, equating to zero and solving for $\boldsymbol{\omega}$ yields

$$\widehat{\boldsymbol{\omega}} = \left(\boldsymbol{\Phi}^T\boldsymbol{\Phi}\right)^{-1}\boldsymbol{\Phi}^T\boldsymbol{y}, \tag{3.7}$$

where

$$\boldsymbol{y} = \left[y(1), \cdots, y(N)\right]^T,$$

and

$$\mathbf{\Phi} = \begin{bmatrix} \phi_0(1) & \phi_1(1) & \cdots & \phi_D(1) \\ \phi_0(2) & \phi_1(2) & \cdots & \phi_D(2) \\ \vdots & \vdots & \ddots & \vdots \\ \phi_0(N) & \phi_1(N) & \cdots & \phi_D(N) \end{bmatrix}$$

Next I will discuss the convergence properties of the Ordinary Least Squares estimator for the different model structures:

Convergence

The convergence of the least-squares estimates can be studied by asking what happens as the number of data points goes to infinity. If $\boldsymbol{\omega}^*$ are the true parameters values then

$$\begin{aligned} \widehat{\boldsymbol{\omega}} - \boldsymbol{\omega}^* &= \left(\mathbf{\Phi}^T\mathbf{\Phi}\right)^{-1}\mathbf{\Phi}^T\boldsymbol{y} - \boldsymbol{\omega}^*, \\ &= \left(\mathbf{\Phi}^T\mathbf{\Phi}\right)^{-1}\mathbf{\Phi}^T\boldsymbol{y} - \left(\mathbf{\Phi}^T\mathbf{\Phi}\right)^{-1}\left(\mathbf{\Phi}^T\mathbf{\Phi}\right)\boldsymbol{\omega}^* \\ &= \left(\mathbf{\Phi}^T\mathbf{\Phi}\right)^{-1}\left(\mathbf{\Phi}^T\left(\boldsymbol{y} - \mathbf{\Phi}\boldsymbol{\omega}^*\right)\right) \\ &= \left(\mathbf{\Phi}^T\mathbf{\Phi}\right)^{-1}\left(\mathbf{\Phi}^T\left(\boldsymbol{y} - \left[\boldsymbol{y} - \mathbf{\Phi}^T\boldsymbol{v}\right]\right)\right) \\ &= \left(\mathbf{\Phi}^T\mathbf{\Phi}\right)^{-1}\left(\mathbf{\Phi}^T\boldsymbol{v}\right). \end{aligned}$$

It is necessary to distinguish between two of models structure:

- Non-parametric models (FIR filters):

  The output is a function of an external variable, $u(t_k)$, the controlled

input, that is, $A(q^{-1}) = 1$. Consequently, the matrix $\mathbf{\Phi}$ is

$$\mathbf{\Phi} = \begin{bmatrix} u(1) & u(0) & \cdots & u(1-m) \\ u(2) & u(1) & \cdots & u(2-m) \\ \vdots & \vdots & \ddots & \vdots \\ u(N) & u(N-1) & \cdots & u(N-m) \end{bmatrix}$$

As $u(t_k)$ and $v(t_k)$ are independent, and $v(t_k)$ is zero mean, then

$$\widehat{\boldsymbol{\omega}} - \boldsymbol{\omega}^* = \left(\mathbf{\Phi}^T \mathbf{\Phi}\right)^{-1} (\mathbf{0}),$$

$$\widehat{\boldsymbol{\omega}} - \boldsymbol{\omega}^* = 0.$$

Thus, estimates of the FIR parameters given by the least-squares approach are unbiased provided the noise sequence $v(t_k)$ is zero-mean.

- Parametric models:

  For these models, the output is a function of the controlled input, $u(t_k)$ and past output values, that is

  $$A(q^{-1}) = 1 + a_1 q^{-1} + \cdots a_{n_a} q^{-n_a}.$$

  Consequently, $\mathbf{\Phi}$ is

  $$\mathbf{\Phi} = \begin{bmatrix} y(1) & \cdots & y(1-n) & u(1) & \cdots & u(1-m) \\ y(2) & \cdots & y(2-n) & u(2) & \cdots & u(2-m) \\ \vdots & \ddots & \vdots & \vdots & \ddots & \vdots \\ y(N) & \cdots & y(N-n) & u(N) & \cdots & u(N-m) \end{bmatrix}$$

or

$$\boldsymbol{\Phi} = \begin{bmatrix} x(1) & \cdots & x(1-n) & u(1) & \cdots & u(1-m) \\ x(2) & \cdots & x(2-n) & u(2) & \cdots & u(2-m) \\ \vdots & \ddots & \vdots & \vdots & \ddots & \vdots \\ x(N) & \cdots & x(N-n) & u(N) & \cdots & u(N-m) \end{bmatrix} + \begin{bmatrix} v(1) & \cdots & v(1-n) & 0 & \cdots & 0 \\ v(2) & \cdots & v(2-n) & 0 & \cdots & 0 \\ \vdots & \ddots & \vdots & \vdots & \ddots & \vdots \\ v(N) & \cdots & v(N-n) & 0 & \cdots & 0 \end{bmatrix}$$

$$= \boldsymbol{\Phi}_{xu} + \boldsymbol{\Phi}_{v0}$$

As $u(t_k)$ and $x(t_k)$ are independent of $v(t_k)$ then

$$\widehat{\boldsymbol{\omega}} - \boldsymbol{\omega}^* = \left(\boldsymbol{\Phi}^T\boldsymbol{\Phi}\right)^{-1}\left(\boldsymbol{\Phi}_{xu} + \boldsymbol{\Phi}_{v0}\right)\boldsymbol{v},$$

$$\widehat{\boldsymbol{\omega}} - \boldsymbol{\omega}^* = \left(\boldsymbol{\Phi}^T\boldsymbol{\Phi}\right)^{-1}\boldsymbol{\Phi}_{v0}\boldsymbol{v}.$$

Now, if $C(q^{-1}) = D(q^{-1}) = 1$ (*i.e.,* $v(t_k)$ is a white, zero-mean signal), then $\boldsymbol{\Phi}_{v0}\boldsymbol{v} = 0$ and

$$\widehat{\boldsymbol{\omega}} - \boldsymbol{\omega}^* = 0,$$

so that estimates converge asymptotically to the true values. However, if $C(q^{-1}) \neq 1$ and/or $D(q^{-1}) \neq 1$, so that $v(t_k)$ is non-white,

then $\boldsymbol{\Phi}_{v0}\boldsymbol{v} \neq 0$

$$\widehat{\boldsymbol{\omega}} = \boldsymbol{\omega}^* + \left(\boldsymbol{\Phi}^T\boldsymbol{\Phi}\right)^{-1}\boldsymbol{\Phi}_{v0}\boldsymbol{v}.$$

Which demonstrates that the estimates do not converge to the true values but are biased. Furthermore, the bias term is a function of the measured input, output, and the unmeasurable noise $v(t_k)$.

Instrumental variables: The ordinary least-squares approach can be extended to give unbiased estimates of the parametric models by using instrumental variables in the estimation equation [136, 101, 141, 142]. Here, the estimation equation (3.7), is replaced by

$$\widehat{\boldsymbol{\omega}} = \left(\boldsymbol{\Phi}^T\widehat{\boldsymbol{\Phi}}\right)^{-1}\widehat{\boldsymbol{\Phi}}^T\boldsymbol{y}, \tag{3.8}$$

where

$$\widehat{\boldsymbol{\Phi}} = \begin{bmatrix} \widehat{\phi}_0(1) & \widehat{\phi}_1(1) & \cdots & \widehat{\phi}_D(1) \\ \widehat{\phi}_0(2) & \widehat{\phi}_1(2) & \cdots & \widehat{\phi}_D(2) \\ \vdots & \vdots & \ddots & \vdots \\ \widehat{\phi}(N) & \widehat{\phi}_1(N) & \cdots & \widehat{\phi}_D(N) \end{bmatrix}$$

where $\widehat{\phi}_j(t_k)$ are the instrumental variables. The instrumental variables must satisfy three conditions [141, 142]:

- $\boldsymbol{\Phi}^T\widehat{\boldsymbol{\Phi}} \neq 0$
- $\boldsymbol{\Phi}^T\widehat{\boldsymbol{\Phi}}$ is full rank
- $\widehat{\boldsymbol{\Phi}}^T\boldsymbol{v} = 0$

The first condition guarantees that the instrumental variable is correlated with the input signal, the second condition guarantees that the inverse of (3.8) exists; the third one guarantees the estimates provided by the instrumental variable approach are asymptotically unbiased. Any signal that fulfills these conditions can be used as instrumental variable. Multiple signals, such as an estimate of the noise-free output, and past input values, have been used for different applications [142]. In consequence, selecting the best instrumental variable must be part of the identification process for each application.

Regularization and Bayesian estimation: One problem with the least-square and instrumental variable estimation approaches is the need to select the model order determined by the number of elements $D+1$ (3.3). So far, it has been assumed that the model order is known *a priori* so that the matrices in (3.7) can be constructed from input and output samples. However, in practice the order is rarely known and so selecting it is an important part of the identification procedure.

One common approach to select the model order is to add a regularization term to the objective function (3.6) that penalizes the complexity of the model. That is

$$E\left(\boldsymbol{\omega}\right) = \underbrace{\frac{1}{2}\sum_{t_k=1}^{N}\left[y(t_k) - \boldsymbol{\omega}^T\boldsymbol{\phi}(t_k)\right]^2}_{\text{Ordinary least squares}} + \underbrace{\frac{\lambda}{2}\sum_{j=1}^{D}|\omega_j|^p}_{\text{Regularization}}, \tag{3.9}$$

where $0 < \lambda < 1$ controls the relative weight of each component, and p defines the type of regularization. A value of $p = 2$ is called to quadratic regularization, while $p = 1$ is known as *lasso* regularization [143]. For $p = 2$ there is an exact

solution for $\boldsymbol{\omega}$, given by

$$\widehat{\boldsymbol{\omega}} = \left(\lambda \boldsymbol{I} + \boldsymbol{\Phi}^T \boldsymbol{\Phi}\right)^{-1} \boldsymbol{\Phi}^T \boldsymbol{y}, \tag{3.10}$$

where $\boldsymbol{I}$ is the unitary matrix.

The parameter estimates $\widehat{\boldsymbol{\omega}}$ will depend heavily on the regularization parameter λ; for example, if $\lambda \approx 0$ then the regularization term will play an insignificant role and the results will be similar to those of the ordinary least squares method. Therefore, several methods have been used to find the optimal value of λ [144]. One popular method is to create a grid of possible values for the regularization parameters and evaluate the cost function at each parameter, and select the value of λ that provides the minimum error [145]. This approach is not ideal as is time consuming and the algorithm often results in a non-optimal λ as it is impossible to test all possible values.

Bayesian learning

An alternative approach to solve the regularization problem is to use Bayesian or probabilistic learning algorithms for parameter estimation [143, 146]; in particular, the *relevance vector machine* [147, 148, 149]. Going through the full details of this algorithm is beyond the scope of this thesis. Consequently, only the foundation and main results will be presented.

In probabilistic learning, the unknown parameters ω_j are regarded as samples from a pre-defined probability distribution (the *prior*) instead of fixed numbers. The objective is then to estimate the parameters that define

this probability distribution (the *posterior*), called hyper-parameters, using the information from the measured data (the *evidence*). In particular, one method, the relevance vector machine, defines the *priors* of ω_j as Gaussian distributions with zero mean and precision (inverse of variance) α_j:

$$p\left(\boldsymbol{\omega}|\boldsymbol{\alpha}\right) = \prod_{j=0}^{J} \mathcal{N}\left(\omega_j|0, \alpha_j^{-1}\right).$$

The use of Gaussian, zero-mean probability distributions as *priors* yields a sparse solution, because the mean of the *posterior* distribution of a parameter that is not needed to explain the measured will also be zero, while the mean of *posterior* distribution of a parameter that is needed to explain the measured will be centered around the true value.

In the Bayesian learning setting, the measured data is considered to be sampled from a probability distribution defined by the input data, the true model parameters and the noise, that is

$$p\left(y(t_k)|\boldsymbol{\phi}(t_k), \boldsymbol{w}, \beta^{-1}\right) = \mathcal{N}\left(y(t_k)|x(t_k), \beta\right)$$

where β is the precision of the noise signal $v(t_k)$. For the N samples, this function, the *likelihood*, becomes

$$p\left(\boldsymbol{y}|\boldsymbol{\Phi}, \boldsymbol{w}, \beta\right) = \prod_{t_k=1}^{N} \mathcal{N}\left(y(t_k)|\boldsymbol{\Phi}, \boldsymbol{w}, \beta^{-1}\right).$$

Using the *prior*, the *likelihood* and the *evidence*, the *posterior* distribution of the model parameters is [143]

$$
\begin{aligned}
&p\left(\boldsymbol{\omega}|\boldsymbol{y}, \boldsymbol{\Phi}, \boldsymbol{\alpha}, \beta\right) = \mathcal{N}\left(\boldsymbol{\omega}|\boldsymbol{m}, \boldsymbol{\Sigma}\right), \\
&\boldsymbol{\Sigma} = \left(\boldsymbol{A} + \beta \boldsymbol{\Phi}^T \boldsymbol{\Phi}\right)^{-1}, \\
&\boldsymbol{m} = \beta \boldsymbol{\Sigma} \boldsymbol{\Phi}^T \boldsymbol{y}.
\end{aligned}
$$

With $\boldsymbol{A} = diag(\alpha_i)$. The problem is reduced to finding the hyper-parameters β and α_i. The relevance vector machine does this by computing the marginal likelihood of the evidence given the input ($\boldsymbol{\Phi}$), and the hyper-parameters, using the product rule of probability, that is

$$
p\left(\boldsymbol{y}|\boldsymbol{\Phi}, \boldsymbol{\alpha}, \beta\right) = \int p\left(\boldsymbol{y}|\boldsymbol{\Phi}, \boldsymbol{w}, \beta\right) p\left(\boldsymbol{\omega}|\boldsymbol{\alpha}\right).
$$

The parameters that maximize the marginal likelihood of the evidence are found by differentiating and equating it to zero. This leads to the following iterative procedure for parameter estimation [143]

$$
\begin{aligned}
\alpha_i =& \frac{\gamma_i}{m_i^2}, \\
\beta_i =& \frac{N - \sum \gamma_i}{\sum \left[y(t_k) - \boldsymbol{\omega}^T \boldsymbol{\phi}(t_k)\right]^2} \\
\gamma_i =& 1 - \alpha_i \Sigma_{ii},
\end{aligned}
$$

where Σ_{ii} is the i^{th} diagonal element of $\boldsymbol{\Sigma}$. The relevance vector machine is an iterative algorithm where the user provides initial values for $\boldsymbol{\alpha}$ and β, and uses them estimate $\boldsymbol{m}$ and $\boldsymbol{\Sigma}$. These are then used to update α_i,

γ_i and β. This process is repeated until there are no significant chances in the parameter values.

3.2 Hammerstein Systems

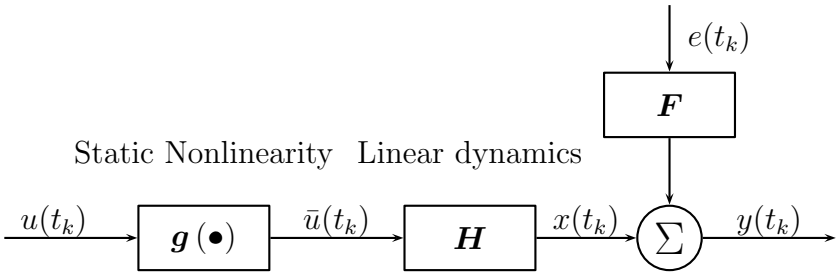

Figure 3–2: Block diagram representing a Hammerstein System.

As Fig. 3–2 shows, the Hammerstein system is a structure comprising a series connection of a static nonlinearity followed by a linear dynamic element. This is an important block-oriented structure that combines the simplicity of linear systems with the generalization capacity of nonlinear systems. It has been successfully used in a variety of research areas including biomedical engineering [12], signal processing [150], and others [151, 152].

3.2.1 Identification of Hammerstein systems

Many different techniques have been developed for the identification of its parameters from input-output data. These techniques make different assumptions regarding the static nonlinearity, the linear system, the input characteristics and the output noise [151]. The most commonly used techniques assume a parametric form for the static nonlinearity, *e.g.*, polynomial nonlinearity, radial basis functions, and then estimate the parameters of the parametric, static nonlinearity and the linear system. Other methods that make no assumptions regarding the structure of the

static nonlinearity are restricted to a particular input, which severely limits their applications [153, 154, 155].

Non-Iterative techniques: Arguably the most commonly used, and perhaps the simplest, way to estimate the parameters of a Hammerstein system is to assume a parametric model for the input nonlinearity and transform the *Single-Input - Single-Output* (SISO) nonlinear systems into a *Multiple-Input - Single-Output* (MISO) linear system. The linear systems identification techniques can be used to estimate the parameters of the new, linear model. This approach has been used to identify joint dynamics using different linear identification algorithms, including correlation [12], sub-space [156, 157], and instrumental variable [64] approaches.

The main advantage of this algorithms is that they estimate all the elements of the Hammerstein system in one single step. However, they have some important drawbacks. The first is that this method significantly increases the dimension of the unknown parameter vector, so that large data sets are required for reliable parameter estimation. Secondly, it is not straightforward to convert the resulting MISO system back into the original SISO system, making it difficult to interpret the estimated parameters.

Iterative approaches: Iterative approaches estimate the elements of the Hammerstein system in separate steps and does not require the estimation of additional parameters. There are two types of iterative identification algorithms for Hammerstein systems: In the first approach, the linear element is estimated and its inverse is used to predict $\bar{u}(t_k)$, the output of the static-nonlinearity. Then, the

shape of the static-nonlinearity is estimated using $u(t_k)$ and $\bar{u}(t_k)$. Now that the shape of $g(\bullet)$ is available, is possible to update intermediate signal $\bar{u}(t_k)$, which is then used to update the estimate of the linear element [158]. One main limitation of this method is that it requires Gaussian input signals [159].

The second approach divides the parameters of the static nonlinearity and linear element in two sets, and defines a cost function for the estimation of each parameter set. However, the estimated parameters related to the static nonlinearity are a function of the input, output and the linear element; and the estimated parameters related to the linear element are a function of the input, output and static nonlinearity. This approach tackles this problem by finding an initial estimate of the linear element, then the parameters related to the static-nonlinearity are estimated using the current values of the linear element. The linear element is then updated using the current estimate of the static-nonlinearity. The algorithm iterates between those steps there are no significant changes in the parameters [160]. Different versions of this algorithm have been used for the estimation of joint [104, 159] and muscle dynamics [161, 162].

A series of papers by P. Stoica [163], E. Bai *et.al* [151, 164, 165] and G. Li *et. al* [166] showed that this iterative identification approach for Hammerstein systems converges to the true values starting from any arbitrary non-zero initial condition provided that a normalization stage is included at the end of each iteration. Additionally, this method is more robust to noise and less sensitive to the input properties that the first class of iterative approaches [167].

The iterative approach developed by E. Bai *et.at* [151] is probably the best approach for identification of Hammerstein systems from biological systems as it: i) Can be used with non-white inputs with arbitrary amplitude distributions, ii) is guaranteed to converge to the true values, iii) requires minimum information about the linear and nonlinear elements, and iv) provides consistent estimates for non-white output noise.

3.3 Linear, Time-Varying Systems

The identification methods discussed so far assume that the system's dynamics is time-invariant. However, most biological system are time-varying, that is, their dynamics changes with time or some other independent variable.

Methods for the identification of time-varying systems can be divided into three categories depending on their underlying assumptions: i) Adaptive methods, these methods use recursive identification algorithm to estimate the model parameters at each time [101]. They assume that the time-varying parameters are random signals. ii) Temporal expansion methods, expand time-varying parameters using a set of predefined basis functions, transforming the time-varying identification problem into a time-invariant problem [168]. They assume that the time-varying parameters can be appropriately described by a linear combination of predefined basis functions. iii) Ensemble methods, estimate the time-varying parameters from a series of responses each exhibiting the same underlying time-varying behavior. Once the ensemble of responses have been obtained, ensemble methods use time-invariant identification techniques to estimate the time-varying parameters at each time [108]. They assume

that is possible to obtain multiple input-output trials presenting the same underlying time-varying behavior.

Each methods has its advantages and limitations. Thus, adaptive methods can be used online, updating the estimated parameters with every new measurement. These methods are commonly used in adaptive control and tracking, where the accuracy of the parameter estimates is less important than the possibility of having online predictions. Ensemble methods cannot be used online as they require multiple realization of the same time-varying process. However, provided that enough data is available, these methods can accurately track fast, large changes in the system dynamics. Temporal expansion methods cannot be used for online prediction either. However, unlike ensemble approaches, temporal expansion methods can estimate the model parameters from one single input-output realization. There are two main limitations associated with temporal expansion methods. First, the quality of the estimate depends on the appropriate selection of the basis functions; this usually requires some *a priori* knowledge of the time-varying dynamics. Second, the temporal expansion transforms the low-dimensional, time-varying system into a high-dimensional, time-invariant system, with a large number of free parameters. This implies that large data records are required for parameter estimation.

3.3.1 Parametric representation of time-varying systems

Using the vector notation introduced of (3.4), a time-varying system can be expresses as

$$x(t) = \boldsymbol{\omega}^T(t)\boldsymbol{\phi}(t), \tag{3.11}$$

the dependency on time is made explicit and

$$\boldsymbol{\omega}(t) = [w_0(t), \cdots, w_J(t)]^T,$$
$$\boldsymbol{\phi}(t) = [\phi_0(t), \cdots, \phi_J(t)].$$

where $\omega_j(t)$ are time-varying parameters and $\phi_j(t)$ are, possibly nonlinear, functions of input ($u(t)$) and output ($x(t)$) variables.

In this representation, the weights $\omega_j(t)$ are continuous-time functions. This continuous-time, time-varying system can be approximated by a set of discrete-time, *frozen* equations at each sample time as

$$x(t_k) = \boldsymbol{\omega}^T(t_k)\boldsymbol{\phi}(t_k), \tag{3.12}$$

the continuous-time system is approximated by a set of *frozen*, discrete-time system at each sample time t_k. As Figure 3–3 shows, this approximation applies a *zero-order-hold* to the time-varying parameters, so that they are treated as being constant, or *frozen* between samples. There other approaches for this approximation of time-varying system, Toth surveyed their advantages and drawbacks, concluding that *zero-order-hold* approximation is adequate when the parameters are instantaneous function of time (i.e, the current parameters value depends on the current time, not on past or future time values), when this assumption is violated, other techniques are required [169].

3.3.2 Identification of linear, time-varying systems

Next I will discuss in more detail the ensemble and temporal expansion methods for identification of time-varying systems.These methods will be used in this thesis as

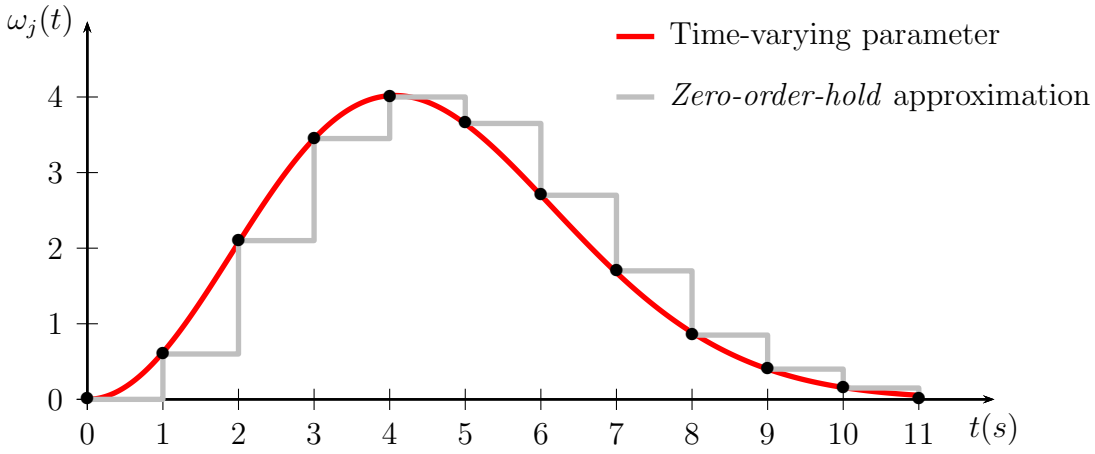

Figure 3–3: Approximation of a continuous-time, time-varying parameter by a set of frozen, discrete-time parameters.

the parameter identification will be performed offline and they provide more accurate estimate that adaptive methods [108, 170].

Ensemble-based approach The ensemble approach relies on having an ensemble of input-output trials with the same time-varying behavior, that is

$$\begin{aligned} y_1(t_k) &= x_1(t_k) + v_1(t_k), \\ &\vdots \\ y_M(t_k) &= x_M(t_k) + v_M(t_k), \end{aligned}$$

where M is the number of elements in the ensemble. Given that each trial has the same time-varying behavior then

$$\begin{aligned} y_1(t_k) &= \boldsymbol{\omega}^T(t_k)\boldsymbol{\phi}_1(t_k) + v_1(t_k), \\ &\vdots \\ y_M(t_k) &= \boldsymbol{\omega}^T(t_k)\boldsymbol{\phi}_M(t_k) + v_M(t_k). \end{aligned}$$

For time t_k

$$\boldsymbol{y}(t_k) = \boldsymbol{\omega}^T(t_k)\Phi(t_k) + \boldsymbol{v}(t_k),$$

where

$$\begin{aligned}
\boldsymbol{y}(t_k) &= \left[y_1(t_k), \cdots, y_M(t_k)\right]^T, \\
\boldsymbol{v}(t_k) &= \left[v_1(t_k), \cdots, v_M(t_k)\right]^T, \\
\boldsymbol{\omega}(t_k) &= \left[w_0(t_k), \cdots, w_J(t_k)\right]^T
\end{aligned}$$

and

$$\boldsymbol{\Phi}(t_k) = \begin{bmatrix}
\phi_{1,0}(t_k) & \phi_{1,1}(t_k) & \cdots & \phi_{1,J}(t_k) \\
\phi_{2,0}(t_k) & \phi_{2,1}(t_k) & \cdots & \phi_{2,J}(t_k) \\
\vdots & \vdots & \ddots & \vdots \\
\phi_{M,0}(t_k) & \phi_{M,1}(t_k) & \cdots & \phi_{M,J}(t_k)
\end{bmatrix}.$$

So that at each discrete-time t_k, the parameters can be estimated using least-squares as

$$\widehat{\boldsymbol{\omega}}(t_k) = \left[\boldsymbol{\Phi}^T(t_k)\boldsymbol{\Phi}(t_k)\right]^{-1}\boldsymbol{\Phi}^T(t_k)\boldsymbol{y}(t_k).$$

Repeating this procedure at each time will map out the time course. This identification procedure can be implemented in matrix form and estimate all the time-varying parameters in a single step.

Basis-expansion approach: The basis expansion approach assumes that the time course of the model parameters can be described by a linear combination of

pre-defined basis functions, that is

$$\omega_j(t_k) = \sum_{i=0}^{i=Q} r_i \Gamma_i\left(t_k\right),$$

where $\Gamma_i(t_k)$ are the basis functions and r_i their weights. Using this parametrization, the time-varying system can be described by

$$y(t_k) = \sum_{i=0}^{i=Q} \sum_{j=0}^{J} r_{i,j} \Gamma_i\left(t_k\right) \phi_j(t_k) + v(t_k).$$

In vector notation, this equation becomes

$$\boldsymbol{y} = \boldsymbol{r}\boldsymbol{\Phi} + \boldsymbol{v},$$

where

$$\begin{aligned}
\boldsymbol{y} &= \left[y(1), \cdots, y(N)\right]^T, \\
\boldsymbol{v} &= \left[v(1), \cdots, v(N)\right]^T, \\
\boldsymbol{r} &= \left[r_{0,0}, \cdots, r_{0,D}, \cdots, r_{Q,0}, \cdots, r_{Q,J}\right]^T
\end{aligned}$$

and

$$\boldsymbol{\Phi} = \begin{bmatrix}
\Gamma_0\left(1\right)\phi_0(1) & \cdots & \Gamma_0\left(1\right)\phi_J(1) & \cdots & \Gamma_Q\left(1\right)\phi_0(1) & \cdots & \Gamma_Q\left(1\right)\phi_J(1) \\
\Gamma_0\left(2\right)\phi_0(2) & \cdots & \Gamma_0\left(2\right)\phi_J(2) & \cdots & \Gamma_Q\left(2\right)\phi_0(2) & \cdots & \Gamma_Q\left(2\right)\phi_J(2) \\
\vdots & \ddots & \vdots & \ddots & \vdots & \ddots & \vdots \\
\Gamma_0\left(N\right)\phi_0(N) & \cdots & \Gamma_0\left(N\right)\phi_J(N) & \cdots & \Gamma_Q\left(N\right)\phi_0(N) & \cdots & \Gamma_Q\left(N\right)\phi_J(N)
\end{bmatrix}.$$

The model parameters can then be estimated using least-squares as

$$\widehat{\boldsymbol{r}} = \left(\boldsymbol{\Phi}^T\boldsymbol{\Phi}\right)^{-1}\boldsymbol{\Phi}^T\boldsymbol{y}.$$

Using this re-parametrization, the $J + 1$ time-varying parameters are approximated by $(Q + 1) \times (J + 1)$ time-invariant parameters that can be estimated using least-squares.

CHAPTER 4
Identification of a Time-Varying, Box-Jenkins Model of Intrinsic Joint Compliance

Authors: Diego L. Guarin and Robert E. Kearney

Journal: IEEE Transactions on Neural Systems and Rehabilitation Engineering

Year: 2016

In the parallel-cascade for dynamic joint stiffness, intrinsic stiffness is described by a linear, dynamical model. Therefore, the identification of linear, system is important for the characterization of joint neuromechanics. However, most linear identification algorithms are limited to time-invariant models. Available methods for identification of linear, time-varying systems require very long data records or provide coarse, on-line estimates of the parameters time-course. This chapter develops and validates a new algorithm for the identification of linear, time-varying, transfer function models that, contrary to classical algorithms, accurately tracks the fast, large changes in the transfer function model parameters using only a few periodic, input-output data segments of short duration. The new algorithm was applied to the estimation of time-varying, intrinsic joint compliance during simulated walking, showing that the new method is a valuable tool for the study of joint biomechanics during function.

Abstract

The mechanical properties of a joint are determined by the combination of intrinsic and reflex mechanisms. However, in some situations the reflex contributions are small so that intrinsic mechanisms play the dominant role in the control of posture and movement. The intrinsic mechanisms, characterized by the joint compliance, can be described well by a second order, linear model for small perturbations around an operating point defined by mean position and torque. However, the compliance parameters depend strongly on the operating point. Thus, for functional activities, such as walking, where position and torque undergo large, rapid changes, the joint compliance will also present large, fast changes and so will appear to be Time-Varying (TV). Therefore, a TV system identification algorithm must be used to characterize these changes. This paper introduces a novel TV system identification algorithm that achieves this. The method extends an instrumental-variable based algorithm for the identification of linear, TV, parametric, Box-Jenkins models to use periodic data. Simulation studies demonstrate that the new algorithm accurately tracks the changes in intrinsic joint compliance expected during walking. Moreover, the method performs well with the complex noise encountered in practice. Consequently the new method should be a valuable tool for the study of joint mechanics during functional activities.

4.1 Introduction

Joint compliance defines the dynamic relation between the torque generated around a joint and its position. This property of the neuromuscular system plays a vital role in the control of movement and posture as it determines the response of

the joint to unexpected disturbances. Consequently, joint compliance and its inverse, dynamic stiffness or impedance, have been the topic of many investigations [20, 1, 12, 171, 18]. Overall joint compliance is generated by a combination of intrinsic and reflex mechanisms. However, there are many situations where reflex contributions are either absent or small enough to be ignored. For example, recent experiments suggest that reflexes are small during walking in healthy subjects [109, 110, 125]. This paper deals with the identification of intrinsic joint compliance during such situations.

Previous studies have shown that under stationary conditions, joint compliance varies with the joint position and torque generated around it [11, 172]. Thus, when these change continuously during functional tasks, joint compliance is expected to be time-varying (TV). Indeed, recent experimental results have documented large changes in ankle compliance throughout the walking cycle [109, 110, 125]. In addition, the noise present in such experiments is neither white nor Gaussian; rather is composed of: a low-frequency (<0.01Hz) trend, a stochastic component band-limited to 1 Hz, physiological tremor (with power up to 10Hz), and 60Hz noise [173, 174]. Consequently, estimating joint compliance requires a TV identification method capable of tracking large, rapid changes in system dynamics in the presence of complex, colored noise.

There are three general approaches to TV system identification: 1) ensemble methods [108, 175], where a large set of input-output realizations, each having the same time-varying behavior, is used to estimate the time course of the parameters;

2) stochastic identification [176, 101], where changes in the TV parameters are assumed to be small between samples and are modeled as a stochastic process; and 3) deterministic identification [168, 170], where the TV parameters are assumed to change deterministically and are modeled using a combination of predefined basis functions.

Ensemble methods require hundreds of input-output realizations having the same TV behavior; this is time consuming and difficult to obtain experimentally. Nevertheless, ensemble methods have been used to characterize joint compliance during different TV conditions [108, 106, 110, 112, 120, 109]. In contrast, both deterministic and stochastic methods estimate the TV parameters from one or a few input-output trials [170, 103]. However, provided an adequate set of basis functions is selected, deterministic methods perform better than stochastic methods as they can track more rapid parameter changes and have lower estimation errors [170].

Despite these advantages, most deterministic methods identify models with the ARMAX structure, shown in Fig. 4–1A, or its subclasses (*i.e.* ARMA, AR, ARX). These structures assume that the noise is white, or that the process and noise plants share the same dynamics. Neither assumption is valid for compliance experiments. Consequently, using an ARMAX algorithm to identify TV joint compliance, where the noise is not white, will yield biased results [101]. Unbiased results can be obtained by using the Box-Jenkins (BJ) model structure, shown in Fig. 4–1B, where the noise and process are modeled independently [139, 101].

A review of the literature found only one method for the identification of TV-BJ models. This method uses instrumental variables and a deterministic parameter

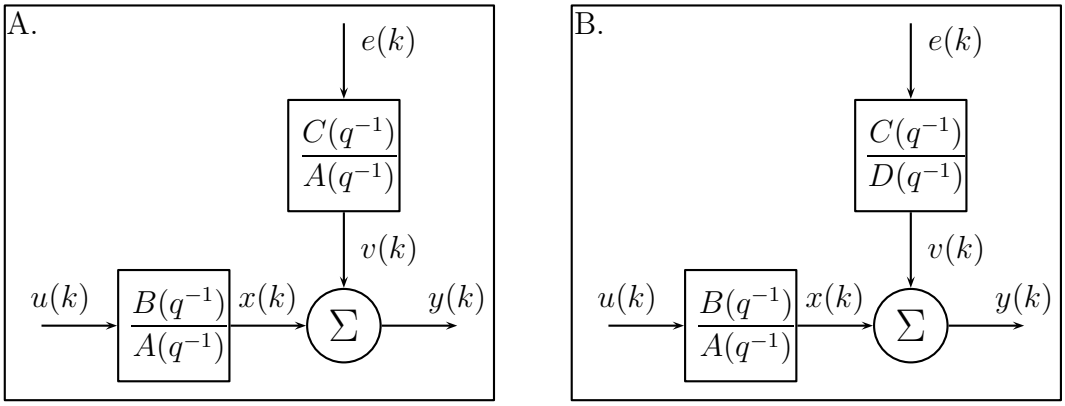

Figure 4–1: Graphical representation of A. ARMAX and B. BJ model structures. $u(k)$ is the controlled input, $x(k)$ is the noise-free output, $y(k)$ is the noise corrupted output, $e(k)$ is the uncontrolled, white disturbances and $v(k)$ is the colored, output noise. $A(q^{-1})$, $B(q^{-1})$, $C(q^{-1})$ and $D(q^{-1})$ are polynomials on q^{-1}.

identification approach [177, 101]. However, it operates on only a single input-output record. This limits its utility for the study of TV systems, such as joint compliance during walking, where due to the short duration of the gait cycle, and the large changes that the joint dynamics undergoes during this short amount of time, multiple cycles will likely be necessary to obtain accurate estimates.

This paper develops and evaluates the performance of an algorithm to estimate TV-BJ models of intrinsic joint compliance. To do so, we: 1) extended the TV-BJ identification algorithm [177] to use periodic, input-output trials of short duration, and 2) developed a TV-BJ model for joint compliance. We demonstrated the utility of the algorithm and explored its performance using data from simulations that mimicked the behavior of intrinsic joint compliance expected during walking.

This paper is organized as follows: Section 4.2 briefly summarizes the instrumental variable approach to the identification of TV-BJ models and then extends it to use periodic, input-output trials of short duration. Section 4.3 formulates a TV,

discrete-time, BJ model of intrinsic joint compliance. Section 4.4 describes the simulation used to evaluate the performance of the new TV-BJ identification algorithm. Section 4.5 presents the results of the simulation study. Section 4.6 summarizes the contributions and discusses some important aspects of the method and its application.

4.2 Time-Varying Box-Jenkins Identification Algorithm

A linear, TV, discrete-time, stochastic, BJ system can be described by [177]:

$$\begin{cases} A\left(k, q^{-1}\right) x(k) = B\left(k, q^{-1}\right) u(k), \\ v(k) = \dfrac{C\left(q^{-1}\right)}{D\left(q^{-1}\right)} e(k), \\ y(k) = x(k) + v(k), \end{cases} \tag{4.1}$$

where $x(k)$ is the noise-free output, $u(k)$ is the controlled input, $v(k)$ is the colored output noise, $y(k)$ is the measured, noisy output, $e(k)$ is a zero-mean, white noise process with normal distribution and variance σ^2 that is uncorrelated with the input, $k \in \mathbb{Z}$ is the discrete time and q^{-1} is the backward shift operator, i.e., $q^{-1}x(t) = x(t-1)$.

$A(k, q^{-1})$ and $B(k, q^{-1})$ are the TV polynomials

$$A\left(k, q^{-1}\right) = 1 + \sum_{i=1}^{n_a} a_i(k) q^{-i}, \tag{4.2a}$$

$$B\left(k, q^{-1}\right) = b_0(k) + \sum_{i=1}^{n_b} b_i(k) q^{-i}, \tag{4.2b}$$

and $C(q^{-1})$ and $D(q^{-1})$ are the time-invariant (TI) polynomials

$$C\left(q^{-1}\right) = 1 + \sum_{i=1}^{n_c} c_i q^{-i}, \tag{4.3a}$$

$$D\left(q^{-1}\right) = 1 + \sum_{i=1}^{n_d} d_i q^{-i}. \tag{4.3b}$$

4.2.1 Model Reparametrization

The TV parameters of $A(k, q^{-1})$ and $B(k, q^{-1})$ can be described as linear combinations of basis functions:

$$a_i(k) = \alpha_{i,0} + \sum_{j=1}^{n_\alpha} \alpha_{i,j}\pi_j(k), \quad i = 1, \cdots, n_a, \tag{4.4a}$$

$$b_i(k) = \beta_{i,0} + \sum_{j=1}^{n_\beta} \beta_{i,j}\pi_j(k), \quad i = 0, \cdots, n_b, \tag{4.4b}$$

where $\alpha_{i,0} \neq 0$, and $\{\pi_j\}_{j=0}^{n_\alpha, n_\beta}$ is the basis function set (*e.g.*. orthogonal polynomials) with $\pi_0(k) = 1, \forall k$. This transforms the TV model into a time-invariant (TI) model with the constant parameters

$$\begin{aligned}\boldsymbol{\rho} = \big[&\alpha_{1,0} \ \ldots \ \alpha_{n_a,0} \ \alpha_{1,1} \ \ldots \ \alpha_{1,n_\alpha} \ \ldots \ \alpha_{n_a,1} \ \ldots \ \alpha_{n_a,n_\alpha} \\ &\beta_{0,0} \ \ldots \ \beta_{0,n_\beta} \ \ldots \ \beta_{n_b,0} \ \ldots \ \beta_{n_b,n_\beta}\big]^T \in \mathbb{R}^{n_\rho},\end{aligned} \tag{4.5}$$

where $n_\rho = n_a(n_\alpha + 1) + (n_b + 1)(n_\beta + 1)$.

4.2.2 Parameter Identification

Laurain *et. al* [177] showed that the parameter set (4.5) can be estimated from input-output data as

$$\hat{\boldsymbol{\rho}} = \left[\frac{1}{N}\sum_{k=1}^{N} \hat{\boldsymbol{\phi}}_{\hat{\boldsymbol{f}}}(\boldsymbol{k})\hat{\boldsymbol{\varphi}}^{\boldsymbol{T}}_{\hat{\boldsymbol{f}}}(\boldsymbol{k})\right]^{-1}\left[\frac{1}{N}\sum_{k=1}^{N} \hat{\boldsymbol{\phi}}_{\hat{\boldsymbol{f}}}(\boldsymbol{k})y^{\hat{f}}(k)\right], \tag{4.6}$$

where

$$\begin{aligned}\hat{\boldsymbol{\varphi}}_{\hat{\boldsymbol{f}}}(\boldsymbol{k}) = \Big[&-y^{\hat{f}}(k-1)\ \ldots\ -y^{\hat{f}}(k-n_a)\ -\hat{x}_1^{\hat{f}}(k-1)\ \ldots\\ &-\hat{x}_{n_\alpha}^{\hat{f}}(k-1)\ \cdots -\hat{x}_1^{\hat{f}}(k-n_a)\ \ldots\ -\hat{x}_{n_\alpha}^{\hat{f}}(k-n_a)\\ &u_0^{\hat{f}}(k)\ \ldots\ u_{n_\beta}^{\hat{f}}(k)\ \ldots\ u_0^{\hat{f}}(k-n_b)\ \ldots\ u_{n_\beta}^{\hat{f}}(k-n_b)\Big]^T,\end{aligned} \tag{4.7a}$$

$$\begin{aligned}\hat{\boldsymbol{\phi}}_{\hat{\boldsymbol{f}}}(\boldsymbol{k}) = \Big[&-\hat{x}^{\hat{f}}(k-1)\ \ldots\ -\hat{x}^{\hat{f}}(k-n_a)\ -\hat{x}_1^{\hat{f}}(k-1)\ \ldots\\ &-\hat{x}_{n_\alpha}^{\hat{f}}(k-1)\ \cdots -\hat{x}_1^{\hat{f}}(k-n_a)\ \ldots\ -\hat{x}_{n_\alpha}^{\hat{f}}(k-n_a)\\ &u_0^{\hat{f}}(k)\ \ldots\ u_{n_\beta}^{\hat{f}}(k)\ \ldots\ u_0^{\hat{f}}(k-n_b)\ \ldots\ u_{n_\beta}^{\hat{f}}(k-n_b)\Big]^T,\end{aligned} \tag{4.7b}$$

and

$$y^{\hat{f}}(k) = \hat{f}\left(q^{-1}\right)y(k), \tag{4.8a}$$

$$u_j^{\hat{f}}(k-i) = \hat{f}\left(q^{-1}\right)u_j(k-i), \tag{4.8b}$$

$$\hat{x}_j^{\hat{f}}(k-i) = \hat{f}\left(q^{-1}\right)\hat{x}_j(k-i). \tag{4.8c}$$

$$\hat{f}\left(q^{-1}\right) = \left(\frac{\hat{D}\left(q^{-1}\right)}{\hat{C}\left(q^{-1}\right)}\right)\left(\frac{1}{\hat{F}\left(q^{-1}\right)}\right). \tag{4.9}$$

With

$$\hat{x}(k) = \frac{1}{\hat{F}(q^{-1})}\left[-\sum_{i=1}^{n_a}\sum_{j=1}^{n_\alpha}\hat{\alpha}_{i,j}\hat{x}_j(k-i) + \sum_{i=0}^{n_b}\sum_{j=0}^{n_\beta}\hat{\beta}_{i,j}u_j(k-i)\right] \tag{4.10a}$$

$$\hat{F}\left(q^{-1}\right) = 1 + \sum_{i=1}^{n_a}\hat{\alpha}_{i,0}q^{-i}. \tag{4.10b}$$

The parameter estimator (4.6) depends on $\hat{\boldsymbol{\varphi}}(k)$ and $\hat{\boldsymbol{\phi}}(k)$; both of these depend in turn on $\hat{x}(k)$, the noise-free output, which is not directly observable. This problem can be overcome through the use of an *Expectation-Maximization* algorithm, that uses a Refined Instrumental Variable procedure [101], in which the current parameter estimates are used to predict the noise-free output - the *instrumental variable* - which is then used to update the parameter estimates. The procedure is repeated to refine the estimates until there are no significant changes in the estimated parameters.

Identification Algorithm

The identification algorithm estimates the model parameters using (4.6) and the refined instrumental variable approach from periodic data. The use of multiple data periods presenting the same time variability allows this algorithm to accurately estimate the parameters' time-course from periods of short duration, such a those observed during walking. Different from the method presented in [177], our algorithm assumes that the model parameters are periodic and so it only estimates their time-courses for one period using all the data. To achieve this, the basis functions are selected to have a length equal to one of the periods and then repeated periodically to match the length of the data record. Therefore, the algorithm estimates only one

parameter set $\hat{\boldsymbol{\rho}}$ which is then used to compute the TV parameters for all periods. The algorithm accounts for the effects of initial conditions, which are important when the duration of each period is short, by exploiting the periodicity of the signals and concatenating the vectors and matrices as expressed in steps 4, 5, and 6 of the algorithm.

Algorithm 1 estimates a TI noise model and a TV process model. However, the estimates of the noise and plant parameters are asymptotically independent [139, 65]. In consequence, when the noise model is not of interest or its structure is unknown, Algorithm 1 can be used assuming the noise is white, *i.e.* $C(q^{-1}) = D(q^{-1}) = 1$, and the estimates of the process plant model will still be unbiased.

Algorithm 1 *Identification TV-BJ from periodic data*

Input: $\{y_m(k)\}_{k=1}^{N}$, $\{u_m(k)\}_{k=1}^{N}$, $\{\pi_j(k)\}_{k=1,\ j=0}^{N,\ max(n_\alpha,n_\beta)}$, n_a, n_b, n_c and n_d. The sub-index $m = 1, \ldots, M$ represents the cycle number.

Output: $\{\hat{A}(k,q^{-1})\}_{k=1}^{N}$, $\{\hat{B}(k,q^{-1})\}_{k=1}^{N}$ and $\{\hat{x}_m(k)\}_{k=1}^{N}$

1. Find an initial estimate of $\hat{\rho}^0$ by assuming that the system is TI and using the Refined Instrumental Variable algorithm from [101]. Set $\hat{D}^0(q^{-1}) = \hat{C}^0(q^{-1}) = 1$ and the counter $r = 0$.
2. Estimate the instrumental variable $\{\hat{x}_m(k)\}_{k=1}^{N}$ via (4.10a)
3. Form the filter

$$\hat{f}^{(r)}\left(q^{-1}\right) = \frac{\hat{D}^{(r)}\left(q^{-1}\right)}{\hat{C}^{(r)}\left(q^{-1}\right)\hat{F}^{(r)}\left(q^{-1}\right)},$$

4. Filter the signals

$$\boldsymbol{u} = [u_1(1)\cdots u_1(N)\cdots u_M(1)\ldots u_M(N)]^T,$$
$$\hat{\boldsymbol{x}} = [\hat{x}_1(1)\cdots \hat{x}_1(N)\cdots \hat{x}_M(1)\ldots \hat{x}_M(N)]^T,$$
$$\boldsymbol{y} = [y_1(1)\cdots y_1(N)\cdots y_M(1)\ldots y_M(N)]^T,$$

with $\hat{f}^{(r)}(q^{-1})$ and then segment the results to generate the associated signals $\{y_m^{\hat{f}}(k)\}_{k=1}^{N}$, $\{u_m^{\hat{f}}(k)\}_{k=1}^{N}$ and $\{\hat{x}_m^{\hat{f}}(k)\}_{k=1}^{N}$.

5. Use the basis functions $\{\pi_j(k)\}_{k=1,\ j=0}^{N,\ max(n_\alpha,n_\beta)}$ to form the regressor-matrices $\{\hat{\boldsymbol{\varphi}}_{\hat{\boldsymbol{f}},\boldsymbol{m}}(\boldsymbol{k})\}_{k=1}^{N}$ and $\{\hat{\boldsymbol{\phi}}_{\hat{\boldsymbol{f}},\boldsymbol{m}}(\boldsymbol{k})\}_{k=1}^{N}$ using (4.7a) and (4.7b).
6. Organize the vectors as

$$\hat{\boldsymbol{\phi}}_{\hat{f}} = \begin{bmatrix} \hat{\boldsymbol{\phi}}_{\hat{\boldsymbol{f}},\mathbf{1}}(\mathbf{1}) \\ \vdots \\ \hat{\boldsymbol{\phi}}_{\hat{\boldsymbol{f}},\mathbf{1}}(\boldsymbol{N}) \\ \vdots \\ \hat{\boldsymbol{\phi}}_{\hat{\boldsymbol{f}},\boldsymbol{M}}(\mathbf{1}) \\ \vdots \\ \hat{\boldsymbol{\phi}}_{\hat{\boldsymbol{f}},\boldsymbol{M}}(\boldsymbol{N}) \end{bmatrix}, \hat{\boldsymbol{\varphi}}_{\hat{f}} = \begin{bmatrix} \hat{\boldsymbol{\varphi}}_{\hat{\boldsymbol{f}},\mathbf{1}}(\mathbf{1}) \\ \vdots \\ \hat{\boldsymbol{\varphi}}_{\hat{\boldsymbol{f}},\mathbf{1}}(\boldsymbol{N}) \\ \vdots \\ \hat{\boldsymbol{\varphi}}_{\hat{\boldsymbol{f}},\boldsymbol{M}}(\mathbf{1}) \\ \vdots \\ \hat{\boldsymbol{\varphi}}_{\hat{\boldsymbol{f}},\boldsymbol{M}}(\boldsymbol{N}) \end{bmatrix}, \boldsymbol{y}^{\hat{f}} = \begin{bmatrix} y_1^{\hat{f}}(1) \\ \vdots \\ y_1^{\hat{f}}(N) \\ \vdots \\ y_M^{\hat{f}}(1) \\ \vdots \\ y_M^{\hat{f}}(N) \end{bmatrix}$$

7. Update the parameter estimates as

$$\hat{\boldsymbol{\rho}}^{(r+1)} = \left[\hat{\boldsymbol{\phi}}_{\hat{f}}\hat{\boldsymbol{\varphi}}_{\hat{f}}^T\right]^{-1}\left[\hat{\boldsymbol{\phi}}_{\hat{f}}\boldsymbol{y}^{\hat{f}}\right].$$

8. Update the instrumental variable $\{\hat{x}_m(k)\}_{k=1}^{N}$ and compute the noise signal as

$$\hat{v}_m(k) = y_m(k) - \hat{x}_m(k).$$

Use the ensemble of noise signals to estimate the noise model parameters using an `ARMAX` identification routine [136].

9. If the difference between $\hat{\boldsymbol{\rho}}^{(r+1)}$ and $\hat{\boldsymbol{\rho}}^{(r)}$ is not significant or, if the maximum number of iterations is exceeded, go to step 10, else increment r and go to step 3.
10. Compute $\hat{A}(k,q^{-1})$ and $\hat{B}(k,q^{-1})$ for all k as

$$\hat{a}_i(k) = \hat{\alpha}_{i,0} + \sum_{j=1}^{n_\alpha}\hat{\alpha}_{i,j}\pi_j(k), \quad \hat{b}_i(k) = \hat{\beta}_{i,o} + \sum_{j=1}^{n_\beta}\hat{\beta}_{i,j}\pi_j(k).$$

4.3 Intrinsic Joint Compliance

At a given operating point, defined by the joint position and torque (τ_0, θ_0), the relation between joint position and torque for small perturbations can be approximated by the continuous-time, second-order, linear system [12, 178, 109]:

$$\tau(t) = I\frac{d^2\left[\theta(t)\right]}{dt^2} + B\frac{d\left[\theta(t)\right]}{dt} + K\theta(t), \tag{4.11}$$

where I, B and K are the joint inertia, viscosity and elasticity; $\theta(t)$ and $\tau(t)$ are the join position and torque; and $t \in \mathbb{R}$ is the continuous time. When the operating point changes with time, the model parameters will be time dependent so that the intrinsic response of the joint to the small perturbations can be approximated about each operating point $(\tau_0(t), \theta_0(t))$ as [106]:

$$\tau(t) = I\frac{d^2\left[\theta(t)\right]}{dt^2} + B(t)\frac{d\left[\theta(t)\right]}{dt} + K(t)\theta(t), \tag{4.12}$$

By assuming a *zero-order-hold* approximation on the TV parameters, this model can be approximated by a set of linear models. Each model is assumed to be fixed at each sampling point so that the model parameters do not change between samples. The TV, joint compliance, at time k, can be expressed as

$$\Theta(s) = \frac{1}{Is^2 + B(k)s + K(k)}\mathcal{T}(s) \tag{4.13}$$

where $\Theta(s)$ and $\mathcal{T}(s)$ are the Laplace transformation of the joint position and torque. Algorithm 1 identifies discrete, TV-BJ systems; therefore, this continuous-time model is approximated by a TV, discrete-time model. Thus, the input-output relation at

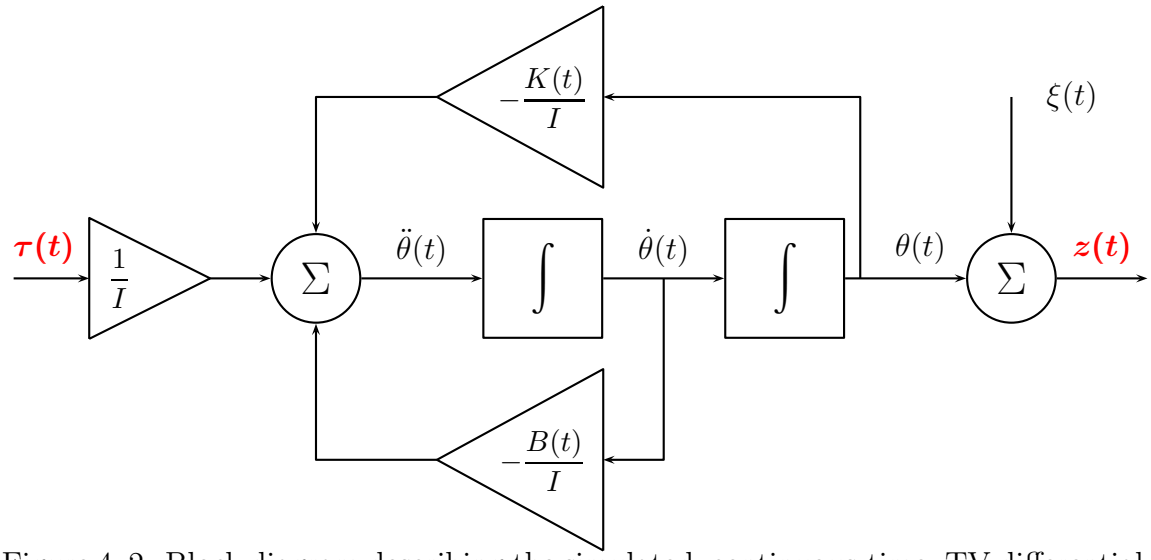

Figure 4–2: Block diagram describing the simulated, continuous-time, TV differential model. The red signals are available for measurements.

time k can be represented by the discrete, TV-BJ model [179]:

$$\theta(k) = \frac{b_0(k)\,(1 + 2q^{-1} + q^{-2})}{1 + a_1(k)q^{-1} + a_2(k)q^{-2}}\tau(k), \tag{4.14}$$

where $b_0(k)$, $a_1(k)$ and $a_2(k)$ are discrete-time, TV parameters. The noise corrupted output can then be expressed as

$$z(k) = \theta(k) + \xi(k), \tag{4.15}$$

where $\xi(k)$ is additive noise.

4.4 Simulation study

4.4.1 Methods

The utility of the new algorithm for the identification of TV joint compliance was evaluated using simulations of human ankle compliance throughout the walking cycle.

The TV, differential equation (4.12) was implemented as shown in Fig. 4–2 and solved numerically using Simulink (MathWorks) to determine the joint position ($\theta(k)$), velocity ($\dot{\theta}(k)$) and acceleration ($\ddot{\theta}(k)$) generated in response to perturbation torque $\tau(k)$. Fig. 4–3 shows the simulated model parameters as a function time. The elastic and viscous parameters varied periodically and the inertial parameter was held constant. The time trajectories during the gait cycle were by obtained interpolating the values reported by Rouse *et. al* [109] and Lee *et. al* [110, 125] at different points through the cycle.

The noise amplitude was adjusted to give an average signal-to-noise ratio (SNR) of 10dB across the record. This SNR is lower than expected experimentally and so it represents a challenge to the identification algorithm [112].

Two types of noise were used in the simulations: (i) white, Gaussian noise, and (ii) experimentally-based noise, derived from a library of experimental signals of ankle torque recorded while subjects maintained a constant torque with fixed ankle position [173]. The library comprised two records, each lasting 120s, from six subjects generating dorsiflexing torques corresponding to 5%, 10% and 15% of their maximum voluntary contractions. For each simulation trial, a section of the recorded torque noise was selected at random, the mean torque was removed and the residual was filtered using the differential, TV model of (4.12) to generate the equivalent, TV position noise signal. Afterwards, a stochastic, white-Gaussian component, representing the measurement noise, was added to the noise sequence. Fig. 4–4 shows examples of these two types of noise, demonstrating their very different characteristics. The top panel show the white-Gaussian noise signal while the bottom panel

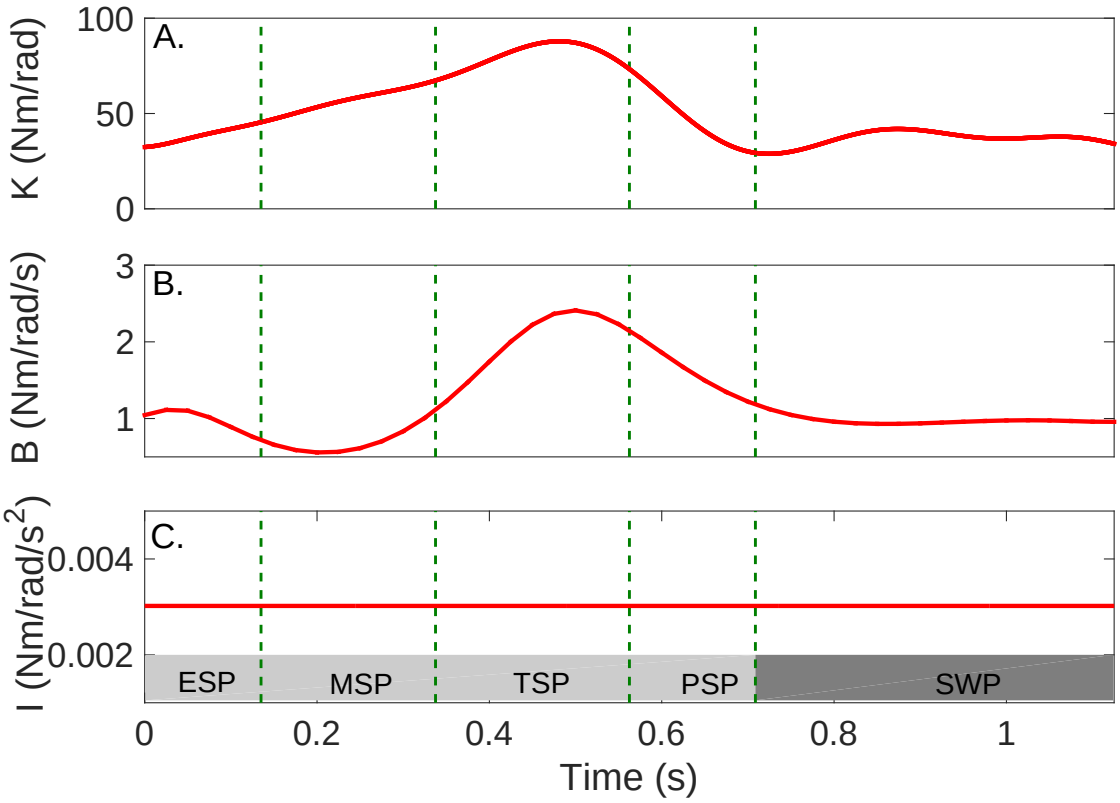

Figure 4–3: Simulated time-varying joint compliance parameters: A) Stiffness , B) viscosity and C) inertia. Vertical lines divide the gait cycle in its sub-phases starting at heel-strike: early stance (ESP), mid-stance (MSP), terminal stance (TSP), pre-swing (PSP), and swing phase (SWP).

shows the experimentally-based noise, composed of experimental data filtered with a TV model (brown line) and a stochastic component.

Simulations were run for durations between 3.375s and 45s, corresponding to 3 until 40 walking cycles with a torque input consisting off a Pseudo-Random Binary Sequence (PRBS) with a peak-to-peak amplitude of 2Nm and a 100ms switching rate. The sampling rate of the simulations was 1kHz and data were decimated to

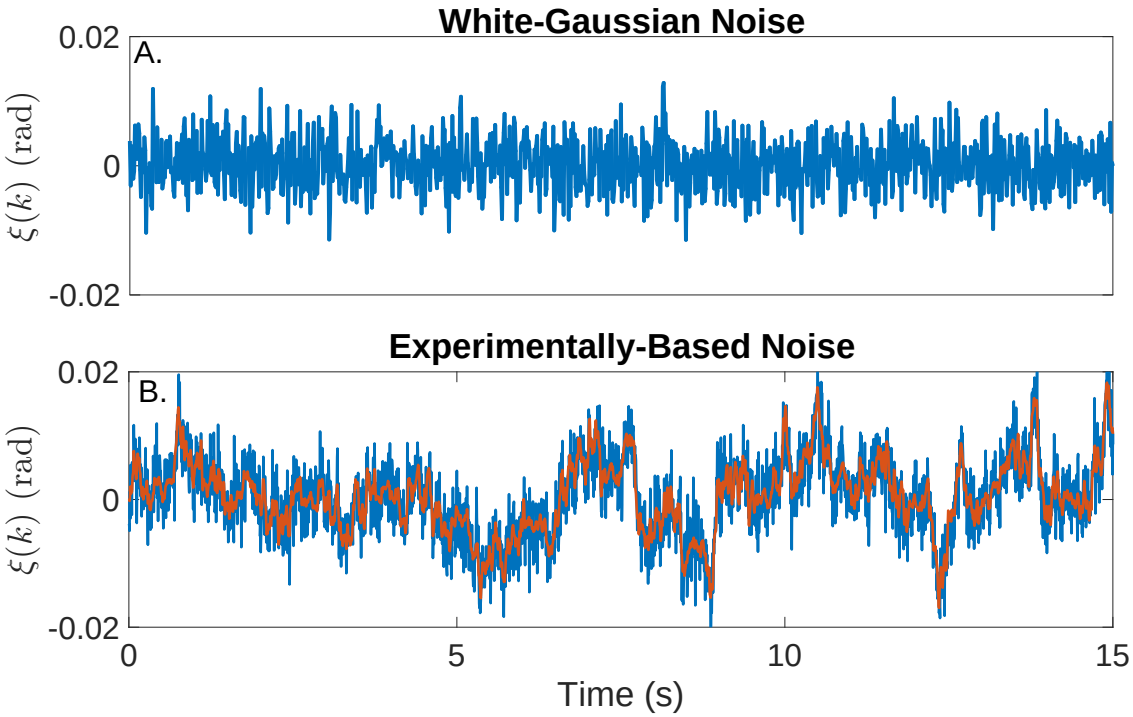

Figure 4–4: Two types of position noise used in the simulations: A) White-Gaussian noise, B) Experimentally-Based noise, composed of experimental data filtered with a TV model (brown line) added to a stochastic, white-Gaussian component (blue line).

200Hz for analysis. Fig. 4–5 shows the torque input ($\tau(k)$), and resulting noise-free and noisy position signals ($\theta(k)$ and $z(k)$) for one cycle of a typical simulation trial.

Each simulation trial comprised two simulation runs using different input realizations. The output of the first run was contaminated with additive noise and used to estimate a TV model; validation was performed using the second run. Monte Carlo experiments comprising 100 trials were used to estimate statistical properties of the estimates.

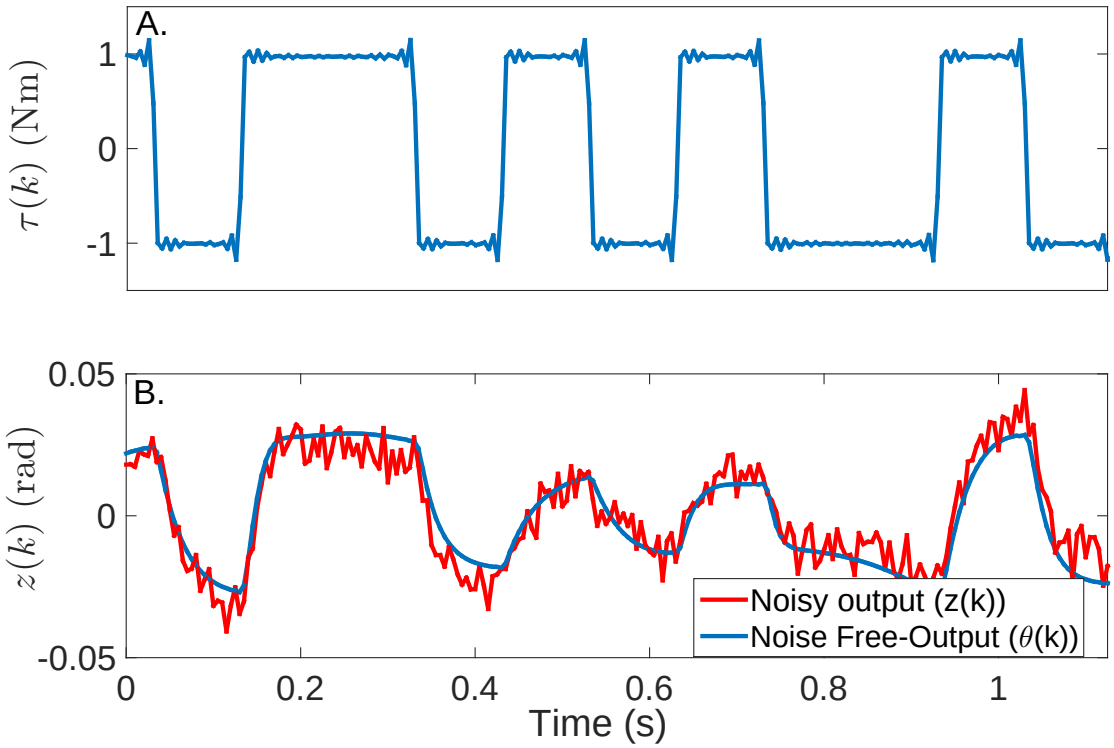

Figure 4–5: Typical simulation results. A) Torque input, B) Position output: Noisy (red line) and Noise-free (blue line).

4.4.2 Parameter Estimation: TV-BJ Model Structure

Algorithm 1 was then used to estimated the discrete-time, TV model parameters and the noise free-output. The noise model was never estimated; it was assumed that $C(q^{-1}) = D(q^{-1}) = 1$ for both types of noise.

Tchebychev polynomials were selected as basis functions because: 1) the polynomial of order 0 is a constant term equal to unity, immediately satisfying the condition imposed to the basis functions (see Section 4.2.1), and 2) their variance is finite in their support, which guarantees that the inverse operation required for parameter

estimation (see eq. (4.6)) will be numerically stable. Tchebychev polynomials of order 0 to 9 were used to represent the three TV parameters resulting a total of 27 parameters to estimate. The number of basis was selected as the minimum order necessary to describe the true TV parameters with a variance accounted for of at least 99%.

4.4.3 Parameter Estimation: TV-ARX Model Structure

For comparison purposes, the TV compliance dynamics were also estimated using a well known, non-iterative, Ordinary Least Squares (OLS) algorithm that estimates the TV parameters of an ARX model of the form [170]

$$z(k) = \frac{b_0(k)\left(1 + 2q^{-1} + q^{-2}\right)}{1 + a_1(k)q^{-1} + a_2(k)q^{-2}}\tau(k) + \frac{1}{1 + a_1(k)q^{-1} + a_2(k)q^{-2}}e(k)$$

This structure assumes that the additive noise, $e(k)$, is a white signal filtered by a system with the same poles as the process plant.

4.4.4 Validation

The predictive ability of model estimates was quantified in terms of the Variance Accounted For (VAF) between the estimated and simulated position for the validation run as:

$$\%VAF = \frac{1}{M}\sum_{m=1}^{M}\left(1 - \frac{\sum_{k=1}^{N}\left(\theta_m(k) - \hat{\theta}_m(k)\right)^2}{\sum_{k=1}^{N}\left(\theta_m(k)\right)^2}\right) \times 100\%,$$

where $\theta_m(k)$ is the noise-free simulated position for trial m and $\hat{\theta}(k)$ is the noise-free predicted position; M is the number of gait cycles and N the number of samples per cycle.

The quality of the parameter estimates was measured in terms of their bias and random errors with respect to the mean estimate in the Monte Carlo simulations, defined as

$$\bar{\hat{b}}_i(k) = \frac{1}{100}\sum_{j=1}^{100}\hat{b}_i(k),$$

where $\hat{b}_i(k)$ is the parameter estimated at each Monte Carlo trial. The bias error at each time k was computed as

$$\epsilon_{b_i}(k) = abs\left(b_i(k) - \bar{\hat{b}}_i(k)\right),$$

where $b_i(k)$ is the true parameter value, and the random error was measured as the standard deviation of the parameter estimates as

$$\sigma_{b_i}(k) = \left[\frac{1}{100}\sum_{j=1}^{100}\left(\hat{b}_i(k) - \bar{\hat{b}}_i(k)\right)^2\right]^{1/2}.$$

Both $\epsilon_{b_i}(k)$ and $\sigma_{b_i}(k)$ are vectors with N samples.

4.4.5 Intrinsic Joint Compliance Parameters

One of the most important aspects of any identification procedure is its the ability to retrieve the physiologically relevant, continuous-time, intrinsic joint compliance parameters: elasticity ($K(k)$), viscosity ($B(k)$) and inertia (I).

The relation between the estimated, discrete-time, model parameters and the continuous-time, intrinsic joint compliance parameters is given by [65]

$$K(k) = \frac{1}{4}\left(\frac{1 + a_1(k) + a_2(k))}{b_0(k)}\right), \tag{4.16a}$$

$$B(k) = \frac{T_s}{4}\left(\frac{1 - a_2(k)}{b_0(k)}\right), \tag{4.16b}$$

$$I(k) = \frac{T_s^2}{16}\left(\frac{1 - a_1(k) + a_2(k))}{b_0(k)}\right), \tag{4.16c}$$

where T_s is the sampling time. It should be noted that the estimated inertia is also TV, however this is an effect created by the discretization step.

4.4.6 Gait Cycle Length and Ensemble Normalization

So far it has been assumed that all the gait cycles in the ensemble have the same length, as this is a requirement of the identification algorithm. However, in practice this is hardly true, as even under controlled experimental settings there is always some degree of variability in the stride length [110]. For an ensemble of gait cycles, this variability can be quantified by the *distortion ratio*, given by

$$Distortion\ Ratio = \left[\frac{1}{M}\sum_{m=1}^{M}\left|\frac{\bar{L} - L_m}{\bar{L}}\right|\right] \times 100\%,$$

where $\bar{L}$ is the average length of the ensemble and L_m the length of each individual cycle. Typically, experiments with healthy subjects present a distortion ratio between 2% and 4% [110, 171]; this value is expected to be larger for patients.

Once the ensemble of gait cycles with different lengths were recorded, they were normalized such that $L_m = \bar{L} = 1.125s$ using the linear time-scaling process described by D. A. Winter [180].

4.5 Results

We first compared the performance of the TV-ARX and TV-BJ methods when used with data records containing 20 cycles.

4.5.1 TV-ARX Model

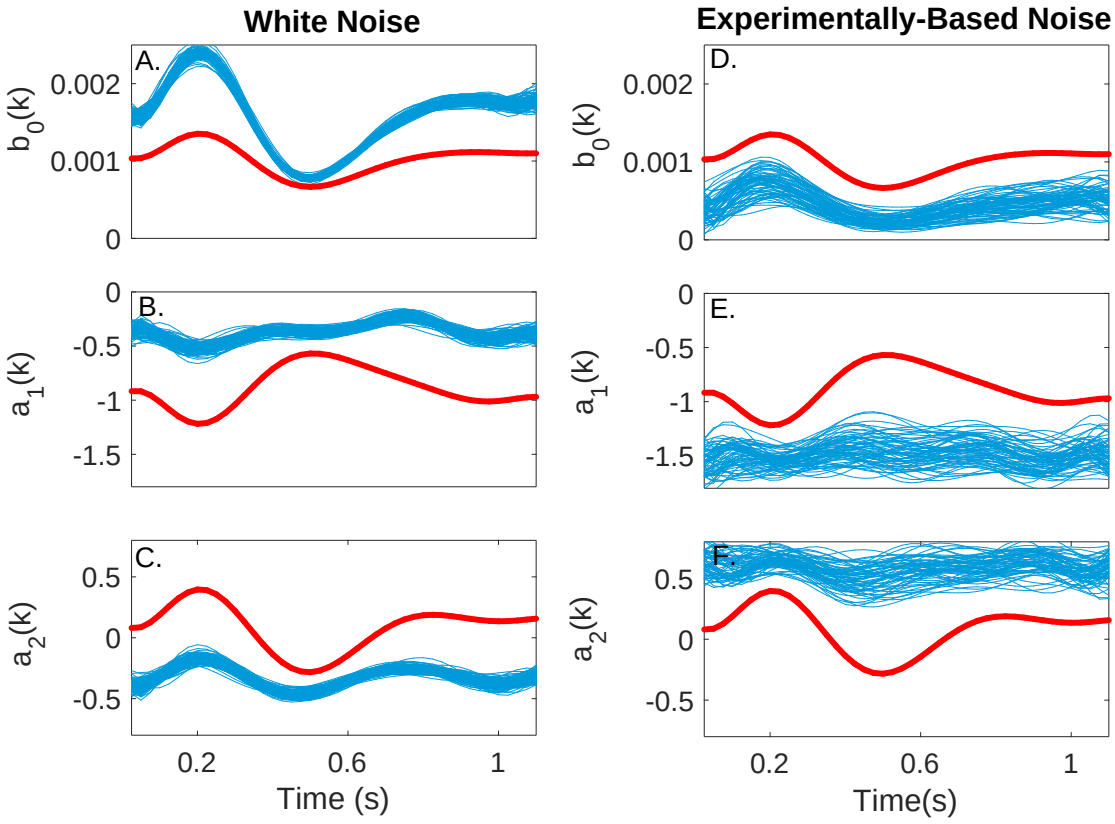

Figure 4–6: TV parameters estimated for the TV-ARX model with white-Gaussian (left column) and experimentally-based (right column) noise. True (red) and estimated (blue) discrete-time, TV parameters for the 100 Monte Carlo simulations.

White-Gaussian noise

The TV-ARX method produced models that predicted the output well with %VAF that were always greater that 99.5%. However, the parameter estimates were

heavily biased as the left column of Fig.4–6 demonstrates. The red lines show the time course of the true model parameters while the blue lines show the estimates from each one of the Monte Carlo trials. It is evident that the time courses of the true and estimated TV parameters were very different in all trials.

Experimentally-Based Noise

For this type of noise TV-ARX method produced a range of models with different predictions abilities. The mean prediction VAF was 94.6% but for some of the Monte Carlo trials it was as low as 87%. The right column of Fig. 4–6 demonstrates that the estimates parameters were very different from the true values.

Fig. 4–7 summarizes the accuracy of the parameter estimates for the two types of noise. In all cases, the TV-ARX estimates had bias errors that were similar in magnitude to the true parameters. The random error was low for white noise but much larger for the experimentally-based noise.

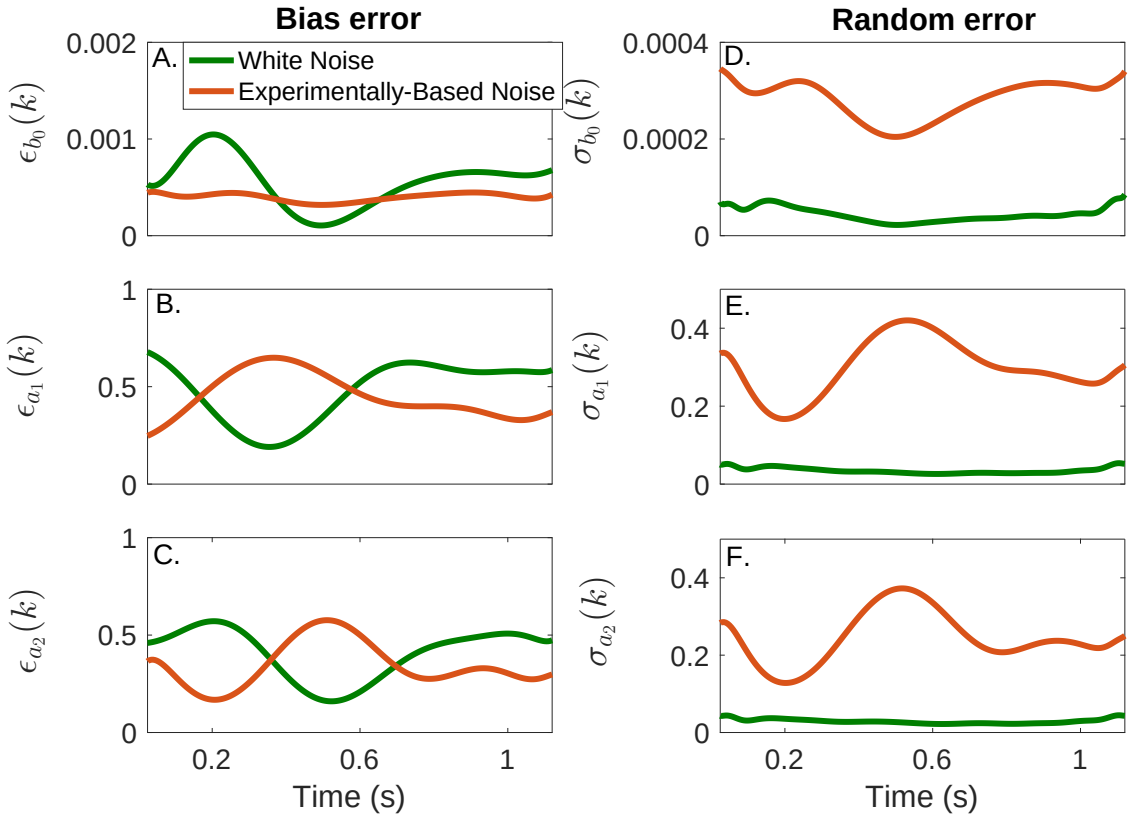

Figure 4–7: Bias (left column) and random (right column) errors for 100 Monte Carlo simulations with the TV-ARX model with white-Gaussian (green lines) and experimentally-based (brown lines) noise. b_0: Top row, a_1: Middle row, and a_2: bottom row.

4.5.2 TV-BJ Model

White-Gaussian noise

The TV-BJ algorithm generated models which predicted the noise free output almost perfectly; the prediction VAF was always greater than 99.9%. Furthermore the left column of Fig. 4–8 demonstrates that the estimated parameters tracked the true values closely with the errors equally distributed around the true values.

Experimentally-Based Noise

The TV-BJ models predicted the noise free output very accurately; the prediction VAF was always greater than 99.9%. The right column of Fig. 4–8 demonstrates that, as happened in the white noise case, the TV parameters were estimated accurately with errors equally distributed around the true values.

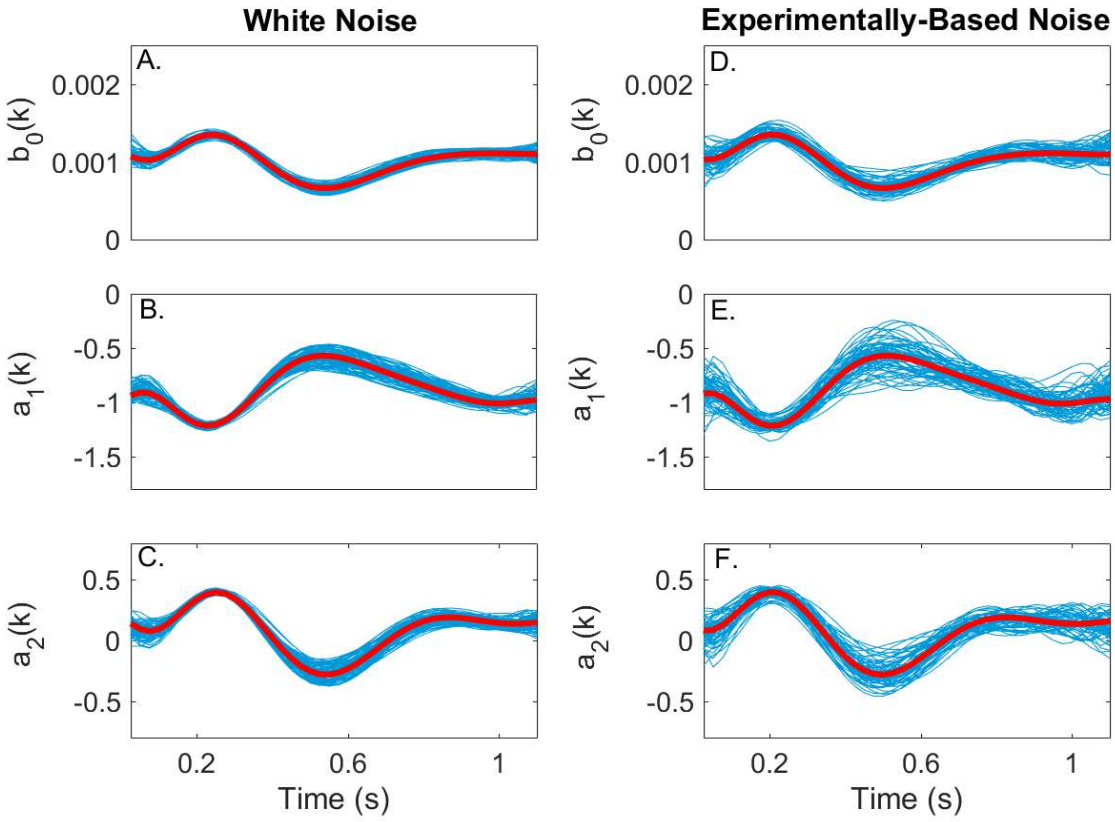

Figure 4–8: TV parameters estimated for the TV-BJ model with white-Gaussian (left column) and experimentally-based (right column) noise. True (red) and estimated (blue) discrete-time, TV parameters for the 100 Monte Carlo simulations.

Fig. 4–9 summarize the accuracy of the parameter estimates for the different types of noise. The bias error obtained with the TV-BJ model were very small

in all the different cases. Furthermore, the bias and random errors obtained with both noise types were very similar, indicating that the estimation results are not significantly influenced by the noise characteristics even though the noise model was not estimated.

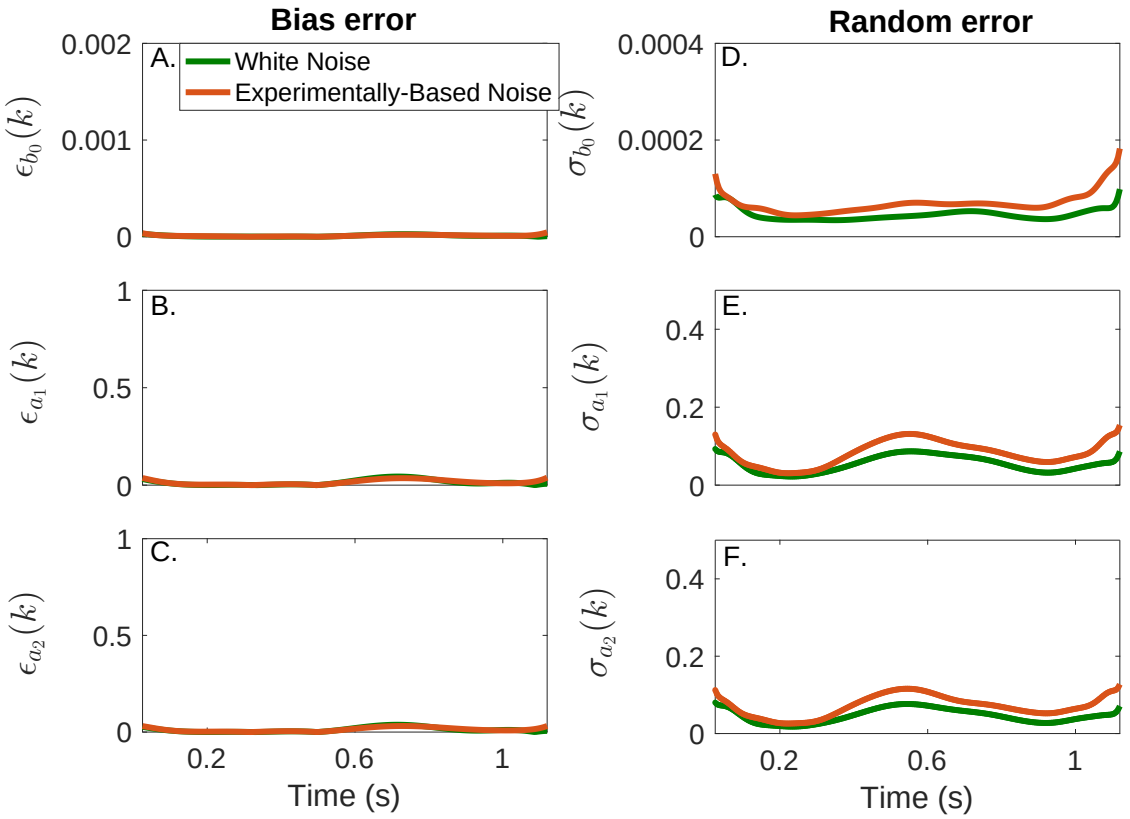

Figure 4–9: Bias (left column) and random (right column) errors for 100 Monte Carlo simulations with the TV-BJ model with white-Gaussian (green lines) and experimentally-based (brown lines) noise. b_0: Top row, a_1: Middle row, and a_2: bottom row.

Table 4–1 summarizes the results; it shows the average over one cycle of the bias and random errors for each parameter, and the $\%\ VAF$ obtained in the Monte Carlo

simulations. The % VAF was close to 100% for TV-BJ estimates with both types of noise and TV-ARX for white noise. However, for experimentally-based noise, the % VAF obtained with the TV-ARX decreased to 94.6%. For all the parameters and both types of noise, the bias error of TV-BJ results were more than an order of magnitude smaller than the TV-ARX estimates. In contrast, the random errors depend strongly on the type of noise. For white noise, TV-ARX results showed the smallest random error and those for the TV-BJ results were only slightly larger. However, for experimentally-based noise, the TV-ARX results presented very large random errors while the TV-BJ results were much smaller and only slightly larger than those observed with white noise.

Table 4–1: Mean of the bias and random errors, and $\%VAF$ for the different model structures and noise types.

	TV-ARX		**TV-BJ**	
	White	Exp-Based	White	Exp-Based
% VAF	99.6	94.6	99.9	99.9
$\epsilon_{b_0} \times 10^{-4}$	5.6	3.9	0.1	0.2
$\epsilon_{a_1} \times 10^{-2}$	51.2	42.3	1.4	1.3
$\epsilon_{a_2} \times 10^{-2}$	41.1	34.5	1.2	1.2
$\sigma_{b_0} \times 10^{-5}$	4.9	28.3	5.1	6.8
$\sigma_{a_1} \times 10^{-2}$	3.6	29.8	5.9	8.2
$\sigma_{a_2} \times 10^{-2}$	3.1	24.4	4.9	7.1

4.5.3 Estimation of Intrinsic Joint Compliance Parameters

The results presented in Figs. 4–6 and 4–8 for the experimentally-based noise were used with eq. 4.16a-4.16c to estimate the TV intrinsic joint compliance parameters; these results are summarized in Fig. 4–10 for the TV-ARX (left column) and

TV-BJ (right column) model structures. The range of each panel was adjusted to properly display the data and facilitate the comparison of the results.

The right column of Fig. 4–10 demonstrates that the results obtained with the TV-ARX algorithm were very variable. The estimated elasticity (K) and viscosity (B) were close to the true value for a few of the Monte Carlo trials but very different for others. On the other hand, the inertia (I) was always biased.

The left column of Fig. 4–10 demonstrates that the estimated parameters with the TV-BJ algorithm tracked the true values closely with small errors located around the areas that presented large changes.

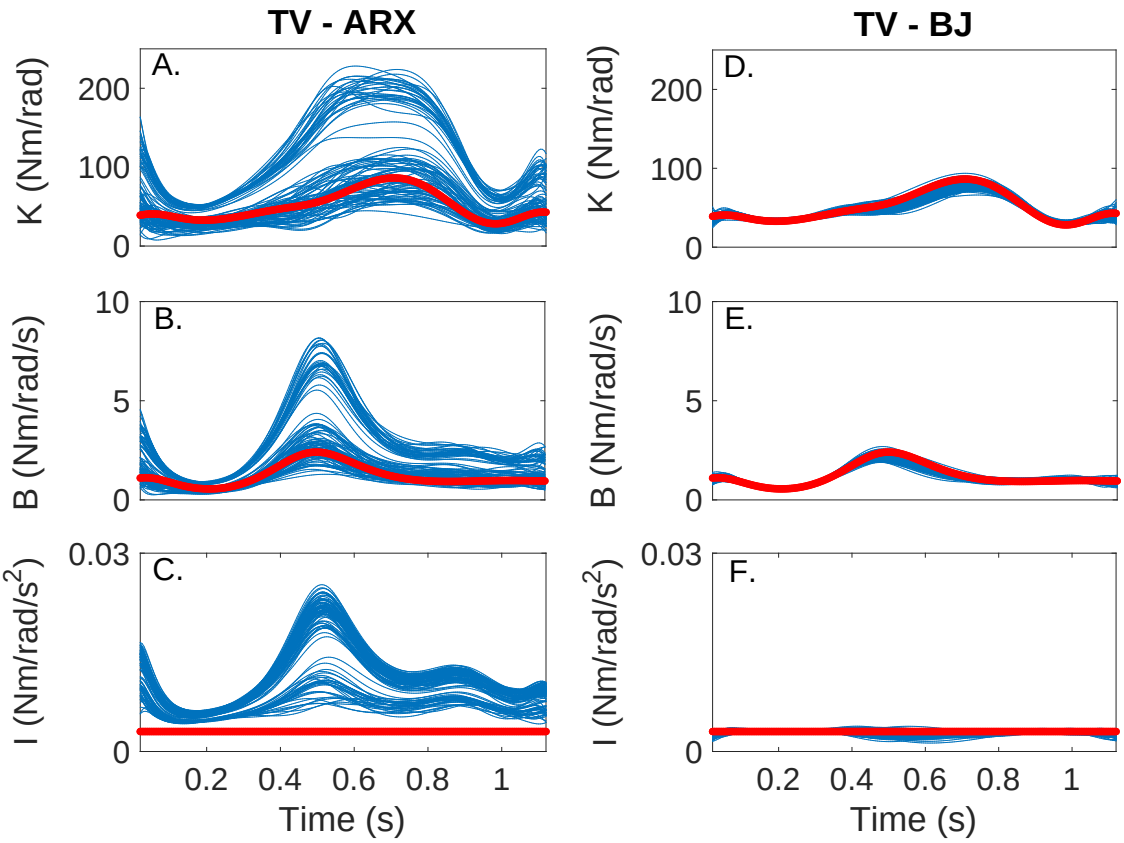

Figure 4–10: TV, intrinsic joint compliance parameters estimated with the the TV-ARX (left column) and TV-BJ (right column) model structures. Results were obtained only for experimentally-based noise. True (red) and estimated (blue) parameters for the 100 Monte Carlo simulations. The range of each panel was adjusted to properly display the results.

4.5.4 Effect of the Number of Trials

To examine the effect of the number of trials on the parameters estimates, the simulation and identification procedures were repeated using different record lengths. Only experimentally-based noise was used since it represents the biggest challenge to the identification algorithm.

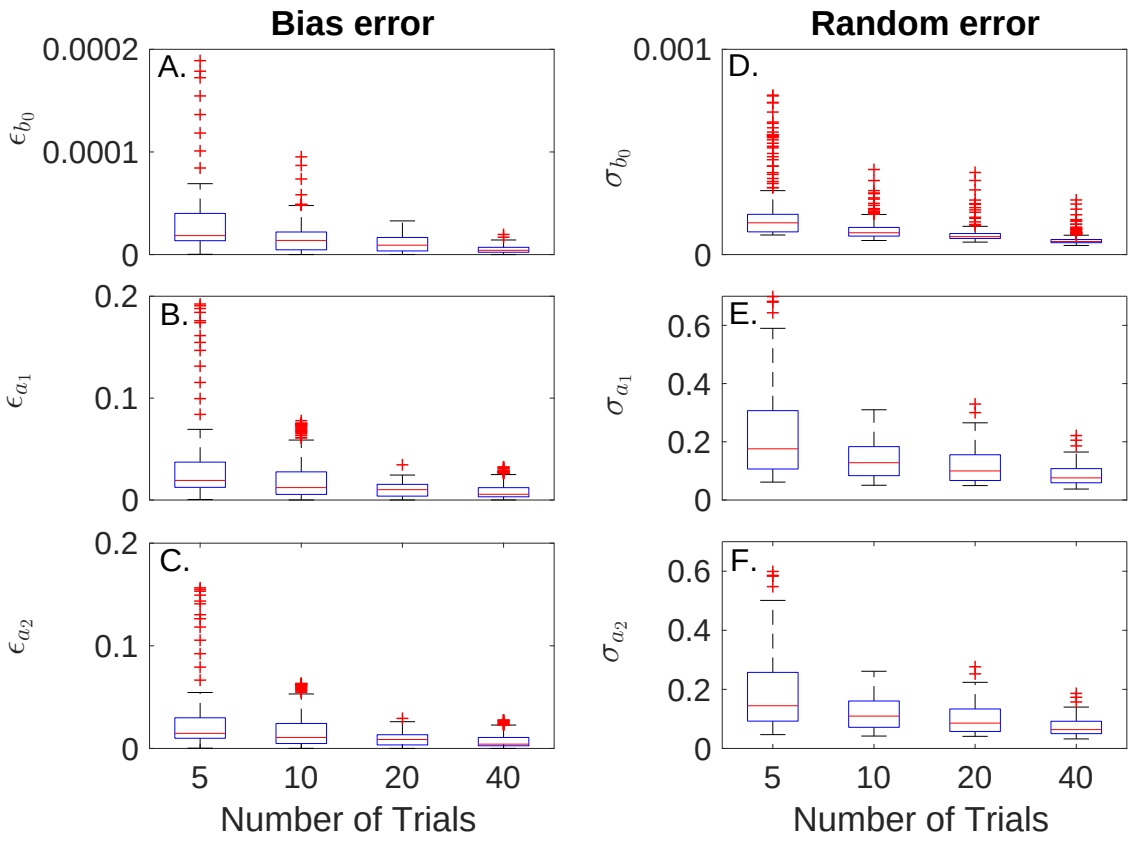

Figure 4–11: Bias and random errors of the parameter estimates computed for the 100 Monte Carlo simulations using the TV-BJ model with experimentally-based noise as a function of the number gait cycles. A. ϵ_{b_0}, B. ϵ_{a_1}, C. ϵ_{a_2}, D. σ_{b_0}, E. σ_{a_1}, and F. σ_{a_2}.

Fig. 4–11 shows the bias and random errors for each parameters as a function of the number of trials. To facilitate the comparison between cases, the bias and random error, which are time sequences with N samples, are presented as box-plots. The median of the signal is presented with a red line, the extremes of the blue box indicate the 25th and 75th percentiles, respectively. The black lines extend to cover the data points not considered outliers and the outliers are plotted using red crosses.

A minimum of five cycles of data were required to obtain reliable results, fewer cycles produced unstable models for some of the Monte Carlo trials. The bias error and random error decreased progressively as the number of cycles increased. However, increasing from 20 to 40 cycles did not show significant reduction in the bias error but there was a noticeable decrease in the parameters variability. The %VAF was similar to that obtained with 20 cycles even with 5 trials.

4.5.5 Effect of Ensemble Normalization

Finally, to examine the effect that the time normalization has on the parameters estimates, the simulation and identification procedures were repeated using ensembles of 20 gait cycles with different length. For this, the length of each cycle was drawn from a Gaussian distribution with mean 1.125s and variance adjusted to obtain distortion ratio between 0% and 9%; for a distortion ratio of 9% the cycles length varied between 0.9s and 1.35s. Once the length of each cycle was defined, the joint compliance parameters of Fig. 4–3 were time-scaled to fit the selected duration of each cycle. Afterwards, the parameters were concatenated and the intrinsic joint compliance model was simulated. Experimentally-based noise was added to the simulated output and data was divided into individual cycles.

Each cycle of input and output data was normalized to the average length of the ensemble using a linear time-scaling process [180]; the normalized data was used for parameter estimation.

Table 4–2 presents the results obtained for different distortion ratios; the TV-ARX results with a distortion ratio of 0% are also included for comparison. These results indicate that the time-normalization process does not severely affects the

Table 4–2: Mean of the bias and random errors, and $\%VAF$ as a function of distortion ratio for the different model structures and Experimentally-bases noise.

	Distortion Ratio					
	0%		3%	5%	7%	9%
	TV-ARX	TV-BJ	TV-BJ			
$\% \ VAF$	94.6	99.9	99.9	99.9	99.8	99.6
$\epsilon_{b_0} \times 10^{-4}$	3.9	0.2	0.3	0.3	0.4	0.4
$\epsilon_{a_1} \times 10^{-2}$	42.3	1.3	3.7	3.3	4.8	6.2
$\epsilon_{a_2} \times 10^{-2}$	34.5	1.2	3.2	3.2	4.2	5.3
$\sigma_{b_0} \times 10^{-5}$	28.3	6.8	10.6	12.2	13.6	13.7
$\sigma_{a_1} \times 10^{-2}$	29.8	8.2	13.0	13.3	14.7	15.5
$\sigma_{a_2} \times 10^{-2}$	24.4	7.1	11.2	11.9	12.6	13.2

$\%VAF$. In contrast, it has a negative effect in both the bias and random errors for all the estimated parameters and that this effect increases with the distortion ratio; a five fold increase in the bias error was observed in the worst case scenario (ϵ_{a_1}). However, even for a distortion ratio of 9% the mean of the bias and random errors obtain with the TV-BJ algorithm were significantly smaller than those obtained with the TV-ARX algorithm for a distortion ratio of 0%.

4.6 Discussion

This paper presents a method for the identification of time-varying intrinsic joint compliance from periodic data segments of short duration using a predefined set of basis functions. This technique estimates the TV parameters of a discrete-time, TV-BJ model and is capable of tracking large, rapid changes in dynamics with no a priori assumption about the noise model dynamics.

4.6.1 Original contributions

This study makes three main contributions:

TV, Intrinsic Joint Compliance

First, this paper presents a new method to quantify intrinsic joint compliance during walking from as few as 5 gait cycles. There is an increased interest in estimating joint compliance during walking [109, 110, 125] as this might help in the design and control of biomimetic prostheses and orthoses [18], the characterization of neuromuscular diseases and lesions [181], and the improvement of electrical stimulation systems aimed at improving or restoring the gait cycle by providing a better description of the relation between joint torque and position [182, 18]. However, the system identification techniques used to date require many (more than 100) trials and assume that: i) the noise added to the output is white and ii) the model parameters remain unchanged during short segments (approximately 100 ms). Our novel algorithm improves over those methods by relaxing these limitations, providing accurate estimates of the intrinsic joint compliance during the gait cycle with short data records.

Our simulation study showed that even with high levels of experimentally-based noise the algorithm only requires 5 gait cycles to yield unbiased estimates of the model parameters; these good results are robust to the time-normalization required when the cycles in the ensemble have different lengths. In addition, our algorithm estimates a new value for the parameters at each sampling interval, effectively computing the parameters time course instead of averages over short time windows. This facilitates the analysis of the parameters variation with time and permits the temporal localization of large changes in the system dynamics. Therefore, our algorithm provides better estimates of joint compliance with less data than previous methods.

Modeling of Biomedical Systems

Second, we demonstrated that the Box-Jenkins model structure is appropriate to describe the intrinsic joint compliance, a TV, biomedical system with complex, non-white additive noise. In general, this model structure can be useful to model any biological system with (approximate) linear dynamics. We showed that selecting simpler model structures, that do not include an independent parametrization of the process and noise plants, to describe biomedical systems can lead to a models with good predictive ability but with biased parameters estimates, which might hamper any possible physiological insight that can be gain from this analysis.

Consequently, the methodology presented here can be applied to model the input-output relation of any biomedical system whose TV dynamics can be well described by a linear system.

Use of Experimentally-Based Noise for Validation of Identification Algorithms

Third, this study makes use of two types of noise for the validation of the proposed algorithm: (i) white-Gaussian noise, and (ii) experimentally-based noise. Our simulation results demonstrated that using only white-Gaussian noise to validate the identification algorithm might falsely overestimate the estimator accuracy. This was observed with the TV-ARX algorithm; the white-Gaussian noise results provided a %VAF close to 100% for all the trials, indicating that the parameters might be correctly estimated. However, the experimentally-based noise results presented a significantly lower %VAF, concurrent with the biased parameter estimates. In contrast, results obtained with the TV-BJ algorithm were equally good for both types of noise, indicating that the estimator should provide accurate results with experimental data.

Ideally, the simulation study should have used experimental noise recorded during walking. Unfortunately, we do not have access to such records and are unaware of any publicly available data base. Nevertheless, we believe that the experimentally-based noise used in this simulations provides a good test for the identification algorithm because: i) the experimentally-based noise is a complex noise signal based on torque measurements whose frequency content is similar to that of the system of interest, ii) the signal contains a physiological, colored-noise and an instrumental, white-noise components, which is characteristic of the noise encountered in physiological system, iii) the signal properties change as a function of the gait cycle, which is expected from the experimental noise measured during walking, and iv) the selected SNR (10dB) is much larger than that expected experimentally.

4.6.2 Limitations

The results presented here were obtained under the assumption that reflex contributions are small and can be ignored; though this assumption seems to be valid for healthy subjects during walking [109, 110], it might not hold for patients suffering of spasticity, which present exaggerated reflex responses [17]. In that case, the changes in position due to the torque perturbations will excite the stretch reflex mechanism, which will produce an additional joint torque that will result in changes of joint position. Hence, the system will behave as a closed-loop system with the feedforward and feedback pathways composed by the intrinsic compliance and reflex stiffness respectively. The algorithm described here cannot be used in such situations to estimated the intrinsic joint compliance as it requires knowledge of the torque perturbation and the feedback signal. However, it is possible to use this algorithm in

combination with a method that we recently introduced for the identification of TV stretch reflex dynamics [179], along with a multi-step method for the identification of closed-loop systems [183, 101] to estimate both the intrinsic and reflex components of joint compliance.

The algorithm assumes that the movement is periodic and takes advantage of this to overcome the lack of initial conditions. There different sources or experimental errors that may affect the periodicity of the movement and induce errors in the parameters estimates. For example, there might be a poor detection of the beginning of the cycle, causing the trials in the ensemble to be out of phase, in addition, each cycle might have a slightly different duration, generating an ensemble with elements of varying length. We showed that the algorithm still provides unbiased estimates when the movements are not perfectly periodic and there is large variability in the cycle length. However, these experimental errors should be reduced as much as possible to minimize the estimation errors. In addition, the algorithm can still be used with minimum changes in situations where the movement is non-periodic but the time-varying behavior is the same in each trial of the ensemble (e.g. a ramp-and-hold movement). However, the initial conditions will be unknown in this situation and this will have a negative effect in the parameter estimates.

Finally, in this study, the continuous-time, TV, differential model of joint compliance was approximated by a set of (frozen) discrete-time equations at each sample interval by assuming a *zero-order-hold* discretization in the model parameters (i.e, it is assumed that the parameter value is constant for the duration of the sample interval). Several other approaches for the discretization of TV systems exist and their

advantages and drawbacks were analyzed in [184]. He concluded that the *zero-order-hold* discretization is adequate to represent TV systems when the parameters values are instantaneous function of time (i.e, the current parameters value only depends on the current time, not on past or future time values), when this assumption is violated, other discretization techniques should be used. The excellent results of our simulation study demonstrate that the zero-holder-hold approximation is adequate for the continuous-time model of joint compliance.

CHAPTER 5
Identification of Time Varying, Intrinsic, Dynamic Ankle Stiffness during Passive, Imposed Walking Movements

Authors: Diego L. Guarin and Robert E. Kearney

Journal: Submitted to - IEEE Transactions on Neural Systems and Rehabilitation Engineering

Year: 2016

Chapter 4 introduced a new method for the estimation of linear, time-varying, transfer function models. This model structure provides parsimonious representation of system dynamics; but requires the model order to be defined *a priori*, which can be difficult for complex, biological systems. An alternative is to describe the systems dynamics using a non-parametric model, which requires no information about the system order. However, current algorithms for estimation of time-varying, non-parametric model parameters require hundreds of input-output data segments presenting the same time-varying behavior. These large data set are very difficult to obtain in practice, which severely limits the applications of these algorithms. This chapter develops and validates a new algorithm for the identification of linear, time-varying, non-parametric model parameters using only a few periodic, input-output data segments of short duration. The new method represents a significant improvement over previous algorithms as the reduction in data requirements implies shorter experiments which makes it much easier to acquire enough trials with the same TV

behavior. This algorithm was used to estimate the fast, large changes in intrinsic ankle stiffness, during an imposed walking movements. Results were obtained with as few as 20 gait cycles, while previous studies that used classical algorithms require more than 600 gait cycles for parameter estimation.

Abstract

The mechanical properties of a joint, determined by the intrinsic and reflex mechanisms, play a vital role in the control of posture and movement. However, under passive conditions, the intrinsic mechanisms, defined by the dynamic intrinsic stiffness, play the dominant role. Passive, intrinsic dynamic stiffness defines the relation between joint position and torque; for small variations about a fixed operating point, it can be modeled as a linear system. However, the intrinsic stiffness parameters depend strongly on the operating point. Thus, for functional activities, where position and torque undergo large, rapid changes, the model parameters will appear to be Time-Varying (TV). This paper introduces a novel, non-parametric, system identification method to estimate TV intrinsic dynamic stiffness. The algorithm combines ensemble and deterministic approaches to estimate TV parameters from periodic, input-output data segments of short duration. In this study, the passive intrinsic stiffness of four subjects was estimated during imposed walking movements. The identified TV models predicted the measured output very well, accounting for 94 $\pm$ 2 % of the measured torque variance. The estimated visco-elastic properties of the ankle changed greatly through the gait cycle; passive joint stiffness increased at least four fold between heel-strike and terminal stance phase, and then sharply decreased from pre-swing to swing phase. These results suggest that the modulation in passive, intrinsic mechanisms provides higher stability of the ankle joint during the weight bearing portion of the gait cycle.

5.1 Introduction

The human ankle produces most of the mechanical power generated during the stance phase of walking. The ankle plantarflexors contribute as much as half of the mechanical power needed for walking, help to mobilize the leg during the swing phase, and promote the ankle flexion necessary for toe-off [185]. Moreover, ankle dorsiflexors help to absorb impact forces during heel-strike which might otherwise destabilize the body [186, 187]. Thus, the ankle joint is critical for propulsion, shock absorption and balance during walking so that understanding its mechanical properties is pivotal for the development of ankle–foot prostheses and orthoses, and to gain better insight into neuromuscular diseases that affect function.

The joint mechanical properties may be defined by the *dynamic joint stiffness*, which relates unexpected joint position disturbances to the involuntary torque response [12]. It is composed of intrinsic and stretch reflex components, which for small perturbations around a fix operating point can be represented by a linear and Hammerstein systems acting in parallel [12, 188, 1].

Early studies in the identification of joint dynamic stiffness from position and torque data focused on stationary, non-moving conditions; they showed that the model parameters depend strongly on the operating point, defined by joint position, torque and other factors [70, 52, 189, 11, 64]. Therefore, when the joint position and torque vary significantly with time, as during walking, stiffness model parameters will be time-varying (TV). However, a literature review revealed relatively few studies that attempted to characterize ankle dynamic stiffness during TV conditions [106,

107, 112, 103, 113, 105, 110, 109, 18]. A major finding is that the results from static experiments cannot be interpolated to describe the behavior during TV situations.

With the advent of powered ankle prostheses and orthoses there is now a necessity of characterizing the intrinsic dynamic ankle stiffness throughout the gait cycle so that biomimetic devices can be designed. Recent studies have introduced novel methodologies to do so [18, 110, 109]. However, these studies demonstrate some important analytical challenges that this research field is currently facing. Fist, the ensemble based approach used in these studies for TV identification requires hundreds of input-output trials showing the same TV behavior to accurately estimate the parameters [106, 108]. This is time consuming and difficult to achieve experimentally, which greatly limits the application of these methods to pathological subjects. Second, these studies estimate the average model parameters over short time windows, which may produce large estimation errors when parameters change rapidly.

This paper deals with the identification of intrinsic, ankle dynamic stiffness during passive, imposed movement. These movements comprised the sum of the ankle trajectory during walking and small, high-frequency position perturbations. A novel TV identification method, that estimates the model TV parameters from periodic, input-output data segments, was developed and used to estimate the TV, intrinsic ankle dynamic stiffness throughout the imposed walking movement.

This paper is organized as follows: Section 5.2 presents the experimental protocol and describes the measured data. Section 5.3 introduces the model used to describe the TV, intrinsic, dynamic ankle stiffness and the system identification algorithm. Section 5.4 presents estimated passive, TV, dynamic ankle stiffness for

the four subjects and compares these results with those obtained in stationary experiments. Finally, Section 5.5 discusses the results and compares them with other studies. Possible applications of this method are also presented and the algorithm's limitations are discussed.

5.2 Experimental Methods

5.2.1 Subjects

Four healthy subjects (one female), aged 25 to 31 years, participated in this study. The experimental procedures were approved by the McGill University Research Ethics Office and subjects gave informed consent.

5.2.2 Experimental protocol

Subjects lay supine with their left foot attached to the pedal of an electrohydraulic actuator operating as a position servo by means of a custom made fiberglass boot so that ankle movement was restricted to plantarflexion and dorsiflexion.

Ankle position, torque, and surface EMG from the medial and lateral gastrocnemius (GM and GL), soleus (SOL) and tibialis anterior (TA) were filtered at 400Hz by an anti-aliasing filter and sampled at 1kHz by a 16-bit A/D converter. Surface EMG electrodes were placed according to the SENIAM recommendations [190].

The subjects' ankle angle was moved to the zero position (i.e, a right angle between the foot and shank) and held there for at least one minute. Then, a movement consisting of 50 gait cycles, each lasting 1s, summed with a Pseudo Random Binary Sequence (PRBS) perturbation whose amplitude and switching rate were 0.035 rad and 150 ms, was applied. The subject was instructed to remain relaxed and not react to the movement, this was monitored using the EMG signals. The experiment

was repeated 3 times, each with a new perturbation signal, to obtain a total of 150 perturbed gait cycles. The red lines in Fig. 5–1 show the ankle position and torque for one gait cycle; the blue lines show the average over the 150 cycles.

A stationary experiment was performed with one subject. In this experiment, the imposed ankle movement comprised only of the PRBS perturbation. Trials lasting 30s were applied at joint positions from -0.2 rad to +0.2 rad with increments of 0.05 rad.

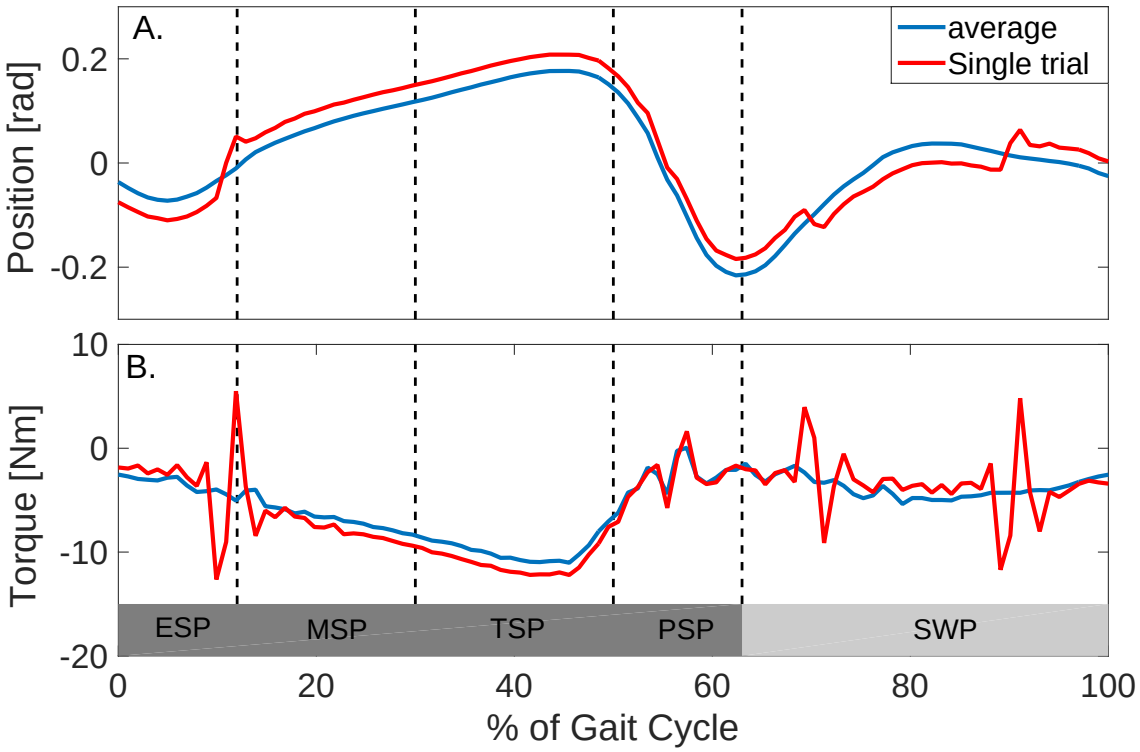

Figure 5–1: A. Ankle trajectory and B. Torque. Red lines show a typical single trials and blue lines show average over 150 cycles. The vertical lines indicate the phases of the gait cycle starting from heel-strike: early stance (ESP), mid-stance (MSP), terminal stance (TSP), pre-swing (PSP) and swing phase (SWP).

5.3 Analytical Methods

5.3.1 Time-varying, intrinsic, dynamic joint stiffness

In general, the relation between joint position and torque can be formulated as [106]:

$$\tau(t_k) = f\left(\theta(t_k), \dot{\theta}(t_k), t_k\right) + I\ddot{\theta}(t_k), \tag{5.1}$$

where $f(\theta(t_k), \dot{\theta}(t_k), t_k)$ is a TV, nonlinear function that describes the net moment due to the viscoelastic properties of the muscle and connective tissue, and stretch reflex feedback; and I is the joint inertia. However, stretch reflexes are usually small for relaxed muscles so that the relation between joint position and torque will be approximated only by its intrinsic component [189, 11].

To estimate joint dynamic stiffness during a large movement small position perturbations must be applied on top of the joint trajectory [75]. Thus, the overall ankle movement is given by:

$$\theta(t_k) = \theta_0(t_k) + \theta_p(t_k),$$

where $\theta_0(t_k)$ is the joint trajectory and $\tau_p(t_k)$ the small position perturbations. We will assume that the overall response is given by:

$$T(t_k) = \tau_0(t_k) + \tau_p(t_k) + \xi(t_k).$$

Which corresponds to the linear combination of the individual responses to the large joint displacements ($\tau_0(t_k)$), the small perturbations ($\tau_p(t_k)$), and an additional term that represent the non-linear effects of applying both movements together ($\xi(t_k)$).

This model differs from previously used models [70, 20, 106, 191, 110, 109] in that it introduces the additional torque component $\xi(t_k)$.

The large joint trajectory and the produced torque, $\theta_0(t_k)$ and $\tau_0(t_k)$, can be estimated by averaging the cycles because $\theta_p(t_k)$ and is zero mean. In contrast, the small, random position perturbation signal is a persistently exciting input and the intrinsic torque that it generates can be well approximated by a linear, dynamic model [188, 1, 12]. The intrinsic, dynamic joint stiffness can then be described by the TV, non-parametric model [110, 107, 112]

$$\tau_p(t_k) = \sum_{k=-L}^{k=L} h(k, t_k)\theta_p(t_k - k), \tag{5.2}$$

where L is the system memory and $h(k, t)$ are elements of a TV Impulse Response Function (IRF).

The torque signal $\xi(t_k)$ depends on nonlinear interactions between the joint trajectory and the small position perturbations. In general, it is expected that this component will be non-zero mean during the gait cycle. Therefore, estimates of intrinsic stiffness will be biased unless $\xi(t_k)$ is removed [136]. This component will be described using cubic B-splines with nodes uniformly distributed across the gait cycle [192], that is:

$$\xi(t_k) \approx \sum_{i=0}^{M} \beta_i B_i\left(t_k\right), \tag{5.3}$$

where β_i are weights and $B_i(t_k)$ the cubic B-splines shown in Fig. 5–2.

5.3.2 Parametrization of TV stiffness model

This section describes the parametrization of the TV, intrinsic, dynamic joint stiffness model. For this, the elements of the TV-IRF in (5.2) are approximated by

a linear combination of basis functions as

$$h\left(k,t_k\right)=\sum_{m=0}^{Q}\gamma_{k,m}B_m\left(t_k\right), \tag{5.4}$$

where $\gamma_{k,i}$ are unknown weights and $B_m(t_k)$ are cubic B-splines. Using this parametrization, the input-output becomes

$$\tau_p(t_k)=\sum_{k=-L}^{L}\sum_{m=0}^{Q}\gamma_{k,m}\theta_{p,m}(t_k-k), \tag{5.5}$$

where

$$\theta_{p,m}(t_k-k)=B_m\left(t_k\right)\theta_p(t_k-k).$$

This procedure transforms the TV identification problem into a time-invariant (TI) problem having additional parameters.

The TI system can be expressed in vector format as the data equation for N samples

$$\boldsymbol{\tau}_p=\boldsymbol{\Theta}_p\boldsymbol{\gamma}, \tag{5.6}$$

where

$$\boldsymbol{\tau}_p=\left[\tau_p(1),\ \cdots\ \tau_p(N)\right]^T,$$
$$\boldsymbol{\gamma}=\left[\gamma_{-L,0},\ \cdots\ \gamma_{-L,Q}\ \cdots\ \gamma_{L,0},\ \cdots\ \gamma_{L,Q}\right]^T,$$

and $\boldsymbol{\Theta}_p$ is

$$\boldsymbol{\Theta}_p=\begin{bmatrix}\theta_{p,0}(1+L) & \cdots & \theta_{p,Q}(1+L) & \cdots & \theta_{p,0}(1) & \cdots & \theta_{p,Q}(1) & \cdots & \theta_{p,0}(1-L) & \cdots & \theta_{p,Q}(1-L)\\ \vdots & \ddots & \vdots & \ddots & \vdots & \ddots & \vdots & \ddots & \vdots & \ddots & \ddots\\ \theta_{p,0}(N+L) & \cdots & \theta_{p,Q}(N+L) & \cdots & \theta_{p,0}(N) & \cdots & \theta_{p,Q}(N) & \cdots & \theta_{p,0}(N-L) & \cdots & \theta_{p,Q}(N-L)\end{bmatrix}$$

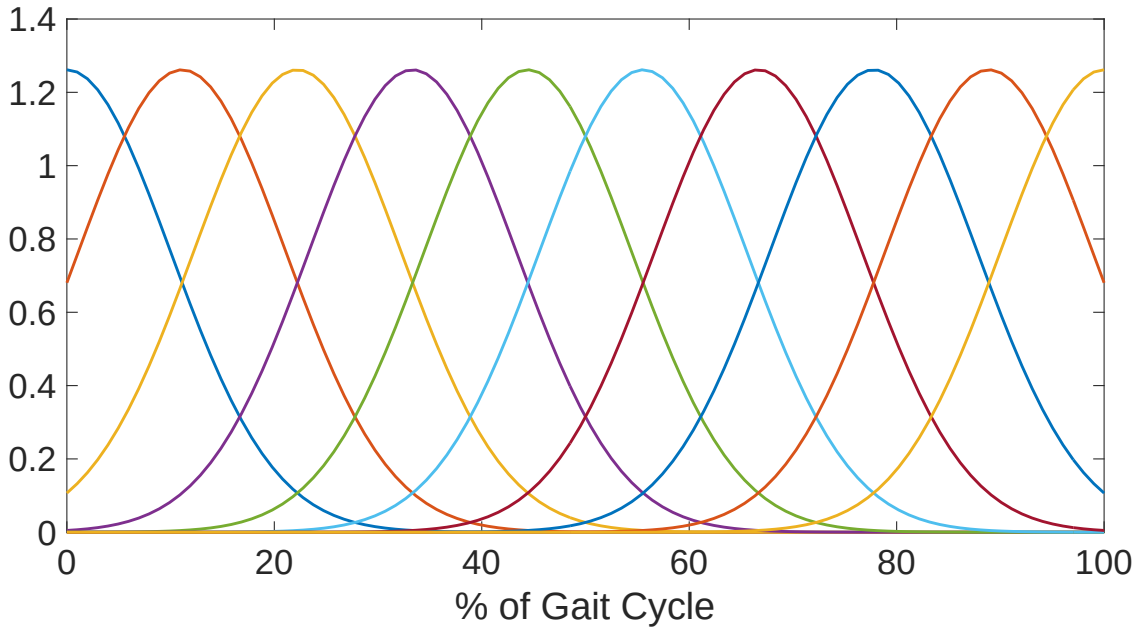

Figure 5–2: Cubic-Splines basis functions used to represent the time-varying parameters as a function of gait cycle.

The parameter set $\boldsymbol{\gamma}$, which defines the TV, IRF elements, can be estimated using this equation and the measured joint position and torque. However, as the duration of the gait cycle is short and changes in the model parameters large and fast, estimating TV, joint intrinsic stiffness from a single gait cycle will provide unreliable estimates. This limitation can be addressed by using an ensemble of gait cycles, each showing the same TV behavior, to refine the parameter estimates.

Using this parametrization, the relation between an ensemble of joint position perturbations and the resulting torques for different gait cycles can be expressed as

$$\begin{bmatrix} \boldsymbol{\tau}_p\{1\} \\ \vdots \\ \boldsymbol{\tau}_p\{n\} \end{bmatrix} = \begin{bmatrix} \boldsymbol{\Theta}_p\{1\} \\ \vdots \\ \boldsymbol{\Theta}_p\{n\} \end{bmatrix} \boldsymbol{\gamma}, \tag{5.7}$$

where n is the number of gait cycles, $\boldsymbol{\tau}_p\{j\}$ is a $[N \times 1]$ vector, $\boldsymbol{\Theta}_p\{j\}$ is a $[N \times (2L+1)]$ matrix, and $\boldsymbol{\gamma}$ is a $[(2L+1) \times 1]$ vector.

Parameter Estimation

Eq. (5.7) is linear in the parameters so we implemented the well known Bayesian, linear regression algorithm known as the *relevance vector machine* in Matlab (Mathworks) and used it for parameter estimation. This is an iterative algorithm that assumes a non-restrictive, Gaussian prior for each parameter. The prior is then updated using the measured data and an Expectation-Maximization algorithm [147, 143].

5.3.3 Identification of passive, dynamic ankle stiffness during an imposed walking movement

Measured joint position and torque data were divided in individual cycles, each starting at heel-strike. The average position and torque signals, $\theta_0(t_k)$ and $\tau_0(t_k)$, were computed as the ensemble average and removed from the measured data to obtain $\theta_p(t_k)$ and $\tau(t_k)$; the blue lines in Fig. 5–3 present these signals for one gait cycle. The acceleration produced by the perturbations was computed and the inertial torque due to the boot and electrohydraulic actuator was computed and subtracted

from the torque. After these steps, the torque signal for the n gait cycles becomes

$$\begin{bmatrix} \boldsymbol{\tau}\{1\} \\ \vdots \\ \boldsymbol{\tau}\{n\} \end{bmatrix} = \begin{bmatrix} \boldsymbol{\tau}_p\{1\} \\ \vdots \\ \boldsymbol{\tau}_p\{n\} \end{bmatrix} + \begin{bmatrix} \boldsymbol{\xi}\{1\} \\ \vdots \\ \boldsymbol{\xi}\{n\} \end{bmatrix}, \tag{5.8}$$

where

$$\boldsymbol{\tau}_p\{j\} = [\tau_p(1)\{j\},\ \cdots\ \tau_p(N)\{j\}]^T,$$
$$\boldsymbol{\xi}\{j\} = [\xi(1)\{j\},\ \cdots\ \xi(N)\{j\}]^T,$$

are the perturbation and additional torques for the j-th cycle. Inserting (5.7) into (5.8) gives

$$\begin{bmatrix} \boldsymbol{\tau}\{1\} \\ \vdots \\ \boldsymbol{\tau}\{n\} \end{bmatrix} = \begin{bmatrix} \boldsymbol{\Theta}_p\{1\} \\ \vdots \\ \boldsymbol{\Theta}_p\{n\} \end{bmatrix} \boldsymbol{\gamma} + \begin{bmatrix} \boldsymbol{\xi}\{1\} \\ \vdots \\ \boldsymbol{\xi}\{n\} \end{bmatrix}. \tag{5.9}$$

Next, the additional torque , $\boldsymbol{\xi}\{j\}$, at each cycle can be expressed as

$$\boldsymbol{\xi}\{j\} = \boldsymbol{B}\boldsymbol{\beta}\{j\}, \tag{5.10}$$

with

$$\boldsymbol{\beta}\{j\} = [\beta_{0,j},\ \cdots\ \beta_{M,j}]^T,$$
$$\boldsymbol{B} = \begin{bmatrix} B_0(1) & \dots & B_M(1) \\ \vdots & \ddots & \vdots \\ B_0(N) & \dots & B_M(N) \end{bmatrix},$$

The objective now is to estimates the parameters that represent the TV, joint dynamic stiffness ($\boldsymbol{\gamma}$) and the additional torque ($\boldsymbol{\beta}\{j\}$) at each cycle. Assuming that the joint stiffness parameters are periodic, their time-courses for one single period can be estimated using all the data. This is achieved by using the same basis functions to represent the TV parameters for all the cycles as expressed in 5.7. Conversely, the additional torque, $\boldsymbol{\beta}\{j\}$, will be different at each cycle and so the parameter set used to represent this signal must be estimated for each cycle.

The identification algorithm estimated the two parameter sets sequentially. It start by an initial estimate of $\widehat{\xi}\{j\}$ at each cycle. Then, this estimated torque is subtracted from the measured torque before finding an estimate of $\widehat{\boldsymbol{\gamma}}$ and computing the torque $\widehat{\tau}_p(t_k)$ for each gait cycle. The estimates of the intrinsic torque are then removed from the measured toque and the estimates of $\widehat{\xi}\{j\}$ are updated. This process is repeated until convergence. This iterative algorithm is described in detail in Algorithm 2.

Algorithm 2 *Identification of TV, intrinsic joint dynamic stiffness*

1. Measure the perturbed and un-perturbed torque and position signals. Compute $\tau(t_k)$ and $\theta_p(t_k)$.
2. Using the set of basis function compute the matrix $\boldsymbol{\theta}_p$ using the recorded signal.
3. Divide the data into each gait cycle to obtain an ensemble of trials as

$$\begin{bmatrix} \boldsymbol{\tau}\{1\} \\ \vdots \\ \boldsymbol{\tau}\{n\} \end{bmatrix}, \quad \text{and} \quad \begin{bmatrix} \boldsymbol{\Theta}_p\{1\} \\ \vdots \\ \boldsymbol{\Theta}_p\{n\} \end{bmatrix}.$$

4. Set a counter $i = 0$. Define a set of n vectors $\widehat{\tau}_p(t_k) = 0$.
5. Find an estimate of the additional torque as

$$\widetilde{\boldsymbol{\xi}}^i\{j\} = \boldsymbol{\tau}\{j\} - \widehat{\boldsymbol{\tau}_p}^i\{j\}$$

where j represent the trial number.
6. Use the estimated residual voluntary torque to identify the elements of (7.9) as

$$\widehat{\boldsymbol{\beta}}^i\{j\} = \boldsymbol{B} \backslash \widetilde{\boldsymbol{\xi}}^i\{j\},$$

where the '\' represents the relevance vector machine algorithm.
7. Update the residual voluntary torque for each trial as

$$\widehat{\boldsymbol{\xi}}\{j\} = \boldsymbol{B}\hat{\boldsymbol{\beta}}\{j\},$$

and remove it from the torque to generate a new signal as

$$\widetilde{\boldsymbol{\tau}_{\boldsymbol{p}}}^i\{j\} = \boldsymbol{\tau}\{j\} - \widehat{\boldsymbol{\xi}}^j\{j\}.$$

8. Use the ensemble of $\widetilde{\boldsymbol{\tau}_{\boldsymbol{p}}}^i$, $\theta_p(t_k)$ signals, and the basis functions to estimate $\boldsymbol{\gamma}$ as

$$\widehat{\boldsymbol{\gamma}}^i = \begin{bmatrix} \boldsymbol{\Theta}_{\boldsymbol{p}}\{1\} \\ \vdots \\ \boldsymbol{\Theta}_{\boldsymbol{p}}\{n\} \end{bmatrix} \backslash \begin{bmatrix} \widetilde{\boldsymbol{\tau}_{\boldsymbol{p}}}^i\{1\} \\ \vdots \\ \widetilde{\boldsymbol{\tau}_{\boldsymbol{p}}}^i\{n\} \end{bmatrix}$$

and use it to compute the perturbation torque at each trial as

$$\widehat{\boldsymbol{\tau}_{\boldsymbol{p}}}^i\{j\} = \boldsymbol{\Theta}_{\boldsymbol{p}}\{j\}\widehat{\boldsymbol{\gamma}}^i$$

9. Define a predicted torque for each trial as

$$\widehat{\boldsymbol{\tau}}^i\{j\} = \widehat{\boldsymbol{\tau}_{\boldsymbol{p}}}^i\{j\} + \widehat{\boldsymbol{\xi}}\{j\}$$

and compute the VAF between the predicted and measured torques as

$$VAF^i\{j\} = max\left[0, \left(1 - \frac{\sum\left(\boldsymbol{\tau}\{j\} - \widehat{\boldsymbol{\tau}}^i\{j\}\right)^2}{\sum\left(\boldsymbol{\tau}^i\{j\}\right)^2}\right)\right],$$

and find the mean VAF of the ensemble as

$$VAF(i) = \frac{1}{n}\sum_{j=1}^{n}\left(VAF^i\{j\}\right).$$

10. If there is a significant difference between $VAF(i)$ and $VAF(i-1)$ then set $i = i + 1$ and go to 5, else finish.

The memory of the IRF must be specifies a priori, here it was selected to be 40 ms, which coincides with the latency of the ankle stretch reflex response [12]. This value was selected so that the stretch reflex mechanisms do not influence the estimated parameters.

5.3.4 Analysis of results

The algorithm estimates $\widehat{\boldsymbol{\gamma}}$, $\widehat{\boldsymbol{\beta}}\{j\}$, and the predicted torques, $\widehat{\tau_p}(t_k)$ and $\widehat{\xi}(t_k)$ for each cycle. The parameter set $\widehat{\boldsymbol{\gamma}}$ and the B-splines basis functions can be used to estimate the TV-IRF as expressed in (5.4). Once the TV-IRF are estimated, the system time-frequency response can be calculated [136] and the DC gain or DC stiffness, and bandwidth (the frequency at which the system gain is 3dB larger than the DC gain) as a function of time can be measured.

5.4 Results

Next we present the results for one typical subject followed by the group results.

5.4.1 Single subject results

The TV, dynamic ankle stiffness was well characterized by a non-parametric model with a memory of 40 ms ($L = 4$); the average VAF for the 130 validation cycles was 96.3 $\pm$ 1.5%.

Fig. 5–3 demonstrates the good agreement between measured and predicted torques, shown in Panel B with blue a purple lines for a typical validation trial. The predicted $\widehat{\xi}(t_k)$ torque, shown in panel D, was small compared with the predicted intrinsic toque, shown in panel C.

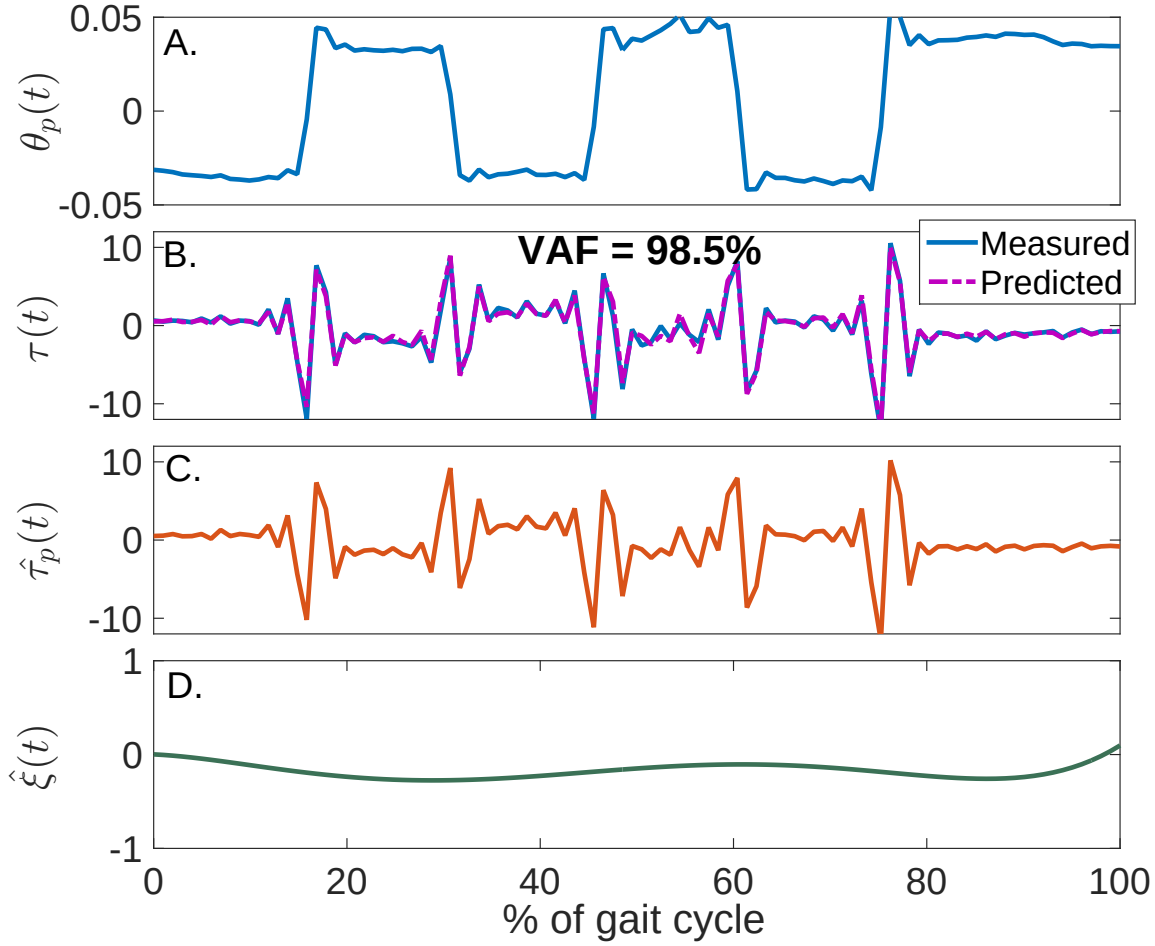

Figure 5–3: Results for a typical validation trial as a function of % of gait cycle. A. Perturbation position input, B. Measured (blue) and predicted (purple) perturbation torque, C. Estimated intrinsic torque, C. Estimated additional torque.

Fig. 5–4A shows the residuals obtained for three gait cycles, this signal is zero-mean for all cycles and small compared with the measured torque. It is mainly composed of high-frequency oscillations, which are likely originated from un-modeled

inertial response. Fig. 5–4B presents the torque $\widehat{\xi}(t_k)$ predicted for the same three cycles, this signal is not only non-zero mean throughout the cycle but shows a different behavior at each cycle.

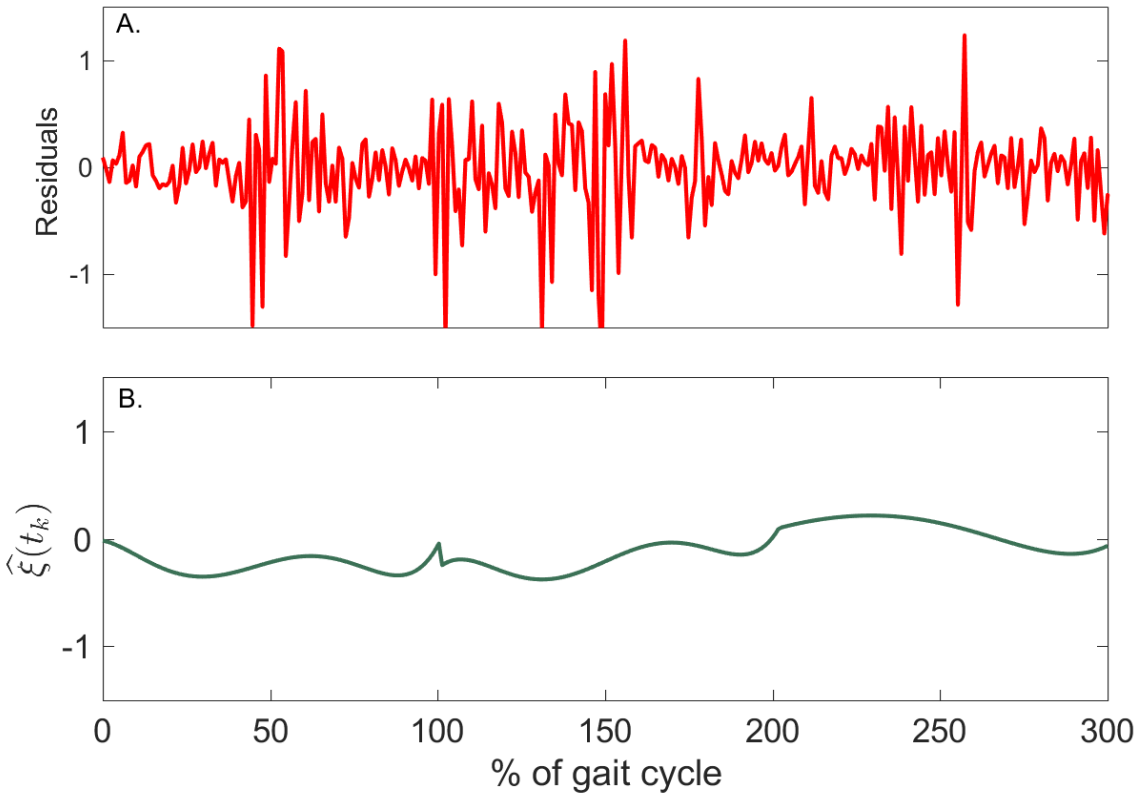

Figure 5–4: A. Residuals obtained for three gait cycles. B. $\widehat{\xi}(t_k)$ predicted for three gait cycles.

Fig. 5–5, presents the time-frequency response of the TV, intrinsic stiffness model. It showed a high-pass behavior, classically observed in this system and changed significantly throughout the gait cycle. Fig. 5–6 characterizes these changes in terms of DC stiffness and system bandwidth during the gait cycle along with

the 95% confidence interval, computed by applying a bootstrap analysis with 100 repetitions [193]. Both increased more than four fold during the stance phase, and then decreased sharply during the pre-swing phase. This drastic change occurred very rapidly, lasting around 100ms. Both then returned to its value at the beginning of the cycle and remained relatively constant through the swing phase. The green dots shown the DC stiffness and bandwidth estimated under stationary conditions at equivalent joint positions. These values are clearly very different from those observed during TV conditions.

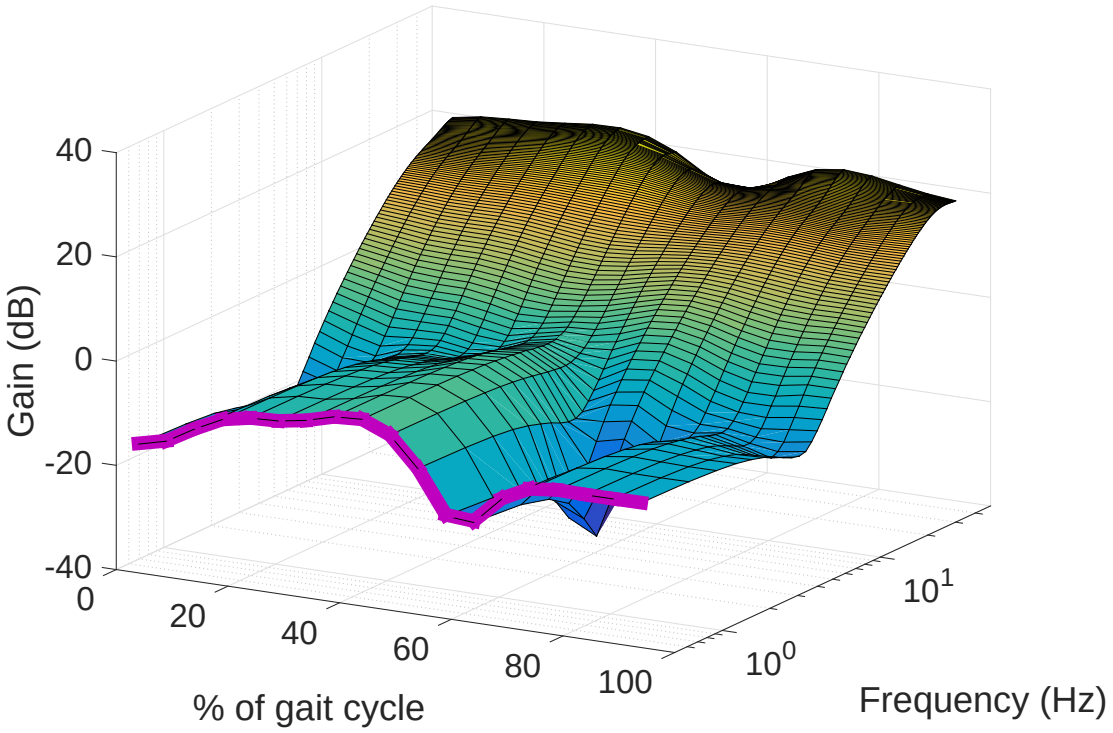

Figure 5–5: Time-Frequency response of the intrinsic, dynamic joint stiffness as a function of gait cycle for one subject.

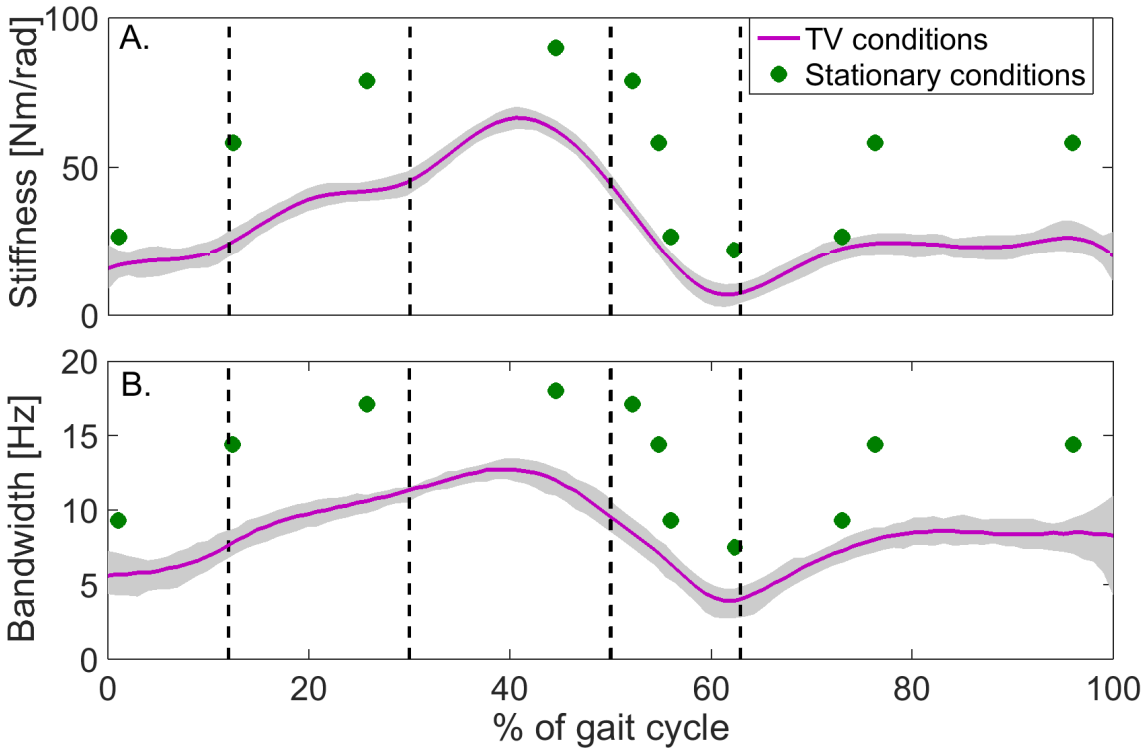

Figure 5–6: A. DC stiffness and B. Bandwidth computed during TV (purple line) and stationary (green dots) conditions. Grey bars indicate 95% confidence interval.

5.4.2 Group results

For all subjects, the TV, dynamic ankle stiffness was well characterized by the estimated non-parametric model with a memory of 40 ms; the average VAF for the 520 validation trials was 94 $\pm$ 2%.

Fig. 5–7 presents the frequency response at different phases of the gait cycle for all subjects. These showed the same general trend in all subjects. In particular, the gain in the low and middle frequencies ($\leqslant$ 15Hz), corresponding to the viscoelastic response of the joint, increased steadily from 0% to 40% of the cycle (corresponding

to the stance phase). Then, it decreased sharply between 40% and 60% of the cycle (corresponding to the pre-swing and initial swing phases). And finally it increased slightly and remained constant until the end of the cycle (corresponding to the swing phase).

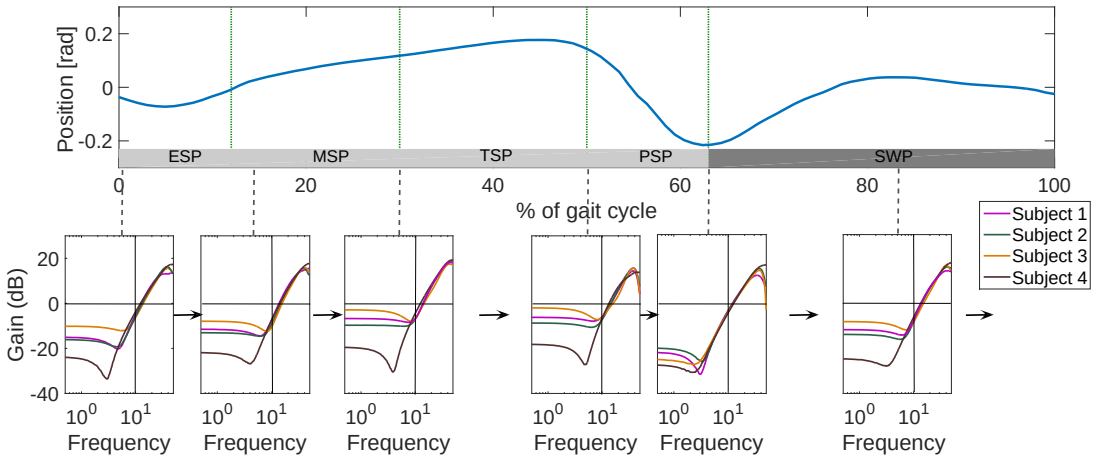

Figure 5–7: Frequency response of intrinsic, dynamic joint stiffness at different phases of the gait cycle for all subjects.

5.5 Discussion

5.5.1 New identification algorithm

This paper describes a new algorithm for the identification of TV, intrinsic, dynamic joint stiffness. The method presents two innovations: First, the algorithm combines the ensemble and deterministic approaches for TV parameter estimation. This permits the estimation of fast, large changes in intrinsic joint stiffness with significantly less data than ensemble methods; only 20 trials were needed to track the changes in joint stiffness through a simulated gait cycle. Previous studies that used ensemble-only methods required hundreds of trials [109, 110]. This reduction

in data requirement translates into much shorter experiments which makes it much easier to acquire enough trials with the same TV behavior.

The second innovation is that our algorithm estimates a novel torque component, $\xi(t_k)$, to account for the non-zeros mean torque that can be produced by nonlinear interactions between the large joint trajectory and the small perturbations, voluntary muscle contractions, and reflex mediated response. Estimating this component ensures that the residuals produced by the intrinsic dynamic stiffness model will be zero mean, which guarantees unbiased parameter estimates [136].

On the other hand, the method also inherits the limitations of both the ensemble and deterministic approaches. First, the method requires that all trials in the ensemble have the same TV behavior. However, the efficiency of the algorithm makes acquiring the data much less demanding than ensemble-only methods. Secondly, the method requires periodic movements to estimate initial conditions correctly. This algorithm can still be used with non-periodic movements; however, if the effects of the initial conditions are non-negligible then a multistep process must be applied to estimate them, otherwise, there will be transients at the beginning of the trial that will corrupt the prediction. The multistep process consists in transforming the estimated TV model into a TV state-space representation, applying a back-casting algorithm to estimate the initial conditions, and then transforming the state-space model into a non-parametric representation [140]. Nevertheless, this procedure requires the knowledge of the model order, which is not always available. Third, quality of the parameter estimates will depend on selecting a set of basis functions capable of efficiently describing the TV parameters changes. We used cubic B-splines which are

well suited for the smoothly changing parameters observed here. However, these basis functions would not be appropriate for parameters undergoing sharp transitions; another set of basis functions, such as Haar wavelets, would be more appropriate for this case. The best choice of type and number of basis functions is an open research problem. We addressed this in part by using the relevance vector machine for parameter estimation; this is a regularized identification algorithm that will force the weights of unnecessary basis functions to zero so they can be discarded.

5.5.2 Passive ankle stiffness throughout the gait cycle

The ankle DC stiffness, increased steadily by three fold from the early to terminal stance phase of the cycle. Next, it decreased by ninefold between the end of the terminal stance and the pre-swing phase. After the toe is lift off, the stiffness remained at a constant, low value until the end of the cycle. Even though these data were acquired from simulated walking experiments, the modulation in stiffness seem functionally appropriate. The increase in stiffness occurs in the portion of the cycle when only one leg supports the body. Thus, an increased ankle stiffness, which increases the joint stability, seems appropriate. Afterwards, both legs support the body so that the large ankle stiffness is no longer necessary. Finally, during the swing phase, the leg is no longer used for support so the stiffness remains constant.

These results indicate that ankle DC stiffness is functionally related to joint position. However, as Fig. 5–8 demonstrates, ankle stiffness can take different values for the same joint position. This indicates that this relation is not static, and most likely, nonlinear.

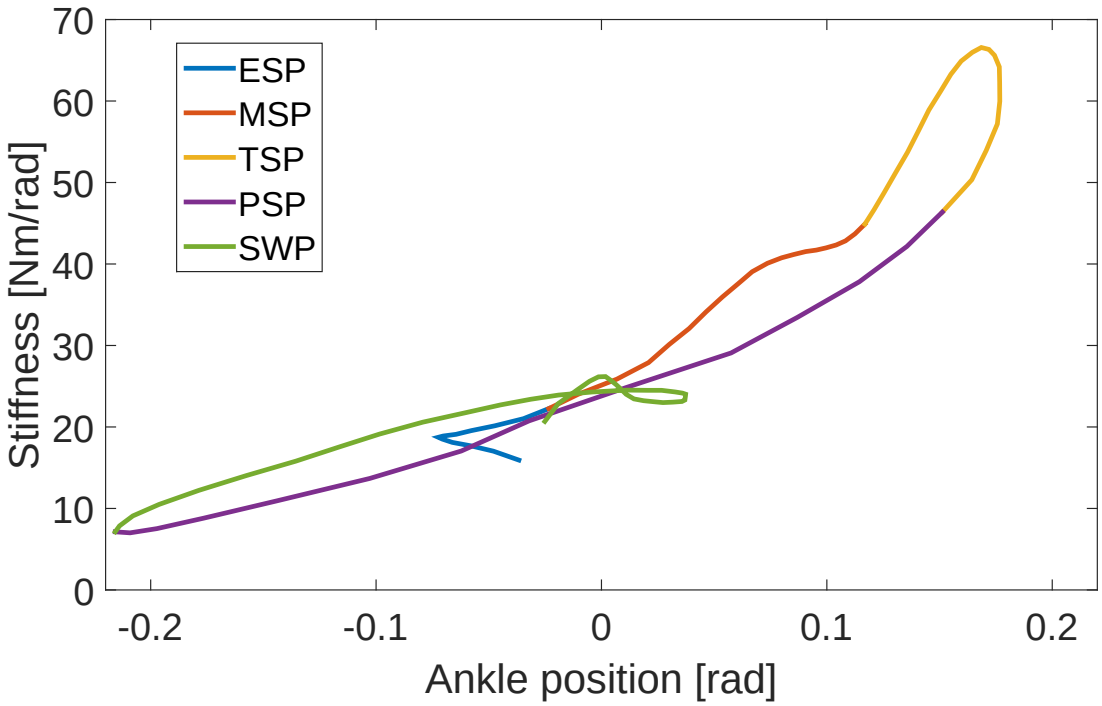

Figure 5–8: Relation between joint position and DC stiffness for the difference phases of the gait cycle.

5.5.3 Comparison with other studies

No one has measured joint dynamic stiffness throughout the entire gait cycle. E. Rouse *et. al* [109], measured ankle stiffness during the stance phase of the gait cycle, and H. Lee *et. al* [110], estimated ankle compliance, the inverse of stiffness, during the pre-swing and swing phases of walking. E. Perreault *et. al* [18] combined these results. These active gait results compare favorably with our imposed walking experiments. In all cases, the ankle DC stiffness showed a large increment in the stance phase of the cycle. We observed and increment of around 420% while the

results presented in [18] showed and increase of approximately 700%. Then, the DC stiffness returned sharply to the heel-strike value during the pre-swing phase.

It is likely that the difference in the magnitudes arises from differences in voluntary torque between our passive walking movements and their active gait experiments. However, the similarity in the trends indicate that the mechanisms underlying the modulation in the passive and active joint stiffness share a common source.

5.5.4 Clinical relevance

Differentiation between spastic and non-spastic subjects

Some central nervous system disorders (e.g. stroke, spinal cord injury, cerebral palsy) may alter the dynamic joint stiffness [194, 181]. This pathological behavior might arise from increase intrinsic stiffness, or reflex stiffness, often refereed as spasticity. Differentiating between these is an important and challenging clinical problem, and sometimes, increased intrinsic stiffness might be misdiagnosed as spasticity, or vice-versa [195]. This method can help to characterize pathological joint stiffness and distinguish whether it arises from spasticity or altered intrinsic mechanisms.

For non-spastic patients, the algorithm can be used directly to characterize the subject's joint mechanical properties. This model and the predicted torque can be used for diagnosis and monitoring. On the other hand, spastic patients will have an overactive stretch reflex response so their torque will be a combination of the intrinsic and reflex mechanism. As discussed, the algorithm will produce unbiased estimates of the intrinsic, dynamic stiffness and torque. The predicted intrinsic torque can then be used to estimate of the torque produced by the reflex mechanisms, which

may be large even for relaxed muscles. The magnitude of these torque signals can be used for diagnosis and monitoring.

Functional Electrical Stimulations (FES)

FES systems, which restore function to paralyzed limbs, use mathematical models of limbs and joints to estimate the torque required to produce a movement [196]. Recent advancements in FES have shown that simpler, lumped models of joint mechanics, such as the one presented here, provide less error than more complex, physiologically inspired models [197, 198]. Moreover, experimental results have demonstrated that models used in FES systems must capture the changes in joint mechanics during movement [198]. The model and algorithm presented here are well suited for this application; the model is general, linear in the parameters and can be estimated with relatively small data sets. Therefore, we suggest that our algorithm is well suited for use in FES control.

CHAPTER 6
An Instrumental Variable Approach for the Identification of Time-Varying, Hammerstein Systems

Authors: Diego L. Guarin and Robert E. Kearney

Journal: Proceedings of the 17th IFAC Symposium on System Identification SYSID

Year: 2015

One of the main complexities in the estimation of dynamic joint stiffness is due to the nonlinear, Hammerstein structure used to represent the stretch reflex mechanism. The estimation of time-invariant, Hammerstein systems is a mature subject and many different techniques for the identification of the model parameters are available. However, to our knowledge there are no publicly available algorithms for the estimation of time-varying, Hammerstein systems. This chapter extends the methods developed in chapters 4 and 5 and applies them for the identification of time-varying, Hammerstein system, composed by a series combination of a time-varying, static-nonlinearity and Box-Jenkins model. This is the first available algorithm that estimates the elements of the time-varying, Hammerstein system model from input-output data without *a priori* assumptions about the shape of the static nonlinearity of the linear model structure.

abstract

This paper introduces an iterative algorithm for the identification of time-varying (TV)-Hammerstein systems. This system is composed by a TV static nonlinearity followed by a TV Box-Jenkins linear model. The algorithm uses two basis function expansions: one to represent the TV parameters and a second to approximate the output of the static nonlinearity. A simulation study showed that the algorithm accurately identified the shape of the TV static nonlinearity and linear dynamic elements even though the noise model structure was unknown.

6.1 Introduction

The Hammerstein system, a series connection of a static nonlinearity followed by a linear dynamic element, is an important block-oriented structure that combines the simplicity of linear systems with the generalization capacity of nonlinear systems. Because of this, it has been successfully used in a variety of research areas including biomedical engineering ([12]), chemical engineering ([199]) and signal processing ([150]).

Several methods have been proposed to identify the parameters of this kind of models in a time-invariant (TI) situation. Among these, the iterative approach, discussed in [151], is particularly appalling because different from other approaches, it does not artificially increase the dimensionality of the search space. On the other hand, the identification of time-varying (TV) Hammerstein systems is still an open problem. Some methods have been presented but all have important limitations. For example, [200] proposed a recursive method for the special case where the parameters had a piece-wise linear time dependency; [201] described an ensemble based algorithm

that requires hundreds of input-output realizations having the same time variation; and [202] combined the ensemble and basis function expansion approaches in a non-parametric method that requires large data sets.

This paper presents an algorithm for the identification of TV Hammerstein systems modeled using the structure presented in Fig 6–1. The nonlinear and linear elements are described by a TV polynomial and a TV Box-Jenkins (BJ) model where the system and noise plants are parametrized independently. The noise is assumed to be TI.

The algorithm combines three identification approaches: *i*) the TV parameters of the nonlinear and linear elements are represented using basis function expansions; this transforms the TV identification problem into TI at the cost of increasing the number of parameters ([203]), *ii*) the BJ model parameters are estimated using a modified version of the *Refined Instrumental Variable* algorithm, whose convergence properties have been discussed elsewhere ([204]), and *iii*) the Hammerstein model is identified using an normalized iterative approach similar to that proposed by [151]. The identification is performed in two steps; one concerned with the identification of the linear dynamic element and the second with the identification of the static nonlinearity. After an initial estimate of the TV linear dynamical element is found, it is used to estimate the elements of the TV static nonlinearity; which in turn are used to update the estimates of the TV linear element. The algorithm iterates between these two steps updating the estimates iteratively until convergence.

This paper is structured as follows: Section 6.2 describes the algorithm. It presents a *Refined Instrumental Variable* algorithm for the identification of TV BJ

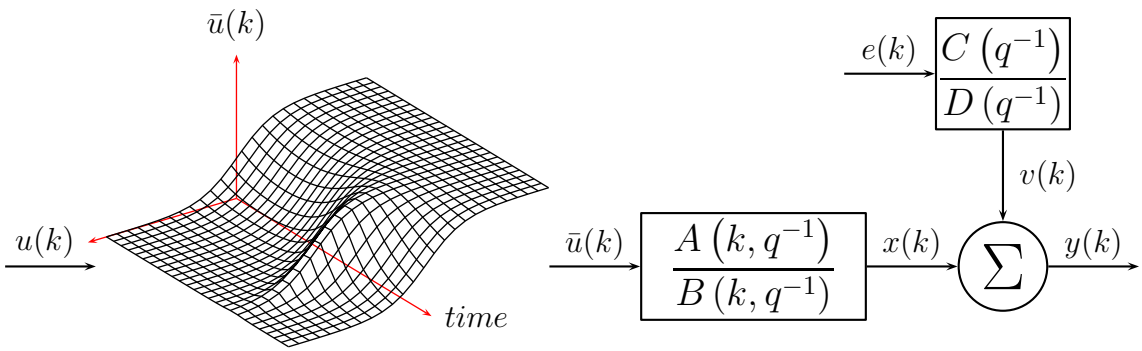

Figure 6–1: Time-varying Hammerstein comprising the series connection of a TV, static nonlinearity followed by a TV, BJ model with a TI noise plant.

models where the TV parameters are described by basis function expansions. This algorithm is then used to define an iterative method for the identification of TV, Hammerstein systems. Section 6.3 presents a simulation study demonstrating that the new algorithm performs well in our example. Finally, Section 6.4 discusses some important contributions of the paper.

6.2 Methods

6.2.1 Identification of Time-Varying, Box-Jenkins Models

Consider the discrete, TV-BJ system

$$\begin{cases} A\left(k,q^{-1}\right)x(k) = B\left(k,q^{-1}\right)\bar{u}(k), \\ v(k) = \dfrac{C\left(q^{-1}\right)}{D\left(q^{-1}\right)}e(k), \\ y(k) = x(k) + v(k), \end{cases} \tag{6.1}$$

where $x(k)$ is the noise-free output, $\bar{u}(k)$ the input, $v(k)$ the output noise, $y(k)$ the noisy output, $e(k)$ a zero mean, normally distributed noise signal with variance σ^2 that is uncorrelated with the input, and q^{-1} is the backward shift operator. The TV

system polynomials are

$$A\left(k, q^{-1}\right) = 1 + \sum_{i=1}^{n_a} a_i(k) q^{-i}, \tag{6.2a}$$

$$B\left(k, q^{-1}\right) = b_0(k) + \sum_{i=1}^{n_b} b_i(k) q^{-i}. \tag{6.2b}$$

The TV parameters are approximated using a basis function expansion

$$a_i(k) = \alpha_{i,0} + \sum_{j=1}^{n_\alpha} \alpha_{i,j} \pi_j(k), \quad i = 1, \cdots, n_a, \tag{6.3a}$$

$$b_i(k) = \beta_{i,0} + \sum_{j=1}^{n_\beta} \beta_{i,j} \pi_j(k), \quad i = 0, \cdots, n_b, \tag{6.3b}$$

where $\alpha_{i,0} \neq 0$, $\beta_{i,0} \neq 0$, and $\{\pi_j\}_{j=1}^{n_\alpha, n_\beta}$ is a set of predefined basis functions. Using this parametrization The TV-BJ model is then defined by the TI parameter set

$$\begin{aligned} \rho = \big[& \alpha_{1,0} \ \ldots \ \alpha_{n_a,0} \ \alpha_{1,1} \ \ldots \ \alpha_{1,n_\alpha} \ \ldots \ \alpha_{n_a,1} \ \ldots \ \alpha_{n_a,n_\alpha} \\ & \beta_{0,0} \ \ldots \ \beta_{0,n_\beta} \ \ldots \ \beta_{n_b,0} \ \ldots \ \beta_{n_b,n_\beta} \big]^T . \end{aligned} \tag{6.4}$$

The TI noise polynomials are

$$C\left(q^{-1}\right) = 1 + \sum_{i=1}^{n_c} c_i q^{-i}, \tag{6.5a}$$

$$D\left(q^{-1}\right) = 1 + \sum_{i=1}^{n_d} d_i q^{-i}. \tag{6.5b}$$

Using (6.3a) and (6.3b), the noise-free output ($x(k)$) can be expressed as the linear, TI model

$$x\left(k\right)=\frac{1}{F\left(q^{-1}\right)}\left[-\sum_{i=1}^{n_a}\sum_{j=1}^{n_\alpha}\alpha_{i,j}x_j\left(k-i\right)+\sum_{i=0}^{n_b}\sum_{j=0}^{n_\beta}\beta_{i,j}\bar{u}_j\left(k-i\right)\right]. \tag{6.6}$$

Where $\pi_0(k)=1$ for all k and

$$x_j\left(k-i\right)=\pi_j(k)x\left(k-i\right), \tag{6.7a}$$

$$u_j\left(k-i\right)=\pi_j(k)u\left(k-i\right). \tag{6.7b}$$

$F\left(q^{-1}\right)$ is a polynomial with constant coefficients given by

$$F\left(q^{-1}\right)=1+\sum_{i=1}^{n_a}\alpha_{i,0}q^{-i}. \tag{6.8}$$

Now define a cost function based on the *one-step-ahead prediction error*

$$V_N\left(\theta\right)=\frac{1}{2N}\sum_{k=1}^{N}\epsilon^2(k), \tag{6.9}$$

where

$$\epsilon(k)=\frac{\hat{D}\left(q^{-1}\right)}{\hat{C}\left(q^{-1}\right)}\left[y(k)-\hat{x}(k)\right].$$

The "ˆ" indicates the expected value estimated from past data up to time $k-1$. For simplicity, $\epsilon(k)$ is expressed as

$$\epsilon(k) = \hat{F}\left(q^{-1}\right)y^{\hat{f}}(k) + \sum_{i=1}^{n_a}\sum_{j=1}^{n_\alpha}\hat{\alpha}_{i,j}\hat{x}_j^{\hat{f}}(k-i) - \sum_{i=0}^{n_b}\sum_{j=0}^{n_\beta}\hat{\beta}_{i,j}\bar{u}_j^{\hat{f}}(k-i), \tag{6.10}$$

where the new variables

$$y^{\hat{f}}(k) = \hat{f}\left(q^{-1}\right)y(k), \tag{6.11a}$$

$$\bar{u}_j^{\hat{f}}(k-i) = \hat{f}\left(q^{-1}\right)\bar{u}_j(k-i), \tag{6.11b}$$

$$\hat{x}_j^{\hat{f}}(k-i) = \hat{f}\left(q^{-1}\right)\hat{x}_j(k-i), \tag{6.11c}$$

have been used. In addition we defined

$$\hat{f}\left(q^{-1}\right) = \left(\frac{\hat{D}\left(q^{-1}\right)}{\hat{C}\left(q^{-1}\right)}\right)\left(\frac{1}{\hat{F}\left(q^{-1}\right)}\right). \tag{6.12}$$

The cost function, (6.9), will be at a minimum when it's partial derivatives with respect to each parameter equal zero; as shown by [204] for the TI case, this leads to the following relation:

$$\hat{\rho} = \left[\frac{1}{N}\sum_{k=1}^{N}\hat{\phi}_{\hat{f}}(k)\hat{\varphi}_{\hat{f}}^T(k)\right]^{-1}\left[\frac{1}{N}\sum_{k=1}^{N}\hat{\phi}_{\hat{f}}(k)y^{\hat{f}}(k)\right], \tag{6.13}$$

with the new variables

$$\hat{\alpha}_{n_a,n_\alpha}\ \hat{\beta}_{0,0}\ \ldots\ \hat{\beta}_{0,n_\beta}\ \ldots\ \hat{\beta}_{n_b,0}\ \ldots\ \hat{\beta}_{n_b,n_\beta}\Big]^T, \tag{6.14a}$$

$$\begin{aligned}\hat{\varphi}_{\hat{f}}(k) = \Big[&-y^{\hat{f}}(k-1)\ \ldots\ -y^{\hat{f}}(k-n_a)\ -\hat{x}_1^{\hat{f}}(k-1)\\ &\ldots\ -\hat{x}_{n_\alpha}^{\hat{f}}(k-1)\ \cdots-\hat{x}_1^{\hat{f}}(k-n_a)\ \ldots\ -\hat{x}_{n_\alpha}^{\hat{f}}(k-n_a)\\ &\bar{u}_0^{\hat{f}}(k)\ \ldots\ \bar{u}_{n_\beta}^{\hat{f}}(k)\ \ldots\ \bar{u}_0^{\hat{f}}(k-n_b)\ \ldots\ \bar{u}_{n_\beta}^{\hat{f}}(k-n_b)\Big]^T\end{aligned} \tag{6.14b}$$

$$\begin{aligned}\hat{\phi}_{\hat{f}}(k) = \Big[&-\hat{x}^{\hat{f}}(k-1)\ \ldots\ -\hat{x}^{\hat{f}}(k-n_a)\ -\hat{x}_1^{\hat{f}}(k-1)\\ &\ldots\ -\hat{x}_{n_\alpha}^{\hat{f}}(k-1)\ \cdots-\hat{x}_1^{\hat{f}}(k-n_a)\ \ldots\ -\hat{x}_{n_\alpha}^{\hat{f}}(k-n_a)\\ &\bar{u}_0^{\hat{f}}(k)\ \ldots\ \bar{u}_{n_\beta}^{\hat{f}}(k)\ \ldots\ \bar{u}_0^{\hat{f}}(k-n_b)\ \ldots\ \bar{u}_{n_\beta}^{\hat{f}}(k-n_b)\Big]^T.\end{aligned} \tag{6.14c}$$

Where $y^{\hat{f}}(k)$ and $u^{\hat{f}}(k)$ are the input and output signals filtered $\hat{f}(q^{-1})$; $\hat{x}^{\hat{f}}(k)$ is an estimate of the noise-free output and satisfies the conditions required of an *instrumental variable*, an auxiliary variable that is used to reduce the influence of the noise in the estimates ([204]). This instrumental variable can not be measured directly but can be estimated from (6.6) using estimates of the parameter set $\hat{\rho}$. This leads to an iterative or *refined* procedure where the current values of the parameter set are used to estimate the *instrumental variable* and in turn this is used to update the parameter set.

Algorithm 3 presents the resulting *Refined-Instrumental-Variable* (RIV) algorithm for the identification of TV-BJ models. This algorithm is a simple modification of the method proposed by [101] and has been already introduced elsewhere ([177]).

Algorithm 3 *TV-RIV*

Input: $\{y(k)\}_{k=1}^{N}$, $\{\bar{u}(k)\}_{k=1}^{N}$, $\{\pi_j(k)\}_{k=1,\ j=0}^{N,\ max(n_\alpha,n_\beta)}$, n_a, n_b, n_c and n_d
Output: $\{\hat{A}(k,q^{-1})\}_{k=1}^{N}$, $\{\hat{B}(k,q^{-1})\}_{k=1}^{N}$ and $\{\hat{x}(k)\}_{k=1}^{N}$

1. Find an initial estimate of $\hat{\rho}^0$ by assuming that the system is LTI and using the Refined Instrumental Variable algorithm [101, Chap. 7]. Set $\hat{D}^0(q^{-1}) = \hat{C}^0(q^{-1}) = 1$ and the counter w to 0.
2. Use (6.6) to estimate the instrumental variable $\{\hat{x}(k)\}_{k=1}^{N}$. 3. Form the filter

$$\hat{f}^{(w)}\left(q^{-1}\right) = \frac{\hat{D}^{(w)}\left(q^{-1}\right)}{\hat{C}^{(w)}\left(q^{-1}\right)\hat{F}^{(w)}\left(q^{-1}\right)},$$

4. Generate the filtered input $\{y(k)^{\hat{f}}\}_{k=1}^{N}$, and output $\{u(k)^{\hat{f}}\}_{k=1}^{N}$, $\{\hat{x}(k)^{\hat{f}}\}_{k=1}^{N}$ signals.
5. Use the basis functions $\{\pi_j(k)\}_{k=1,\ j=0}^{N,\ max(n_\alpha,n_\beta)}$ to form the regressor matrices $\{\hat{\varphi}_{\hat{f}}(k)\}_{k=1}^{N}$ and $\{\hat{\phi}_{\hat{f}}(k)\}_{k=1}^{N}$ using (6.14b) and (6.14c).
6. Use (6.13) to update the parameter estimates.
7. Update the instrumental variable $\{\hat{x}(k)\}_{k=1}^{N}$ and compute the noise signal as

$$\hat{v}(k) = y(k) - \hat{x}(k).$$

Use this to estimate the noise model parameters with any of the well known method to estimate `ARMAX` models.
8. If the difference between $\hat{\rho}^{(w+1)}$ and $\hat{\rho}^{(w)}$ is not significant or, if the maximum number of iterations is exceeded, go to step 9, else increment w and go to step 3.
9. Compute the elements of $\hat{A}(k,q^{-1})$ and $\hat{B}(k,q^{-1})$ for all k using (4.15) and (**??**).

6.2.2 Identification of Time-Varying, Hammerstein Systems

Consider the discrete, TV Hammerstein system

$$\begin{cases} \bar{u}(k) = g(k, u(k)), \\ A\left(k, q^{-1}\right) x(k) = B\left(k, q^{-1}\right) \bar{u}(k), \\ v(k) = \dfrac{C\left(q^{-1}\right)}{D\left(q^{-1}\right)} e(k), \\ y(k) = x(k) + v(k), \end{cases} \tag{6.15}$$

where $g(k, \bullet)$ is a TV, static nonlinearity. It can have any shape as long as its effect on the input can be approximate as

$$\bar{u}(k) = g(k, u(k)) \approx \sum_{i=0}^{M} r_i(k) \Gamma_i\left(u(k)\right), \tag{6.16}$$

where $\Gamma_0(u(k)) = 1$ for all k. The TV behavior of the coefficients $(r_i(k))$ is in turn described by the basis function expansion

$$r_i(k) = \sum_{j=0}^{n_\gamma} \gamma_{i,j} \pi_j(k), \quad i = 1, \cdots, M. \tag{6.17}$$

Inserting (6.16) and (6.17) into (6.15) yields

$$\begin{cases} x(k) = \frac{B\left(k, q^{-1}\right)}{A\left(k, q^{-1}\right)} \sum_{i=0}^{M} \sum_{j=0}^{n_\gamma} \gamma_{i,j} \pi_j(k) \Gamma_i\left(u(k)\right), \\ v(k) = \dfrac{C\left(q^{-1}\right)}{D\left(q^{-1}\right)} e(k), \\ y(k) = x(k) + v(k), \end{cases} \tag{6.18}$$

With this parametrization the TV-Hammerstein model is now defined by two TI parameter sets: ρ, given by (7.5), and

$$\eta = \left[\gamma_{0,0} \ \ldots \ \gamma_{M,0} \ \ldots \ \gamma_{0,n_\gamma} \ \ldots \ \gamma_{M,n_\gamma}\right]^T. \tag{6.19}$$

It is clear from (6.18) that if η, the TV-static nonlinearity, is known then the identification of the TV-Hammerstein systems reduces to the identification of a TV-BJ model. On the other hand, if ρ, which defines the TV linear dynamics, is known then the input-output relation reduces to

$$y(k) = \sum_{i=0}^{M} \sum_{j=0}^{n_\gamma} \gamma_{i,j} z_{i,j}(k) + v(k), \tag{6.20}$$

where

$$z_{i,j}(k) = \frac{B\left(k, q^{-1}\right)}{A\left(k, q^{-1}\right)} \left[\pi_j(k) \Gamma_i\left(u(k)\right)\right]. \tag{6.21}$$

and the parameter set that minimizes the *one-step-ahead prediction error* is then given by the least-squares solution

$$\hat{\eta} = \left[\frac{1}{N} \sum_{k=1}^{N} \hat{Z}(k) \hat{Z}^T(k)\right]^{-1} \left[\frac{1}{N} \sum_{k=1}^{N} \hat{Z}(k) y^T(k)\right], \tag{6.22}$$

where

$$\begin{aligned} \hat{Z}(k) = \big[&\hat{z}_{0,0}(k) \ \ldots \ \hat{z}_{M,0}(k)(k) \ \ldots \ \hat{z}_{0,n_\gamma}(k) \\ &\ldots \ \hat{z}_{M,n_\gamma}(k)\big]^T, \end{aligned} \tag{6.23}$$

where $\hat{z}_{i,j}(k)$ is estimated from (6.21) using the current values of $\hat{A}(k, q^{-1})$ and $\hat{B}(k, q^{-1})$.

Algorithm 4 combines these solutions to give a RIV algorithm for the identification of TV-Hammerstein systems.

Algorithm 4 *TV-RIV for Hammerstein systems*

Input: $\{y(k)\}_{k=1}^{N}$, $\{u(k)\}_{k=1}^{N}$, $\{\pi_j(k)\}_{k=1,\ j=0}^{N,\ max(n_\alpha,n_\beta,n_\gamma)}$, $\{\Gamma_j(\bullet)_{j=0}^{M}\}$ n_a, n_b, n_c, n_d, n_α, n_β, n_γ and M.

Output: $\{\hat{A}(k,q^{-1})\}_{k=1}^{N}$, $\{\hat{B}(k,q^{-1})\}_{k=1}^{N}$, $\{\hat{r}_i(k)\}_{k=1,j=0}^{N,M}$, and $\{\hat{x}(k)\}_{k=1}^{N}$

1. Find an initial estimate of $\hat{\rho}^0$, $\hat{D}^0(q^{-1})$ and $\hat{C}^0(q^{-1})$ using $y(k)$, $u(k)$ and the Algorithm 1. Set the counter m to 1.
2. Compute $\hat{Z}(k)$ for all k using (6.21) and (6.23) and use (6.22) to update the estimate of the static nonlinearity.
3. Compute $\hat{\bar{u}}(k)$ using (6.16) and (6.17).
4. Estimate $\hat{\rho}^m$, $\hat{D}^m(q^{-1})$ and $\hat{C}^m(q^{-1})$ using $y(k)$, $\hat{\bar{u}}(k)$ and Algorithm 1.
5. Compute $\hat{b}_i^m(k)$ for all i and k using (6.3b) and normalize it as

$$\hat{b}_i^m(k) = \xi_m \hat{b}_i^m(k)||\hat{\eta}^m||,$$

also normalize the elements of the static nonlinearity as

$$\hat{\eta}^m = \xi_m \frac{\hat{\eta}^m}{||\hat{\eta}^m||}.$$

Where $\xi_m = \pm 1$ is the sign of the first nonzero element of $\hat{\eta}^m$.
6. If the difference between $\hat{\rho}^{(m+1)}$ and $\hat{\rho}^{(m)}$, and $\hat{\eta}^{(m+1)}$ and $\hat{\eta}^{(m)}$ is not significant or, if the maximum number of iterations is exceeded, go to 6. Otherwise increment m and go to step 2.
6. Compute the elements of $\hat{A}(k,q^{-1})$, $\hat{B}(k,q^{-1})$ and $\hat{r}_i(k)$ for all k using (6.3a), (6.3b) and (6.17)

6.2.3 Estimation of the noise model

Algorithm 3 estimates models for both the noise and the system at each iteration and uses these estimates to compute the filter $\hat{f}(q^{-1})$. However, estimating the noise model may be difficult since the input to the noise plant cannot be measured and its order is usually unknown *a priori*. However, the BJ structure parametrizes the system and noise plants independently so that estimates of their parameters are asymptotically independent. That is, provided there is enough data, the estimates of the system polynomials ($\hat{A}(k, q^{-1})$, and $\hat{B}(k, q^{-1})$) are not dependent on the estimates of the noise polynomials ($\hat{C}(q^{-1})$, and $\hat{D}(q^{-1})$). In practice, this means that if it is assumed that $C(q^{-1}) = D(q^{-1}) = 1$ the estimates $\hat{A}(k, q^{-1})$, and $\hat{B}(k, q^{-1})$ will not differ significantly from those obtained when the noise model is estimated ([205, 101, 204]).

6.3 Simulation Example

The algorithm was validated using simulated data from the TV-Hammerstein system

$$\begin{cases} \bar{u}(t) = g(t, u(t)), \\ x(t) = -G(t)\frac{\omega^2(t)}{s^2+2\zeta(t)\omega(t)s+\omega^2(t)}\bar{u}(t), \\ v(k) = \frac{1-0.2q^{-1}}{1-q^{-1}+0.2q^{-2}}e(k), \\ y(k) = x(k) + v(k). \end{cases} \tag{6.24}$$

This is an hybrid model where the system is continuous but the noise and the measured output are discrete. This model was selected because it is a good representation of stretch reflex dynamics ([64]) and therefore has applications in motor control research. The model parameters where selected to resemble those observed

(a) Static Nonlinearity

(b) Linear Element

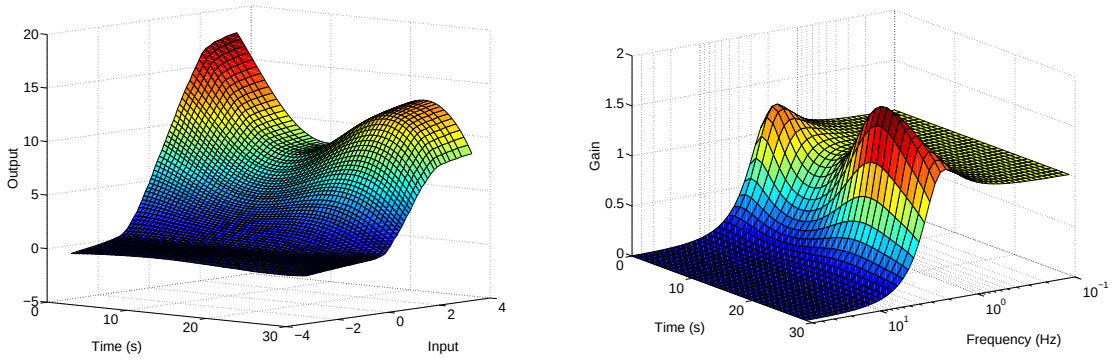

Figure 6–2: Elements of the simulated TV-Hammerstein system: (a) TV static nonlinearity, and (b) TV frequency response of the linear, dynamic.

experimentally ([64]). Fig. 6–2a shows the simulated TV static nonlinearity; it resembles a half-wave rectifier whose threshold, slope, and saturation vary with time. The TV, linear, dynamic element was a low-pass filter with TV resonant frequency. Fig. 6–2b shows its frequency response gain as a function of time.

The noise plant was modeled by a low-pass filter with a cut-off frequency of 5 Hz; the plant and noise model did not share any poles.

6.3.1 Simulation

The continuous time system was simulated using Matlab (The Mathworks) for 30s at a sampling rate of 1KHz and then decimated to 100 Hz for further analysis. The ratio between the variances of the output and noise signals was 15dB.

Fig. 6–3 shows a typical simulation trial. The input (top panel) was TI with a normal distribution and a bandwidth of 30Hz. The characteristics of the noise-free

output (middle panel) show a clear time dependency. The bottom panel shows the colored noise signal.

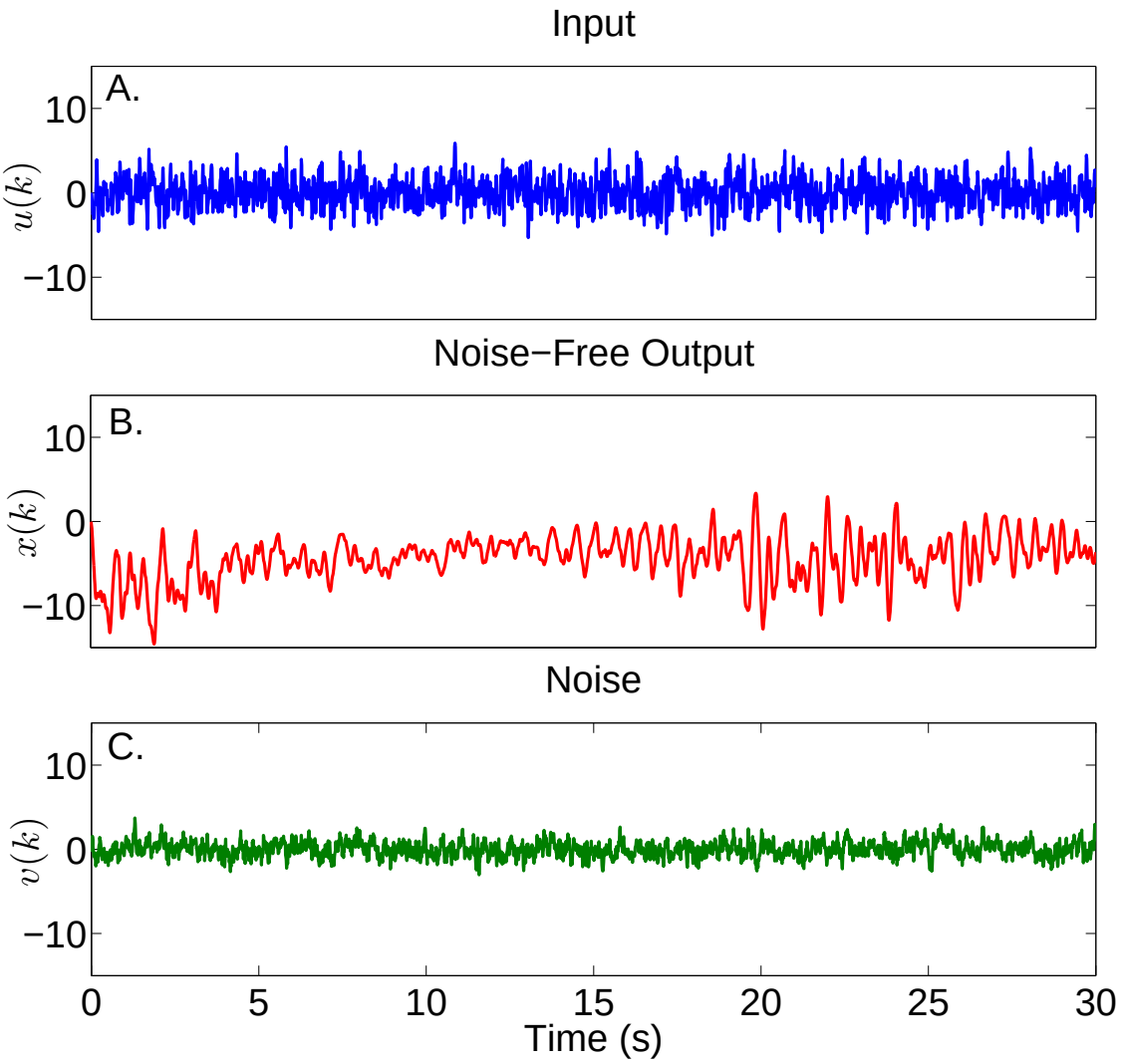

Figure 6–3: Typical simulation trial: a) Input signal, b) noise-free output and c) additive noise.

6.3.2 Parametrization

The new algorithm describes the linear, dynamic element as a discrete-time, TV, BJ system and the static nonlinearity as a basis function expansion. Consequently, before starting the identification procedure it was necessary to *i*) find the discrete-time equivalent of the simulated continuous-time model, and *ii*) find an appropriate parametric representation of the static nonlinearity.

Discrete-time system:

Using the bi-linear transformation and considering the noncommutativity of the backshift operator (*i.e.*, $q^{-1}x(k)u(k) = x(k-1)u(k-1)$), the continuous-time model of (6.24) can be shown to be equivalent to the discrete-time model

$$x(k) = \frac{h(k)\left(1 + 2q^{-1} + q^{-2}\right)}{1 + p_1(k)q^{-1} + p_2(k)q^{-2}}\bar{u}(k), \tag{6.25}$$

where $h(k)$, $p_1(k)$ and $p_2(k)$ are the TV, discrete-time parameters.

Time-varying parameters:

The basis function set used to describe the time-varying parameters comprised the Tchebychev polynomials of order 0 to 6. These were selected because: *i*) The variances of all the polynomials are similar and so the estimation problem should remain well scaled. *ii*) Experience has shown they generate well-conditioned regressors. *iii*) The simulated values were generated as power functions of time, so using Tchebychev polynomials as basis functions can help to validate the robustness of the algorithm to the lack of information regarding the true basis functions.

Static nonlinearity:

The basis functions used to model the static nonlinearity were Tchevichev polynomials of order 0 to 4.

6.3.3 Results

Two points should be noted with respect to the results presented in this section: *i*) The identification procedure did not attempt to estimate the noise model. This is equivalent to incorrectly assuming that the noise model was $C(q^{-1}) = D(q^{-1}) = 1$ but as is argued in Section 6.2.3 this should not influence the estimation of the system parameters. *ii*) The DC gain of a Hammerstein system may be partitioned arbitrarily between the static nonlinearity and the linear dynamics. Consequently, for consistency, in the results presented here all the gain was assigned to the static nonlinearity and that of the linear dynamic element forced to be one for all t.

Single trial results:

For comparison purposes, a TI model was estimated between the input and noisy output for a typical trial using the new algorithm by setting the order of the Tchebychev polynomials used to represent the TV parameters to zero, and the order of the linear model equal to that of (6.25). The Variance Accounted For (%VAF) between the TI model predicted output and the noise-free simulated output was only 65%; demonstrating the need for a TV model.

Next, the TV-RIV algorithm was applied with the full basis function set. The resulting TV model predicted output accounted almost all (98.4%) of the noise-free output variance. Fig. 6–4 shows the model predicted output and its residuals. The

residuals are TI, showing that TV behavior of the plant has been fully captured by the estimated model.

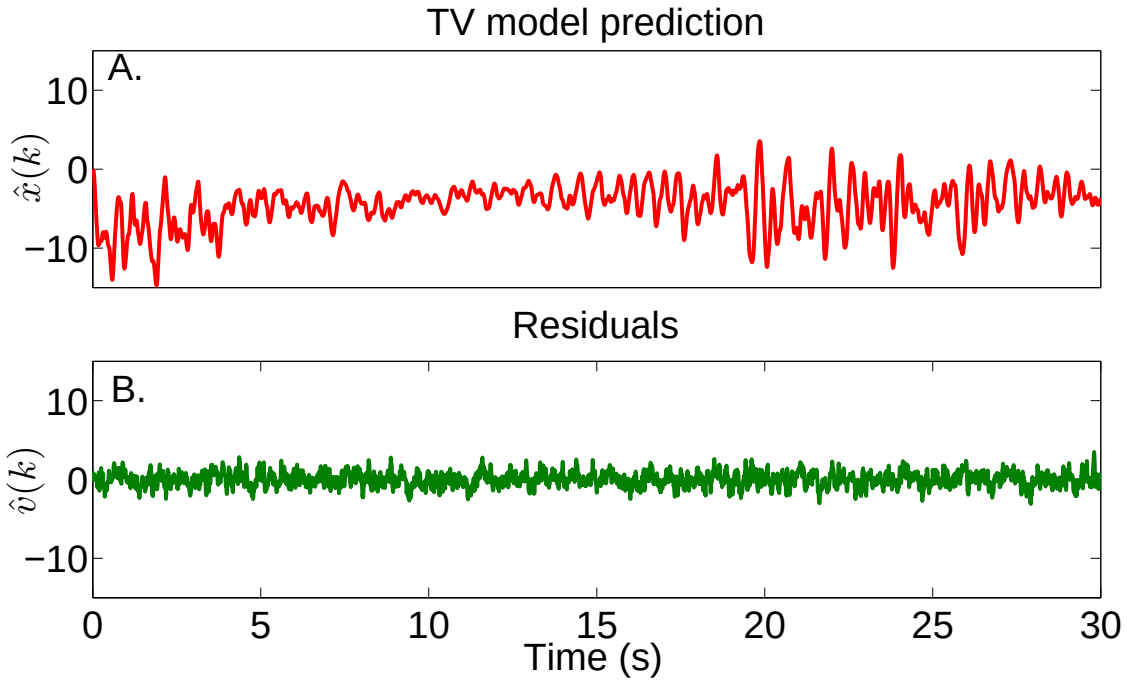

Figure 6–4: Results obtained with the estimated TV model. a) Predicted output, and b) residuals.

Monte Carlo results:

To further examine the performance of the TV-RIV algorithm the simulations were repeated 200 times and TV models were estimated for each realization. The algorithm needed less than 10 iterations to converge in all trials; the %VAF between the simulated and predicted outputs was always larger than 98%. Fig. 6–5 shows the simulated (blue) and estimated (red) static nonlinearities at three times. Fig. 6–6 presents the simulated and estimated frequency response gains. The similarity

of the estimated curves to each other and to the simulated curves demonstrate that the TV-RIV estimates had low variance and were accurate.

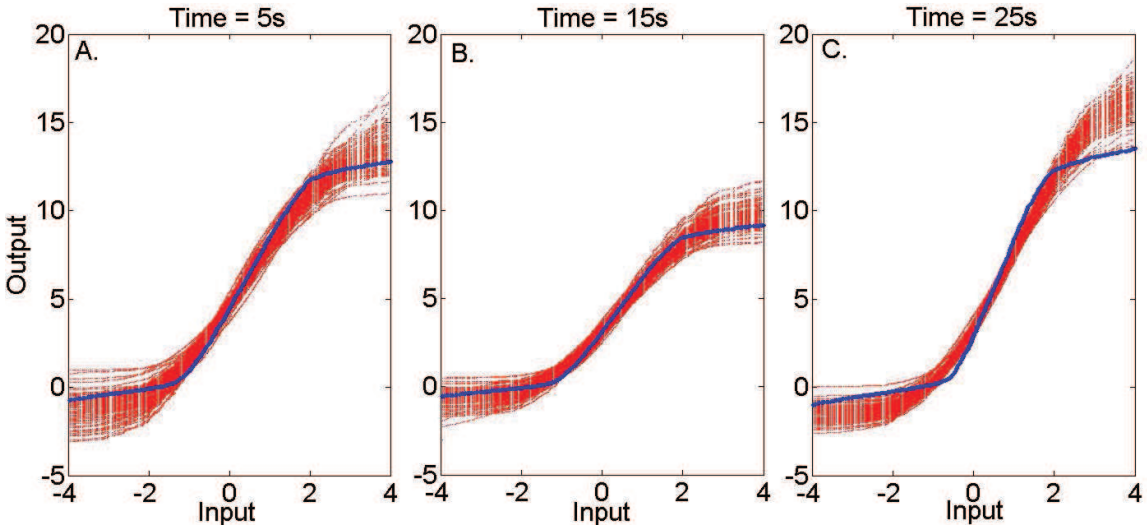

Figure 6–5: True (blue) and estimated (red) static nonlinearities at three times. a) 5s, b) 15s and c) 25s.

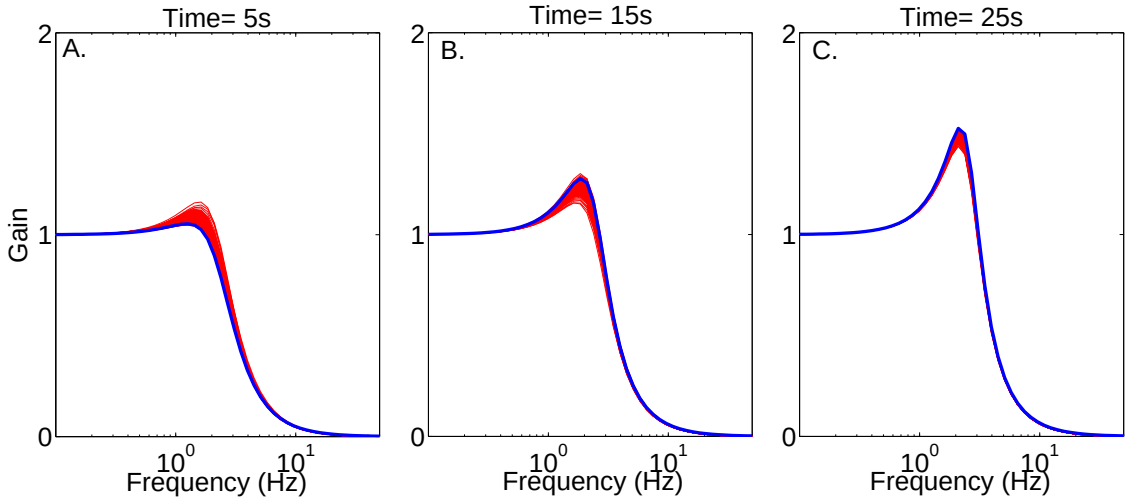

Figure 6–6: True (blue) and estimated (red) frequency response gains at three times. a) 5s, b) 15s and c) 25s.

6.4 Discussion

We have presented an algorithm for the identification of TV-Hammerstein systems composed of a TV static nonlinearity, represented as a combination of predefined basis functions, followed by a TV linear dynamic element, represented by a TV-BJ model. Our algorithm approximates the TV model parameters by a linear combination of basis functions; this approximation guarantees that, provided an appropriate set of basis functions is selected, any kind of static nonlinearity and time-dependency can be modeled. However, it adds the additional constraint of having to determine what is the appropriate set of basis functions. While this problem has no solution in general, our experience with the method has shown that the Tchevicheb polynomials provide a good initial approximation of the parameters time-dependency. Once this is available it may be possible to find other basis functions that provide more accurate results.

Another important aspect of the algorithm is the selection of the order of the approximation; this dictates the number of free parameters of the model and thus the dimension of the search space. Fortunately, there is a fracture point were adding additional basis functions will increase the prediction error, restricting in this way the maximum number of basis that can be used. The selection of the optimal number of basis functions to use is more complicated and some approaches haven been proposed ([202, 203]) but there is yet no definitive solution. We are studying the possibility of using an sparse optimization algorithm that will force the parameters associated with non-contributing basis functions to zero.

CHAPTER 7
Identification of Time-Varying, Intrinsic and Reflex Dynamic Ankle Stiffness during Imposed Walking

Authors: Diego L. Guarin and Robert E. Kearney

Journal: To be submitted - IEEE Transactions on Neural Systems and Rehabilitation Engineering

Year: 2017

This chapter develops a new methodology for the identification of joint dynamic stiffness during time-varying conditions that facilitates the characterization of joint neuromechanical properties during function. Overall joint stiffness is modeled by a parallel-cascade structure composed of intrinsic and reflex pathways. Intrinsic stiffness is described by a time-varying, non-parametric, linear model, and reflex stiffness is described by a time-varying, Hammerstein system, composed by a series combination of a time-varying, static-nonlinearity and Box-Jenkins model. The algorithms developed in Chapters 4, 5 and 6 are combined to estimate the intrinsic and reflex components of the dynamic joint stiffness sequentially, iterations are used to refine the parameters estimates. This method is applied to measure the intrinsic and reflex dynamic stiffness from one subject in an imposed walking movement experiment with constant muscle activation. Results show, for the first time, how the intrinsic

and reflex components of dynamic ankle stiffness change during movement, and provide new evidence of how the neuromechanical joint properties are modulated during function.

Abstract

Dynamic joint stiffness determines the relation between joint position and torque, and plays a vital role in the control of posture and movement. It is usually quantified during stationary conditions using disturbance experiments, were small position perturbations are applied to the joint and the produced torque is recorded. However, dynamic joint stiffness is composed of intrinsic and reflex mechanisms, these act and change together, so that nonlinear, mathematical models and specialized system identification techniques are required to separate their individual contributions. Experimental evidence has shown that dynamic joint stiffness is heavily modulated by the operating point, defined by joint position and voluntary torque, so that during function, where the operating point undergoes large, rapid changes, the model parameters will appear to be Time-Varying (TV). This study introduces a new methodology to quantify the intrinsic and reflex components of joint dynamic stiffness during movement. The algorithm combines ensemble and deterministic approaches to estimate the parameters of a TV, dynamic joint stiffness model from position and torque records. A Simulation study demonstrated that the new algorithm accurately tracks the changes the model parameters expected during walking using as little as 40 gait cycles. Furthermore, the method was applied to estimate the intrinsic and reflex dynamic stiffness during an imposed walking movement with constant muscle activation. The identified TV models predicted the measured torque very well, accounting for more than 95 % of the signal variance. Results showed that both intrinsic and reflex dynamic stiffness changed greatly through the gait cycle; in

particular, the gain of both pathways increased at least three fold during the stance phase of the gait cycle.

7.1 Introduction

The role of the short-latency stretch reflex during movement remains controversial [206, 207, 208]. While some studies suggest that reflex response serves to facilitate all voluntary movements [209, 210], others have proposed that the myotatic response plays a role only in extreme or pathological cases [43], or during early adaptation to a new tasks or conditions [178].

EMG is often used to study the functional role of reflexes [206, 211, 208, 178]. However, EMG is influenced by reflex response and other factors, such as voluntary activity. In addition, the relation between EMG and joint torque is influenced by muscle length and contraction velocity, so that is difficult to estimate the mechanical contributions of stretch reflex during function using only EMG [48, 212, 59].

H-reflexes have also been used to quantify the reflex activity [49]. Studies involving H-reflexes apply electrical stimulation to excite the system, bypassing the fusimotor systems and the mechanical stimulus to muscle spindles, which can be heavily modulated during function via γ-motor neurons [207]. In addition, direct stimulation of the nerve might result in the excitation of different afferent mechanisms that project to the $\alpha-$motorneurons (e.g. skin sensors, Golgi tendon organs) so that the resultant response will be generated by combination of the different pathways [47]. Consequently, the functional relevance of these studies is not completely clear.

A better approach would be to directly measure the mechanical consequences of the reflex activity. However, it is difficult to separate the myotatic response from that due to the intrinsic properties of the muscle and connective tissue surrounding the joints. Experimentally this has been achieved by comparing the mechanical behavior of a joint before and after deafferentation using surgery, anaesthesia, cuffing or other manipulation [43, 213]. However, is difficult to validate to what extent this process affects the intrinsic properties of the joint [47, 12].

An alternative approach would be to perform the deafferentation analytically using mathematical models and system identification techniques to separate the mechanical effects of the intrinsic and reflex mechanisms. System identification techniques, using small, random perturbations to excite the intrinsic and reflex dynamics, have been successfully applied to multiple joints with different model types [70, 214, 47, 215]. These models have typically been linear; however, the mechanical response produced by stretch reflexes are highly nonlinear [59], so that these models fail to completely characterize the stretch reflex mechanisms or simply ignore it. The parallel-cascade model, proposed by R. E. Kearney *et at.*, describes the intrinsic and stretch reflex mechanisms in terms of dynamic joint stiffness, that determines the dynamic relation between joint position and the torque acting about it. Intrinsic dynamic stiffness arises from the mechanical properties of the joint, passive tissue, and active muscle fibers, and is described by a linear model relating joint position and torque. Reflex dynamic stiffness arises from changes in muscle activation due to the short-latency stretch reflex, and is described by a nonlinear, Hammerstein model relating joint velocity and torque [12].

Successful application of these analytical techniques have been typically limited to stationary conditions, where the operating point, defined by the joint position and voluntary torque, remains relatively constant throughout the experiment. Stationary experiments have shown that the parallel-cascade model parameters change significantly with the operating point [11, 64]. Consequently, when the operating point changes continuously, as during walking, stiffness model parameters will become time-varying (TV).

Several studies have characterized the intrinsic dynamic stiffness during TV conditions, ignoring the stretch reflex contributions [106, 107, 108, 109, 110, 125, 216]. We have introduced methods for the estimation of intrinsic and stretch reflex mechanisms using the parallel-cascade model structure during TV conditions; however, these methods require very large data sets for parameter estimation, which severely limits their application [111, 112, 103, 113]. Results show that interpolation of parameter values obtained from stationary experiments does not describe joint dynamic stiffness during TV conditions. Therefore, methods that can track parameters changes during TV conditions are required to capture the modulation of the dynamic joint stiffness during function.

This paper develops and validates a novel method to estimate the intrinsic and reflex components of joint dynamic stiffness during periodic, movements, such as walking. This method improves over previous algorithms in several ways: i) it significantly reduces the data requirements for accurate parameter estimation; ii) it parametrizes the system and noise plants independently, diminishing the negative effect that the complex, non-white noise encountered in physiological system, has on

the parameter estimates; and iii) it is not based on correlation analysis, so it can be easily reformulated to work with data measured in closed-loop.

This paper is organized as follows: Section 7.2 presents the TV, parallel-cascade model of joint dynamic stiffness and introduces a novel re-parametrization that approximates, the non-linear, TV model with a set of linear, time-invariant models. It then introduces an algorithm to estimate the parameters of this model using data acquired during periodic, TV conditions. Section 7.3 describes the simulation study used to evaluate the performance of the new model parametrization and identification algorithm. Section 7.4 demonstrates the practical application of the algorithm to estimate intrinsic and reflex ankle dynamic stiffness during imposed walking movements with constant voluntary torque. Section 7.5 summarizes the contributions and discusses some important aspects underlying the method and its application.

7.2 Model Formulation and Parameter Identification

7.2.1 Joint position perturbations and torque

To estimate joint dynamic stiffness during movement, small position perturbations must be applied on top of the joint trajectory [75]. Thus, the overall, perturbed joint trajectory is

$$\theta(t_k) = \theta_0(t_k) + \theta_p(t_k), \tag{7.1}$$

where $\theta_0(t_k)$ is the joint trajectory and $\theta_p(t_k)$ the perturbations.

Under stationary conditions, where the joint position, θ_0, is an offset that is fix throughout the experiment, and the voluntary joint torque is constant, the net

moment at the joint is

$$TQ(t_k) = TQ_0 + TQ_p(t_k) + \xi(t_k),$$

where TQ_0 is a constant torque, produced by passive mechanisms due to the position offset θ_0, and by active mechanisms due to the constant muscle activation; $TQ_p(t_k)$ is a perturbation torque, produced by the excitation of intrinsic and reflex mechanisms by the position perturbations; and $\xi(t_k)$ is a noise signal produced by the combination of physiological and measurement noise [173, 174]. Experimental evidence has shown that for small, zero-mean position perturbations, the perturbation torque is given by

$$TQ_p(t_k) = TQ_I(t_k) + TQ_R(t_k)$$

where $TQ_I(t_k)$ and $TQ_R(t_k)$ are the torques produced by the intrinsic and reflex mechanisms, which cannot be measured directly. However, under stationary condition, a noisy version of the perturbation torque can be retrieved from the net moment at the joint by removing the constant offset TQ_0 from the measured data. Once the perturbation position and torque are computed, specialized analytical methods and models can be used to estimate the individual contributions of the intrinsic and reflex mechanisms [12].

On the other hand, under TV conditions, the joint trajectory $\theta_0(t_k)$ and/or the muscle activation level vary during the experiment, so that $TQ_0(t_k)$, the torque produced by passive and voluntary mechanisms is no longer constant. Consequently, estimating the perturbation torque from the net joint moment now requires a three step procedure: First, a perturbed joint trajectory is applied and the net joint torque,

given by

$$TQ(t_k) = TQ_0(t_k) + TQ_p(t_k) + \xi(t_k),$$

is recorded. Then, a un-perturbed joint trajectory is applied an the net joint torque $TQ_0^*(t_k)$ is recorded. Finally, the torque recorded in both experiments is subtracted to compute a noisy estimate of the perturbed torque. However, it is not realistic to expect that the joint will follow the exact same trajectory and/or that the subject will exert exactly the same voluntary torque in the perturbed and un-perturbed experiments. Therefore, under TV conditions, the perturbation torque is given by

$$TQ_p(t_k) = TQ_I(t_k) + TQ_R(t_k) + TQ_\Delta(t_k), \tag{7.2}$$

where $TQ_\Delta(t_k)$ represents the possible non-zero difference between passive and voluntary torques produced during the perturbed and un-perturbed experiments.

7.2.2 Time-varying dynamic joint stiffness

Once the perturbation joint position and torque are available, a system identification procedure can be applied to analytically separate the intrinsic and reflex components. Under stationary conditions, this can be achieved by modeling the overall dynamic joint stiffness with a parallel-cascade structure, where the intrinsic stiffness is described by a linear systems relating joint position and intrinsic torque, and the reflex stiffness is described by a Hammerstein systems relating joint velocity and reflex torque [12, 64, 62].

Under TV conditions, a TV version of the parallel-cascade structure, shown in Fig. 7–1, has been successfully applied to describe the overall dynamic joint stiffness [111, 112, 103, 113]. However, the identification algorithms used to estimated

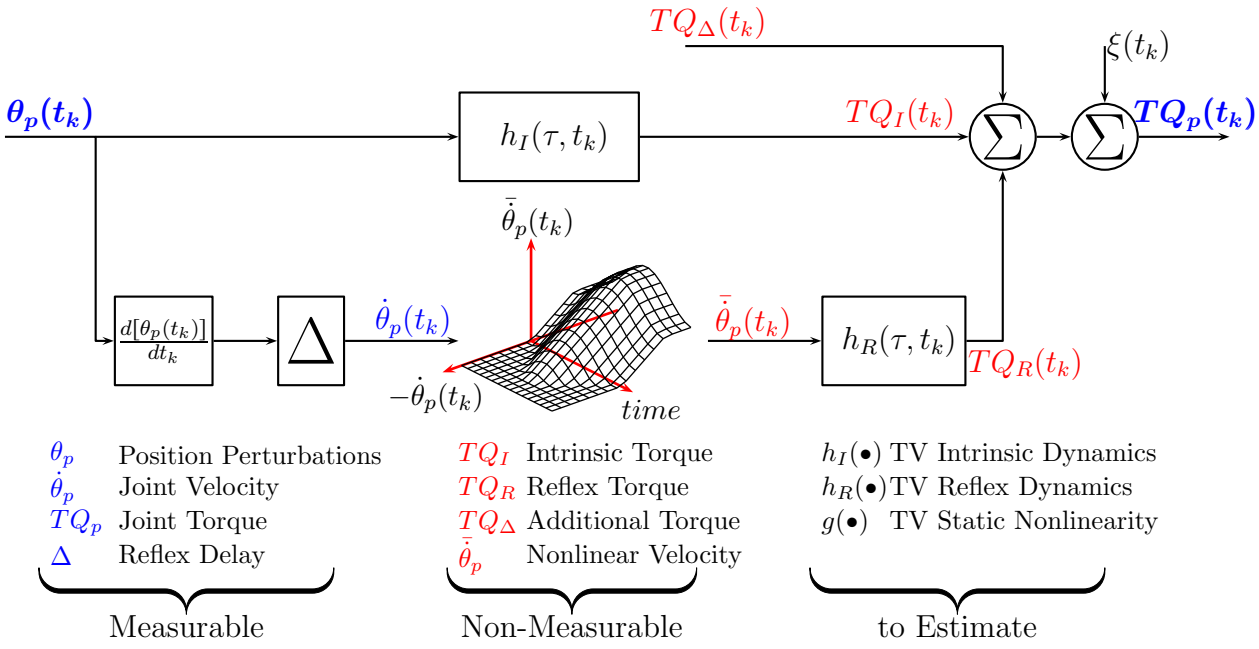

Figure 7–1: Time-Varying, Parallel-Cascade model structure representing the intrinsic and reflex response of the joint to small position perturbations. Measurable signals are shown in blue while those that can only be estimated are shown in red.

the TV model parameters require very large data sets and are difficult to use in practice.

We introduce an alternative parametrization of the TV, nonlinear, parallel-cascade model of dynamic joint stiffness that transforms it into a set of pseudo-linear, time-invariant models.

Intrinsic dynamic stiffness

are usually described by a second order, linear model relating position and torque [1]

$$TQ_I(t_k) = K(t_k)\theta_p(t_k) + B(t_k)\frac{d[\theta_p(t_k)]}{dt_k} + I\frac{d^2[\theta_p(t_k)]}{d^2t_k}, \tag{7.3}$$

where $K(t_k)$, $B(t_k)$ and I are the intrinsic elasticity, viscosity and inertia. However, recent experimental evidence suggests that the intrinsic dynamics stiffness is more complex than second-order [217]. Therefore, we choose to describe intrinsic stiffness with the TV, non-parametric model

$$TQ_I(t_k) = \sum_{\tau=-L}^{\tau=L} h_I(\tau, t_k)\theta_p(t_k - \tau), \tag{7.4}$$

where $h_I(\tau, t_k)$ is a TV, impulse response function (IRF) that requires no a priori assumption of model order. The length of the system memory must be specified but there is much evidence a memory of 40 ms is adequate [12, 216, 217].

***Model re-parametrization*:**

The TV-IRF can be approximated as a linear combination of basis functions

$$h_I(\tau, t_k) = \sum_{j=0}^{j=n_\lambda} \lambda_{\tau,j}\Lambda_j(t_k),$$

where $\{\Lambda_j(t_k)\}_{j=0}^{j=n_\lambda}$ are a set of pre-defined basis functions and $\lambda_{\tau,j}$ their coefficients.

The intrinsic dynamic stiffness can then be approximated by the linear, time-invariant model

$$TQ_I(t_k) = \sum_{\tau=-L}^{\tau=L} \sum_{j=0}^{j=n_\lambda} \lambda_{\tau,j}\Lambda_j(t_k)\,\theta_p(t_k - \tau). \tag{7.5}$$

Reflex dynamic stiffness

can be described by a Hammerstein system, comprising a series combination of a static-nonlinearity and a second-order, linear dynamic system, relating joint velocity

and reflex torque [113, 64, 62].

$$\bar{\dot{\theta}}_p(t_k) = g\left(\dot{\theta}_p(t_k), t_k\right), \tag{7.6a}$$

$$\frac{d^2[TQ_R(t_k)]}{dt_k^2} + 2\zeta(t_k)\omega(t_k)\frac{d[TQ_R(t_k)]}{dt_k} + \omega^2(t_k)TQ_R(t_k) = G(t_k)\omega^2(t_k)\bar{\dot{\theta}}_p(t_k), \tag{7.6b}$$

where $\dot{\theta}_p(t_k)$ is the joint velocity, and $g(\bullet, t_k)$ is a TV, static non-linearity; and $\zeta(t_k)$, $\omega(t_k)$ and $G(t_k)$ are the damping, natural frequency and gain respectively.

This continuous-time, TV, differential can be approximated by a set of frozen, discrete-time, transfer function models given by

$$TQ_R(t_k) = \frac{b_0(t_k)\left(1 + 2q^{-1} + q^{-1}\right)}{1 + a_1(t_k)q^{-1} + a_2(t_k)q^{-2}}\bar{\dot{\theta}}_p(t_k), \tag{7.7}$$

where $b_0(t_k)$, $a_1(t_k)$ and $a_2(t_k)$ are discrete-time, TV parameters and q^{-1} is the backward shift operator. The continuous-time and discrete-time parameters are related to each other by

$$G(t_k) = 4\left[\frac{b_0(t_k)}{1 + a_1(t_k) + a_2(t_k)}\right],$$

$$\omega(t_k) = \frac{2}{T}\left[\frac{1 + a_1(t_k) + a_2(t_k)}{1 - a_1(t_k) + a_2(t_k)}\right]^{1/2},$$

$$\zeta(t_k) = \frac{1 - a_2(t_k)}{\left[\left(1 + a_1(t_k) + a_2(t_k)\right)\left(1 - a_1(t_k) + a_2(t_k)\right)\right]^{1/2}}.$$

***Model re-parametrization*:**

The TV, static non-linearity can be approximated by the linear combinations of Kernel functions

$$\bar{\dot{\theta}}_p(t_k) = g\left(\dot{\theta}_p(t_k), t_k\right) \approx \sum_{i=0}^{i=n_c} c_i(t_k)\, C_i\left(\dot{\theta}_p(t_k)\right),$$

where $C_i(\bullet)$ are a set of pre-defined Kernels (e.g. polynomials, radial basis) and c_i are their TV coefficients. Following the same procedure as before, these are approximated by a linear combination of basis functions as

$$c_i(t_k) = \sum_{j=0}^{j=n_\gamma} \gamma_{i,j}\Gamma_j(t_k),$$

where $\{\Gamma_j(t_k)\}_{j=0}^{j=n_\gamma}$ are a set of basis functions and $\gamma_{i,j}$ their coefficients.

Similarly, the TV parameters of the linear system can be approximated by a linear combination of basis functions

$$b_0(t_k) = \sum_{j=0}^{j=n_\beta} \beta_{0,j}\Psi_j(t_k),$$

$$a_i(t_k) = \alpha_{i,0} + \sum_{j=1}^{j=n_\alpha} \alpha_{i,j}\Pi_j(t_k), \quad i = 0, \ldots, n_a.$$

where $\alpha_{i,0} \neq 0$. $\{\Psi_j(t_k)\}_{j=0}^{j=n_\beta}$ and $\{\Pi_j(t_k)\}_{j=0}^{j=n_\alpha}$ are sets of basis functions with $\Pi_0(t_k) = 1, \forall t_k$; $\beta_{0,j}$, and $\alpha_{i,j}$ their coefficients.

Using these definitions, the relation between the reflex torque ($TQ_R(t_k)$) and joint velocity can be approximated by the discrete-time, time-invariant, Hammerstein system

$$\bar{\dot{\theta}}_p(t_k) = \sum_{i=0}^{i=n_c} \sum_{j=0}^{j=n_\gamma} \gamma_{i,j}\Gamma_j(t_k)\, C_i\left(\dot{\theta}_p(t_k)\right), \tag{7.8a}$$

$$TQ_R(t_k) = \frac{1}{F(q^{-1})}\left[-\sum_{i=1}^{n_a}\sum_{j=1}^{n_\alpha}\alpha_{i,j}\Pi_j(t_k)\,TQ_R(t_k-i) + \sum_{j=0}^{n_\beta}\beta_{i,j}\Psi_j(t_k)\,\bar{\dot{\theta}}_p(t_k)\right], \tag{7.8b}$$

where $F(q^{-1})$ is the polynomial

$$F\left(q^{-1}\right) = 1 + \alpha_{1,0}q^{-1} + \alpha_{2,0}q^{-2},$$

Other components

$TQ_\Delta(t_k)$ is expected to be an stochastic, low-frequency signal. It can be described by a linear combination of basis functions

$$TQ_\Delta(t_k) = \sum_{j=0}^{j=n_p} p_i P_i(t_k), \tag{7.9}$$

where $\{P_i(t_k)\}_{j=0}^{j=n_p}$ are a set of basis functions and p_i their coefficients.

Overall joint stiffness

Using these re-parameterizations, the overall relation between joint position and torque, shown in Fig. 7–1, can be approximated by the linear, TI models shown in equations (7.5), (7.8a), (7.8b), and (7.9) with coefficients

$$\boldsymbol{\rho}_I = \left[\lambda_{-L,0}\cdots\lambda_{-L,n_\lambda}\cdots\lambda_{L,0}\cdots\lambda_{L,n_\lambda}\right], \tag{7.10a}$$

$$\boldsymbol{\rho}_R = \left[\alpha_{1,0}\cdots\alpha_{1,n_\alpha}\cdots\alpha_{2,0}\cdots\alpha_{2,n_\alpha}\ \beta_{0,0}\cdots\beta_{0,n_\beta} \gamma_{0,0}\cdots\gamma_{0,n_\gamma}\cdots\gamma_{n_c,0}\cdots\gamma_{n_c,n_\gamma}\right], \tag{7.10b}$$

$$\boldsymbol{\rho}_A = \left[p_0\cdots p_{n_p}\right], \tag{7.10c}$$

7.2.3 Identification of TV, dynamic joint stiffness

We now describe an algorithm for the identification of the re-parametrized models of the intrinsic, reflex and $TQ_{\Delta}(t_k)$. There are four key elements to the algorithm. First, as Fig. 7–1 shows, $TQ_I(t_k)$, $TQ_R(t_k)$ and $TQ_{\Delta}(t_k)$ cannot be measured directly so the models that describe each component cannot be estimated directly from measured data. This problem is addressed using an iterative algorithm that estimates the models sequentially by removing the influence of the other pathways before estimating the parameters of each component [12, 113].

Second, the parameters of the Hammerstein system that represents the reflex component are identified using an additional iterative algorithm, that estimates the static nonlinearity and linear element are sequentially. This method identifies the coefficients representing the static nonlinearity and reflex dynamics iteratively and is guaranteed to converge to the true values under general conditions [172, 151]

Third, an Ordinary Least-Squares (OLS) algorithm used to estimate the reflex linear dynamics will give biased estimates if the noise is not white [101]. To avoid this, we use an instrumental variable approach, that provides unbiased estimates of the model parameters even in the presence of non-white noise [177, 218].

Finally, the identification algorithm assumes that the parameters' time-course is repeated periodically so that it is possible to measure multiple trials presenting the same time-varying behavior. The algorithm exploits the periodicity and estimates only one period of the model parameters' time-course using multiple cycles of the input and output data. This algorithm combines two different methodologies for TV

identification: temporal expansion and ensemble approaches. This hybrid identification algorithm was recently introduced by us, and simulation results showed that it can track faster changing parameters than the temporal expansion method and requires significantly less data than the ensemble approach [218].

Identification algorithm

assume that n cycles, each with N data points, of joint position and torque were measured for both the un-perturbed and perturbed joint trajectories. The perturbation position and torque signal are computed by aligning and subtracting the measured position and torque signals during the perturbed and un-perturbed experiments. Following eq. (7.2), the noise-free perturbation torque for n cycles can organized in matrix form as

$$\begin{bmatrix} \boldsymbol{TQ_p}\{1\} \\ \vdots \\ \boldsymbol{TQ_p}\{n\} \end{bmatrix} = \begin{bmatrix} \boldsymbol{TQ_I}\{1\} \\ \vdots \\ \boldsymbol{TQ_I}\{n\} \end{bmatrix} + \begin{bmatrix} \boldsymbol{TQ_R}\{1\} \\ \vdots \\ \boldsymbol{TQ_R}\{n\} \end{bmatrix} + \begin{bmatrix} \boldsymbol{TQ_\Delta}\{1\} \\ \vdots \\ \boldsymbol{TQ_\Delta}\{n\} \end{bmatrix}, \tag{7.11}$$

where

$$\boldsymbol{TQ_p}\{j\} = \left[TQ_p(1)\{j\} \cdots TQ_p(N)\{j\}\right]^T,$$

is the perturbed torque for the j-th cycle. The identification algorithm assumes that intrinsic and reflex dynamics have the same time-varying behavior in each cycle so that the model parameters are periodic. In contrast, $TQ_\Delta(t_k)$ is assumed to be different for each cycle, consequently, the parameters describing this torque are different for each cycle.

The identification algorithm proceeds as follows:

1. Initialize

$$\widehat{\boldsymbol{TQ}}_{\boldsymbol{I}}\{j\} = \widehat{\boldsymbol{TQ}}_{\boldsymbol{R}}\{j\} = \boldsymbol{O}, \quad j = 1, \cdots, n.$$

2. Estimate the TQ_{Δ} for each cycles as

$$\widetilde{\boldsymbol{TQ}}_{\Delta}\{j\} = \boldsymbol{TQ}_{p}\{j\} - \left(\widehat{\boldsymbol{TQ}}_{\boldsymbol{I}}\{j\} + \widehat{\boldsymbol{TQ}}_{\boldsymbol{R}}\{j\}\right)$$

   - Use $\widetilde{\boldsymbol{TQ}}_{\Delta}\{j\}$ and the linear, identification algorithm introduced in [216] to estimate $\hat{\boldsymbol{\rho}}_{A}$. The algorithm estimates a new set of coefficients for each cycle.

   - Use the identified parameters to update the estimate of $\widehat{\boldsymbol{TQ}}_{\Delta}\{j\}$ for each cycle.

3. Estimate the intrinsic torque as

$$\widetilde{\boldsymbol{TQ}}_{I}\{j\} = \boldsymbol{TQ}_{\boldsymbol{p}}\{j\} - \left(\widehat{\boldsymbol{TQ}}_{\boldsymbol{R}}\{j\} + \widehat{\boldsymbol{TQ}}_{\boldsymbol{\Delta}}\{j\}\right)$$

   - Use the estimated intrinsic torque, the perturbation position and the identification algorithm introduced in [216] to estimate $\hat{\boldsymbol{\rho}}_{I}$. The algorithm estimates one single set of coefficients using all the cycles assuming periodicity in the joint trajectory.

   - Use the identified parameters and the perturbation position to update the estimate of $\widehat{\boldsymbol{TQ}}_{I}\{j\}$ for each gait cycle.

4. Estimate the reflex torque as

$$\widetilde{\boldsymbol{TQ}}_{R}\{j\} = \boldsymbol{TQ}_{\boldsymbol{p}}\{j\} - \left(\widehat{\boldsymbol{TQ}}_{\boldsymbol{I}}\{j\} + \widehat{\boldsymbol{TQ}}_{\boldsymbol{\Delta}}\{j\}\right)$$

   - Use the estimated reflex torque, the perturbation velocity and the identification algorithm introduced in [172] to estimate $\hat{\boldsymbol{\rho}}_{R}$. The algorithm estimates one single set of coefficients using all the cycles assuming periodicity in the joint trajectory.

   - Use the identified parameters and the perturbation velocity to update the estimate of $\widehat{\boldsymbol{TQ}}_{R}\{j\}$ for each cycle.

5. Compute the net predicted torque for all the gait cycles as

$$\widehat{\boldsymbol{TQ}}_p\{j\} = \widehat{\boldsymbol{TQ}}_{\boldsymbol{I}}\{j\} + \widehat{\boldsymbol{TQ}}_{\boldsymbol{R}}\{j\} + \widehat{\boldsymbol{TQ}}_{\boldsymbol{\Delta}}\{j\}$$

and calculate the percentage of variance accounted for ($\%VAF$) between the predicted and measured torque signals as

$$\%VAF = max\left[0, \frac{\sum_{t_k=1}^{t_k=N*n}\left(TQ_p(t_k) - \widehat{TQ}_p(t_k)\right)^2}{\sum_{t_k=1}^{t_k=N*n}\left(TQ_p(t_k)\right)^2}\right],$$

where $N * n$ is the total length of the data record.

6. The procedure is repeated from step 2 until successive iterations fail to improve $\%VAF$.

The identification algorithm provides estimates of the intrinsic ($\widehat{TQ}_I(t_k)$), reflex ($\widehat{TQ}_R(t_k)$) and additional ($\widehat{TQ}_\Delta(t_k)$) torques, along with the model parameters $\hat{\boldsymbol{\rho}}_I$ and $\hat{\boldsymbol{\rho}}_R$.

7.3 Simulation Study

7.3.1 Methods

The utility of the new algorithm was evaluated using simulations of TV, dynamic ankle stiffness throughout the gait cycle.

Simulated model

Fig. 7–2 presents the TV, joint dynamic stiffness model. The intrinsic stiffness was simulated as a time-varying, continuous-time, second-order system. The reflex stiffness as a series connection of a delay, fixed to 40ms, a differentiator, and a Hammerstein system; the TV, static-nonlinearity was given by a half-wave rectifier

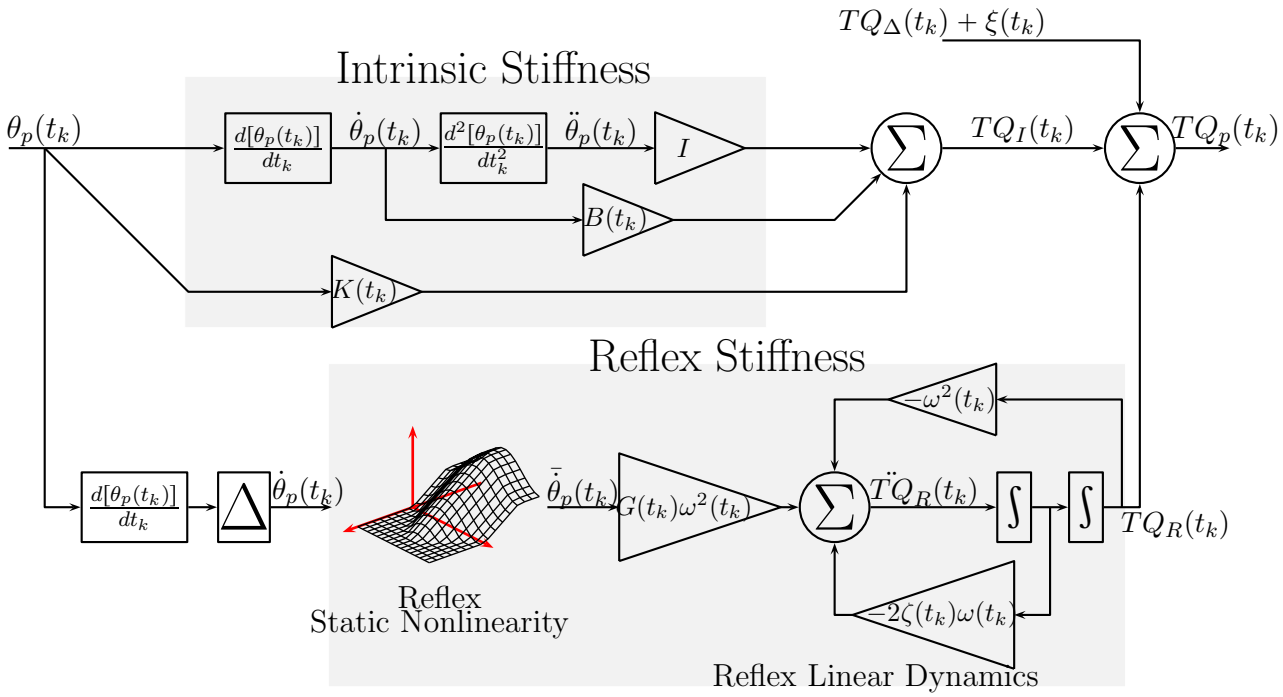

Figure 7–2: Simulated, TV, Parallel-Cascade model. Intrinsic dynamic stiffness was modeled as a TV, second order, continuous-time system, and reflex dynamic stiffness was modeled as a Hammerstein system with TV static-nonlinearity followed by a second order, continuous-time system.

with a TV threshold ($th(t_k)$) and the reflex, linear dynamics was a continuous-time, second-order system.

Model parameters

Fig. 7–3 show the time-course of the simulated parameters as a function of the gait cycle.

The top three panels in the left column of Fig. 7–3 show the time-course of the intrinsic stiffness parameters, these values were originally reported by Lee *et. al* [125].

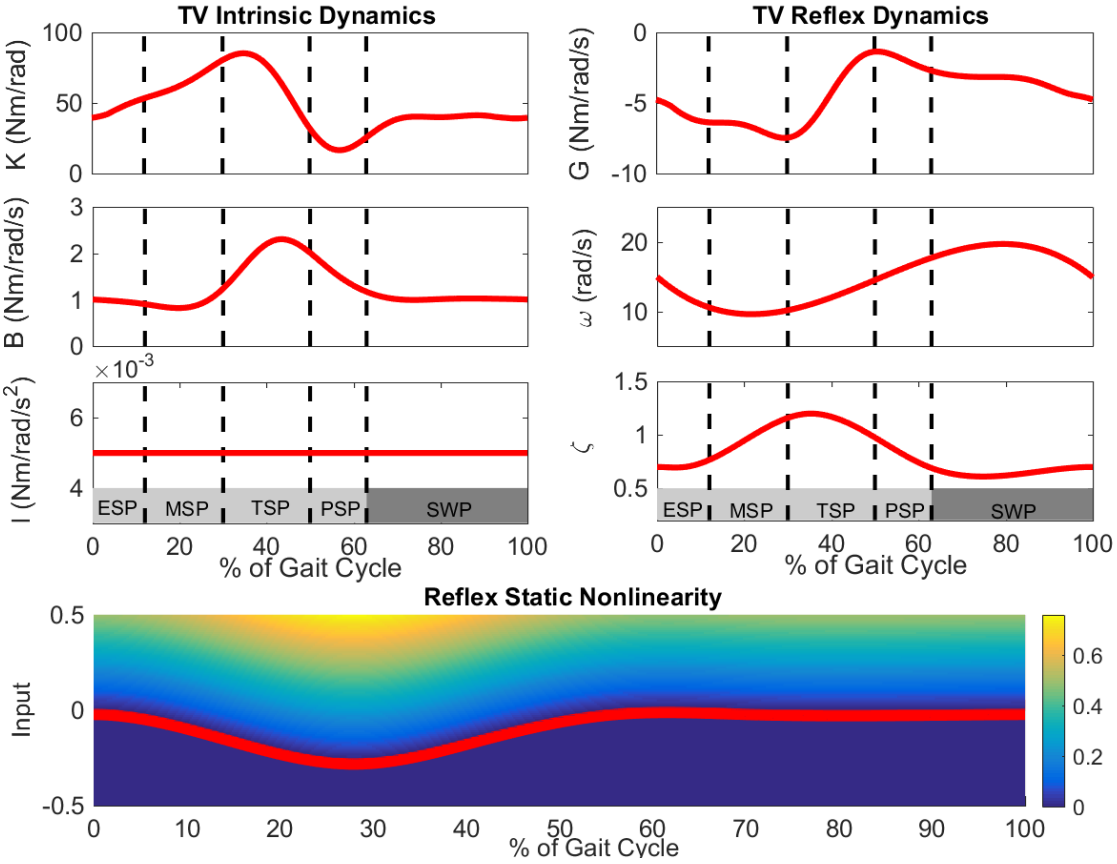

Figure 7–3: Simulated time-varying model parameters as a function of gait cycle. Top three panes - Left column: Intrinsic Stiffness (K), viscosity (B), and inertia (I). - Right column: Reflex gain (G), natural frequency (ω), and damping (ζ). Bottom panel presents the reflex static-nonlinearity with the red line showing the TV threshold. Vertical lines divide the gait cycle in its sub-phases starting at heel-strike: early stance (ESP), mid-stance (MSP), terminal stance (TSP), pre-swing (PSP), and swing phase (SWP).

The top three panels in the right column of Fig. 4–3 show the linear, reflex dynamics parameters. The reflex gain was originally reported by Sinkjaer *et. at* [207], whereas the simulated reflex natural frequency and damping were generated by interpolating results from static experiments with matched position [64]. Finally, the

bottom panel of Fig. 4–3 shown the reflex static-nonlinearity. The TV threshold was selected to change significantly during the stance phase of walking, where the reflex gain is largest, and to remain constant at zero during the pre-swing and swing phases.

Input

Fig. 7–4A shows the input sequence, corresponding to a *Pseudo Random Arbitrary Level Distributed Signal* (PRALDS) with a random switching rate drawn from a uniform distribution between 250ms and 350m, and a peak-to-peak amplitude of 0.06 rad. The PRALDS has velocities distributed over the whole range of possible values and so it provides a rich set of values with which to estimate the reflex static-nonlinearity [156].

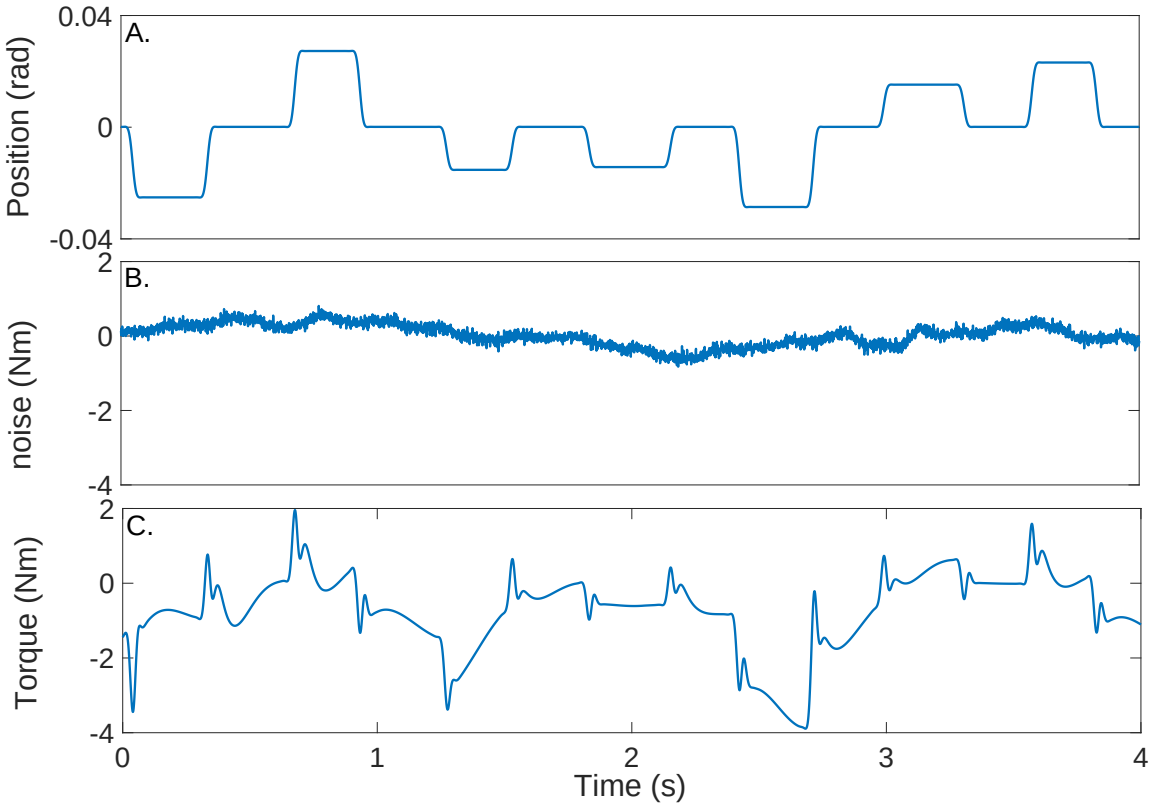

Figure 7–4: Typical simulation results: A) Joint position input, B) experimental noise and C) joint torque output.

Noise

Fig. 7–4B shows the noise used in the simulations. It was obtained from a library of experimental signals of ankle torque recorded while subjects maintained a constant torque with fixed ankle position [173]. The library comprised 100 records each lasting 60s, from six subjects generating dorsiflexing torques corresponding to 5%, 10% and 15% of their maximum voluntary torque. For each simulation trial, a section of the recorded torque noise was selected at random and its mean was removed. This noise signal is composed of a low-frequency trend (corresponding

to $TQ_{\Delta}(t_k)$), physiological tremor, 60Hz noise, and white-Gaussian measurement noise [173, 174]. The noise amplitude was adjusted to give an average signal-to-noise ratio (SNR) of 20dB across the record. The SNR is lower than expected experimentally, which has been shown to be around 40 dB [219].

Simulation

Fig. 7–4C shows the noise-free output, produced by the sum of the simulated intrinsic and reflex torques. The model was simulated using Simulink (the MathWorks) using a third order solver with a sampling rate of 1KHz. Each simulated step lasted for 1.4s, which is equivalent to slow walking [207]; 40 gait cycles were simulated so that each trial lasted for 56s. Afterwards, perturbation position and torque were decimated to 100Hz for analysis.

The 56s trial was repeated 100 times with a new input and noise sequence to compute statistical properties of the parameter estimates.

7.3.2 Basis functions

Cubic B-splines were selected as basis functions to represent the coefficients of the intrinsic TV-IRF ($\{\Lambda_j(t_k)\}_{j=0}^{j=n_\lambda}$); the TV, reflex static-nonlinearity ($\{\Gamma_j(t_k)\}_{j=0}^{j=n_\gamma}$); and the numerator of the TV, reflex linear dynamics ($\{\Psi_j(t_k)\}_{j=0}^{j=n_\beta}$). The B-splines knots were uniformly distributed along the gait cycle, 10 basis functions we used to represent each TV parameter. The number of basis was selected as the minimum order necessary to describe the true TV parameters with a variance accounted for of at least 99%.

Tchebichev polynomials were selected as basis functions to represent the coefficients in the denominator of the TV, reflex linear dynamics ($\{\Pi_j(t_k)\}_{j=0}^{j=n_\alpha}$) and

$TQ_\Delta(t_k)$ ($\{P_j(t_k)\}_{j=0}^{j=n_p}$). Polynomials of order 0 to 7 were used to represent the denominator of the TV, reflex linear dynamics, whereas polynomials of order 0 to 4 were used to represent $TQ_\Delta(t_k)$.

Tchebichev polynomials were used as Kernels to represent the reflex, static-nonlinearity ($\{C_j(\dot{\theta}_p(t_k))\}_{j=0}^{j=n_c}$). There are some advantages of using this type of Kernels: i) the first-order Kernel is linear, $C_1(\dot{\theta}_p(t_k)) = \dot{\theta}_p(t_k)$, so that the estimated parameters can be used to validate whether a nonlinear model is needed or not; and ii) the variance of the output is finite in its support, which guarantees the numerical stability of the estimation process. Polynomials of order 0 to 4 were used as Kernels to approximate the TV static-nonlinearity.

7.3.3 Estimated parameters

Table 7–1: Number of free parameters in simulated and estimated models

	Simulated model (TV coefficients)	Estimated model (TI coefficients)
Intrinsic linear dynamics	3	90
Reflex static-nonlinearity	1	40
Reflex linear dynamics	3	34
Additional torque	-	200

Table 7–1 presents the number of parameters in the simulated and estimated models, showing that the proposed re-parametrization transforms the low-order, TV modes, whose parameters cannot be directly estimated into high-order, TI models, whose parameters can be easily estimated using linear identification algorithms.

$TQ_\Delta(t_k)$ was approximated with 5 coefficients at each cycle, so that a total of 200 coefficients were estimates in the 40 cycles.

A property of the Hammerstein systems is that the gain can be arbitrarily assigned to the static-nonlinearity or the linear dynamic element without affecting the output. For consistency, we decided to assign the gain of the reflex pathway to the static-nonlinearity, fixing the linear dynamics gain ($G(t_k)$) to unity.

7.3.4 Validation

The predictive ability of the estimated model was quantified in terms of the Variance Accounted For (VAF) between the predicted and simulated intrinsic and reflex torques. An average-VAF was computed using all the data for each simulation trial as shown in step 5 of the identification algorithm. In addition, a TV-VAF was computed, this measure was obtained by dividing each gait cycle into 20 segments and computing the VAF between predicted and simulated signals for each segment.

As it is difficult to compute the intrinsic viscosity and inertia directly from the estimated TV-IRF, the simulated and estimated intrinsic, TV models were compared in terms of their time-frequency response, that were calculated for the parametric and non-parametric models [136]. Moreover, the TV intrinsic elasticity (K) was computed, by summing the elements of the estimated IRF at each point in time, and compared with the simulated parameter.

The shape of the estimated reflex, TV, static-nonlinearity (which includes the reflex gain) was compared with the simulated TV, half-wave rectifier. The TV, reflex natural frequency (ω) and damping (ζ) were computed directly from the estimated, discrete-time parameters and compared with the simulated parameters.

Time-invariant, dynamic joint stiffness model

For comparison purposes, a time-invariant (TI), dynamic joint stiffness model was estimated between the perturbation position and noisy torque signals using the all the cycles. The TI, intrinsic and reflex model parameters were estimated using the new algorithm by fixing the basis functions used to represent the intrinsic a reflex models coefficients to be a single basis, given by an all-ones vector.

7.3.5 Results

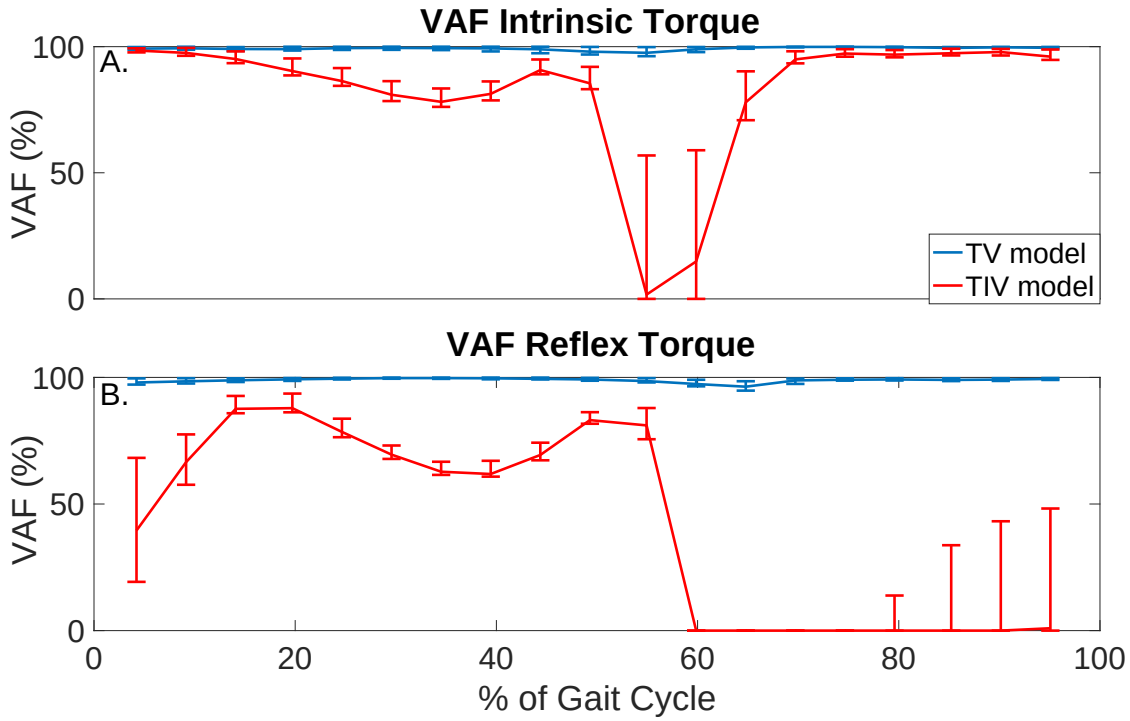

Figure 7–5: TV-VAF between the noise-free torque and the output of the time-invariant (red lines) and time-varying (blue lines) models, each bar presents the mean, 5th and 95th percentile computed for the 4000 simulated gait cycles. A) Intrinsic torque, and B) reflex torque.

Time-invariant results

The TI model did a poor job at predicting the simulated data, the average-VAF was always lower than 70% for both intrinsic and reflex torques. Furthermore, Fig. 7–5 presents the TV-VAF obtained for the 4000 simulated gait cycles. Is clear that the TI models were not able to capture the time-varying system dynamics, indicating the need for TV models.

Time-varying results

The TV model predicted the output extremely well, the average-VAF was always larger than than 99% for both intrinsic and reflex torques. Fig. 7–5 shows that the TV-VAF for the intrinsic and reflex torques was always greater than 97%; the lowest values were observed around the pre-swing and early-swing phases of the cycle, where the gain of the intrinsic and reflex pathways are smallest.

TV intrinsic dynamic stiffness

Fig. 7–6A presents the simulated (red) and estimated (blue) intrinsic elasticity, demonstrating that the estimated parameter tracked the true values very closely in all the 100 trials. Furthermore, the bottom panels of the figure present snapshots at different landmarks of the gait cycle of the time-frequency response for both the estimated TV-IRF (blue lines) and the simulated, second-order model (red lines). There was a remarkable similitude in the time-frequency response of the estimated and simulated systems up to around 30 Hz, corresponding to the input's band-width, with the results obtained in the 100 simulations falling very close to the simulated system frequency response.

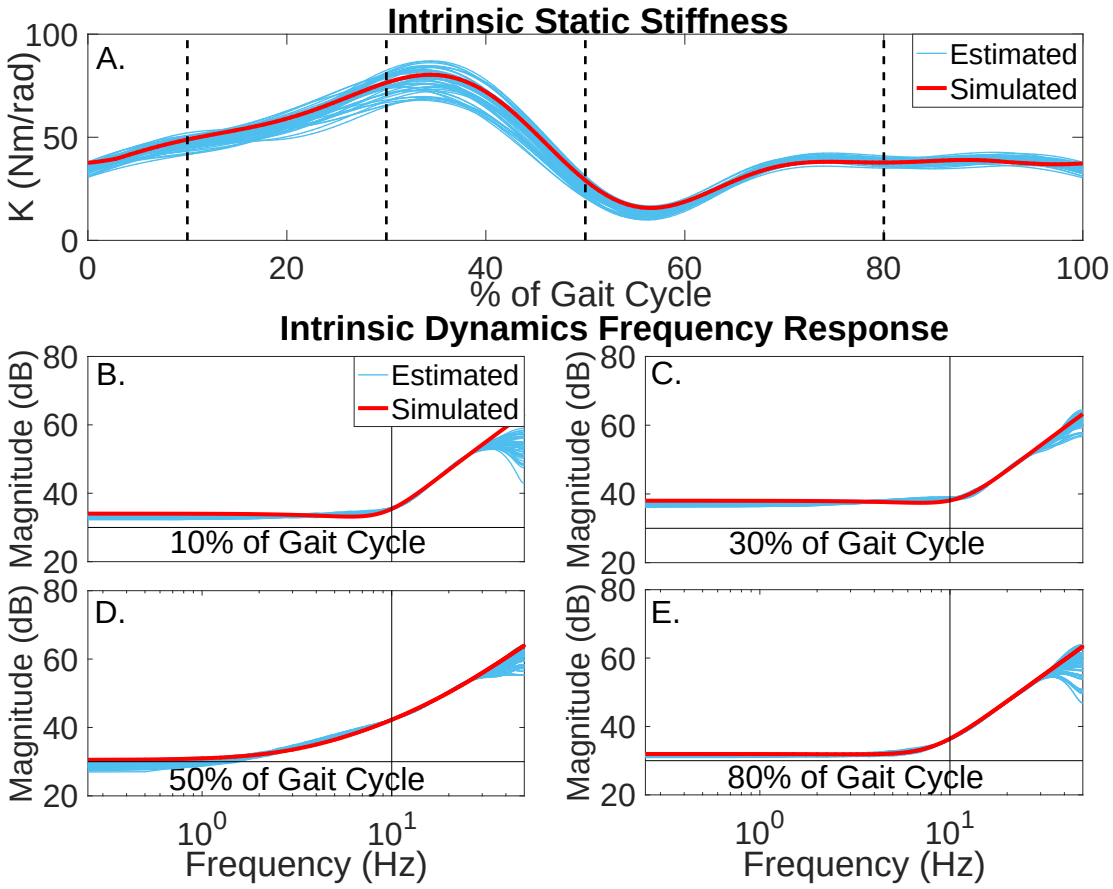

Figure 7–6: Intrinsic dynamic stiffness. Top panel :Simulated (red line) and estimated (blue lines) intrinsic stiffness ($K(t_k)$) as a function of gait cycle. Bottom four panels: Snapshots of the time-frequency response of the simulated (red lines) and estimated (blue lines) systems at different landmarks of the gait cycle, these instances are indicated in the top panel with vertical lines and correspond to: the beginning of the mid-stance phase, the beginning and end of the terminal-stance phase, and the middle of the swing-phase.

TV reflex dynamic stiffness

The top four panels of Fig. 7–7 present snapshots at different landmarks of the gait cycle of the estimated and simulated TV static-nonlinearity. As the different

panels demonstrate, the estimated, polynomial static-nonlinearity was able to accurately track both the TV threshold and slope of the simulated half-wave rectifier. The bottom panels of the figure shown the simulated and estimated natural frequency and damping of the reflex, linear dynamics model, demonstrating that the estimated parameters tracked the true values closely. The reflex damping was slightly underestimated; however, this did not significantly affected the VAF.

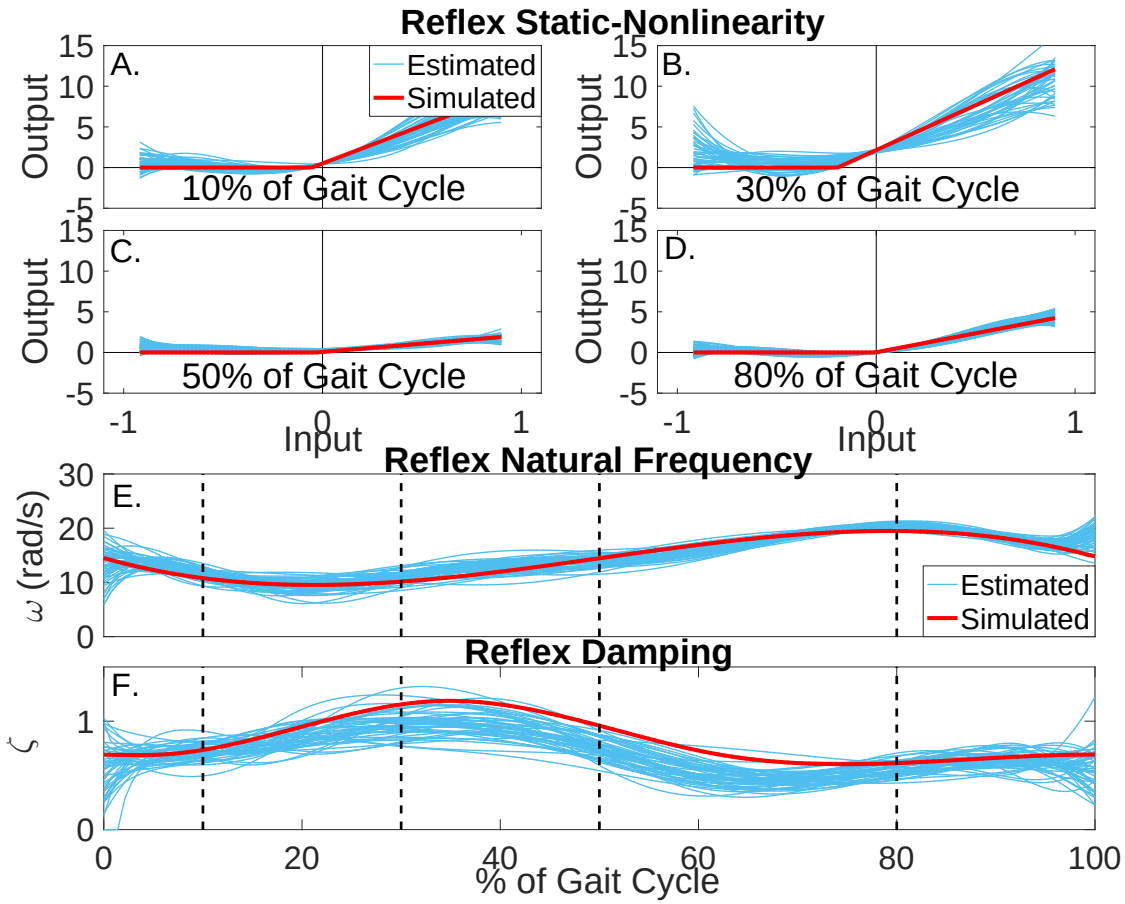

Figure 7–7: Reflex dynamic stiffness. Top four panels: Snapshots of the the simulated (red lines) and estimated (blue lines) TV, static nonlinearity at different landmarks of the gait cycle, these instances are indicated in the bottom panels with vertical lines. Bottom panels: Simulates (red line) and estimated (blue lines) reflex natural frequency ($\omega(t_k)$) and damping ($\zeta(t_k)$) as a function of gait cycle.

7.4 Experimental Study

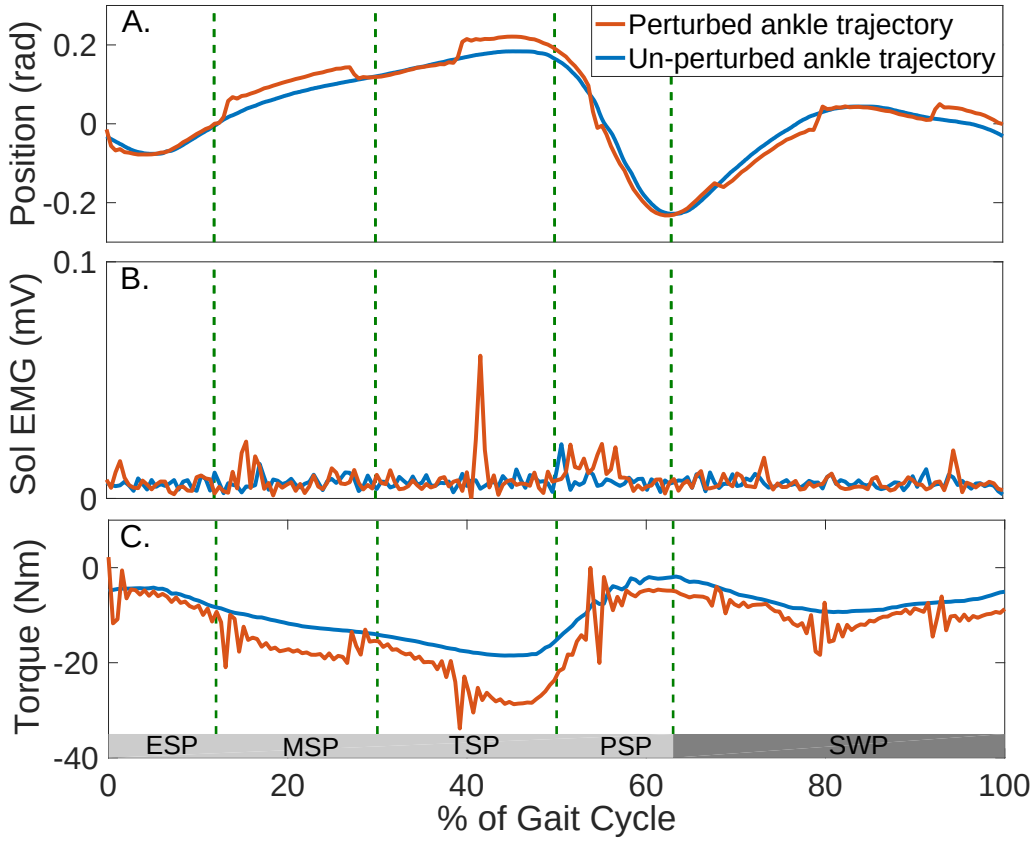

Figure 7–8: Typical data recorded during a un-perturbed (blue lines) and perturbed (brown lines) gait cycle. A) Ankle trajectory, B) Soleus EMG and C) ankle torque.

The utility of the new TV, identification algorithm was demonstrated by estimating the ankle dynamic stiffness during an imposed walking movement with constant voluntary torque from measured joint position and torque data acquired from one healthy subject, who provided written informed consent. The experiment was approved by the McGill University Research Ethics Office.

7.4.1 Experimental methods

The subject lay supine with his left foot attached to the pedal of an electrohydraulic actuator operating as a position servo by means of a custom made fiberglass boot [12]. The ankle movement was restricted to plantarflexion and dorsiflexion.

Ankle position, torque, and surface EMG from the medial and lateral gastrocnemius (GM and GL), soleus (SOL) and tibialis anterior (TA) were measured, filtered at 400Hz to prevent aliasing and sampled at 1kHz by a 16-bit A/D converter. Data were decimated to 100Hz for analysis.

During the experiment, the actuator moved the ankle to zero position (i.e., there was a right angle between the foot and shank) and held there for a one minute. Then, a un-perturbed ankle trajectory consisting of 30 gait cycles, each lasting for 2 s, was applied. This experiment was repeated 2 times to obtain a total of 60 un-perturbed gait cycles. The experiment was then repeated but this time a perturbed ankle trajectory was applied. The perturbed trajectory was obtained by adding a PRALDS, similar to that used in the simulation study, to the walking trajectory.

The subject was required to maintain a constant plantarflexion torque corresponding to 10% of his maximum torque but not react to the imposed movement. For this, the subject was presented with a visual feedback consisting of a low-pass filtered (0.7Hz) version of the measured torque minus the passive torque produced during the un-perturbed ankle trajectory, which was measured beforehand. The subject was allowed to train for several minutes before the beginning of the trial.

Perturbed and un-perturbed ankle trajectories and torque signals were subtracted to compute the perturbation position ($\theta_p(t_k)$) and torque ($TQ_p(t_k)$). Data

was then divided into identification and validation segments; 40 gait cycles were used for parameters estimation and the remaining 20 cycles for model validation. The model was validated by computing the average-VAF between the measured and predicted torques for the validation data.

Fig. 7–8 shows the perturbed and un-perturbed ankle trajectories, soleus EMG, and ankle torques measured during one imposed gait cycle. Furthermore, top panels of Fig. 7–9 present with blue lines the perturbation position ($\theta_p(t_k)$) and torque ($TQ_p(t_k)$) signals for two gait cycles.

7.4.2 Results

Time-invariant results

An estimated TI model did a poor job at predicting the measured data, the average-VAF was always lower than 75%. This result indicate the need for a TV model to capture the system dynamics.

Time-varying model

An estimated TV model predicted the measured torque very well, the average-VAF for the validation trials was always larger than 95%. Fig. 7–9B presents the predicted total torque for two of the validation gait cycles with a brown line. For these particular cycles, the average-VAF was 96%. The good agreement between the measured and predicted torques indicates that the estimated model was able to accurately capture the system dynamics. In addition, panels C, D and E of the same figure present the predicted intrinsic,reflex and $TQ_\Delta(t_k)$ as a function of time.

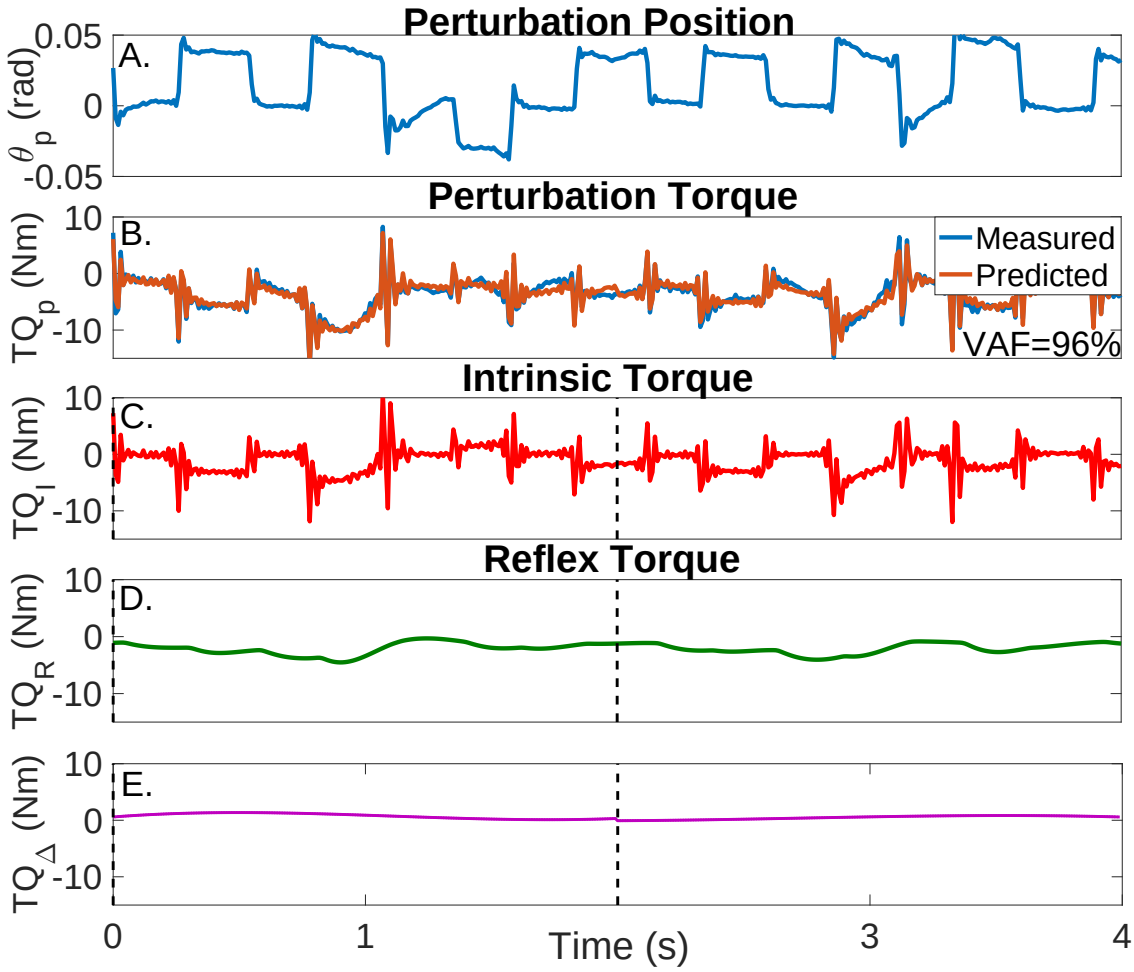

Figure 7–9: Results for a typical validation trial as a function of % of gait cycle. A) Perturbation position input, B) Measured (blue) and predicted (brown) perturbation torque, C) Estimated intrinsic torque, D) Estimated reflex torque and C) Estimated additional torque.

TV intrinsic dynamic stiffness

The parameters of the TV-IRF used to represent the intrinsic dynamic stiffness underwent large, fast changes throughout the gait cycle. Fig. 7–10A presents the variation in the intrinsic elasticity, which was computed directly from the TV-IRF,

along with the 95% confidence interval, computed by applying a bootstrap analysis with 100 repetitions [193]. The intrinsic elasticity increased three fold (from 30 Nm/rad to 90 Nm/rad) during the stance phase, and sharply decreased during the pre-swing phase (to around 20Nm/rad). Then, it returned to its initial value and remained constant throughout the swing phase.

In addition, Fig. 7–10C presents the intrinsic elasticity as a function of ankle position. This plot indicates that: i) the intrinsic elasticity is larger in plantarflexion than dorsiflexion; ii) the relation between joint position and intrinsic elasticity is nonlinear and seems to be influenced by the phase of the gait cycle.

Furthermore, the upper pathway of Fig. 7–11 shows the time-frequency response of the TV-IRF as a function of the gait cycle. The purple line indicated the ankle elasticity. The intrinsic dynamic stiffness showed a high-pass behavior, typically observed during stationary experiments [212], and underwent large, fast changes throughout the gait cycle

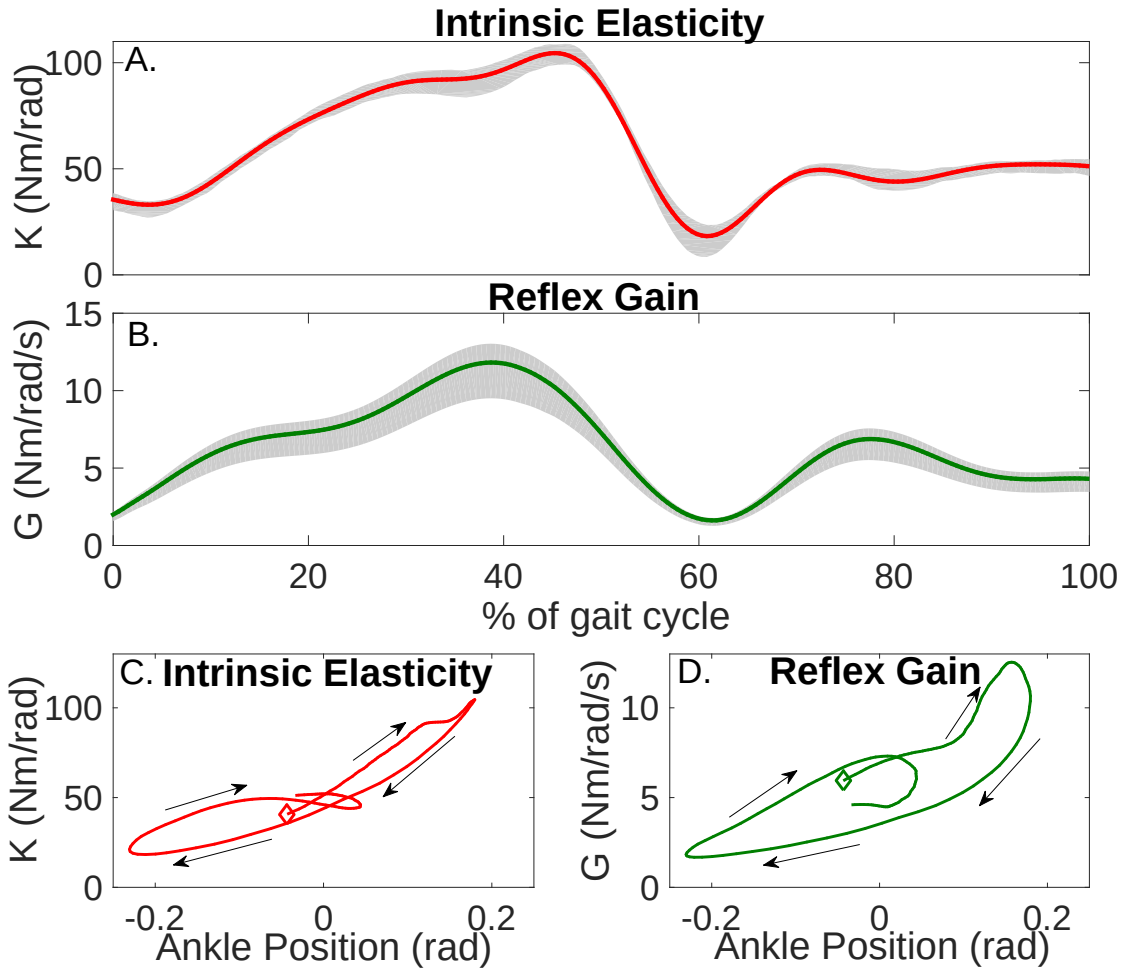

Figure 7–10: A) Intrinsic and B) reflex gains as a function of ankle position. Heel-strike is indicated with an un-filled diamond, arrows show the progression of the gait cycle.

TV reflex dynamic stiffness

The parameters of the polynomial nonlinearity used to represent the reflex, static-nonlinearity underwent large, fast changes throughout the gait cycle. Fig. 7–10B presents the variation in the reflex gain, computed as the slope of the static nonlinearity, along with the 95% confidence interval. The reflex gain increased two

fold (from 6 Nm/rad/s to 12 Nm/rad/s) during the stance phase, and decreased to almost zero during the pre-swing phase. Then, it increased and remained constant throughout the swing phase.

In addition, Fig. 7–10D presents the reflex gain as a function of ankle position. This plot indicates that: i) the reflex gain is larger in plantarflexion than dorsiflexion; ii) the relation between joint position and reflex gain is nonlinear and seems to be influenced by the phase of the gait cycle.

Furthermore, the parameters of the second-order, linear system used to represent the reflex, linear dynamics did not vary significantly. The lower pathway of Fig. 7–11 shows the TV, static-nonlinearity as a function of gait cycle and the frequency response of the reflex linear dynamic model. The estimated static-nonlinearity resembles a half-wave rectifier; the gain underwent large, fast changes throughout the gait cycle. The linear dynamics, which presents a low-pass behavior, did not vary throughout the gait cycle. The shape of the static nonlinearity and the cut-off frequency of the linear dynamic element coincide with what has been observed in stationary experiments [212].

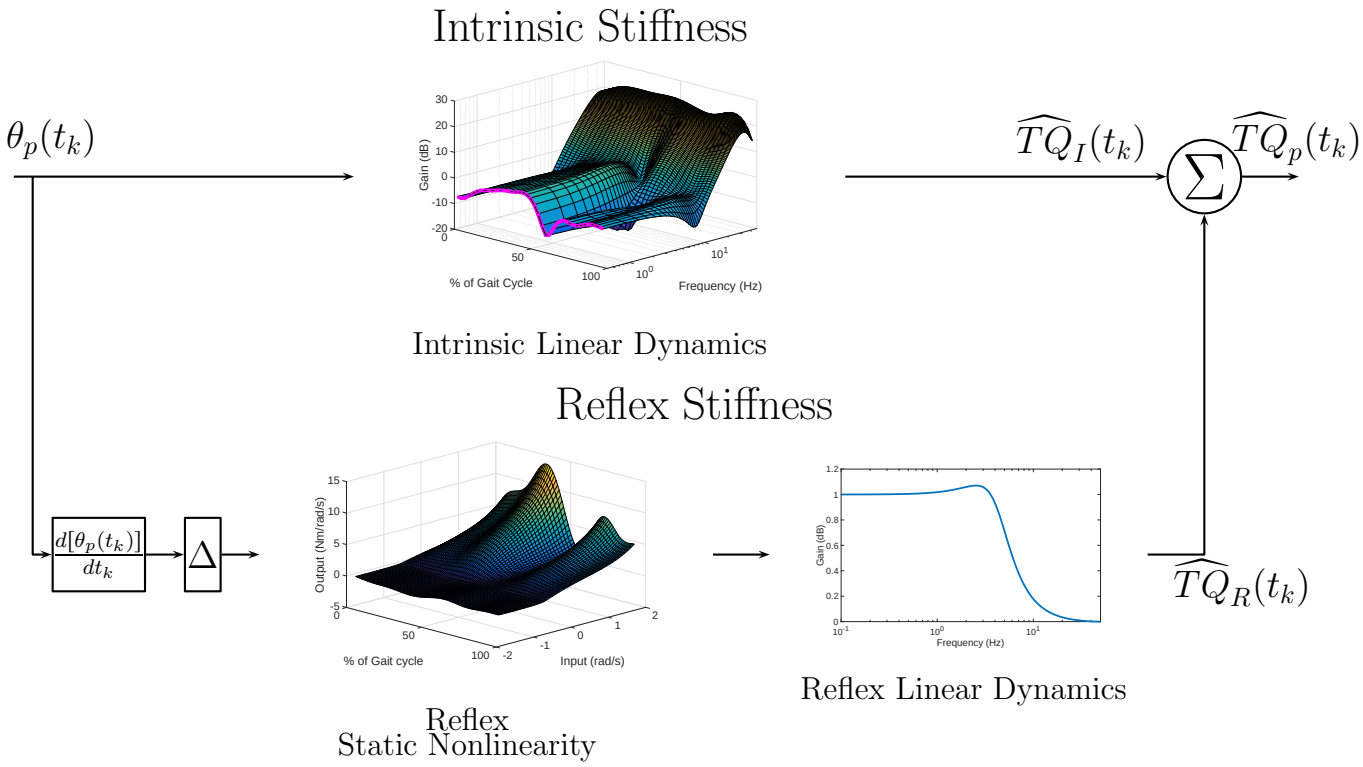

Figure 7–11: Estimated, TV, Parallel-Cascade model. Intrinsic dynamic stiffness was modeled as a TV-IRF model, and reflex dynamic stiffness was modeled as a Hammerstein system with TV static-nonlinearity followed by a time-invariant, low-pass filter.

7.5 Discussion and Conclusions

This paper presents a new model parametrization and identification algorithm for the accurate estimation of the intrinsic and stretch reflex components of TV dynamic joint stiffness. The algorithm combines ensemble and deterministic approaches to estimate the parameters of the TV model from position and torque records. Simulations demonstrated that the new algorithm successfully decomposed the dynamic joint stiffness into its intrinsic and reflex components from position and total torque signals, and accurately tracked the fast, large changes in the parameters of each

pathway using as few as 40 gait cycles even in the presence of experimental noise. Furthermore, the method was successfully applied for dynamic joint stiffness estimation during an imposed walking experiment. The good agreement between the predicted and measured torques demonstrated that the new methodology was able to accurately describe the overall TV, ankle dynamic stiffness.

7.5.1 Methodological issues and limitations

Methods that estimate TV, joint dynamic stiffness make three underlying assumptions: i) The small perturbations applied to the joint do not modify the operating point [12]; ii) the mechanical response of the joint to small perturbations and to large changes in the operating point, such as the changes in the joint trajectory observed during the experimental trial, are linearly superimposed [70]; and iii) the system dynamics, which changes as a function of the operating point, can be described by a set of *frozen*, local models at each point in time [106]. The good agreement between the predicted and measured torques suggests that these assumptions hold for the type of movements produced during slow walking. It remains to be validated if this assumptions are valid during fast movements such as running.

Our methodology leverages on these assumptions and introduces a novel parameterization of the parallel-cascade model where the time-course of the frozen, local models parameters is approximated by a linear combination of basis functions, effectively transforming the TV model into a set of TI models at the cost of increasing the number of free parameters. This points out two of the main limitations of the identification algorithm:

First, the type and number of basis functions used to parametrize the TV coefficients must be known a priori. The quality of the parameter estimates will depend on selecting a set of basis functions capable of efficiently describing the TV parameters changes. In this study B-splines and Tchebichev polynomials were used to represent the parameters variation. Both basis functions are well suited for describing smooth changing parameters; however, B-splines are commonly used to approximate fast changing parameters, whereas Tchebichev polynomials are commonly used to approximate very-low-frequency trends. For parameters undergoing sharp transitions; another set of basis functions, such as Haar wavelets, which are formed as a sequence of rescaled "square-shaped" functions, would be more appropriate.

Second, as the number of free-parameters is significantly increased, the identification algorithm requires large data sets for accurate parameter estimation. This limitation was addressed here by combining the basis function expansion with an ensemble identification approach, which assumes that there are multiple, input-output trials showing the same TV behavior. However, compared with ensemble-only identification methods, our algorithm requires significantly less repetitions. This reduction in data requirement translates into much shorter experiments which makes it easier to acquire enough trials with the same TV behavior.

Finally, the algorithm relies on the reflex response delay to accurately separate the intrinsic and reflex components from the measured position and torque data. Furthermore, it is assumed that the delay remains constant throughout the gait cycle. The reflex day was measured using joint velocity and EMG signals, and no modulation with the gait cycle was found. However, this observation is only valid

for the particular experimental conditions analyzed here; if these change, then this assumption must be validated under the new conditions.

7.5.2 Simulation study

System identification methods are often validated using idealistic input and noise sequences. However, the performance of these algorithms might degrade when applied to experimental data, with non-ideal inputs and non-zero mean, non-white noise. Our simulation was intended to mimic real experiments, with model parameters based on those reported in the literature, non-ideal inputs with limited bandwidth, and experimental, non-white noise sequences. Doing so guarantees that the results obtained in the simulations are more relevant to experimental conditions.

The simulated, intrinsic time-frequency response was fully captured by the estimated model up to around 30Hz, which corresponds to the input's band-width. The gain and threshold of the simulated half-wave rectifier were also accurately tracked by the estimated polynomial nonlinearity. The large variability in the polynomial nonlinearity for large velocities is likely related to the fact that the amplitude distribution of the velocity signal is highly concentrated around zero, so that there is little information about the nonlinearity's shape for high velocities [156]. Finally, the reflex, natural frequency was accurately estimated, while the reflex damping was slightly underestimated. However, this did not affect the prediction ability of the estimated models, indicating that the model output is not very sensitive these small differences in the damping.

7.5.3 Experimental study

Application of the new methodology allowed us to estimate the intrinsic and reflex ankle dynamic stiffness during an imposed walking movement from measured ankle position and torque data. Results showed that the proposed model structure was able to accurately predict the output torque to novel perturbation sequences, indicating that the estimated model successfully captured the TV, nonlinear dynamics.

The intrinsic elasticity underwent drastic changes during the imposed gait cycle, showing a significant increase during the stance-phase and a stepped decrease during the pre-swing phase. The reflex gain showed a similar behavior, increasing during the stance-phase and then returning to its original value during the pre-swing and swing phases. Similar to stationary experiments results, the intrinsic elasticity and reflex gain observed during the imposed movement were heavily modulated by the ankle angle; however, their values were also dependent on the phase of the gait cycle. These results indicate that past values of the ankle trajectory influence its neuromechanical properties.

The other components of the reflex pathway did not show any significant change. However, this result might be caused by the relatively small amplitude of the reflex torques compared to the intrinsic torques, which limits the ability of the algorithm to capture the variation in the reflex parameters.

Finally, even though the results presented here were acquired from simulated walking experiments, the modulation in intrinsic and reflex stiffness seem functionally appropriate. The increase in stiffness occurs in the portion of the cycle when only

one leg supports the body. Thus, an increased ankle stiffness, which increases the joint stability, seems appropriate. Afterwards, both legs support the body so that the large ankle stiffness is no longer necessary. Finally, during the swing phase, the leg is no longer used for support so the intrinsic and reflex stiffness remain low and constant.

We conclude that the new algorithm will be a useful tool in the study of joint dynamic stiffness during TV conditions and that it will help further the understanding of the modulation of this system during function.

CHAPTER 8
Discussion and Conclusions

The four studies described in this thesis were motivated by the desire to measure the neuromechanical properties of joints and their modulation during function. Such measurements would have an important impact in several research fields. The ability to characterize join neuromechanics during function would advance motor control research by providing evidence needed to test different hypothesis regarding the neural control of movement. It would also lead to better understanding of neuromuscular diseases and to development objective measurements to asses the effectiveness of treatment. Furthermore, the it would lead to significant improvements in prosthetics and orthotic devices and would be important in the development of robots that are capable of interacting with humans and the environment in a natural, compliant manner.

The neuromechanical properties of joints can be characterized in terms of dynamic joint stiffness, that describes the relation between joint position and torque. Dynamic joint stiffness composed of intrinsic and reflex stiffness acting in parallel. Intrinsic stiffness arises from the mechanical properties of the joint, passive tissue, and active muscle, and can described by a linear, TV model relating joint position and intrinsic torque. Reflex dynamic stiffness arises from changes in muscle activation due to the excitation of the short-latency stretch reflex, and can be described by a nonlinear, TV, Hammerstein model, made up of a series connection of a TV

static-nonlinearity and a linear, TV system, relating joint velocity and reflex torque. These mechanisms act and change together so their individual contributions to dynamic joint stiffness cannot be measured directly.

In this thesis, I applied mathematical models and systems identification techniques to measurements of joint position and total torque made during function to analytically separate the torques due to intrinsic and reflex mechanisms. These methods make it possible for the first time to characterize the neuromechanical properties of human joints during function. This will provide information that is essential to understand the neural control of posture and movement, to objectively characterize mechanical consequences of neuromuscular diseases, and to the develop biomimetic prosthetics and orthotic devices.

8.1 Identification algorithms

8.1.1 Identification of linear, time-varying systems

Linear, time-varying (LTV) systems play a vital role in describing the neuromechanical properties of human joints during function. The relation between joint position and intrinsic torque can be fully described by a LTV systems, and that of the joint position and reflex torque can be described by a series connection of a static nonlinearity and a LTV system. Consequently, accurate identification of LTV systems a basic requirement for measuring the neuromechanical properties of joints during function.

Time-varying parametric models

Chapter 4 develops and validates a new algorithm to identify time-varying, Box-Jenkins models. This model structure is characterized by an independent parametrization of the systems and noise plants, which makes it useful for modeling biomedical systems whose output is usually contaminated by complex, non-white noise. The technique combines two approaches for TV systems identification: temporal expansion and ensemble methods. In contrast to classical temporal expansion algorithms, which are limited to systems whose parameters vary slowly with time, and classical ensemble algorithms, which require data sets with hundreds of input-output realizations presenting the same TV behavior, this hybrid technique can track fast, large changes in the model parameters using relatively few short, periodic, input-output trials.

This hybrid technique also inherits the limitations of both the ensemble and temporal expansion approaches: First, the method requires that all trials in the ensemble present the same TV behavior, acquiring such data may be difficult experimentally. However, the efficiency of the algorithm, which allows it to deliver reliable estimates with relatively few trials, makes acquiring the data much less demanding than classical ensemble methods. Secondly, the quality of the parameter estimates will depend on selecting a set of basis functions capable of efficiently describing the TV parameters changes. Here, I used cubic B-splines and Tchebychev polynomials; these basis functions are well suited to describe the smooth changes in the systems dynamics observed in the experimental conditions studied here. However, these basis functions would not be appropriate if the parameters underwent sharp transitions;

another set of basis functions, such as Haar wavelets, would be more appropriate for such a case. The selection of the best basis functions is an open research problem, and is often necessary to test a variety of basis functions to select the set most appropriate for a specific task.

Furthermore, the new algorithm uses an instrumental-variable approach for parameter estimation that guarantees that the parameter estimates will be unbiased even when the output contains significant levels of complex, non-white noise. This represents a clear advantage over classical least-squares methods that produce biased parameter estimates when the output noise is not white. Simulations results demonstrated that the algorithm accurately tracked the modulation of the intrinsic joint compliance during a periodic movement using as few as 5 cycles of input-output data contaminated with significant levels of realistic noise. This represents a substantial improvement over the classical ensemble algorithm used in previous studies that require hundreds of cycles to track the parameters modulation throughout a movement [110]. This dramatic reduction in data requirements translates into much shorter experiments making it much easier to acquire trials with the same TV behavior. It also facilitates studies of joint neuromechanics in patients suffering from neuromuscular diseases, who typically have limited endurance and are not able to withstand the long, fatigue inducing experiments that were required in the past.

Time-varying non-parametric models

Parametric models, and in particular Box-Jenkins models, are adequate to describe biomedical systems when the model order is known, the usefulness of the results depends on the validity of the selected model order. Alternatively, when the

order of the system dynamics is not known, the input-output relation can be described by a non-parametric model, which does not require the definition of a model order. However, non-parametric models usually have more free parameters than parametric models, so that when the order of the system dynamics is known, parametric models provide a more parsimonious representation of the system dynamics and is easier to provide a physical interpretation to the estimated parameters.

Chapter 5 develops and validates a new algorithm to identify linear, time-varying, non-parametric models. This algorithm combines the temporal expansion and ensemble approaches for parameter estimation and therefore can track fast, large changes in the model parameters using just a few periodic input-output segments of short duration. Furthermore, this method uses a Bayesian identification algorithm for parameter estimation. This identification procedure imposes a ridge regularization that forces the parameters associated to unnecessary basis functions to zero so they can be discarded, this reduces the number of free-parameters in the model, lessening the data requirements for parameter estimation.

The hybrid algorithm for identification of linear, time-varying, non-parametric models suffer from similar limitations that those discussed in the parametric model identification. The algorithm requires an ensemble of input-output trials presenting the same TV behavior, and the quality of the parameter estimates depends on the appropriate selection of basis functions.

8.1.2 Identification of time-varying Hammerstein systems

Hammerstein systems, the series connection of a static-nonlinearity and a linear dynamic systems, combine the simplicity of linear systems with the generalization

capacity of nonlinear systems. Therefore it does not come as a surprise that many physical systems can be described well by Hammerstein models. In particular, reflex stiffness, the relation between joint velocity and reflex torque, can be described by a Hammerstein system [12]. There is strong evidence that the gain of the system, the sensitivity of the spindle and the muscle's dynamic response are modulated by joint position, background torque and other factors [11, 59, 62] so that during function, reflex stiffness must be described by a time-varying, Hammerstein systems.

Chapter 6 develops and validates a new algorithm for identification of TV, Hammerstein systems. The algorithm approximates the static-nonlinearity using a linear combination of basis functions, this transforms the single-input, single-output nonlinear model into a multiple-input, single-output, linear model. The parameters corresponding to the static-nonlinearity and linear dynamic system are estimated sequentially using the algorithms developed in chapters 4 and 5. The new algorithm improves on previous methods in several ways: i) it does not require the inversion of the static-nonlinearity, so that it can estimate the shape of any static-nonlinearity, not only those that can be inverted, and ii) is guaranteed to converge under general conditions, so that it does not require white, Gaussian inputs to yield unbiased parameter estimates. Simulations demonstrated that the algorithm provides unbiased estimated of the TV static-nonlinearity and linear dynamic elements even in the presence of physiological noise. However, as the algorithm is based on the methods introduced in Chapters 4 and 5, it inherits its limitations, namely, it requires an ensemble of input-output trials presenting the same TV behavior for accurate

parameter estimation, and the quality of the parameter estimates depends on the appropriate selection of basis functions.

8.1.3 Identification of time-varying parallel-cascade systems

Chapter 7 develops and validates a new algorithm to estimate joint dynamic stiffness during function. This algorithm combines the methods developed in Chapters 4, 5 and 6 to estimate the intrinsic and reflex components of dynamic joint stiffness from position and total torque measurements. The algorithm finds an initial estimate of intrinsic stiffness and with it predicts the intrinsic torque, this is then removed from the measured torque and the residuals are used to estimate the reflex stiffness. This model is then used to predict the reflex torque, which is then removed from the total torque and the residuals are used to update the intrinsic stiffness model. The algorithm iterates until there are no further changes in the model parameters. Simulations showed that the new algorithm successfully decomposed the overall joint torque into its intrinsic and reflex components from position and total torque signals with significant levels of experimental noise.

As the algorithm is based on the methods introduced in chapters 4, 5 and 6, it inherits its limitations, namely, it requires an ensemble of input-output trials presenting the same TV behavior for accurate parameter estimation, and the quality of the parameter estimates depends on the appropriate selection of basis functions. Furthermore, though the two estimation steps involved in the algorithm are guarantee to converge to the true values under general conditions, the overall iterative algorithm might suffer from converge issues. However, extensive practical experience has shown that the algorithm fails to converge only when the reflex contribution

to the overall torque is significantly smaller than that of the intrinsic mechanisms. This situation, which seems to be common during movement [59], will require other specialized methods that are under development.

8.2 Simulation issues

Systems identification algorithms are often validated using idealistic simulations that use ideal inputs with power in all the frequencies of interest, and zero-mean, white noise. Furthermore, model parameters are often selected to obtain the best performance of the identification algorithm. However, the performance of these algorithms might degrade when applied to experimental data, with non-ideal inputs and noise.

The algorithms presented here were validated using realistic simulations, intended to mimic real experiments. These simulations used non-ideal inputs with limited band-width, non-zero mean, non-white, noise that was acquired experimentally, and the model parameters were based on values recently reported in the literature [64, 65, 109, 110, 125, 220]. Results presented in this thesis demonstrated that the utility of the identification algorithms must be evaluated using realistic simulations. Chapter 4 showed that the $\%VAF$ between the prediction of the classical TV-ARX identification algorithm and the output of the idealistic simulation was always larger than 99.5%; however, when a realistic simulation was used, the $\%VAF$ decreased to 84%, consistent with the poor quality of the parameter estimates.

The model parameters time-trajectories were delivered from those reported by Rouse *et.al* [109] and Lee *et. al* [110, 125] for the gait cycle. The values were then adjusted to match those previously found in quasi-stationary experiments that

were performed in the same experimental device used in this thesis, that involves subjects lying supine with their left foot attached to the pedal of an electrohydraulic actuator operating as a position servo [64, 65, 220]. However, during walking, the joint elasticity is significantly larger that the values used in our simulations, likely due to the activation of the leg muscles to support and propel the body. Consequently, to validate that the new algorithms for identification of ankle compliance, introduced in Chapter 4, and intrinsic ankle stiffness, introduced in Chapters 5 and 7, can estimate the ankle mechanical properties during walking, I performed a simulation study with increased values of joint elasticity.

Fig. 8–1 and 8–2 present the results of estimating the intrinsic joint compliance using the parametric method introduced in Chapter 4 and the intrinsic joint dynamic stiffness using the non-parametric method introduced in Chapters 5 and 7. The simulated model was identical to that reported by Lee *et. al* for a 70kg subject [125]. Input and noise sequences are the same as those given in Chapters 5 and 7, the SNR was adjusted to give an average value of 10dB. The excellent agreement between simulated and estimated model parameters presented in Fig. 8–1 and 8–2 demonstrate that the algorithms for identification of linear, time-varying systems can be potentially used to estimate the time-varying mechanical ankle properties during walking.

8.3 Experimental results

The algorithms presented in this thesis were used to estimate the dynamic ankle stiffness during an imposed, periodic movement. The results from these pilot experiments demonstrated for the first time, the accurate estimation of the ankle

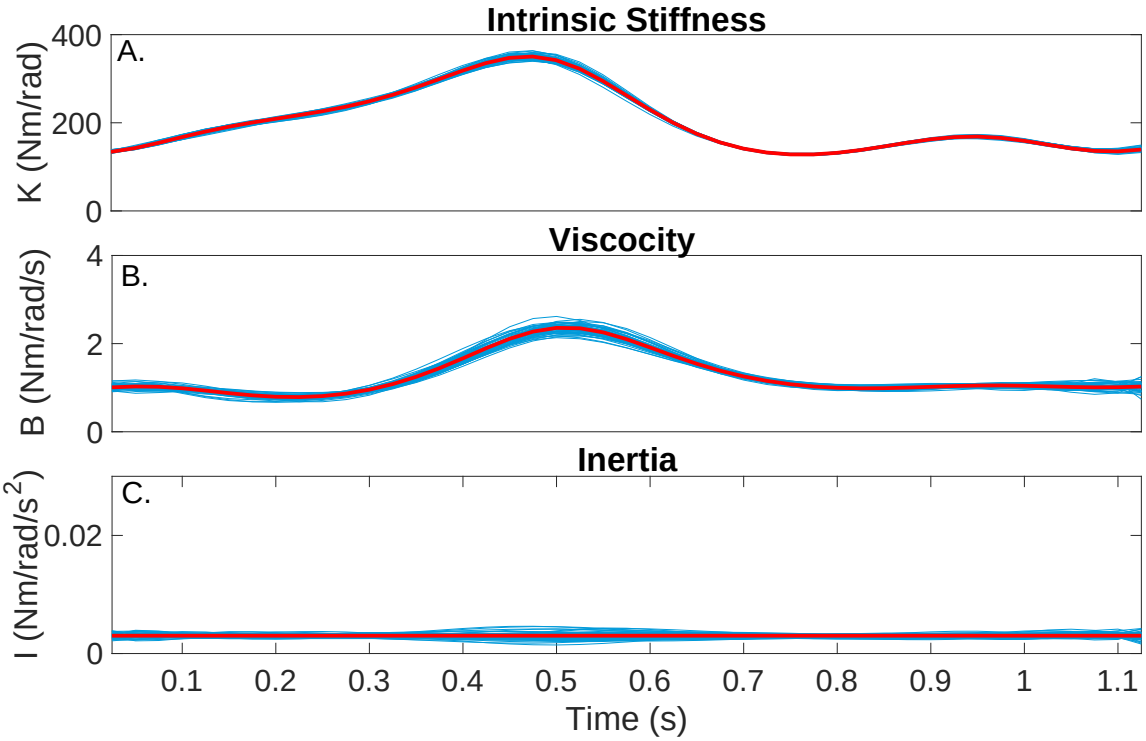

Figure 8–1: TV intrinsic joint compliance parameters estimated with the TV-BJ identification algorithm introduced in Chapter 4, simulated parameters values (red) are similar to those observed during walking, estimation results of 100 Monte Carlo trials (blue) followed closely the true parameters.

neuromechanical properties during functionally relevant situations. These results demonstrates a true TV behavior in the joint neuromuscular properties, and not just a static-nonlinear dependency on joint position, as has been previously assumed [105, 221].

Two different experiments were performed: first, the ankle was displaced in a walking trajectory while the subject was relaxed. Second, the ankle was displaced in a walking trajectory while the subject was exerting a constant level of torque using the ankle flexors.

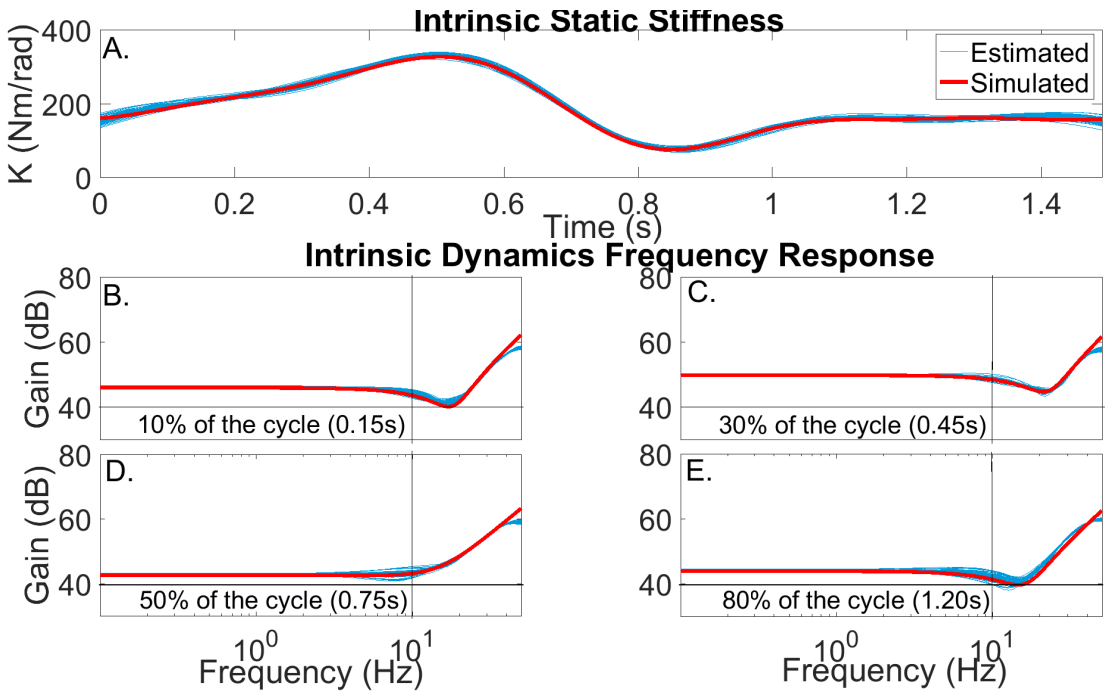

Figure 8–2: Intrinsic dynamic stiffness estimated with the TV-IRF identification algorithm introduced in Chapter 5. Top panel :Simulated (red) and estimated (blue) intrinsic stiffness ($K(t_k)$) during the gait cycle. Bottom four panels: Snapshots of the time-frequency response of the simulated (red) and estimated (blue) systems at different moments of the gait cycle, corresponding to A. 10%, B. 30%, C. 50% and E. 80% of the cycle. Simulated parameters values (red) are similar to those observed during walking, estimation results of 100 Monte Carlo trials (blue) followed closely the true parameters.

8.3.1 Imposed movement with relaxed muscles

Intrinsic stiffness

The new algorithm was applied to estimate the dynamic ankle stiffness during passive movements. Here, the contribution of the reflex mechanisms is negligible so that the overall ankle stiffness can be described only by the intrinsic component, which is modeled by a linear, time-varying, non-parametric model. The TV model

parameters were estimated using only 20 input-output trials, and the predicted output torque accounted for more than 94% of the measured torque variance, demonstrating that the estimated TV, non-parametric model accurately described the joint mechanical properties during movement. Results showed that the ankle visco-elastic properties, change drastically during movement, demonstrating that the joint passive mechanical properties are heavily modulated by joint position.

These results also demonstrated that joint dynamics stiffness during function cannot be inferred from stationary experiments at matched operating points. Intrinsic stiffness was lower during movement than during constant posture experiments at matched positions. The discrepancy between time-varying and quasi-stationary results has been previously reported in experiments with voluntary muscle activation [106, 107, 124].

The results presented in Chapter 4 were obtained for relaxed muscles only. However, the origins of passive muscle tension are not fully understood, some suggest that passive muscles can be described as visco-elastic elements, and that cross-bridges are not involved in production of passive force [222, 223]. Others have hypothesized that passive muscle tension is produced by a combination of the muscle's visco-elastic properties and by cross-bridges engaged between actin and myosin in resting muscle fibres [224, 225]. Our results are consistent with the latter hypothesis, since the discrepancy between time-varying and quasi-stationary results can only be explained by the presence of engaged cross-bridges in the production of passive muscle tension. Consequently, our results suggest that a simple visco-elastic element does not adequately describes the passive behavior of skeletal muscle during movement.

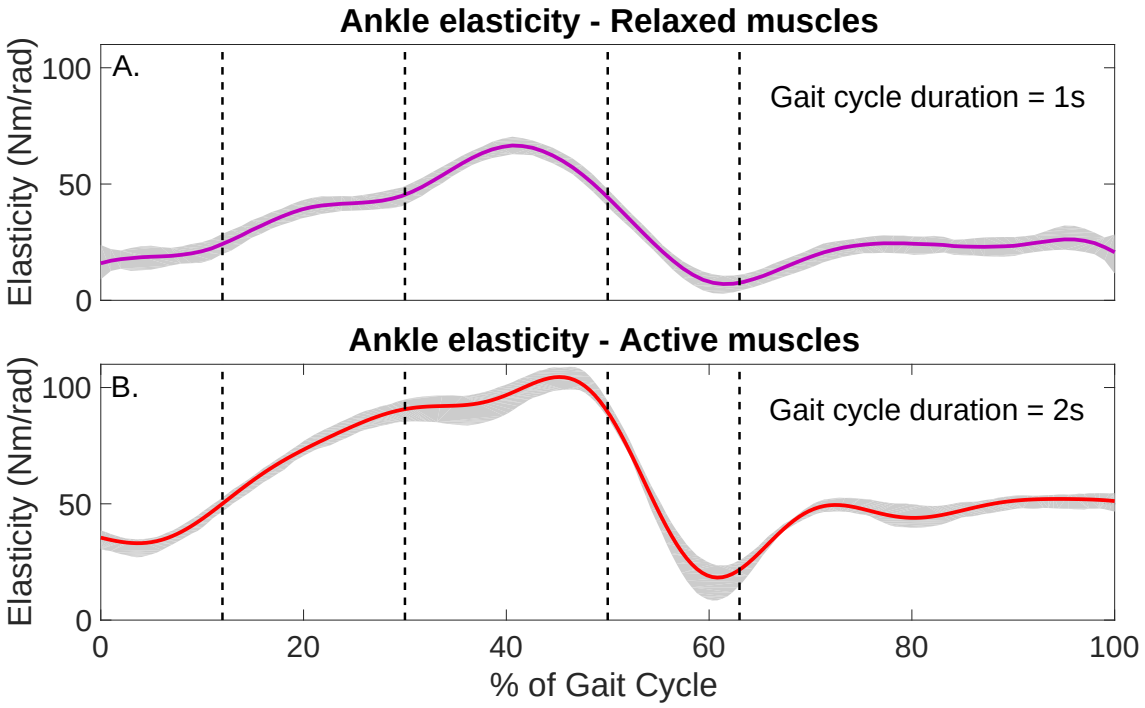

Figure 8–3: Ankle elasticity as a function of gait cycle during imposed walking movement. A) Relaxed muscles, B) Active extensors muscles, 10% of MVC. Shaded regions represent the 95% confidence interval. The vertical lines divide the gait cycle in its different phases starting from heel-strike: early stance, mid-stance, terminal stance, pre-swing and swing phase.

8.3.2 Imposed movement with muscle activation

Intrinsic stiffness

Fig. 8–3 presents the ankle elasticity as a function of gait cycle estimated during relaxed (presented in Chapter 5) and active (presented in Chapter 7) experiments with the same subject. The joint elasticity observed during passive and active experiments shows the a similar trend, increasing during the first portion of the movement, then rapidly decreasing between 50% and 60% of the cycle, and then staying constant, at a low value for the remainder of the movement. Joint elasticity estimated with

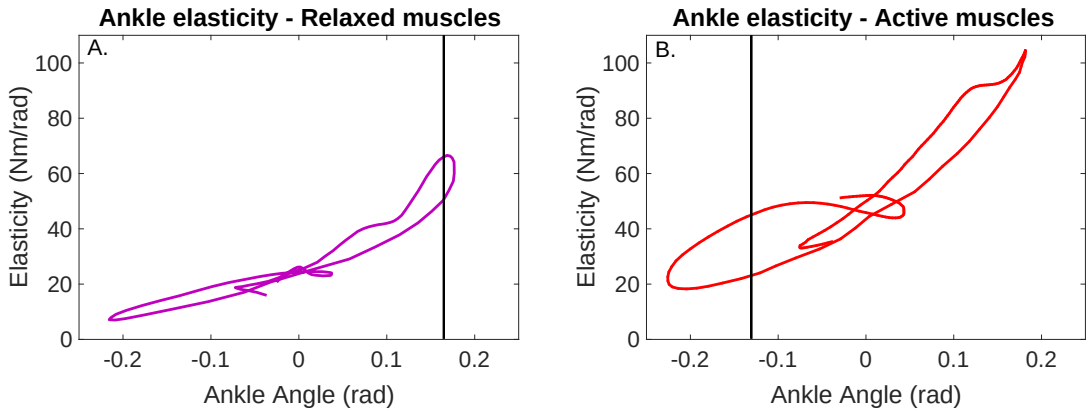

Figure 8–4: Ankle elasticity as a function of ankle angle during imposed walking movement. A) Relaxed muscles, B) Active extensors muscles, 10% of MVC.

constant voluntary torque increased three fold during the simulated stance phase, while that estimated with relaxed muscles increased four fold. As the cycle duration in the passive and active experiments was different, and given that the passive properties of muscles are velocity dependent [224, 226], it is not possible to rule out that the observed differences are not due to a velocity-dependent effect.

Furthermore, Fig. 8–4 demonstrates that joint elasticity estimated during movement can take different values for the same ankle angle depending on the immediate history of the movement. For the relaxed experiment, the vertical line in Fig. 8–4A shows that differences in the ankle elasticity up to 30% were observed, while for the active experiment, the vertical line in Fig. 8–4B shows that the the ankle elasticity almost doubled for certain angles. These results provide additional evidence that cross-bridges contribute to the tension during stretch of passive muscle, because during passive movements, when the number of engaged cross-bridges is small, the

history dependent effects are small; and when the subject voluntarily activate its muscles, engaging more cross-bridges, these effects are increased.

Reflex stiffness

Reflex stiffness is generated only by active mechanisms, so that the observed dependency of stretch reflex responses on the immediate history of contraction and length changes is expected. Moreover, modulation of reflex stiffness during movement can be attributed to the force-length, and force-velocity relations of active muscle fibers. However, the fact that reflex EMG was also modulated during the movement, combined with the observation that the reflex gain reached its maximum value and started decreasing at least 100 ms before intrinsic stiffness reached its peak value, suggest that the modulation also arises from neural mechanisms. One possible mechanisms underlying these changes is the increase in the number of active spindle afferent when the muscle is lengthened [227, 228]. This could increase the effective neural gain by bringing additional spindle afferents into the response, producing a maximum reflex torque ahead of the maximum intrinsic torque, which is influence by both passive and active mechanisms.

8.4 Implications

In summary, the new algorithms provided accurate estimates of time-varying, intrinsic and reflex dynamic stiffness using only a few periodic, input-output data segments of short duration. These methods greatly facilitate the study of joint neuromechanics during function, and provide new analytical tools to: i) validate hypothesis regarding the neural control of movement, ii) study and characterize neuromuscular diseases, iii) advance the field of prosthesis design by providing a better

understanding of the neuromechanics of human joints. The contributions of this thesis to these research fields is discussed in detail next

8.4.1 Neural control of movement

Accurate measurements of intrinsic and reflex stiffness and their modulation during movement could help to solve the ongoing debate between different theories regarding the neural control of movement. Two of the most widely discussed theories, the equilibrium point hypothesis and the internal model hypothesis, consider that the modulation of dynamic joint stiffness is either a precursor or a consequence of the movement. The equilibrium point hypothesis postulates that the central nervous systems controls the movement of limbs by controlling the stiffness of associated joints. In this theory, movement is accomplished by modulating the visco-elastic properties of muscle via the tonic stretch reflex, whose threshold of activation is altered during voluntary movements by central control signals, signals from sensory receptors in other muscles, and history of activation [13, 14, 229]. The internal model hypothesis suggests that the central nervous system learns internal models of the complex interactions within the body and between the body and the environment,and predicts the exact forces needed to generate the movement [15, 16].

Our results presented for the first time the modulation of the intrinsic and reflex components of dynamic joint stiffness during an imposed movement. They show that the gain of these mechanisms change significantly during the movement and that the gain of the stretch reflex seems to lead that of the intrinsic stiffness. It was also observed that the elastic properties of the joint are lower during movement than that observed during constant posture experiments at matching positions.

Our results are more consistent with the equilibrium point framework, as this hypothesis predicts modulation in joint neuromechanical properties during movement due to the excitation of stretch reflex mechanism at certain muscle length. However it is impossible to reach any conclusion based on the results presented here as they do not involve voluntary movements. Other experiments exploring the modulation of intrinsic and reflex mechanisms during voluntary movements must be performed to validate these hypothesis; the methods introduced in this thesis can be used to verify if the modulation in dynamics stiffness precedes the movement, as indicated by the equilibrium point hypothesis, or is a consequence of the movement, as indicated by the internal model hypothesis.

8.4.2 Neuromuscular diseases and clinical applications

Clinical manipulations of joints to assess pathologies in muscle tone involve movement, as clinicians know that movement is required to fully characterize the joint neuromechanical properties. However, clinicians can only provide a subjective measure of the joint properties, and current methods for the objective measurement of joint dynamic stiffness are limited to constant posture experiments, limiting their ability to provide clinically relevant information [17]. The methods developed here be useful to diagnose neuromuscular diseases and the evaluate the effectiveness of treatment programs because they can provide objective measurements of the joint neuromechanical properties during time-varying experiments, which involve movement and/or variation of voluntary muscle activation, and can be used to complement the information provided by current methods.

Another application of the methods and models introduced in this thesis is in the improvement of Functional Electrical Stimulation (FES) systems. These systems restore function to paralyzed limbs, using mathematical models of the limbs and joints biomechanics to estimate the torques required to produce a desired movement [196]. Recent advancements in FES have shown that simple, lumped models of joint biomechanics, such as the ones presented here, provide less error than more complete, physiologically inspired models [197, 198]. Moreover, experimental results have demonstrated that models used in FES systems must be able to capture the modulation of joint biomechanics during movement [198]. Therefore, we suggest that our model and identification algorithms are well suited for use in FES control and will provide an improvement over existing technologies.

8.4.3 Design of prosthesis devices

State of the art powered prosthesis makes use of series elastic components that included a series stiffness tuned to the stiffness of the biological joint to minimize the mechanical work required by an electric motor [230]. Alternatively, a control system may be used to emulate a series of passive impedance functions at the artificial joint in order to reproduce the behavior of a healthy joint [231]. Both these technologies require an accurate measurement of the joint stiffness during the desired movement, something that was not possible in the past and can now be achieved using the methods introduced here.

8.5 Future Work

8.5.1 Closed-loop identification

The pilot experiments presented here involved the interaction of the ankle joint with an infinitely stiff load. However, most functional situations involve the interaction of the joint with a compliant load. In those cases, joint position and torque are connected by a feedback loop, and the estimation of joint neuromechanical properties becomes a closed-loop identification problem.

Here, non-linear, closed-loop identification methods are required to estimate the parameters of the intrinsic and reflex components. Furthermore, during function, the parameters of the parallel-cascade model will be time-varying, so that novel, time-varying identification algorithms that work with closed-loop data are required. The methods proposed here, that make use of instrumental-variables, can be modified to deal with closed-loop system by selecting an appropriate instrumental variable [183]. Furthermore, the basis function expansion approach for identification of time-varying systems, is not bounded to the model structure, so that it can be directly applied to closed-loop systems. Therefore, the new algorithm can be applied to data acquired in closed-loop by selecting an adequate instrumental-variable.

This time-varying, closed-loop identification algorithm can be useful to the study of ankle dynamic stiffness during upright stance where the body is considered as a compliant load with that the ankle is interacting.

8.5.2 Linear-parameter-varying methods

LPV models are an alternative to TV models that assume that the model parameters are modulated by a measurable or estimable signal called scheduling variable, and relate the changes in the model parameters with an underlying modulating signal. Given the advantages and a limitations of the time-varying and linear-parameter-varying approaches, is clear that both methods are complementary. The time-varying method, which makes little assumptions about the parameters time-course, can be used as a first step to determine possible scheduling variables and their relations with the model parameters. Afterwards, the linear-parameter-varying approach can be used to determine a global model that describes the system as a function of the underlying, modulation variables.

The results presented here indicate that determining the scheduling variables and their relations with the intrinsic and reflex stiffness during function will be a daunting task, as both mechanisms seem to be influenced by the immediate history of contraction and muscle length changes, and so any model that attempt to capture the nonlinear characteristics of joint neuromechanics must include these dynamic relations.

APPENDIX A
Background

This chapter provides a summary of the characteristics and properties of the neuromuscular system, and presents some background information related to the anatomy and function of the ankle joint. It starts by introducing some basic concepts in muscle physiology and peripheral sensor receptors, it then introduces the stretch reflex and the neuromuscular mechanisms involved in it. It ends with an overview of the anatomy and function of the ankle joint.

A.1 Neuromuscular system

There are three types of muscles in the human body: skeletal, smooth and cardiac. Skeletal muscles are in charge of moving the limbs under voluntary and involuntary activation, and providing postural support for the body. Smooth muscles are involuntary activated muscles that line blood vessels, airways and the gut. Cardiac muscles are found in the heart and their purpose is to involuntarily contract the heart and pump blood through the body.

A.1.1 Skeletal muscle physiology

Skeletal muscle is divided into parallel fascicles, composed of smaller, string-like, multinucleated cells called muscle fibers. Thus, as Figure A–1A shows, each muscle is composed of hundreds of thousands of independent contractile elements arranged in parallel, and in series for longer muscles.

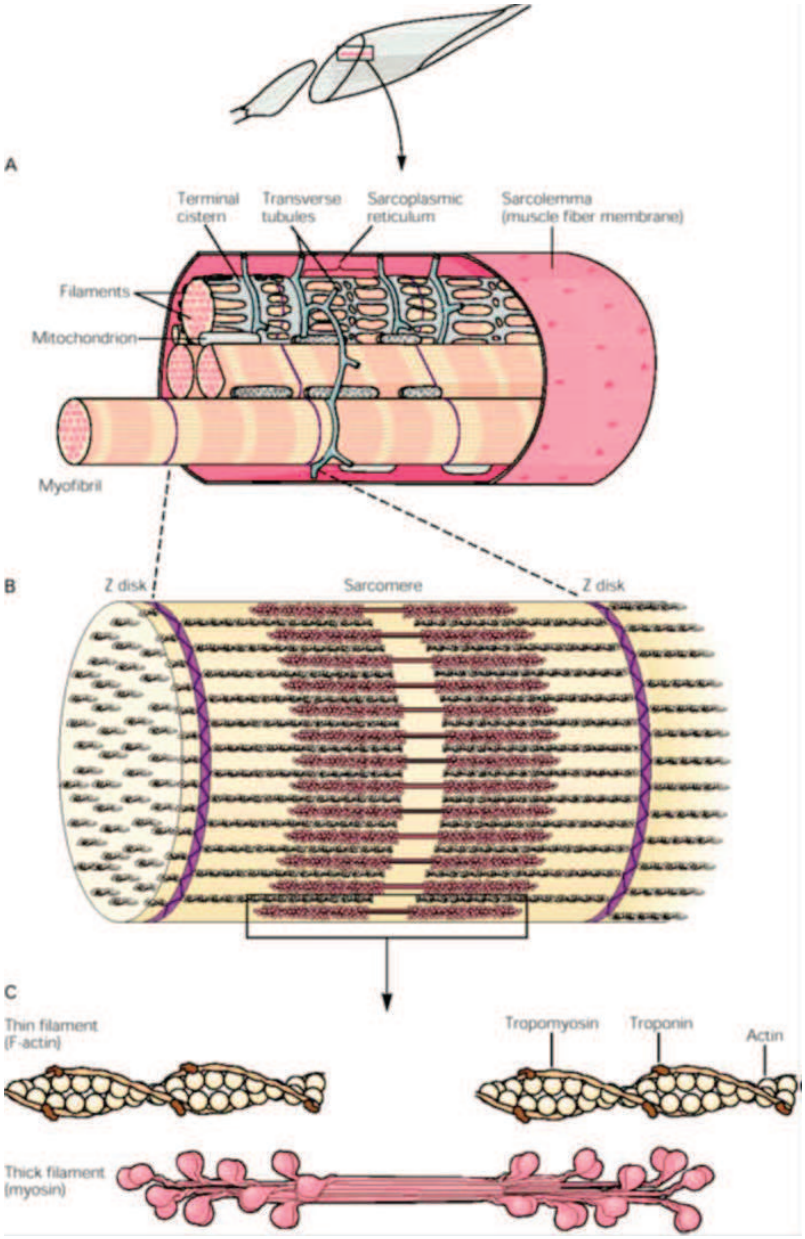

Figure A–1: Organization of skeletal muscle. A. Relationship between myofibrils, membrane, transverse tubule system, and sarcoplastic reticulum. B. Sarcomere. C. Details of the thin and tick filaments. Adapted from [3]

As Figure A–1B shows, each muscle fiber contains many myofibrils, consisting of longitudinally repeated cylindrical units, called sarcomeres. Each sarcomere contains contractile proteins, organized into a regular matrix of thick and thin filaments, and bounded by Z-disks. The sarcomere is the functional unit in skeletal muscle, all myofibrils in a muscle fiber change length together due to the non-contractile elements that link them. Each muscle fiber has about 20.000 sarcomeres in series [3].

The thin filaments project in both directions from the Z-disks. On the other hand, the thick filaments are discontinuous and float in the middle of the sarcomere. As Figure A–1C shows, the thin filaments are composed by polymerized actin monomeres arranged as a helix, troponin and tropomyosin. The thick filaments are comprised of myosin molecules entwined together. These molecules have globular heads that stick out from the sides of the thick filaments.

Organization

Muscles are usually controlled by large motor neurons whose cell bodies lie in the spinal cord or brain stem. As Figure A–2 shows, the axon of each motor neuron exits the spinal cord through a ventral root, or when located in the brain stem, the axon exits via a cranial nerve. Once it reaches the muscle it controls, it branches widely to innervate hundreds of fibers scattered over the muscle. Each muscle fiber is innervated by one motor unit around its midpoint. A muscle unit refers to the ensemble of fibers innervated by a single motor neuron; the motor neuron and muscle unit together are called motor unit.

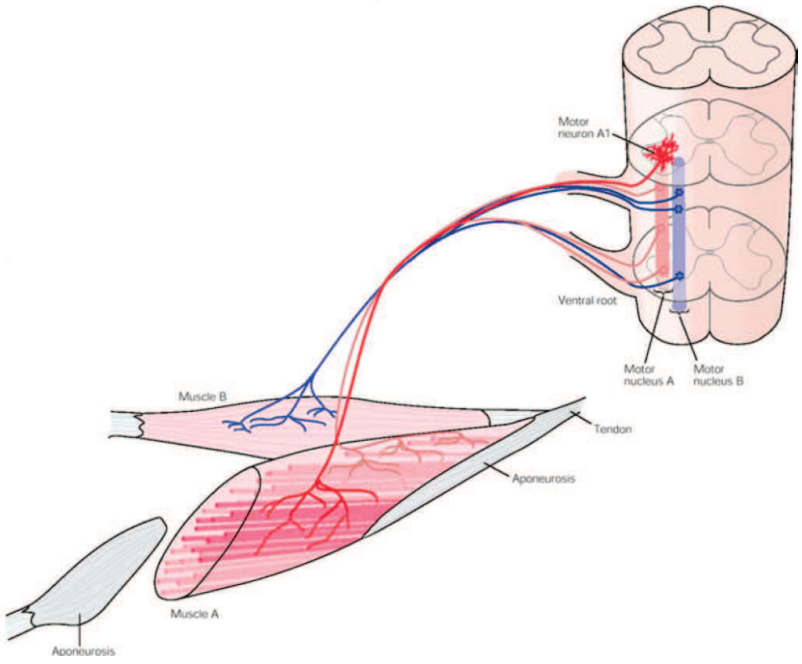

Figure A–2: Organization of the neuromuscular system. Adapted from [3]

Contractile mechanics

The connection between a motor neuron and a muscle fiber is by way of a chemical synapse called an *end-plate*. As Figure A–3 shows, the motor neuron terminal is filled with vesicles containing the neurotransmitter acetylcholine, while the motor end plate contains many acetylcholine receptors. Once the neuron releases enough neurotransmitter, these bind to ligand-gated ion channels in the postsynaptic membrane in the muscle and produce the diffusion of sodium and potassium across the receptors depolarizing the end-plate; this opens voltage-gated sodium channels, further increasing the inflow of ions allowing for firing of an action potential. The acetylcholine released from the motor neuron is rapidly hydrolyzed by acetylcholinesterase, leaving the muscle fiber ready to respond to the next action potential.

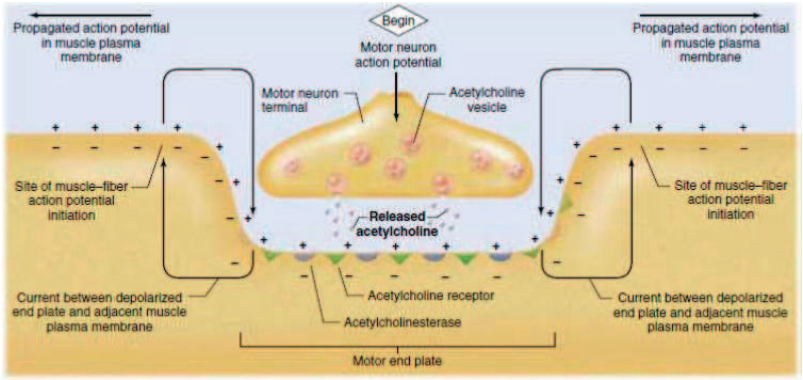

Figure A–3: Chemical connection between nervous system and muscle. Adapted from [4]

The action potential propagates relatively slowly (3-5 m/s) in both directions away from the end-plate region [3]. These give rise to relatively large potential gradients in the extracellular fluid around the muscle fiber.

When the action potential propagates along the surface of the muscle fiber, it depolarizes the transverse tubules within the muscle fiber, motivating the realize of calcium from the sacroplasmic reticulum, which diffuses passively among the myofilaments, and binds reversibly to troponin in the thin filaments.

As Figure A–4 shows, once the calcium binds into the troponin, there is a conformational change in the thin filament that exposes actin-binding sites, allowing the myosin heads to attach and form cross bridges between the thick and thin filaments. The attached myosin heads rotate, in a movement called power stroke, releasing ADP and Pi, and exerting longitudinal forces that pull the thick and thin filaments into greater overlap, shortening the muscle fiber and producing force. At the end of the power stroke ATP binds to the myosin head, detaching it from the thin filament.

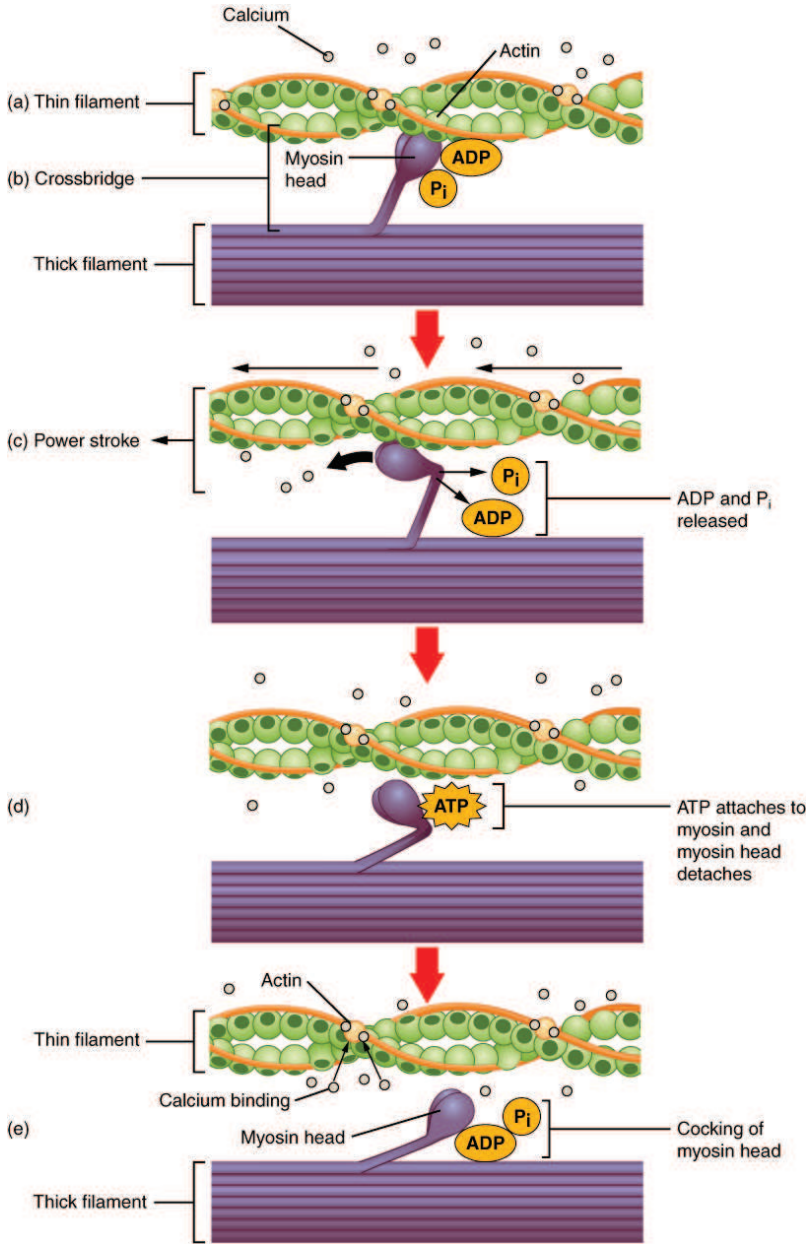

Figure A–4: Contraction is produced by cyclical attachment and detachment of myosin heads on adjacent thin filaments. Adapted from [5]

The chemical energy released by dephosphrylation of the ATP is used to recock the myosin heads for attachment to another binding site and produce other power stoke.

The release of calcium by the sacroplasmic reticulum is very rapid, but it may take up to 50ms to activate the thin filaments fully and for cross bridges to form. The free calcium is rapidly taken up causing the number of cross bridges to decrees over a period of 80 to 200 ms [3]. Consequently, the force produced by a single action potential is small. If another action potential occurs before all the calcium released by the first action potential has been taken up, more cross bridges will form, resulting in a greater output force. The higher the frequency of action potentials, the higher the force that will be generated up to the point where all cross bridge binding sites are continuously activated and the force output no longer shows any ripples. Figure A–5 depicts this phenomenon which is called a fused tetanus, or maximal tetanic contraction.

Force-length, force-velocity relations

The total force that can be measured at the tendon reflects the sum of the passive tension generated in the muscle plus the active tension generated by the cross bridges. This force depends on three factors: the force produced by each cross-bridge, the number of cross-bridges and the velocity of the cross bridge motion.

Cross bridges can form only in regions of the sarcomere where myosin heads lie adjacent to actin filaments. Thus, as Figure A–6A illustrates, when a muscle fiber is stretched far enough, the overlap region decreases so that no active force can be generated. However, the passive force, produced by stretched fibers, increases substantially with the muscle length. Similarly, when the muscle is shortened, the

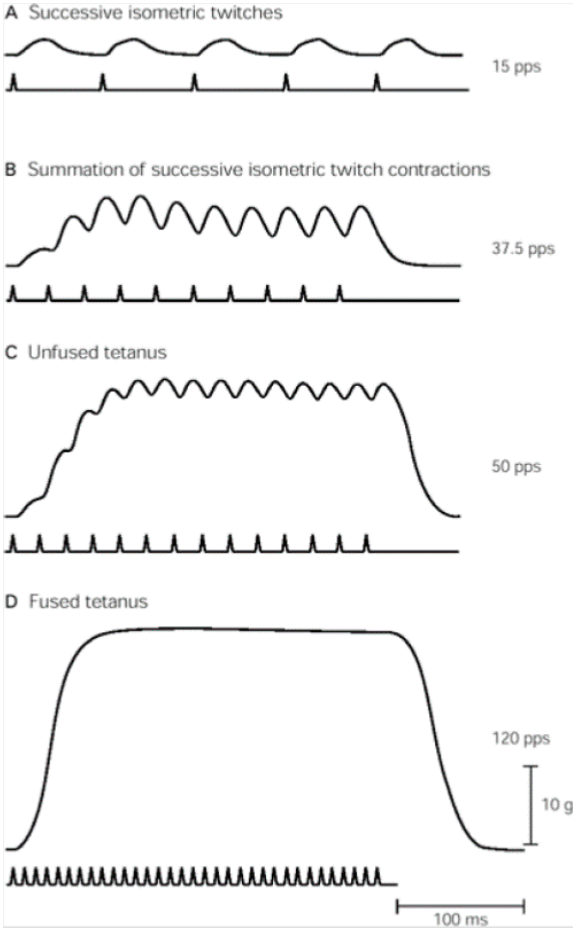

Figure A–5: The active tension in a muscle varies with the rate of stimulation of the muscle nerve. Adapted from [3]

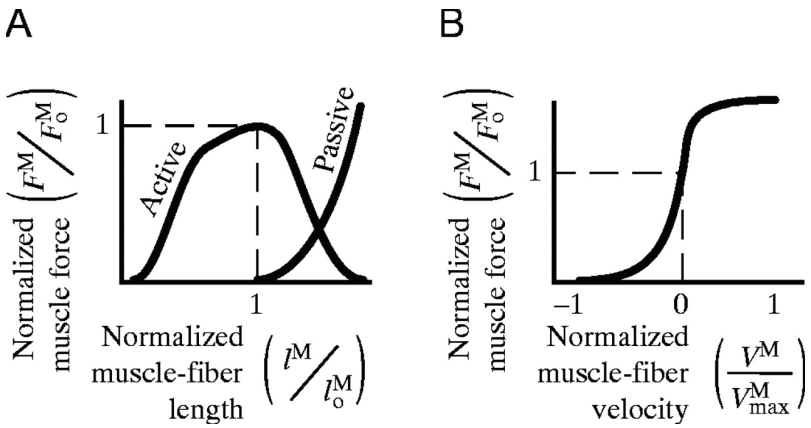

Figure A–6: Force-Length, and Force-Velocity relations for individual muscle fibers. Adapted from [6]

progressive overlap of thin filaments will occlude the potential attachment sites and no more cross bridges can be formed. Once the Z-disks reach their minimum distance, no more active force can be produced.

The rate at which cross bridge motion occurs is also an important factor in force generation. Shortening the muscle causes the myosin heads to spend more time near the end of their power stroke, where they produce less contractile force, and in detaching, recocking, and reattaching, where they produce no force. On the other hand, when the muscle is lengthening, the mysion heads spend more time stretched past their angle of attachment and little time in the unattached state because they do not need to be recocked after being pulled away from the actin. Consequently, contractile force rises rapidly and tends to stay high.

Types of muscle fibers

There are three different types of muscle fibers, each specialized for certain task and with different metabolic properties. Most muscles are composed of a mix of

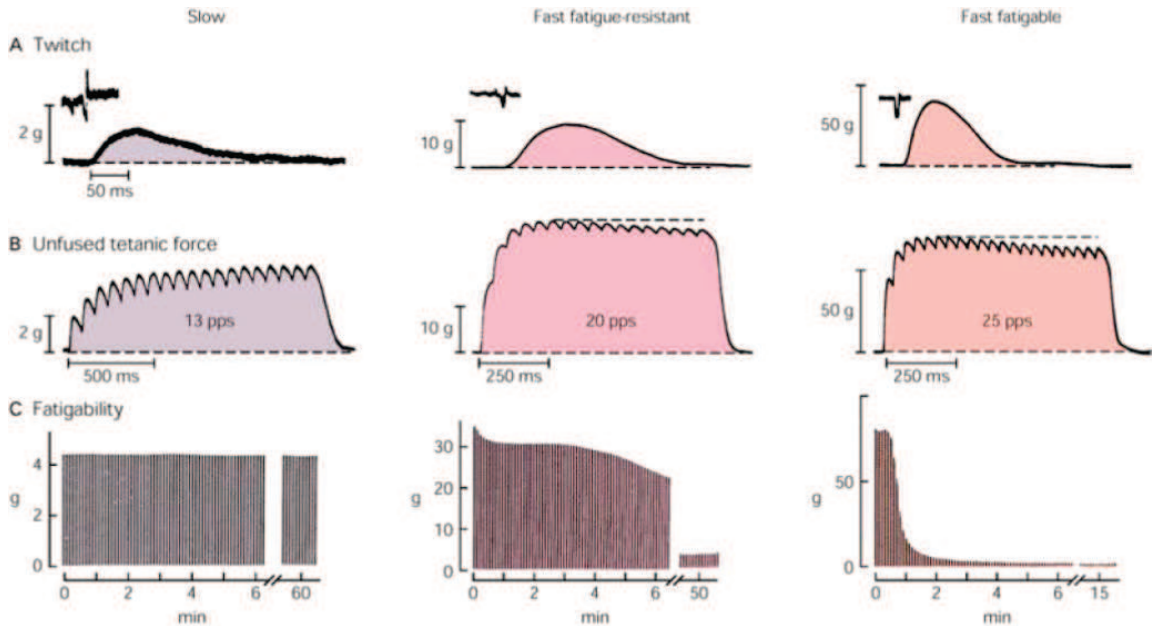

Figure A–7: Slow, fast fatigue-resistant, and fast fatigable motor units vary in twitch, tetanic force, and fatigability. Adapted from [3]

these three fiber types: slow twitch fiber, and two types of fast twitch fibers. All the muscle fibers innervated by a single motor neuron are of the same type.

As Figure A–7 shows, slow-twitch or type I fibers, produce a force that rises and falls slowly in response to an action potential. Muscles composed mainly of type I fibers can produce relatively small amounts of force for long periods of time. This types of fibers use oxygen and glucose supplied by the bloodstream to generate the ATP needed for force production. In fast-twitch, or type II fibers, the force produces rises and falls rapidly. There are two different types of fast-twitch fibers according to the metabolic process. Type IIA fibers are fatigue resistant, fast-twitch fibers; they are slower that type IIB but can generate force for longer periods of time.

A.1.2 From muscle force to movement

The human body has over 250 muscles, each with a distinct mechanical action at one or more joints. The simplest type of joint is a hinge, which allows movement in only one plane. Because muscles can only pull, these joint require two muscles pulling in opposite directions. Other types of joints permit movement in all the axes of rotation, and a few move primary in translation. The degrees of freedom of a joint are the number of independently controllable axes of motion and ranges from one, for a simple hinge joint, up to a maximum of six. In a multiarticular limb the degrees of freedom are the sum of the degrees of freedom of all of its joints.

Each muscle produces a joint torque that is the product of the contractile force and its moment arm at that joint. As Figure A–8 shows, the moment arm is the length of a perpendicular from the line of pull of the muscle to the center of rotation of the joint. Unlike the idealized view presented in the figure, the moment arm of real muscle often changes when the joint angle changes [7]. The net torque at a joint is the sum of the torques produced by the muscles that cross the joint.

A.1.3 Peripheral sensor receptors

Muscle spindles

Muscle spindles are small encapsulated sensory receptors that have a spindle-like shape located within the fleshy part of the muscle. Their main function is to signal changes in muscle length. As changes in the muscle length are related to changes in the angles of the joints that the muscle cross, muscle spindles can also inform the central nervous system about the relative positions of the body segments.

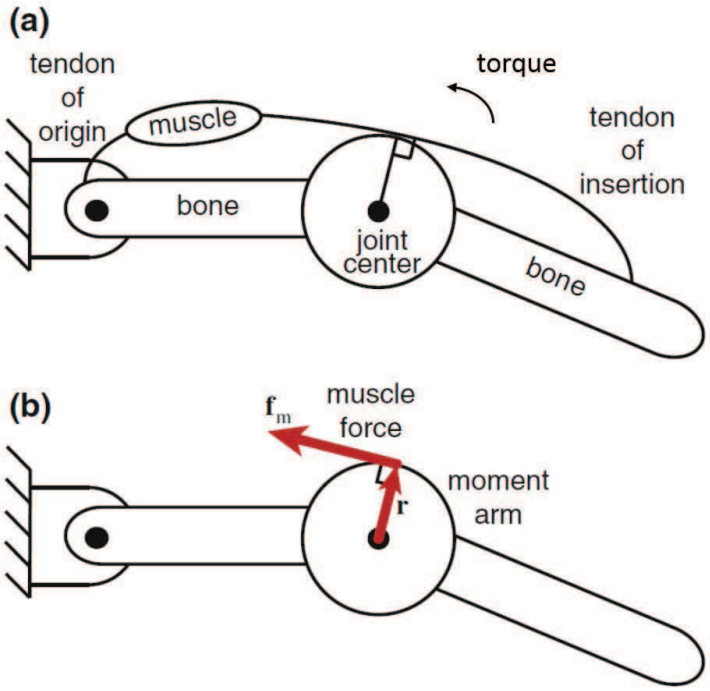

Figure A–8: a) Idealized view of a hinge joint actuated by a single muscle. b) The torque at the joint can be estimated by measuring the force produced by the muscle (f_m) and the moment arm (r). Adapted from [7]

As Figure A–9A shows, the three main components of the muscle spindle are : 1) intrafusal muscle fibers whose central regions are non-contractile; 2) sensory endings that originate from the central region of the intrafusal fibers; and 3) sensory endings that originate from the polar region of the intrafusal fibers.

When the central region of the spindle is stretched, the sensory endings are also stretched and increase their firing rate. Muscle spindles are arranged in parallel with the fibers in the body of the muscle, the extrafusal fibers; consequently, the intrafusal fibers change length with the rest of the muscle. Thus, when the muscle is stretched, the activity in the sensory ending increases; and when the muscle is shortened, spindles activity decreases.

The muscle spindles are innervated by small-diameter, motor neurons, called gamma-motor neurons. These are different from the large-diameter, motor neurons that innervate the extrafusal fibers that form the body of the muscle. The contraction of the intrafusal fibers does not contribute to the force produced by the muscle. Rather, the gamma-motor neurons provide a mechanism to adjust the sensitivity of the muscle spindles.

As Figure A–9B shows, there are two types of intrafusal fibers: nuclear bags and nuclear chain fibers. There are two types of nuclear bags: dynamic and static groups. Moreover, there are two types of sensory endings: primary or Ia, and secondary or II fibers. Ia fibers spiral around the central region of the intrafusal fibers, the endings of the type II fibers are located adjacent to the center of the static nuclear bag and the nuclear chain. The gamma-motor neuron can also be divided in two classes:

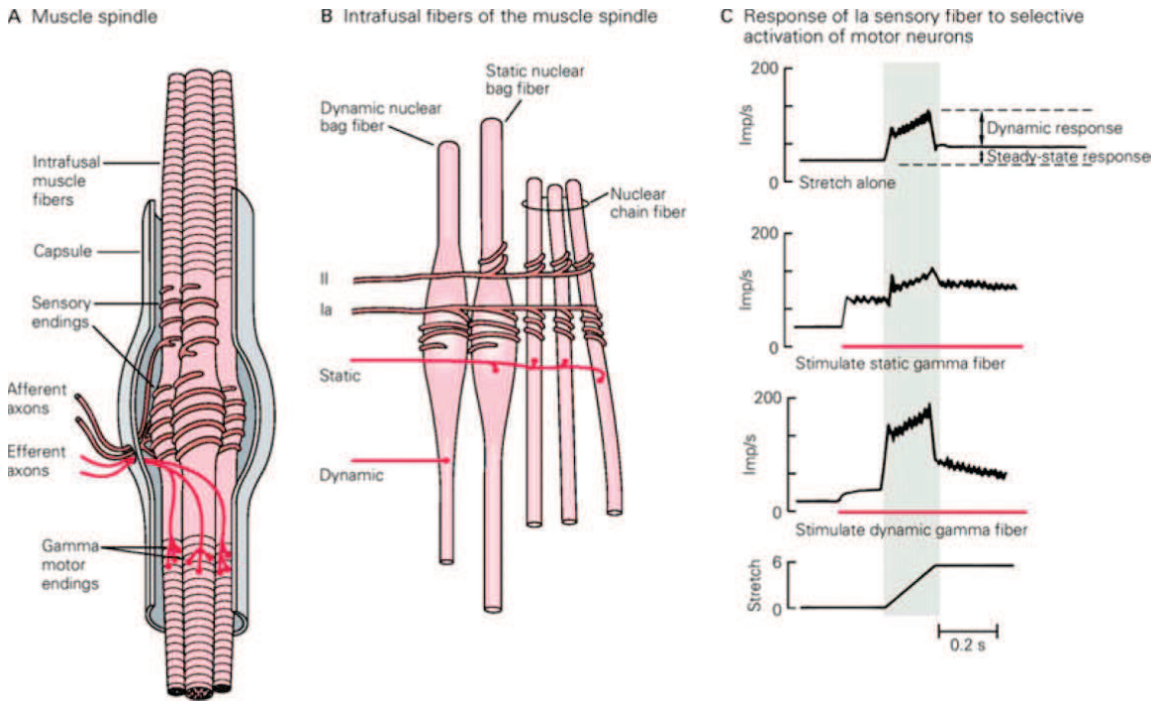

Figure A–9: Muscle spindle: A. The main components of the muscle spindle are intrafusal muscle fibers, afferent sensory fiber endings, and efferent motor fiber endings. B. The muscle spindle contains three types of intrafusal fibers: dynamic nuclear bag, static nuclear bag, and nuclear chain fibers. Two types of motor neurons innervate different intrafusal fibers. Dynamic gamma motor neurons innervate only dynamic bag fibers; static gamma motor neurons innervate various combinations of chain and static bag fibers. C. Selective stimulation of the two types of gamma motor neurons has different effects on the firing of the primary sensory endings in the spindle. Adapted from [3]

dynamic gamma neurons that innervate the dynamic nuclear bag fibers, and static gamma-motor neurons that innervate the remaining intrafusal fibers.

This complex internal structure gives the spindle the possibility to differentiate between steady-state and dynamic activities. The tonic discharge of both primary and secondary afferents inform the central nervous system of the steady-state length of the muscle. In addition, the primary endings are very sensitive to changes in muscle velocity, so that they are able to inform about the speed of movement and small, unexpected changes in muscle length.

The central nervous system can independently adjust the dynamic and static sensitivity of the sensory fibers from muscle spindles via the dynamic and static gamma motor neurons. In addition, gamma motor neurons maintain the tension in the muscle spindles during muscle contraction. Without this *alpha-gamma co-activation*, the spindle would slack during muscle contraction and loss its responsiveness to changes in muscle length. This mechanism assures that the intrafusal fibers in the spindle remain under tension over the full range of muscle lengths.

Golgi tendon organ

Golgi tendons organs are sensory receptors connected in series with a group of muscle fibers and located in the junction between the muscle fibers and the tendon. These encapsulated organs are innervated by a single axon (Ib fibers), this axon losses its myelination when it enters the capsule and branches into many fine endings, each of which intertwines among the braided collagen fascicles. Stretching of the tendon organ straightens the collagen fibers, thus compressing the nerve endings and causing them to fire.

Tendon organs are most sensitive to changes in muscle tension. Studies have shown that the average level of activity in the tendon organs in a muscle gives a fairly good measure of the total force in a contracting muscle [232]. Thus, tendon organs continuously inform the central nervous system about the force in a contracting muscle.

Other sensors

There are other sensors that inform the central nervous system about the current state of the limbs. Among those, the cutaneous and joint receptors are the most important for movement control. Information from these sensors converges along with the information from the golgi tendon organ and muscle spindles in the spinal column. The integration of this information may allow for precise spinal control of muscle tension in activities such as grasping a delicate object [3].

A.1.4 Spinal reflexes

The central nervous system uses the sensory information provided by the different sensors to regulate movement, without this sensory input movements tend to imprecise and tasks that require fine coordination are impossible [3].

Spinal reflexes arise from sensory stimuli from receptors in the skin, muscle, tendons and joints. Its neural circuitry is contained in the spinal cord and so their mechanical involved response is involuntary. However, spinal reflexes are heavily modulated by central commands, which allows them to be modified and adapt to different tasks [3, 178].

Stretch reflex

The stretch reflex refers to an involuntary contraction of the muscle that occurs when this is lengthened. This muscle spindle mediated mechanism was firs described by Liddell and Sherrington [233], who carried their experiment in de-cerebrated cats. During their experiments, they flexed passively the extended cat's hindlimb and increased contraction of the muscles being stretched. They also found that stretching the muscle caused the antagonist muscle to relax. It is now known that de-cerebrate animals have stronger reflex responses than normal animals because descending pathways from the cerebral cortex and other higher centers of the brain continuously modulate the strength of stretch reflexes. [3].

As seen in Figure A–10, the muscle spindle, which are responsible for sensing the muscle stretch or myotasis, make direct connection on the alpha motor neurons, creating a monosynaptic pathway. Ia fibers from the muscle spindle excite the motor neuron innervating the same muscle (homonymous connections) and those innervating muscles having a similar mechanical function (heteronymous connection). In addition, Ia fiber have an inhibitory action on alpha motor neurons innervating antagonist muscles via inhibitory inter-neurons in the spinal column. This mechanism facilitates the reciprocal inhibition of an antagonist muscle to prevent further lengthening of the stretched muscle.

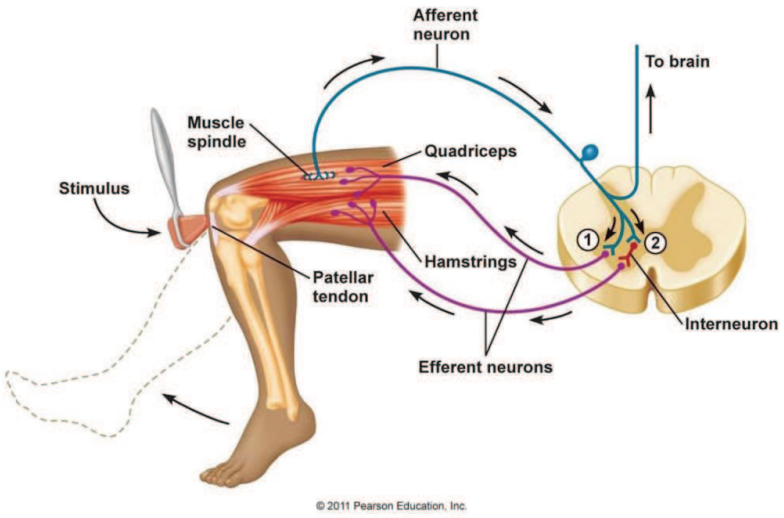

Figure A–10: Neural pathways involved in the knee stretch reflex. Adapted from [8]

A.2 The Ankle Joint

A.2.1 Anatomy

Bones

The lower limbs are extensions from the trunk that originate in the gluteal region, see Figure A–11. Their main functions are to support the body weight and locomotion. The leg region, the part that lies between the knee and the distal part of the leg includes the tibia and fibula, the ankle, or talocrular region includes the medial and lateral malleoli that flank the ankle joint. Finally, the foot region is the distal part of the lower limb and contains the tarsus, metatarsus and phalanges.

The tibia is the second largest bone of th body, its particular shape at the ends provides an increase area for articulation and weight transfer. The proximal end of the tibia possess two smooth articular surfaces that articulate with the large condyles of the femur. The distal end of the tibia is smaller that the proximal end, the inferior

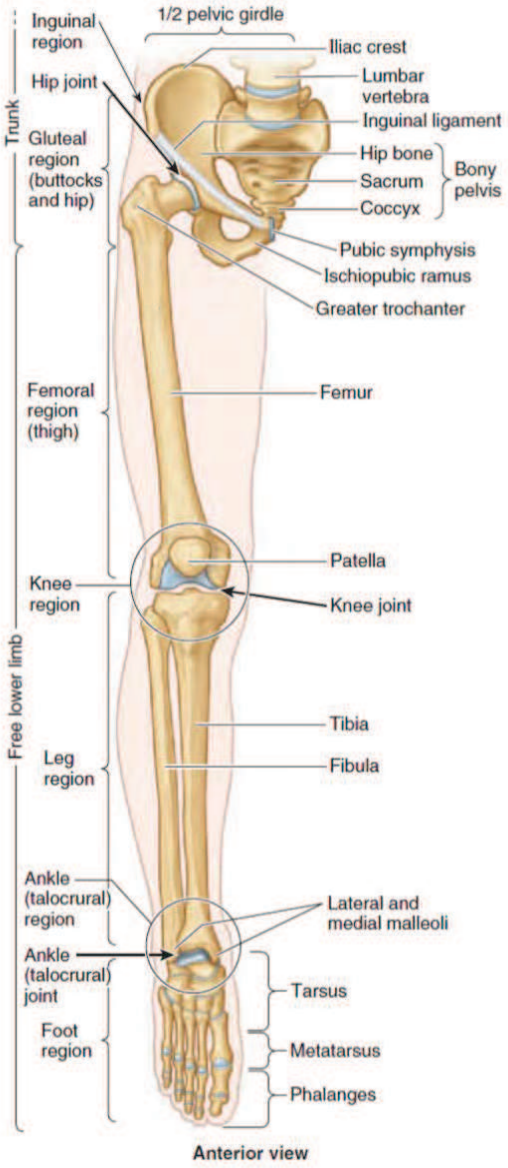

Figure A–11: Regions and bones of the lower limb. Adapted from [9]

surface of the shaft and the surface of the medial malleolus articulate with the talus and are covered with articular cartilage. The fibula is slender than the tibia and lies posterolateral to it. Both bones are firmly attached by the tibiofibular syndesmosis. The tibia serves no role in weight-bearing, its main function is for muscle attachment. The lateral malleolus at the distal end of the tibia forms the superior component of the ankle joint, it provides attachment for the ligaments and helps to stabilize the joint.

As shown in Figure A–12, the talus has a body, neck and head. The superior surface is griped by both malleoli and receives the body weight from the tibia. The talus transfers the weight to the calcaneus and forefoot. Most of the talus surface is covered with articular cartilage. The calcaneus is the largest and strongest bone in the foot, when standing it transfers most of the body weight from the talus to the ground

Movements

The ankle joint is a hinge type joint, with movements only in one plain. Dorsiflexion, bringing the toes closer to the shin, and plantarflexion, moving the toes away from the shin, are the only movements that occur at the ankle. Figure A–13 presents these movements and the general localization of the muscles involved in each one.

Studies have reported that the ankle's range of motion (ROM) for healthy young males is between 30° to 60° in plantarflexion and 8° to 20° in dorsiflexion [234, 235]; these values are reduced with aging and disease [236].

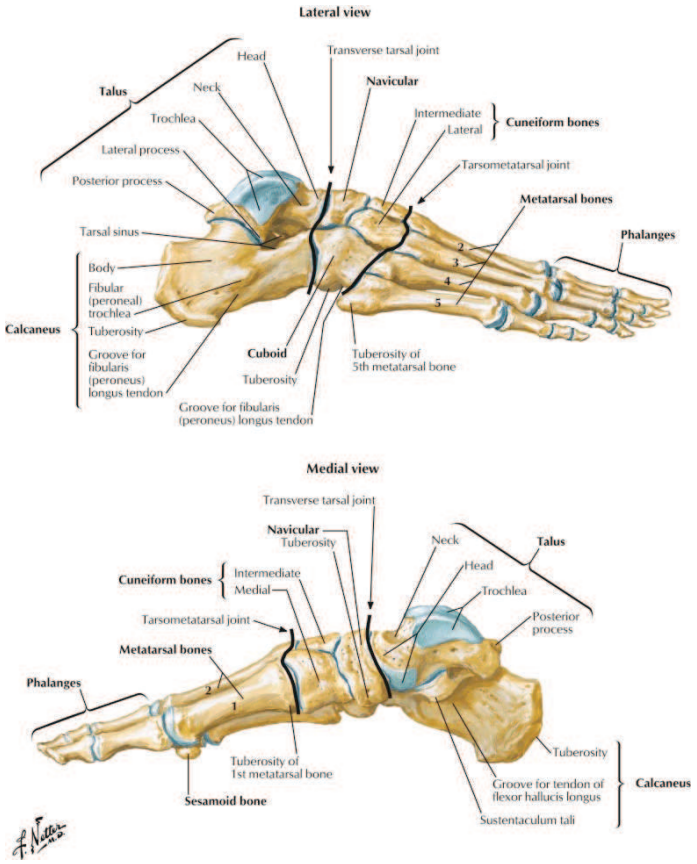

Figure A–12: Bones of the foot. Adapted from [10]

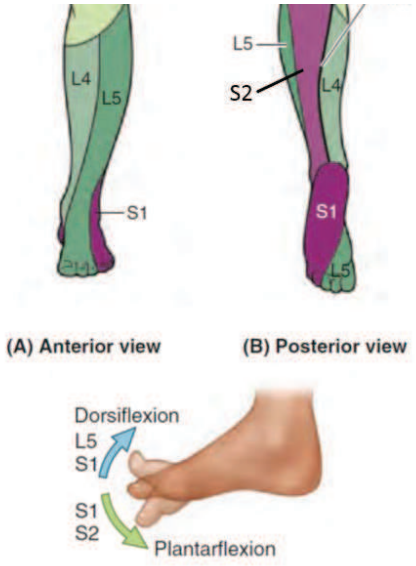

Figure A–13: Movements of the ankle and general localization of the involved muscles. Adapted from [9]

Muscles

As shown in Figure A–14, the leg is organized in three compartments: Anterior, lateral and posterior. The four muscles in the anterior compartment of the leg are tibialis anterior, extensor digitorum longus, extensor hallucius longus, and fibularis tertius. These muscles are dorsiflexors of the ankle joint. The long extensors also serve as extensors of the toes.

As depicted in Figure A–15, the tibialis anterior is the most superficial dorsiflexor. It is a slender muscle that lies against the lateral surface of the tibia. Its tendon is located the farthest from the axis of the ankle joint so that this muscles is the strongest dorsiflexor.

The muscles in the posterior compartment are in charge of ankle platarflexion, inversion at the subtalar and transverse tarsal joints, and flexion of the toes. In

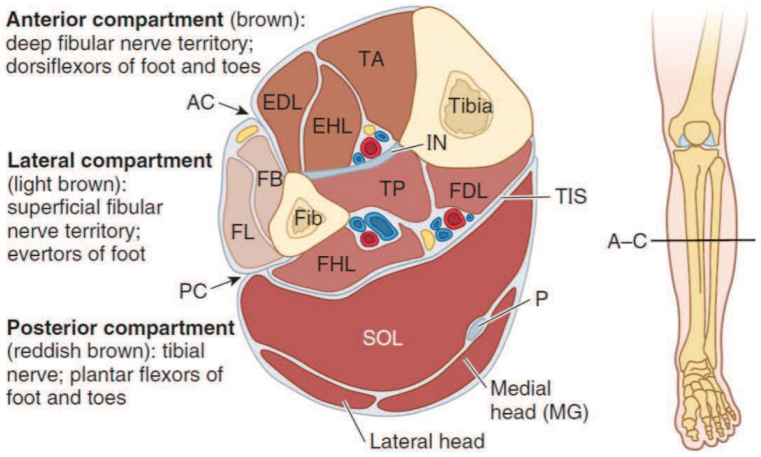

Figure A–14: Compartment of the leg. TA: Tibialis anterior, EDL: Extensor digitorum longus, EHL: Extensor hallucis longus, FB: Fibularis brevis, FL: Fibularis longus, TP: Tibialis posterior, FDL: Flexor digitorum longus, FHL: Flexor hallucis longus, SOL: Soleus, MG: Medial Gastrocnemius. Adapted from [9]

particular, the triceps surae, the collection of the gastrocnemius and soleus muscles, generates more than 90% of the plantarflexion force [9]. Figure A–16 shows the origins and attachments of these two muscles; the gastrocnemius is the most superficial muscle in the posterior compartment. It is a two-heads, two-joints muscle, its acts both in the knee and ankle joints. However, it cannot exerts its full power in both joints at the same time. The gastronemius muscle is composed mainly of white, fast-twitch fibers. The soleus is a large muscle located deep to the gastrocnemius, it is attached to the fibula and tibia so that it only acts on the ankle joint. The soleus muscle is composed mainly of red, fatigue resistant, slow-twitch fibers, which makes them the predominant plantarflexor muscle for standing and strolling.

Both muscles connect to the calcaneal tendon, the thickest and stronger tendon in the body. As seen in Figure A–16, this tendon is a continuation of the aponeurosis

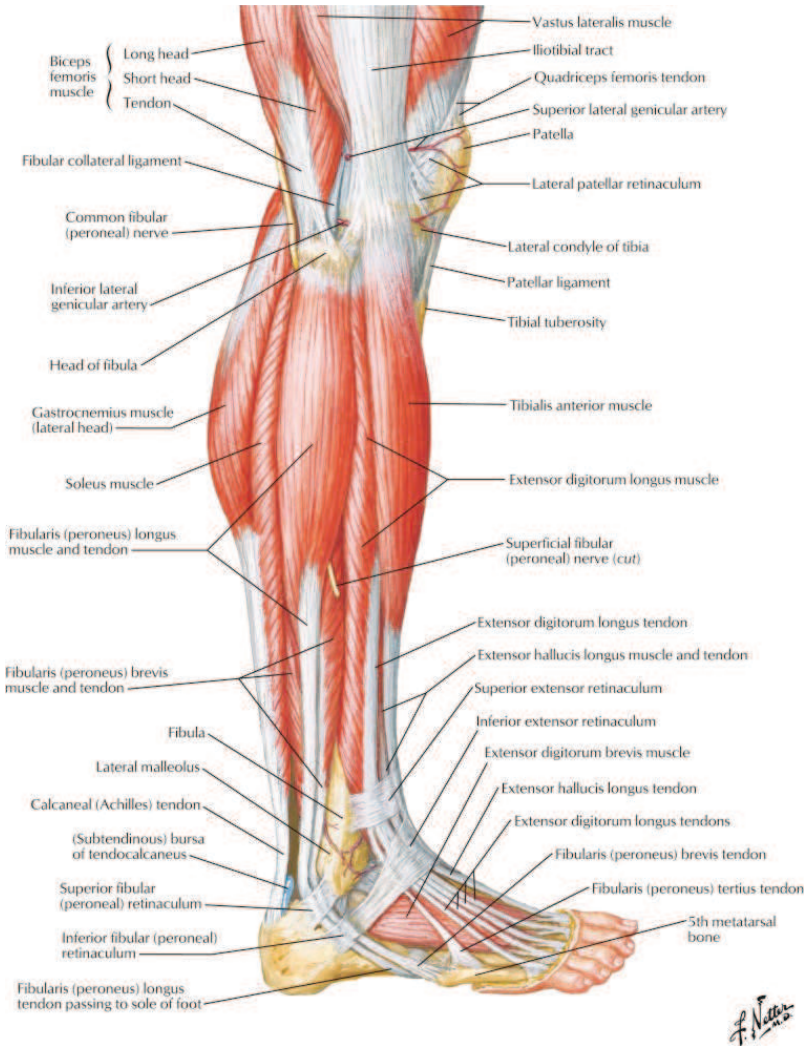

Figure A–15: Muscles in the leg. Lateral view. Adapted from [10]

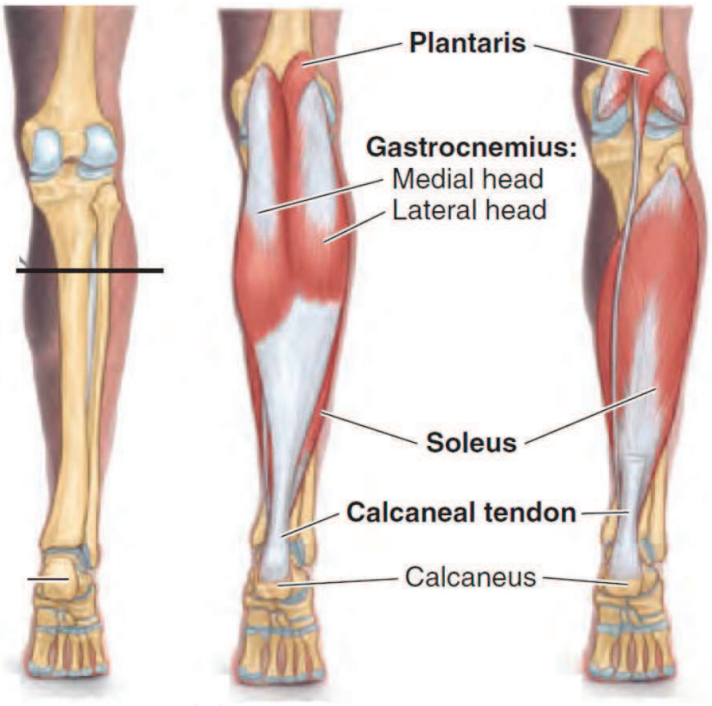

Figure A–16: Muscles in the leg. Posterior view. Adapted from [9]

formed where the bellies of the gastrocnemius terminate. This tendon receives fibers from the soleus and gastrocnemius muscles, at the distal end the tendon is tick and has an almost-round cross section; it then inserts on the posterior surface of the calcaneal tuberosity by making a 90° turn.

A.2.2 Function

The main function of the lower limbs are standing and walking [9]. When the person is standing upright only a few of the back and lower limb muscles are active. The hip and knee joints are in their most stable position (maximal contact of the articular surfaces for weight transfer) and, as shown in Figure A–17, the ankle joint

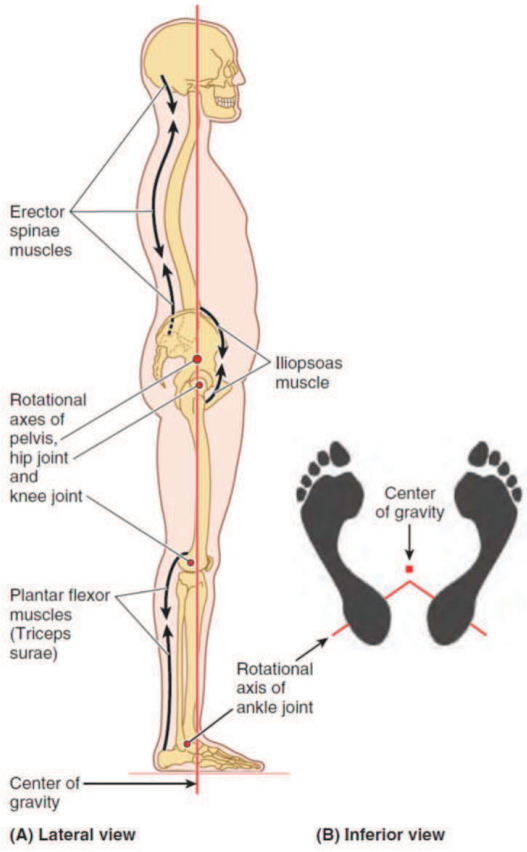

Figure A–17: Relaxed standing. A. Relationship of the line of gravity with the rotation axis to the hip, knee and ankle joints. B. Asymmetrical weight distribution around the center of gravity during standing. Adapted from [9]

is less stable, with the line of gravity falling just anterior to the ankle joint. In consequence, the tendency to fall forward must be counter balanced by activation of the ankle plantaflexor muscles.

Figure A–18 shows the different phases of locomotion. During the gait cycle, the ankle joint and related muscles play multiple and vital roles [9]: During heel strike, the ankle dorsiflexors help to lower the forefoot to the ground, during the early and mid-stance, when the foot is flat in the ground, the ankle plantarflexors perform

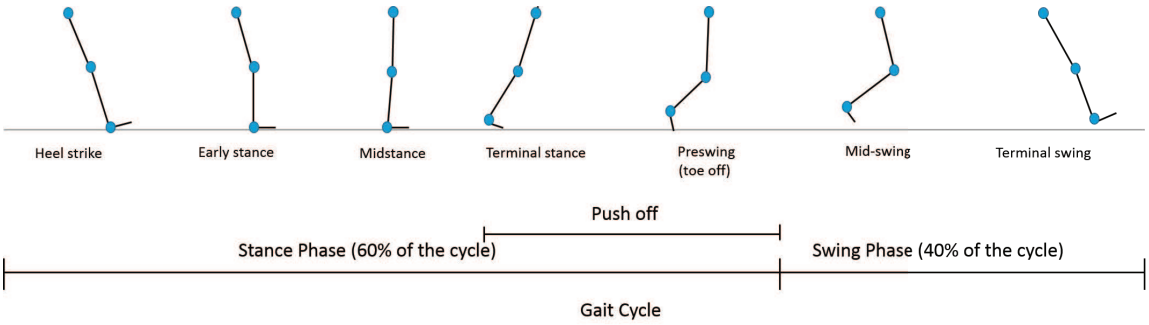

Figure A–18: Relative position of the hip, knee and ankle joints during the gait cycle. The stance phase of the cycle was divided into five sub-phases and lasts for about 60% of the step duration. The swing phase was divided into two sub-phases and composes about 40% of the cycle.

an eccentricly contraction to stop dorsiflexion. Furthermore, during the terminal stance, the plantarflexors are in charge of the push off that moves the body forward, providing more than half of the mechanical power needed for walking [185]. During the initial and mid-swing, the ankle dorsiflexors are in charge of lifting the foot from the ground. Finally, these muscles help to position the foot in the correct angle for heel-strike. In addition, to facilitate the movement of the foot during the difference phases of walking, ankle dorsiflexors and plantarflexors help to absorb impact forces during heel-strike which might otherwise destabilize the body [186, 237].

References

[1] R. E. Kearney and I. W. Hunter, "System identification of human joint dynamics," *Crit. Rev. Biomed. Eng*, vol. 18, no. 1, pp. 55 – 87, 1990.

[2] M. Verhaegen and P. Dewilde, "Subspace model identification part 1. the output-error state-space model identification class of algorithms," *International journal of control*, vol. 56, no. 5, pp. 1187–1210, 1992.

[3] E. R. Kandel, J. H. Schwartz, T. M. Jessell, S. A. Siegelbaum, and A. Hudspeth, *Principles of neural science*. McGraw-hill New York, 2000, vol. 4.

[4] A. J. Vander and D. JH Luciano, *Humanphysiology: the mechanisms of body function*. McGraw-Hill book company, 2001.

[5] J. G. Betts *et al.*, *Anatomy & physiology*. Open Stax, 2013.

[6] F. E. Zajac, "Muscle and tendon properties models scaling and application to biomechanics and motor," *Critical reviews in biomedical engineering*, vol. 17, no. 4, pp. 359–411, 1989.

[7] F. J. Valero-Cuevas, *Fundamentals of neuromechanics*. Springer, 2016.

[8] F. H. Martini, J. L. Nath, and E. F. Bartholomew, *Fundamentals of Anatomy & Physiology*. Pearson Education, 2015.

[9] K. L. Moore, A. F. Dalley, and A. M. Agur, *Clinically oriented anatomy*. Lippincott Williams & Wilkins, 2013.

[10] F. H. Netter, *Atlas of human anatomy*. Elsevier Health Sciences, 2010.

[11] M. M. Mirbagheri, H. Barbeau, and R. E. Kearney, "Intrinsic and reflex contributions to human ankle stiffness: Variation with activation level and position," *Exp Brain Res*, vol. 135, no. 4, pp. 423 – 436, 2000.

[12] R. E. Kearney, R. B. Stein, and L. Parameswaran, "Identification of intrinsic and reflex contributions to human ankle stiffness dynamics," *IEEE Trans. on Biomedical Eng*, vol. 44, no. 6, pp. 493 – 504, 1997.

[13] A. G. Feldman and M. L. Latash, "Testing hypotheses and the advancement of science: recent attempts to falsify the equilibrium point hypothesis," *Experimental Brain Research*, vol. 161, no. 1, pp. 91–103, 2005.

[14] A. G. Feldman and M. F. Levin, "The equilibrium-point hypothesis–past, present and future," in *Progress in motor control*. Springer, 2009, pp. 699–726.

[15] D. M. Wolpert, R. C. Miall, and M. Kawato, "Internal models in the cerebellum," *Trends in cognitive sciences*, vol. 2, no. 9, pp. 338–347, 1998.

[16] M. Kawato, "Internal models for motor control and trajectory planning," *Current opinion in neurobiology*, vol. 9, no. 6, pp. 718–727, 1999.

[17] M. M. Mirbagheri, H. Barbeau, M. Ladouceur, and R. E. Kearney, "Intrinsic and reflex stiffness in normal and spastic, spinal cord injured subjects," *Exp Brain Res*, vol. 141, no. 4, pp. 446 – 459, 2001.

[18] E. Perreault, L. Hargrove, D. Ludvig, H. Lee, and J. Sensinger, "Considering limb impedance in the design and control of prosthetic devices," in *Neuro-Robotics*. Springer, 2014, pp. 59–83.

[19] R. Van Ham, T. G. Sugar, B. Vanderborght, K. W. Hollander, and D. Lefeber, "Compliant actuator designs," *IEEE Robotics & Automation Magazine*, vol. 16, no. 3, pp. 81–94, 2009.

[20] G. C. Agarwal and G. L. Gottlieb, "Compliance of the human ankle," *Trans. Am. Sot. mech. Eng*, vol. 19, pp. 166 – 170, 1979.

[21] S. Siegler, J. Chen, and C. Schneck, "The three-dimensional kinematics and flexibility characteristics of the human ankle and subtalar jointspart i: Kinematics," *Journal of biomechanical engineering*, vol. 110, no. 4, pp. 364–373, 1988.

[22] H. Lee, H. I. Krebs, and N. Hogan, "Multivariable dynamic ankle mechanical impedance with active muscles," *IEEE Transactions on Neural Systems and Rehabilitation Engineering*, vol. 22, no. 5, pp. 971–981, 2014.

[23] P. L. Weiss, R. Kearney, and I. Hunter, "Position dependence of ankle joint dynamicsii. active mechanics," *Journal of biomechanics*, vol. 19, no. 9, pp. 737–751, 1986.

[24] S. Siegler, G. Moskowitz, and W. Freedman, "Passive and active components of the internal moment developed about the ankle joint during human ambulation," *Journal of biomechanics*, vol. 17, no. 9, pp. 647–652, 1984.

[25] R. Stein, "Peripheral control of movement." *Physiological Reviews*, vol. 54, no. 1, pp. 215–243, 1974.

[26] W. F. Genadry, R. E. Kearney, and I. W. Hunter, "Dynamic relationship between emg and torque at the human ankle: variation with contraction level and modulation," *Medical and Biological Engineering and Computing*, vol. 26, no. 5, pp. 489–496, 1988.

[27] S. C. Cannon and G. I. Zahalak, "The mechanical behavior of active human skeletal muscle in small oscillations," *Journal of biomechanics*, vol. 15, no. 2, pp. 111–121, 1982.

[28] R. A. Brand, R. D. Crowninshield, C. E. Wittstock, D. R. Pedersen, C. R. Clark, and F. M. V. Krieken, "A model of lower extremity muscular anatomy," *J Biomech Eng*, vol. 104, no. 4, pp. 304–314, 1982.

[29] C. Hogfors, G. Sigholm, and P. Herberts, "Biomechanical model of the human shoulderi. elements," *Journal of Biomechanics*, vol. 20, no. 2, pp. 157 – 166, 1987. [Online]. Available: http://www.sciencedirect.com/science/article/pii/0021929087903071

[30] M. G. Pandy, "Computer modeling and simulation of human movement," *Annu. Rev. Biomed. Eng*, no. 3, pp. 245–273, 2001.

[31] K.-N. An, B. Kwak, E. Chao, and B. Morrey, "Determination of muscle and joint forces: a new technique to solve the indeterminate problem," *Journal of biomechanical engineering*, vol. 106, no. 4, pp. 364–367, 1984.

[32] R. D. Crowninshield and R. A. Brand, "A physiologically based criterion of muscle force prediction in locomotion," *Journal of biomechanics*, vol. 14, no. 11, pp. 793–801, 1981.

[33] A. Erdemir, S. McLean, W. Herzog, and A. J. van den Bogert, "Model-based estimation of muscle forces exerted during movements," *Clinical biomechanics*, vol. 22, no. 2, pp. 131–154, 2007.

[34] M. Sartori, M. Maculan, C. Pizzolato, M. Reggiani, and D. Farina, "Modeling and simulating the neuromuscular mechanisms regulating ankle and knee joint stiffness during human locomotion," *Journal of Neurophysiology*, vol. 114, no. 4, pp. 2509–2527, 2015.

[35] M. Willerslev-Olsen, J. B. Andersen, T. Sinkjaer, and J. B. Nielsen, "Sensory feedback to ankle plantar flexors is not exaggerated during gait in spastic hemiplegic children with cerebral palsy," *Journal of neurophysiology*, vol. 111, no. 4, pp. 746–754, 2014.

[36] J. A. Hoffer and S. Andreassen, "Regulation of soleus muscle stiffness in premammillary cats: Intrinsic and reflex components," *Journal of Neurophysiology*, vol. 45, no. 2, pp. 267 – 285, 1981.

[37] T. R. Nichols and J. C. Houk, "Improvement in linearity and regulation of stiffness that results from actions of stretch reflex," *J. of Neurophysiology*, vol. 39, no. 1, pp. 119 – 142, 1976.

[38] J. Lehmann, R. Price, B. DeLateur, S. Hinderer, and C. Traynor, "Spasticity: quantitative measurements as a basis for assessing effectiveness of therapeutic intervention." *Archives of physical medicine and rehabilitation*, vol. 70, no. 1, pp. 6–15, 1989.

[39] A. Hufschmidt and K. Mauritz, "Chronic transformation of muscle in spasticity: a peripheral contribution to increased tone." *Journal of Neurology, Neurosurgery & Psychiatry*, vol. 48, no. 7, pp. 676–685, 1985.

[40] R. Herman and H. Schaumburg, "Alterations in dynamic and static properties of the stretch reflex in patients with spastic hemiplegia." *Archives of physical medicine and rehabilitation*, vol. 49, no. 4, p. 199, 1968.

[41] S. Fellows, F. Dömges, R. Töpper, A. Thilmann, and J. Noth, "Changes in the short-and long-latency stretch reflex components of the triceps surae muscle during ischaemia in man." *The Journal of physiology*, vol. 472, no. 1, pp. 737–748, 1993.

[42] T. Sinkjær and R. Hayashi, "Regulation of wrist stiffness by the stretch reflex," *Journal of biomechanics*, vol. 22, no. 11, pp. 1133–1140, 1989.

[43] V. Dietz, K.-H. Mauritz, and J. Dichgans, "Body oscillations in balancing due to segmental stretch reflex activity," *Experimental brain research*, vol. 40, no. 1, pp. 89–95, 1980.

[44] A. Berardelli, M. Hallett, C. Kaufman, E. Fine, W. Berenberg, and S. Simon, "Stretch reflexes of triceps surae in normal man." *Journal of Neurology, Neurosurgery & Psychiatry*, vol. 45, no. 6, pp. 513–525, 1982.

[45] G. C. Agarwal and G. L. Gottlieb, "Effect of virration on the ankle stretch reflex in man," *Electroencephalography and clinical neurophysiology*, vol. 49, no. 1, pp. 81–92, 1980.

[46] M. L. Latash and V. Zatsiorsky, *Biomechanics and Motor Control: Defining Central Concepts*. Academic Press, 2015.

[47] F. C. Van der Helm, A. C. Schouten, E. de Vlugt, and G. G. Brouwn, "Identification of intrinsic and reflexive components of human arm dynamics during postural control," *Journal of neuroscience methods*, vol. 119, no. 1, pp. 1–14, 2002.

[48] E. Toft, T. Sinkjær, S. Andreassen, and K. Larsen, "Mechanical and electromyographic responses to stretch of the human ankle extensors," *Journal of Neurophysiology*, vol. 65, no. 6, pp. 1402 – 1410, 1991.

[49] T. Sinkjær, E. Toft, K. Larsen, S. Andreassen, and H. J. Hansen, "Non-reflex and reflex mediated ankle joint stiffness in multiple sclerosis patients with spasticity," *Muscle Nerve*, vol. 16, no. 1, pp. 267 – 285, 1993.

[50] R. R. Carter, P. E. Crago, and M. W. Keith, "Stiffness regulation by reflex action in the normal human hand," *Journal of Neurophysiology*, vol. 64, no. 1, pp. 105 – 123, 1990.

[51] M. Heyters, A. Carpentier, J. Duchateau, and K. Hainaut, "Twitch analysis as an approach to motor unit activation during electrical stimulation," *Can J Appl Physiol*, vol. 19, no. 4, pp. 451–461, 1994.

[52] P. L. Weiss, R. E. Kearney, and I. W. Hunter, "Position dependence of ankle joint dynamics. i passive mechanics," *Journal of Biomechanics*, vol. 19, no. 9, pp. 727 – 735, 1986.

[53] G. I. Zahalak and R. Pramod, "Myoelectric response of the human triceps brachii to displacement-controlled oscillations of the forearm," *Experimental Brain Research*, vol. 58, no. 2, pp. 305–317, 1985. [Online]. Available: http://dx.doi.org/10.1007/BF00235312

[54] P. E. Crago, J. Houk, and Z. Hasan, "Regulatory actions of human stretch reflex," *Journal of Neurophysiology*, vol. 39, no. 5, pp. 925–935, 1976.

[55] F. Lacquaniti, F. Licata, and J. Soechting, "The mechanical behavior of the human forearm in response to transient perturbations," *Biological Cybernetics*, vol. 44, no. 1, pp. 35–46, 1982.

[56] R. E. Kearney and I. W. Hunter, "System identification of human triceps surae stretch reflex dynamics," *Experimental Brain Research*, vol. 51, no. 1, pp. 117–127, 1983. [Online]. Available: http://dx.doi.org/10.1007/BF00236809

[57] ——, "System identification of human stretch reflex dynamics: Tibialis anterior," *Experimental Brain Research*, vol. 56, no. 1, pp. 40–49, 1984. [Online]. Available: http://dx.doi.org/10.1007/BF00237440

[58] G. L. Gottlieb and G. C. Agarwal, "Response to sudden torques about ankle in man: myotatic reflex," *Journal of Neurophysiology*, vol. 42, no. 1, pp. 91–106, 1979.

[59] R. B. Stein and R. E. Kearney, "Nonlinear behavior of muscle reflexes at the human ankle joint," *J. of Neurophysiology*, vol. 73, no. 1, pp. 65 – 72, 1995.

[60] G. L. Gottlieb and G. C. Agarwal, "Dynamic relationship between isometric muscle tension and the electromyogram in man," *Journal of applied physiology*, vol. 30, no. 3, pp. 345–351, 1971.

[61] E. A. Clancy and N. Hogan, "Relating agonist-antagonist electromyograms to joint torque during isometric, quasi-isotonic, nonfatiguing contractions," *IEEE Transactions on Biomedical Engineering*, vol. 44, no. 10, pp. 1024–1028, 1997.

[62] S. Jalaleddini, E. Sobhani Tehrani, and R. Kearney, "A subspace approach to the structural decomposition and identification of ankle joint dynamic stiffness." *IEEE transactions on bio-medical engineering*, 2016.

[63] Y. Zhao, D. T. Westwick, and R. E. Kearney, "Subspace methods for identification of human ankle joint stiffness," *IEEE Trans. on Biomedical Eng*, vol. 58, no. 11, pp. 3039 – 3048, 2011.

[64] D. L. Guarin, K. Jalaleddini, and R. E. Kearney, "Identification of a parametric, discrete-time model of ankle stiffness," in *Engineering in Medicine and Biology Society (EMBC), 2013 Annual International Conference of the IEEE*, 2013, pp. 5065 – 5070.

[65] D. L. Guarin, "Identification of multiple-input, single-output discrete transfer function models. application to ankle stiffness." Master's thesis, McGill University, Montreal, 2013.

[66] L. Q. Zhang, G. Nuber, J. Butler, M. B., and W. Z. Rymer, "In vivo human knee joint dynamic properties as functions of muscle contraction and joint position," *Journal of Biomechanics*, vol. 31, no. 1, pp. 71 – 76, 1997.

[67] H. Lee, H. I. Krebs, and N. Hogan, "Linear time-varying identification of ankle mechanical impedance during human walking," in *ASME 2012 5th Annual Dynamic Systems and Control Conference joint with the JSME 2012 11th Motion and Vibration Conference*. American Society of Mechanical Engineers, 2012, pp. 753–758.

[68] J. Mizrahi, "Mechanical impedance and its relations to motor control, limb dynamics, and motion biomechanics," *Journal of medical and biological engineering*, vol. 35, no. 1, pp. 1–20, 2015.

[69] D. T. Westwick and E. J. Perreault, "Closed-loop identification: Application to the estimation of limb impedance in a compliant environment," *IEEE Trans Biomed Eng*, vol. 58, no. 3, pp. 521 – 530, 2011.

[70] G. L. Gottlieb and G. C. Agarwal, "Dependence of human ankle compliance on joint angle," *Journal of Biomechanics*, vol. 11, no. 4, pp. 177 – 181, 1978.

[71] A. C. Schouten, E. de Vlugt, J. B. van Hilten, and F. C. van der Helm, "Design of a torque-controlled manipulator to analyse the admittance of the wrist joint," *Journal of neuroscience methods*, vol. 154, no. 1, pp. 134–141, 2006.

[72] D. Ludvig, S. A. Antos, and E. J. Perreault, "Joint impedance decreases during movement initiation," in *2012 Annual International Conference of the IEEE Engineering in Medicine and Biology Society*. IEEE, 2012, pp. 3304–3307.

[73] M. L. Latash and V. M. Zatsiorsky, "Joint stiffness: Myth or reality?" *Human movement science*, vol. 12, no. 6, pp. 653–692, 1993.

[74] A. H. Hansen, D. S. Childress, S. C. Miff, S. A. Gard, and K. P. Mesplay, "The human ankle during walking: implications for design of biomimetic ankle prostheses," *Journal of biomechanics*, vol. 37, no. 10, pp. 1467–1474, 2004.

[75] E. J. Rouse, R. D. Gregg, L. J. Hargrove, and J. W. Sensinger, "The difference between stiffness and quasi-stiffness in the context of biomechanical modeling," *IEEE Transactions on Biomedical Engineering*, vol. 60, no. 2, pp. 562–568, 2013.

[76] T. I. H. Brown, P. M. H. Rack, and H. F. Ross, "Forces generated at the thumb interphalangeal joint during imposed sinusoidal movements," *Journal of Physiolgy*, vol. 332, no. 1, pp. 69 – 85, 1982.

[77] G. C. Joyce, P. M. Rack, and H. F. Ross, "The forces generated at the human elbow joint in response to imposed sinusoidal movements of the forearm," *Journal of Physiolgy*, vol. 240, no. 2, pp. 351 – 374, 1974.

[78] C. M. Evans, S. J. Fellows, P. M. R. H. F. Ross, and D. K. Walters, "Response of the normal human ankle joint to imposed sinusoidal movements," *Journal of Physiolgy*, vol. 344, no. 1, pp. 483 – 502, 1983.

[79] G. I. Zahalak and S. J. Heyman, "A quantitative evaluation of the frequency-response characteristics of active human skeletal muscle in vivo," *Journal of Biomechanical Engineering*, vol. 101, no. 1, pp. 28 – 37, 1979.

[80] E. J. Perreault, R. F. Kirsch, and P. E. Crago, "Effects of voluntary force generation on the elastic components of endpoint stiffness," *Experimental Brain Research*, vol. 141, no. 3, pp. 312–323, 2001.

[81] E. J. Perreault, R. F. Kirsch, and A. M. Acosta, "Multiple-input, multiple-output system identification for characterization of limb stiffness dynamics," *Biological cybernetics*, vol. 80, no. 5, pp. 327–337, 1999.

[82] A. Roy, H. I. Krebs, D. J. Williams, C. T. Bever, L. W. Forrester, R. M. Macko, and N. Hogan, "Robot-aided neurorehabilitation: a novel robot for ankle rehabilitation," *IEEE transactions on robotics*, vol. 25, no. 3, pp. 569–582, 2009.

[83] D. T. Westwick and E. J. Perreault, "Estimates of acausal joint impedance models," *IEEE Transactions on Biomedical Engineering*, vol. 59, no. 10, pp. 2913–2921, 2012.

[84] E. de Vlugt, A. C. Schouten, and F. C. van der Helm, "Closed-loop multivariable system identification for the characterization of the dynamic arm compliance using continuous force disturbances: a model study," *Journal of neuroscience methods*, vol. 122, no. 2, pp. 123–140, 2003.

[85] W. Mugge, D. A. Abbink, A. C. Schouten, J. P. Dewald, and F. C. van der Helm, "A rigorous model of reflex function indicates that position and force feedback are flexibly tuned to position and force tasks," *Experimental brain research*, vol. 200, no. 3-4, pp. 325–340, 2010.

[86] A. C. Schouten, E. De Vlugt, J. Van Hilten, and F. C. Van Der Helm, "Quantifying proprioceptive reflexes during position control of the human arm," *IEEE Transactions on Biomedical Engineering*, vol. 55, no. 1, pp. 311–321, 2008.

[87] E. De Vlugt, J. H. de Groot, K. E. Schenkeveld, J. Arendzen, F. C. van der Helm, and C. G. Meskers, "The relation between neuromechanical parameters and ashworth score in stroke patients," *Journal of neuroengineering and rehabilitation*, vol. 7, no. 1, p. 1, 2010.

[88] S. Van Eesbeek, J. H. De Groot, F. C. Van der Helm, and E. De Vlugt, "In vivo estimation of the short-range stiffness of cross-bridges from joint rotation," *Journal of biomechanics*, vol. 43, no. 13, pp. 2539–2547, 2010.

[89] E. De Vlugt, S. Van Eesbeek, P. Baines, J. Hilte, C. G. Meskers, and J. H. De Groot, "Short range stiffness elastic limit depends on joint velocity," *Journal of biomechanics*, vol. 44, no. 11, pp. 2106–2112, 2011.

[90] E. J. Perreault, P. E. Crago, and R. F. Kirsch, "Estimation of intrinsic and reflex contributions to muscle dynamics: a modeling study," *IEEE transactions on biomedical engineering*, vol. 47, no. 11, pp. 1413–1421, 2000.

[91] L. Galiana, J. Fung, and R. Kearney, "Identification of intrinsic and reflex ankle stiffness components in stroke patients," *Experimental brain research*, vol. 165, no. 4, pp. 422–434, 2005.

[92] M. M. Mirbagheri, X. Niu, and D. Varoqui, "Prediction of stroke motor recovery using reflex stiffness measures at one month," *IEEE Transactions on Neural Systems and Rehabilitation Engineering*, vol. 20, no. 6, pp. 762–770, 2012.

[93] M. M. Mirbagheri, T. Lilaonitkul, and W. Z. Rymer, "Prediction of natural history of neuromuscular properties after stroke using fugl-meyer scores at 1 month," *Neurorehabilitation and Neural Repair*, vol. 25, no. 5, pp. 458–468, 2011.

[94] K. M. Moorhouse and K. P. Granata, "Trunk stiffness and dynamics during active extension exertions," *Journal of biomechanics*, vol. 38, no. 10, pp. 2000–2007, 2005.

[95] ——, "Role of reflex dynamics in spinal stability: intrinsic muscle stiffness alone is insufficient for stability," *Journal of biomechanics*, vol. 40, no. 5, pp. 1058–1065, 2007.

[96] R. Xia, M. Radovic, A. J. Threlkeld, and Z.-H. Mao, "System identification and modeling approach to characterizing rigidity in parkinson's disease: Neural and non-neural contributions," in *Bioinformatics and Biomedical Engineering (iCBBE), 2010 4th International Conference on*, 2010, pp. 1–4.

[97] S. M. Tare, "Estimation of stretch reflex contributions of wrist using system identification and quantification of tremor in parkinson's disease patients," Ph.D. dissertation, University of Pittsburgh, 2009.

[98] W. Harwin, A. Murgia, and E. Stokes, "Assessing the effectiveness of robot facilitated neurorehabilitation for relearning motor skills following a stroke," *Medical & biological engineering & computing*, vol. 49, no. 10, pp. 1093–1102, 2011.

[99] A. K. Swain, D. T. Westwick, and E. J. Perreault, "Frequency domain identification of a parallel-cascade joint stiffness model," in *Proceedings of the 2010 American Control Conference*. IEEE, 2010, pp. 4367–4372.

[100] C. Larivière, D. Ludvig, R. Kearney, H. Mecheri, J.-M. Caron, and R. Preuss, "Identification of intrinsic and reflexive contributions to low-back stiffness: medium-term reliability and construct validity," *Journal of biomechanics*, vol. 48, no. 2, pp. 254–261, 2015.

[101] P. C. Young, *Recursive Estimation and Time-Series Analysis*. Berlin: Springer, 2011.

[102] S. L. Kukreja, H. L. Galiana, and R. E. Kearney, "Narmax representation and identification of ankle dynamics," *IEEE Trans. on Biomedical Eng*, vol. 50, no. 1, pp. 70 – 81, 2003.

[103] D. L. Guarin and R. E. Kearney, "A narmax method for the identification of time-varying joint stiffness," in *Engineering in Medicine and Biology Society (EMBC), 2012 Annual International Conference of the IEEE*, 2012, pp. 6518 –6521.

[104] K. Jalaleddini and R. E. Kearney, "Estimation of the gain and threshold of the stretch reex with a novel subspace identication algorithm," in *Engineering in Medicine and Biology Society (EMBC), 2011 Annual International Conference of the IEEE*, 2011, pp. 4431 – 4434.

[105] K. Jalaleddini, M. A. Golkar, D. L. Guarin, E. S. Tehrani, and R. E. Kearney, "Parametric methods for identification of time-invariant and time-varying joint stiffness models," *IFAC-PapersOnLine*, vol. 48, no. 28, pp. 1375–1380, 2015.

[106] D. Bennett, J. M. Hollerbach, Y. Xu, and I. Hunter, "Time-varying stiffness of human elbow joint during cyclic voluntary movement," *Experimental Brain Research*, vol. 88, no. 2, pp. 433–442, 1992.

[107] R. F. Kirsch and R. E. Kearney, "Identification of time-varying stiffness dynamics of the human ankle joint during an imposed movement," *Experimental brain research*, vol. 114, no. 1, pp. 71–85, 1997.

[108] J. B. MacNeil, R. E. Kearney, and I. W. Hunter, "Identification of time-varying biological systems from ensemble data (joint dynamics application)," *Biomedical Engineering, IEEE Transactions on*, vol. 39, no. 12, pp. 1213–1225, 1992.

[109] E. Rouse, L. Hargrove, E. Perreault, and T. Kuiken, "Estimation of human ankle impedance during the stance phase of walking," *Neural Systems and Rehabilitation Engineering, IEEE Transactions on*, vol. 22, no. 4, pp. 870–878, 2014.

[110] H. Lee and N. Hogan, "Time-varying ankle mechanical impedance during human locomotion," *Neural Systems and Rehabilitation Engineering, IEEE Transactions on*, vol. 23, no. 5, pp. 755–764, 2015.

[111] H. Giesbrecht, M. Baker, D. Ludvig, R. Wagner, and R. Kearney, "Identification of time-varying intrinsic and reflex joint stiffness," in *Engineering in*

Medicine and Biology Society, 2006. EMBS'06. 28th Annual International Conference of the IEEE. IEEE, 2006, pp. 288–291.

[112] D. Ludvig, T. S. Visser, H. Giesbrecht, and R. E. Kearney, "Identification of time-varying intrinsic and reflex joint stiffness," *IEEE Trans. on Biomedical Eng*, vol. 58, no. 6, pp. 1715 – 1723, 2011.

[113] D. L. Guarin and R. E. Kearney, "Time-varying identification of ankle dynamic joint stiffness during movement with constant muscle activation," in *Engineering in Medicine and Biology Society (EMBC), 2015 37th Annual International Conference of the IEEE*. IEEE, 2015, pp. 6740–6743.

[114] D. B. Lipps, E. M. Baillargeon, D. Ludvig, and E. J. Perreault, "System identification of multidimensional shoulder impedance during volitional contractions," *IFAC-PapersOnLine*, vol. 48, no. 28, pp. 1369–1374, 2015.

[115] Y. Xu and J. M. Hollerbach, "A robust ensemble data method for identification of human joint mechanical properties during movement," *IEEE transactions on biomedical engineering*, vol. 46, no. 4, pp. 409–419, 1999.

[116] D. Ludvig and R. E. Kearney, "Real-time estimation of intrinsic and reflex stiffness," *IEEE Transactions on Biomedical Engineering*, vol. 54, no. 10, pp. 1875–1884, 2007.

[117] D. Ludvig, I. Cathers, and R. E. Kearney, "Voluntary modulation of human stretch reflexes," *Experimental brain research*, vol. 183, no. 2, pp. 201–213, 2007.

[118] S. van Eesbeek, F. van der Helm, M. Verhaegen, and E. de Vlugt, "Lpv subspace identification of time-variant joint impedance," in *Neural Engineering (NER), 2013 6th International IEEE/EMBS Conference on*. IEEE, 2013, pp. 343–346.

[119] E. S. Tehrani, K. Jalaleddini, and R. E. Kearney, "Linear parameter varying identification of ankle joint intrinsic stiffness during imposed walking movements," in *2013 35th Annual International Conference of the IEEE Engineering in Medicine and Biology Society (EMBC)*. IEEE, 2013, pp. 4923–4927.

[120] D. Ludvig and E. J. Perreault, "Task-relevant adaptation of musculoskeletal impedance during posture and movement," in *2014 American Control Conference*. IEEE, 2014, pp. 4784–4789.

[121] P. Weiss, R. Kearney, and I. Hunter, "Position dependence of stretch reflex dynamics at the human ankle," *Experimental brain research*, vol. 63, no. 1, pp. 49–59, 1986.

[122] W. MacKay, D. Crammond, H. Kwan, and J. Murphy, "Measurements of human forearm viscoelasticity," *Journal of Biomechanics*, vol. 19, no. 3, pp. 231–238, 1986.

[123] X. Hu, W. M. Murray, and E. J. Perreault, "Muscle short-range stiffness can be used to estimate the endpoint stiffness of the human arm," *Journal of neurophysiology*, vol. 105, no. 4, pp. 1633–1641, 2011.

[124] D. Ludvig, M. Plocharski, P. Plocharski, and E. Perreault, "Knee stiffness decreases during continuous volitional movement," in *Annual Meeting of the Society for Neuroscience, Neuroscience 2013, 9-13 November 2013, San Diego, Ca, Usa*. Society for Neuroscience, 2013.

[125] H. Lee, E. Rouse, and H. Krebs, "Summary of human ankle mechanical impedance during walking," *IEEE Journal of Translational Engineering in Health and Medicine*, vol. PP, no. 99, pp. 1–7, 2016.

[126] F. Doemges and P. Rack, "Task-dependent changes in the response of human wrist joints to mechanical disturbance." *The Journal of Physiology*, vol. 447, p. 575, 1992.

[127] C. Capaday and R. Stein, "Amplitude modulation of the soleus h-reflex in the human during walking and standing," *The Journal of neuroscience*, vol. 6, no. 5, pp. 1308–1313, 1986.

[128] ——, "Difference in the amplitude of the human soleus h reflex during walking and running." *The Journal of physiology*, vol. 392, p. 513, 1987.

[129] E. Toft, G. T. Espersen, S. Kålund, T. Sinkjær, and B. C. Hornemann, "Passive tension of the ankle before and after stretching," *The American journal of sports medicine*, vol. 17, no. 4, pp. 489–494, 1989.

[130] R. F. Kirsch and W. Rymer, "Neural compensation for fatigue-induced changes in muscle stiffness during perturbations of elbow angle in human," *Journal of neurophysiology*, vol. 68, no. 2, pp. 449–470, 1992.

[131] C. Cobelli and E. Carson, *Introduction to modeling in physiology and medicine*. Academic Press, 2008.

[132] V. Z. Marmarelis, *Nonlinear dynamic modeling of physiological systems*. John Wiley & Sons, 2004, vol. 10.

[133] D. T. Westwick and R. E. Kearney, *Identification of nonlinear physiological systems*. Hoboken, N.J.: IEEE Press, 2003.

[134] K. J. Åström and B. Wittenmark, *Adaptive control*. Courier Corporation, 2013.

[135] A. Oppenheim, *Discrete Time Signal Processing*. Pearson Higher Education, 2010.

[136] L. Ljung, *System Identification - Theory For the User*, 2nd ed. Upper Saddle River, N.J.: Prentice Hall, 1999.

[137] P. C. Young, "An instrumental variable method for real-time identification of a noisy process," *Automatica*, vol. 6, no. 2, pp. 271 – 287, 1970.

[138] G. E. Box, G. M. Jenkins, G. C. Reinsel, and G. M. Ljung, *Time series analysis: forecasting and control*. John Wiley & Sons, 2015.

[139] D. R. Cox and N. Reid, "Parameter orthogonality and approximate conditional inference," *Journal of the Royal Statistical Society. Series B (Methodological)*, vol. 49, no. 1, pp. 1 – 39, 1987.

[140] M. Verhaegen and V. Verdult, *Filtering and system identification: a least squares approach*. Cambridge university press, 2007.

[141] P. C. Young and A. Jakeman, "Refined instrumental variable methods of recursive time-series analysis part i. single input, single output systems," *Int. Journal of Control*, vol. 19, no. 1, p. 1 30, 1979.

[142] T. D. Söderström and P. G. Stoica, *Instrumental variable methods for system identification*. Springer, 1983, vol. 57.

[143] C. M. Bishop, "Pattern recognition," *Machine Learning*, vol. 128, 2006.

[144] J. Friedman, T. Hastie, and R. Tibshirani, *The elements of statistical learning*. Springer series in statistics Springer, Berlin, 2001, vol. 1.

[145] R. Tóth, C. Lyzell, M. Enqvist, P. S. Heuberger, and P. M. Van den Hof, "Order and structural dependence selection of lpv-arx models using a nonnegative garrote approach," in *Decision and Control, 2009 held jointly with the 2009*

28th Chinese Control Conference. CDC/CCC 2009. Proceedings of the 48th IEEE Conference on. IEEE, 2009, pp. 7406–7411.

[146] Z. Ghahramani and S. T. Roweis, "Learning nonlinear dynamical systems using an em algorithm," *Advances in neural information processing systems*, pp. 431–437, 1999.

[147] M. E. Tipping, "Sparse bayesian learning and the relevance vector machine," *Journal of machine learning research*, vol. 1, no. Jun, pp. 211–244, 2001.

[148] A. Tipping and A. Faul, "Analysis of sparse bayesian learning," *Advances in neural information processing systems*, vol. 14, pp. 383–389, 2002.

[149] D. P. Wipf and B. D. Rao, "Sparse bayesian learning for basis selection," *IEEE Transactions on Signal Processing*, vol. 52, no. 8, pp. 2153–2164, 2004.

[150] J. Stapleton and S. Bass, "Adaptive noise cancellation for a class of nonlinear, dynamic reference channels," *IEEE transactions on circuits and systems*, vol. 32, no. 2, pp. 143–150, 1985.

[151] E.-W. Bai and D. Li, "Convergence of the iterative hammerstein system identification algorithm," *IEEE Transactions on Automatic Control*, vol. 49, no. 11, pp. 1929–1940, 2004.

[152] F. Ding, X. P. Liu, and G. Liu, "Identification methods for hammerstein nonlinear systems," *Digital Signal Processing*, vol. 21, no. 2, pp. 215–238, 2011.

[153] W. Greblicki, "Continuous-time hammerstein system identification," *IEEE Transactions on Automatic Control*, vol. 45, no. 6, pp. 1232–1236, 2000.

[154] A. Gardiner, "Frequency domain identification of nonlinear systems," in *3rd IFAC Symp. on Identification and System Parameter Estimation, Hague, Netherlands*, 1973, pp. 831–834.

[155] E.-W. Bai, "Frequency domain identification of hammerstein models," *IEEE transactions on automatic control*, vol. 48, no. 4, pp. 530–542, 2003.

[156] K. Jalaleddini and R. E. Kearney, "Subspace identification of siso hammerstein systems: application to stretch reflex identification," *IEEE Transactions on Biomedical Engineering*, vol. 60, no. 10, pp. 2725–2734, 2013.

[157] M. Verhaegen and D. Westwick, "Identifying mimo hammerstein systems in the context of subspace model identification methods," *International Journal of Control*, vol. 63, no. 2, pp. 331–349, 1996.

[158] I. W. Hunter and M. J. Korenberg, "The identification of nonlinear biological systems: Wiener and hammerstein cascade models," *Biological Cybernetics*, vol. 55, pp. 135 – 144, 1986.

[159] D. T. Westwick and R. E. Kearney, "Separable least squares identification of nonlinear hammerstein models: Application to stretch reflex dynamics," *Annals of Biomedical Engineering*, vol. 29, no. 8, p. 707 718, 2001.

[160] K. Narendra and P. Gallman, "An iterative method for the identification of nonlinear systems using a hammerstein model," *IEEE Transactions on Automatic control*, vol. 11, no. 3, pp. 546–550, 1966.

[161] F. Le, I. Markovsky, C. T. Freeman, and E. Rogers, "Identification of electrically stimulated muscle models of stroke patients," *Control Engineering Practice*, vol. 18, no. 4, pp. 396–407, 2010.

[162] W. Farahat and H. Herr, "A method for identification of electrically stimulated muscle," in *2005 IEEE Engineering in Medicine and Biology 27th Annual Conference*. IEEE, 2005, pp. 6225–6228.

[163] P. Stoica and T. Soderstrom, "Asymptotic behaviour of some bootstrap estimators," *International Journal of Control*, vol. 33, no. 3, pp. 433 – 454, 1981.

[164] E.-W. Bai and Y. Liu, "Least squares solutions of bilinear equations," *Systems & control letters*, vol. 55, no. 6, pp. 466–472, 2006.

[165] Y. Liu and E.-W. Bai, "Iterative identification of hammerstein systems," *Automatica*, vol. 43, no. 2, pp. 346–354, 2007.

[166] G. Li and C. Wen, "Convergence of normalized iterative identification of hammerstein systems," *Systems & Control Letters*, vol. 60, no. 11, pp. 929–935, 2011.

[167] K. Jalaleddini and R. Kearney, "An iterative algorithm for the subspace identification of siso hammerstein systems," *18th IFAC World Congress*, vol. 44, no. 1, pp. 11 779 – 11 784, 2011.

[168] T. S. Rao, "The fitting of non-stationary time-series models with time-dependent parameters," *J. Royal Statist. Society. Series B*, vol. 32, no. 2, pp. 312–322, 1970.

[169] R. Tóth, *Modeling and identification of linear parameter-varying systems*. Springer, 2010, vol. 403.

[170] R. Zou and K. H. Chon, "Robust algorithm for estimation of time-varying transfer functions," *Biomedical Engineering, IEEE Transactions on*, vol. 51, no. 2, pp. 219–228, 2004.

[171] T. Sinkjær, E. Toft, S. Andreassen, and B. C. Hornemann, "Muscle stiffness in human ankle dorsiflexors: intrinsic and reflex components," *Journal of Neurophysiology*, vol. 60, no. 3, pp. 1110–1121, 1988.

[172] D. L. Guarin and R. E. Kearney, "Time-varying identification of ankle dynamic joint stiffness during movement with constant muscle activation," in *Engineering in Medicine and Biology Society (EMBC), 2015 37th Annual International Conference of the IEEE*. IEEE, 2015, pp. 6740–6743.

[173] M. Ranjbaran, K. Jalaleddini, D. L. Guarin, R. E. Kearney, and H. Galiana, "Analysis and modeling of noise in biomedical systems," in *Engineering in Medicine and Biology Society (EMBC), 2013 Annual International Conference of the IEEE*, 2013, pp. 997 – 1000.

[174] S. M. Bezrukov, H. Frauenfelder, and F. Moss, *Fluctuations and Noise in Biological, Biophysical, and Biomedical Systems*. SPIE, 2003.

[175] R. F. Kirsch and R. E. Kearney, "Identification of time-varying dynamics of the human triceps surae stretch reflex. ii. rapid imposed movement." *Experimental brain research*, vol. 97, no. 1, p. 128, 1993.

[176] P. Stoica and T. Soderstrom, "On the convergence properties of a time-varying recursion," *Signal Processing Letters, IEEE*, vol. 2, no. 5, pp. 95–96, 1995.

[177] V. Laurain, M. Gilson, R. Tth, and H. Garnier, "Refined instrumental variable methods for identification of LPV Box-Jenkins models," *Automatica*, vol. 46, no. 6, pp. 959 – 967, 2010.

[178] E. Burdet, D. W. Franklin, and T. E. Milner, *Human robotics: neuromechanics and motor control*. MIT Press, 2013.

[179] D. L. Guarin and R. E. Kearney, "An instrumental variable approach for the identification of time-varying, hammerstein systems," in *17th IFAC Symposium on System Identification*, 2015.

[180] D. A. Winter, *Biomechanics and motor control of human movement*. John Wiley & Sons, 2009.

[181] M. Mirbagheri, C. Tsao, K. Settle, T. Lilaonitkul, and W. Rymer, "Time course of changes in neuromuscular properties following stroke," in *2008 30th Annual International Conference of the IEEE Engineering in Medicine and Biology Society*. IEEE, 2008, pp. 5097–5100.

[182] E. Marsolais and R. Kobetic, "Functional electrical stimulation for walking in paraplegia." *J Bone Joint Surg Am*, vol. 69, no. 5, pp. 728–733, 1987.

[183] M. Gilson, H. Garnier, P. C. Young, and P. M. Van den Hof, "Optimal instrumental variable method for closed-loop identification," *Control Theory & Applications, IET*, vol. 5, no. 10, pp. 1147–1154, 2011.

[184] R. Tóth, *Modeling and identification of linear parameter-varying systems*. Springer, 2008, vol. 403.

[185] D. Gordon, E. Robertson, and D. A. Winter, "Mechanical energy generation, absorption and transfer amongst segments during walking," *Journal of biomechanics*, vol. 13, no. 10, pp. 845–854, 1980.

[186] J. J. Eng and D. A. Winter, "Kinetic analysis of the lower limbs during walking: what information can be gained from a three-dimensional model?" *Journal of biomechanics*, vol. 28, no. 6, pp. 753–758, 1995.

[187] J. Perry, J. R. Davids *et al.*, "Gait analysis: normal and pathological function." *Journal of Pediatric Orthopaedics*, vol. 12, no. 6, p. 815, 1992.

[188] G. C. Agarwal and G. L. Gottlieb, "Oscillation of the human ankle joint in response to applied sinusoidal torque on the foot," *Journal of Physiolgy*, vol. 268, no. 2, pp. 151 – 176, 1977.

[189] P. Weiss, I. Hunter, and R. Kearney, "Human ankle joint stiffness over the full range of muscle activation levels," *Journal of biomechanics*, vol. 21, no. 7, pp. 539–544, 1988.

[190] H. J. Hermens, B. Freriks, C. Disselhorst-Klug, and G. Rau, "Development of recommendations for {SEMG} sensors and sensor placement procedures," *Journal of Electromyography and Kinesiology*, vol. 10, no. 5, pp. 361 – 374, 2000.

[191] F. Lacquaniti, M. Carrozzo, and N. Borghese, "Time-varying mechanical behavior of multijointed arm in man," *Journal of Neurophysiology*, vol. 69, no. 5, pp. 1443–1464, 1993.

[192] H. L. Wei and S. A. Billings, "Identification of time-varying systems using multiresolution wavelet models," *Int. J. systems Sci*, vol. 33, no. 15, pp. 1217 – 1228, 2002.

[193] W. H. Press, *Numerical recipes 3rd edition: The art of scientific computing*. Cambridge university press, 2007.

[194] L. R. Smith, K. S. Lee, S. R. Ward, H. G. Chambers, and R. L. Lieber, "Hamstring contractures in children with spastic cerebral palsy result from a stiffer extracellular matrix and increased in vivo sarcomere length," *The Journal of physiology*, vol. 589, no. 10, pp. 2625–2639, 2011.

[195] M. Willerslev-Olsen, J. Lorentzen, T. Sinkjær, and J. B. Nielsen, "Passive muscle properties are altered in children with cerebral palsy before the age of 3 years and are difficult to distinguish clinically from spasticity," *Developmental medicine & Child neurology*, vol. 55, no. 7, pp. 617–623, 2013.

[196] R. F. Kirsch and A. M. Acosta, "Model-based development of neuroprostheses for restoring proximal arm function," in *Engineering in Medicine and Biology Society, 2001. Proceedings of the 23rd Annual International Conference of the IEEE*, vol. 4. IEEE, 2001, pp. 4075–4079.

[197] E. J. Perreault, C. J. Heckman, and T. G. Sandercock, "Hill muscle model errors during movement are greatest within the physiologically relevant range of motor unit firing rates," *Journal of biomechanics*, vol. 36, no. 2, pp. 211–218, 2003.

[198] E. Schearer, Y.-W. Liao, E. Perreault, M. Tresch, W. Memberg, R. Kirsch, and K. Lynch, "Semiparametric identification of human arm dynamics for flexible control of a functional electrical stimulation neuroprosthesis," *Neural Systems and Rehabilitation Engineering, IEEE Transactions on*, 2016.

[199] E. Eskinat, S. H. Johnson, and W. L. Luyben, "Use of hammerstein models in identification of nonlinear systems," *AIChE Journal*, vol. 37, no. 2, pp. 255–268, 1991.

[200] J. Voros, "Identification of hammerstein systems with time-varying piecewise-linear characteristics," *Circuits and Systems II: Express Briefs, IEEE Transactions on*, vol. 52, no. 12, pp. 865–869, 2005.

[201] M. Lortie and R. E. Kearney, "Identification of time-varying hammerstein systems from ensemble data," *Ann. Biomed. Eng*, vol. 29, pp. 619 – 635, 2001.

[202] B. I. Ikharia and D. T. Westwick, "On the identification of hammerstein systems with time-varying parameters," in *Engineering in Medicine and Biology Society, 2007. EMBS 2007. 29th Annual International Conference of the IEEE*. IEEE, 2007, pp. 6475–6478.

[203] R. Zou, H. Wang, and K. H. Chon, "A robust time-varying identification algorithm using basis functions," *Annals of biomedical engineering*, vol. 31, no. 7, pp. 840–853, 2003.

[204] P. C. Young, "Refined instrumental variable estimation: Maximum likelihood optimization of a unified box–jenkins model," *Automatica*, vol. 52, pp. 35–46, 2015.

[205] D. A. Pierce, "Least squares estimation in dynamic-disturbance time series models," *Biometrika*, vol. 59, no. 1, pp. 73 – 78, 1972.

[206] V. Dietz, D. Schmidtbleicher, and J. Noth, "Neuronal mechanisms of human locomotion," *Journal of Neurophysiology*, vol. 42, no. 5, pp. 1212–1222, 1979.

[207] T. Sinkjaer, J. B. Andersen, and B. Larsen, "Soleus stretch reflex modulation during gait in humans," *Journal of neurophysiology*, vol. 76, no. 2, pp. 1112–1120, 1996.

[208] E. P. Zehr and R. B. Stein, "What functions do reflexes serve during human locomotion?" *Progress in neurobiology*, vol. 58, no. 2, pp. 185–205, 1999.

[209] G. L. Gottlieb and G. C. Agarwal, "Response to sudden torques about ankle in man. iii. suppression of stretch-evoked responses during phasic contraction." *Journal of neurophysiology*, vol. 44, no. 2, pp. 233–246, 1980.

[210] J. Dufresne, J. Soechting, and C. Terzuolo, "Modulation of the myotatic reflex gain in man during intentional movements," *Brain research*, vol. 193, no. 1, pp. 67–84, 1980.

[211] R. B. Stein and C. Capaday, "The modulation of human reflexes during functional motor tasks," *Trends in neurosciences*, vol. 11, no. 7, pp. 328–332, 1988.

[212] R. E. Kearney, M. Lortie, and R. B. Stein, "Modulation of stretch reflexes during imposed walking movements of the human ankle," *Journal of neurophysiology*, vol. 81, no. 6, pp. 2893–2902, 1999.

[213] J. Allum and K. Mauritz, "Compensation for intrinsic muscle stiffness by short-latency reflexes in human triceps surae muscles," *Journal of Neurophysiology*, vol. 52, no. 5, pp. 797–818, 1984.

[214] L.-Q. Zhang and W. Z. Rymer, "Simultaneous and nonlinear identification of mechanical and reflex properties of human elbow joint muscles," *Biomedical Engineering, IEEE Transactions on*, vol. 44, no. 12, pp. 1192–1209, 1997.

[215] A. Klomp, J. H. De Groot, E. de Vlugt, C. G. Meskers, J. H. Arendzen, and F. C. van der Helm, "Perturbation amplitude affects linearly estimated neuromechanical wrist joint properties," *Biomedical Engineering, IEEE Transactions on*, vol. 61, no. 4, pp. 1005–1014, 2014.

[216] D. L. Guarin and R. E. Kearney, "Identification of time varying, intrinsic ankle dynamic stiffness during an imposed walking movement with relaxed muscles," *IEEE Transactions on Neural Systems and Rehabilitation Engineering*, Submitted.

[217] E. Sobhani Tehrani, S. K. Jalaleddini, and R. Kearney, "Ankle joint intrinsic dynamics is more complex than a mass-spring-damper model." *IEEE Transactions on Neural Systems and Rehabilitation Engineering*, Submitted.

[218] D. L. Guarin and R. E. Kearney, "Identification of a time-varying, box-jenkins model of intrinsic joint compliance," *IEEE Transactions on Neural Systems and Rehabilitation Engineering*, vol. PP, no. 99, pp. 1–1, 2016.

[219] D. Ludvig and R. E. Kearney, "Real-time estimation of intrinsic and reflex stiffness," *IEEE Trans. on Biomedical Eng*, vol. 54, no. 10, pp. 1875 – 1884, 2007.

[220] K. Jalaleddini, "Subspace identification of biomedical systems: Application to dynamic joint stiffness," Ph.D. dissertation, McGill University, Montreal, 2015.

[221] E. Sobhani Tehrani, K. Jalaleddini, and R. E. Kearney, "Linear parameter varying identification of ankle joint intrinsic stiffness during imposed walking movements," in *Engineering in Medicine and Biology Society (EMBC), 2013 35th Annual International Conference of the IEEE*. IEEE, 2013, pp. 4923–4927.

[222] J. M. Winters, "Hill-based muscle models: a systems engineering perspective," in *Multiple muscle systems*. Springer, 1990, pp. 69–93.

[223] K. Wang, R. McCarter, J. Wright, J. Beverly, and R. Ramirez-Mitchell, "Regulation of skeletal muscle stiffness and elasticity by titin isoforms: a test of the segmental extension model of resting tension." *Proceedings of the National Academy of Sciences*, vol. 88, no. 16, pp. 7101–7105, 1991.

[224] D. Hill, "Tension due to interaction between the sliding filaments in resting striated muscle. the effect of stimulation," *The Journal of physiology*, vol. 199, no. 3, pp. 637–684, 1968.

[225] U. Proske and D. Morgan, "Do cross-bridges contribute to the tension during stretch of passive muscle?" *Journal of Muscle Research & Cell Motility*, vol. 20, no. 5-6, pp. 433–442, 1999.

[226] M. R. Rehorn, A. K. Schroer, and S. S. Blemker, "The passive properties of muscle fibers are velocity dependent," *Journal of biomechanics*, vol. 47, no. 3, pp. 687–693, 2014.

[227] J. C. Houk, W. Z. Rymer, and P. E. Crago, "Dependence of dynamic response of spindle receptors on muscle length and velocity," *Journal of Neurophysiology*, vol. 46, no. 1, pp. 143–166, 1981.

[228] J. Liebesman and E. Cafarelli, "Physiology of range of motion in human joints: a critical review," *Critical Reviews in Physical and Rehabilitation Medicine*, vol. 6, pp. 131–131, 1994.

[229] M. L. Latash, *Fundamentals of motor control*. Academic Press, 2012.

[230] G. A. Pratt and M. M. Williamson, "Series elastic actuators," in *Intelligent Robots and Systems 95.'Human Robot Interaction and Cooperative Robots',*

Proceedings. 1995 IEEE/RSJ International Conference on, vol. 1. IEEE, 1995, pp. 399–406.

[231] A. H. Shultz, J. E. Mitchell, D. Truex, B. E. Lawson, E. Ledoux, and M. Goldfarb, "A walking controller for a powered ankle prosthesis," in *Engineering in Medicine and Biology Society (EMBC), 2014 36th Annual International Conference of the IEEE*. IEEE, 2014, pp. 6203–6206.

[232] P. E. Crago, J. C. Houk, and W. Z. Rymer, "Sampling of total muscle force by tendon organs," *Journal of neurophysiology*, vol. 47, no. 6, pp. 1069–1083, 1982.

[233] E. G. T. Liddell and C. Sherrington, "Reflexes in response to stretch (myotatic reflexes)," *Proceedings of the Royal Society of London. Series B, Containing Papers of a Biological Character*, vol. 96, no. 675, pp. 212–242, 1924.

[234] D. C. Boone and S. P. Azen, "Normal range of motion of joints in male subjects." *J Bone Joint Surg Am*, vol. 61, no. 5, pp. 756–759, 1979.

[235] A. Roaas and G. B. Andersson, "Normal range of motion of the hip, knee and ankle joints in male subjects, 30–40 years of age," *Acta Orthopaedica Scandinavica*, vol. 53, no. 2, pp. 205–208, 1982.

[236] M. J. Spink, M. R. Fotoohabadi, E. Wee, K. D. Hill, S. R. Lord, and H. B. Menz, "Foot and ankle strength, range of motion, posture, and deformity are associated with balance and functional ability in older adults," *Archives of physical medicine and rehabilitation*, vol. 92, no. 1, pp. 68–75, 2011.

[237] M. Burnfield, "Gait analysis: Normal and pathological function," *Journal of Sports Science and Medicine*, vol. 9, p. 353, 2010.